Peroxin3, a newly identified regulator of melanocyte development and melanosome biogenesis in zebrafish *Danio rerio*

Dissertation
zur
Erlangung des Doktorgrades (Dr. rer. nat.)
der
Mathematisch-Naturwissenschaftlichen Fakultät
der
Rheinischen Friedrich-Wilhelms-Universität Bonn

vorgelegt von
Mirco Brondolin
aus
San Dona' di Piave - Italien

Bonn 2016

Angefertigt mit Genehmigung der Mathematisch-Naturwissenschaftlichen Fakultät der
Rheinischen Friedrich-Wilhelms-Universität Bonn

1. Gutachter
Prof. Dr. rer. nat. Michael Hoch

2. Gutachter
Prof. Dr. phil. nat. Christoph Thiele

Tag der Promotion: 20. März 2017

Erscheinungsjahr: 2017

Per aspera sic itur ad astra

"Through hardships to the stars"

(Lucius Annaeus Seneca, *Hercules furens*, act II, v. 437

Table of contents

1 Introduction

Cells are the basic biological unit of all living organisms. They are the fundamental unit of structure and function. The outer boundary of a cell is the plasma membrane, consisting of a phospholipid bilayer. Within the plasma membrane, enclosed by their own lipid bilayer, distinct compartments, called organelles, can be identified. Organelles are specialized for carrying out specific functions and each of them has a differentiate structure in comparison to any other.

1.1 Peroxisomes

1.1.1 Peroxisome structure and features

Peroxisomes are round to oval organelles surrounded by a single membrane (Figure 1A). They are present in all eukaryotic cells (with the only exception of the erythrocytes and spermatozoa) (Schluter et al. 2006a). Their main functions are to protect the cell by the damaging effects of reactive oxygen species (ROS) and to take part in the fatty acid oxidative metabolism (Cooper & Beevers 1969; Lazarow & Duve 1976). Their size varies between different cell types and within the same cell. Their size usually correlates with number per cell (the more peroxisomes, the smaller they are) and with shape (smaller peroxisome are usually round-shaped, whereas bigger peroxisomes are tubular) (van den Bosch et al. 1992; Wiese et al. 2007; Schrader & Fahimi 2008). Their shape, number and protein repertoire are highly variable in different species, tissues and cell types. Peroxisomes are promptly reacting to different stimuli, physiological conditions and environmental changes (Islinger et al. 2012). They can be rapidly assembled, they increase in number and, if not needed anymore, degraded.

Peroxisomes are similar to lysosomes in morphology. Their biology is unique since they are assembled from proteins synthetized in the cytoplasm on free ribosomes, but they replicate by division, like mitochondria or chloroplasts (Lazarow & Fujiki 1985). In contrast to mitochondria and chloroplasts, peroxisomal proteins are encoded by nuclear DNA. On the membrane and inside the phospholipid by-layer, a multiplicity of proteins and enzymes are located. Electron microscopy observation revealed that enzymes which are present in the peroxisome matrix are electron dense structures; moreover, a crystalline core is described to constitute the centre of the peroxisomal matrix (Figure 1, B and C).

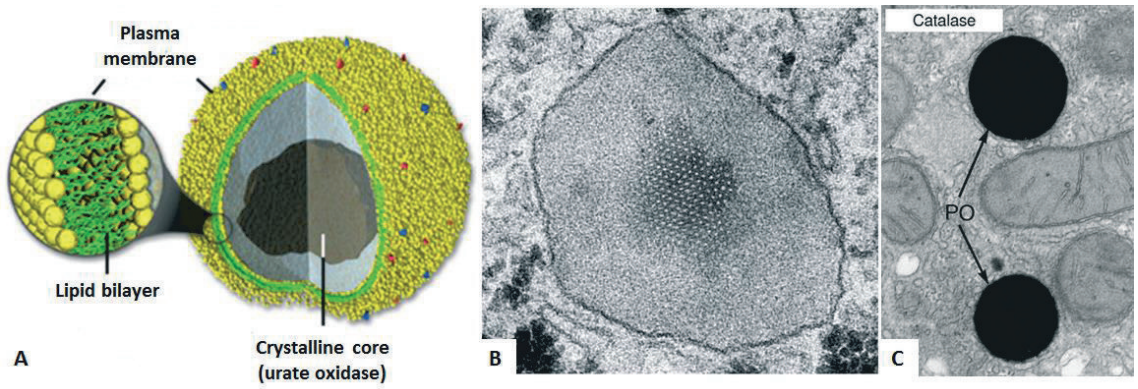

Figure 1 – Simplified schematic representation of peroxisome structure. (**A**) The lipid bilayer-delimited vesicle contains a plethora of enzymes, among which the urate oxidase aggregate in an electron-dense structure in the middle (modified from Molecular Expression; http://micro.magnet.fsu.edu/cells/peroxisomes/peroxisomes.html - The Florida State University). (**B**) View of a peroxisome at the transmission electron microscope. The highly diffractive region in the middle, giving a regular pattern, is representative of the electron-dense urate oxidase enzyme, organized in a crystal structure (modified from Berg et al. 2012). (**C**) Cytochemical localization of catalase stained with the alkaline diamino-benzidine technique in rat hepatic peroxisomes (PO). In the same panel, it is possible to recognize also mitochondria, which are different in shape, structure and morphology (modified from Schrader & Fahimi 2008).

At the time of first description, they were named “microbodies” (Rhodin 1954) and identified as organelles that carry out oxidative reactions, leading to the production of hydrogen peroxide. Since hydrogen peroxide is highly toxic to the cell, damaging nucleic acids, lipids and proteins, peroxisomes contain catalase, which neutralizes hydrogen peroxide toxicity either by converting it to water or by using it to oxidize other organic compounds (Duve & Baudhuin 1966).

1.1.2 **Peroxisomal metabolic activity**

The enzyme content is currently described to consists of more than one hundred different proteins (Wanders 2014). All these enzymes are involved in a variety of metabolic reactions in different biochemical pathways, focused on energy metabolism. Despite differences between species, reactions common to animals, plants and fungi include the oxidation of different fatty acids for energy production and the scavenging of toxic molecules (mainly reactive oxygen species) therefrom derived (Cooper & Beevers 1969; Lazarow & Duve 1976). Fatty acids are processed in a variety of ways, according to their structure: β-oxidation of fatty acids, demethylation of branched fatty acids, oxidation of dicarboxylic and polyunsaturated fatty acids are taking place in peroxisomes. These reactions are important since they provide a major source of metabolic energy. In animals, peroxisomes further specialized with an

extended group of reactions. They are capable also of lipid biosynthesis, in particular of ether phospholipids, cholesterol and dolichol. In the heart and brain, plasmalogens synthesis is especially relevant, since these molecules are important components of cell membranes. In the liver, cholesterol can be further metabolized in bile acids which are then secreted in the gut. In peroxisomes, also other substrates are metabolized: for example, uric acid can be used for synthesis of purine nucleotides and amino acids can be deaminated (Nishikawa et al. 2000) (Figure 2).

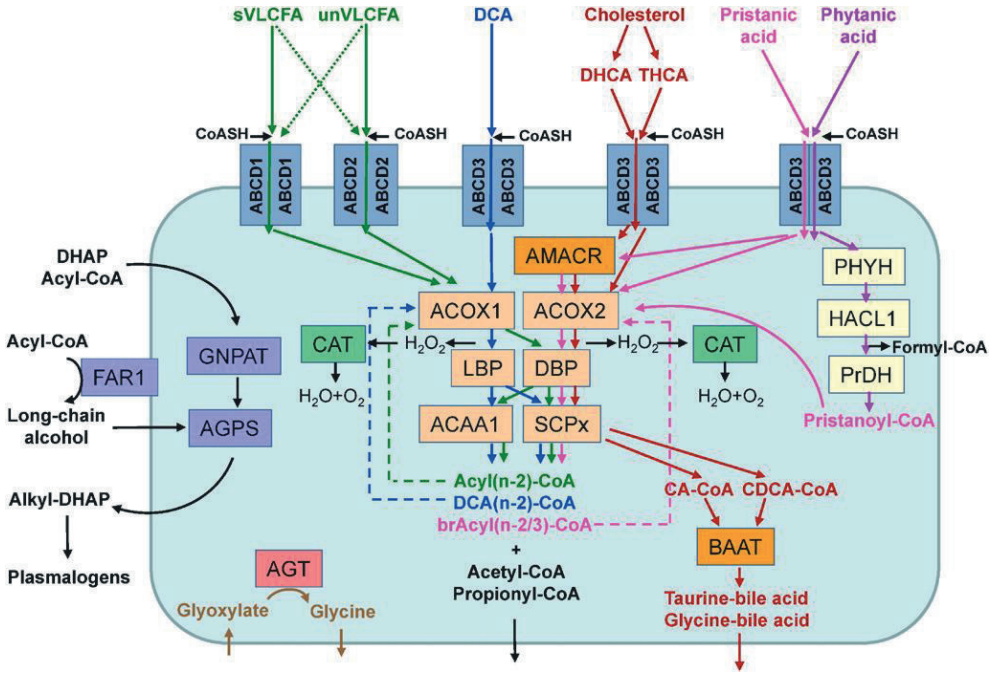

Figure 2 – Main metabolic pathways in peroxisomes. The numerous enzymes in the peroxisomal matrix catalyse reactions involved in the same pathways. Substrates are imported by several ABCD transporters at the membrane (blue boxes). The most important represented pathway is the fatty acid β-oxidation and the enzymes involved are named in light orange boxes. Other pathways are fatty acid α-oxidation (enzymes in yellow), plasmalogens synthesis (enzymes in purple) and bile acid synthesis (enzymes in bright and light orange). All enzymes are indicated with the gene abbreviation. sVLCFA=saturated very long chain fatty acids; unVLCFA=unsaturated very long chain fatty acids; DCA= dicarboxylic acids; DHCA=dihydroxycholestanoic acid; THCA=trihydroxycholestanoic acid; CDCA=chenodeoxycholic acid; DHAP=dihydroxyacetone phosphate; CA=cholic acid. (From Waterham et al. 2016).

In plants and fungi, peroxisomes are associated with an even wider range of metabolic reactions (Islinger et al. 2012), e.g. the synthesis of hormonal signal molecules, like jasmonate and auxins, or secondary metabolites, like biotin or vitamin K1 (Baker et al. 2006; Kienow et al. 2008; Bartoszewska et al. 2011). In *Penicillum* species, it is known that peroxisomes take part in the synthesis of penicillin (Sprote et al. 2009; Meijer et al. 2010). In a similar way, other fungi produce toxins required for host invasion in peroxisomes (Imazaki et al. 2010).

Peroxisomes may also contain enzymes involved in the glyoxylate cycle and for this reason they are also referred as glyoxysomes (Breidenbach & Beevers 1967).

1.1.2.1 Fatty acids β-oxidation

Peroxisomal β-oxidation is found in virtually all cell types and organisms. It usually starts from Very Long Chain Fatty Acids (VLCFA), C22 and longer. Other molecules that can enter the peroxisomal β-oxidation are branched-chain fatty acids (e.g. pristanic acid), bile acid intermediates (such as DiHydroxyCholic Acid – DHCA and TriHydroxyCholic Acid – THCA) and long chain dicarboxylic acids. During β-oxidation, fatty acid molecules undergo multiple cycles, consisting each of four different reactions (dehydrogenation, hydration, dehydrogenation and thiolytic cleavage). At the end of each cycle, fatty acid chains are two carbon atoms shortened and electrons are transferred to oxygen without energy gain, in contrast to mitochondrial oxidation (Wanders et al. 2010). Shortened fatty acid chains, usually with eight carbon atoms, esterified to acyl-CoA molecules, enter then the mitochondrial oxidation, where they undergo the complete oxidation into water and carbon dioxide (Wanders et al. 1995; van Roermund et al. 1995) (Figure 3C).

Slight variations can be observed in the oxidation of the bile acids intermediates, like Di- and TriHydroxyCholestanoic Acid (DHCA and THCA). They undergo one cycle of β-oxidation in peroxisomes to produce the CoA esters of the primary bile acids, chenodeoxycholic acid and cholic acid, respectively. These molecules are then conjugated with taurine or glycine and the product is then transported out of the peroxisomes to be transferred to the bile (Ferdinandusse & Houten 2006; Russell 2003) (Figure 3D).

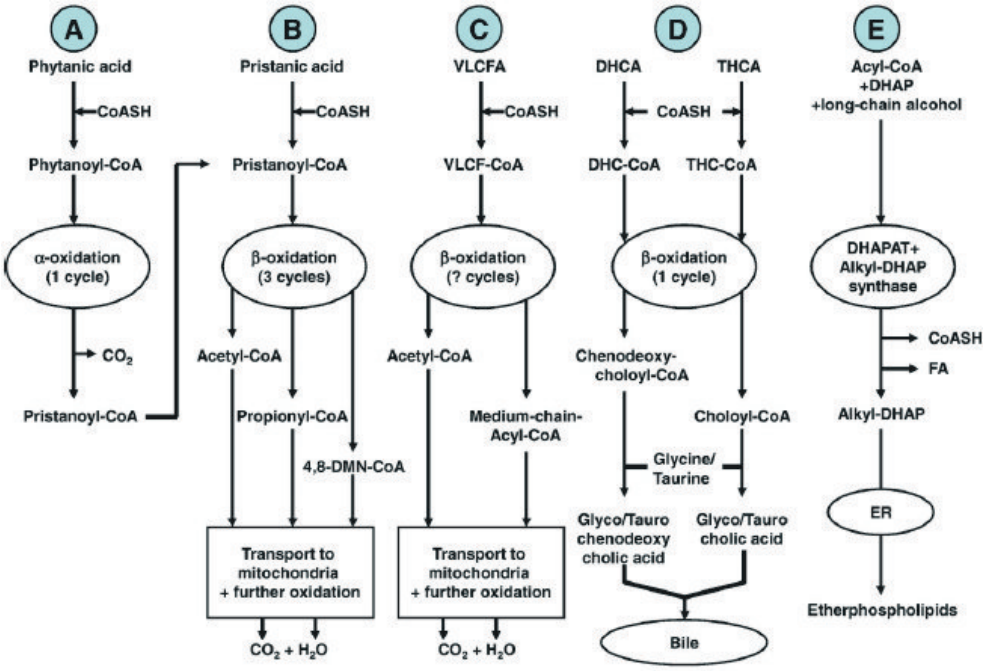

Figure 3 – Lipid metabolism in peroxisomes. Peroxisomes include enzymes able to differently process a variety of substrates. These include the α-oxidation of phytanic acid (**A**) and the β-oxidation of pristanic acid (**B**), very long chain fatty acids (VLCFA – **C**) and dihydroxycholestanoic acid (DHCA) and trihydroxycholestanoic acid (THCA – **D**). All these reactions require the activation of the lipid moiety with Coenzyme A (CoASH). The part of the ether phospholipid synthesis taking place in the peroxisomes is also here represented (**E**). (From Wanders et al. 2010).

1.1.2.2 Fatty acids α-oxidation

Fatty acids with a methyl group at the 3-position (phytanic acid, for example) cannot be directly β-oxidized. For this reason, they need first to be α-oxidized. Specific peroxisomal enzymes (phytanoyl-CoA 2-hydroxylase, 2-hydroxyphytanoyl-CoA lyase, and pristanal dehydrogenase) shorten the fatty acid chain of one carbon obtaining a 2-methyl fatty acid, which can then enter canonical β-oxidation (Jansen & Wanders 2006; Wanders et al. 2011) (Figure 3, A and B).

1.1.2.3 Ether phospholipids synthesis

Ether phospholipids are a special class of phospholipids in which at the sn-1 position of the glycerol backbone an ether bond is present, in contrast to other phospholipids (phosphatidylcholine, phosphatidylethanolamine, and phosphatidylserine) having an ester bond. The major subgroup of ester phospholipid is the plasmalogens, characterized by an unsaturated O-(1-alkenyl)(vinyl ether) group. The biosynthesis of ether phospholipids occurs predominantly in the ER, but it requires two essential intra-peroxisomal steps catalysed by

GlyceroNePhosphate O-Acyl Transferase (GNPAT; also known as DiHydroxyAcetonePhosphate AcylTransferase - DHAPAT) and AlkylGlycerone Phosphate Synthase (AGPS, also known as alkyldihydroxyacetonephosphate synthase), introducing the typical ether bond (Braverman & Moser 2012) (Figure 3E). Another protein on the peroxisomal membrane, Far1, catalyses the cytosolic reduction of fatty acyl-CoA to their respective fatty alcohols, which are subsequently used inside the peroxisome as substrate by AGPS (Buchert et al. 2014).

1.1.2.4 Reactive oxygen species detoxification

All the previously described reactions occurring inside the peroxisomes are highly oxidative and produce massive amounts of H_2O_2, inducing oxidative stress. O_2 is reduced to H_2O_2 by different flavin-containing oxidases (Antonenkov et al. 2010). The most important of those is catalase, a heme-containing enzyme that can form H_2O_2 in a catalytic ($2H_2O_2 \rightarrow 2H_2O + O_2$) and peroxidatic ($H_2O_2 + AH_2 \rightarrow A + 2H_2O$) manner (Kirkman & Gaetani 2007). In the peroxisomal enzyme repertoire, other anti-oxidant enzymes, such as xanthine dehydrogenase, inducible Nitric Oxide Synthase (iNOS), Cu/Zn SuperOxide Dismutase (SOD1), PeroxiReDoXin 5 (PRDX5), Glutathione S-Transferase Kappa (GSTK1), 'Microsomal' Glutathione S-Transferase 1 (MGST-1) and EPoxide Hydrolase 2 (EPHX2) are present (del Rio 2002; Islinger et al. 2009). Typical electron donors are low molecular weight alcohols, formate, nitrite and formaldehyde. Some indirect molecular evidences show that also glutathione and vitamin C may contribute in the regulation of the peroxisomal redox state, since peroxisomal membrane pore proteins may allow their diffusion in the peroxisomal matrix (Rokka et al. 2009; Ivashchenko et al. 2011). Nevertheless, some of these enzymes are sources of superoxide anions ($O^{\bullet-}_2$) and nitric oxide ($^{\bullet}NO$) (Loughran et al. 2013; Stolz et al. 2002). $O^{\bullet-}_2$ and $^{\bullet}NO$ can rapidly combine to form peroxynitrite ($ONOO^-$) (Pacher et al. 2007) (Figure 4). Other reactions, like the synthesis of plasmalogens, are reactive oxygen species scavengers (Wallner & Schmitz 2011; Bonekamp et al. 2009).

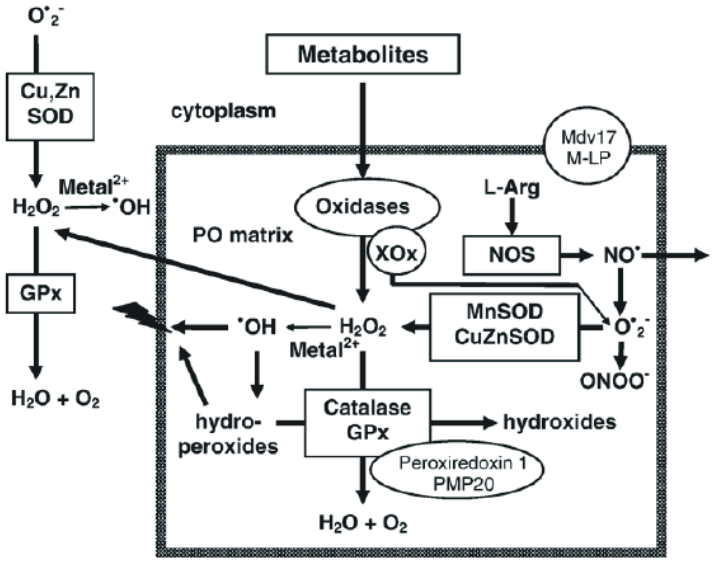

Figure 4 – Reactive oxygen species metabolism in peroxisomes. Oxidations of fatty acids and synthesis of ether phospholipids generate high amounts of H_2O_2, that may damage the cell biomolecules. Thus, H_2O_2 is confined in the peroxisome, where catalase, glutathione-peroxidases (GPx), peroxiredoxins and superoxide dismutase (SODs) neutralize it. In the process also reactive nitrogen species can enter the pathway, through the oxidation of L-arginine operated by the nitric oxide synthase (NOS). (From Schrader & Fahimi 2006a).

Moreover, peroxisomes contribute to the cellular redox metabolism and signalling, with electron-transfer processes playing a messenger role in biological systems (Burgoyne et al. 2012). Cells produce two different types of redox signalling molecules: reactive oxygen species ($O^{\bullet-}_2$, H_2O_2, and the hydroxyl radical $^{\bullet}OH$) and reactive nitrogen species ($^{\bullet}NO$, nitrogen dioxide radical $^{\bullet}NO_2$, nitrite NO^-_2, $ONOO^-$)(Nathan & Ding 2010). These molecules can induce both reversible and irreversible oxidation of proteins and thereby differently influence the activity of kinases, phosphatases, transcription factors, caspases, and metalloproteases (Berridge 2014). Furthermore, lipid peroxidation products can act as important messengers in signalling events that lead to cell proliferation, differentiation, senescence or apoptosis (Ayala et al. 2014).

1.1.3 **Peroxisome biogenesis**

The biogenesis of peroxisomes involves several processes including the formation of peroxisome committed vesicles, the import of peroxisomal membrane and matrix proteins, peroxisomal growth, division and proliferation (Fujiki et al. 2014; Smith & Aitchison 2013). These different processes are controlled by a class of conserved proteins called peroxins (pex), reflecting their role in peroxisome biogenesis. In mammals, 13 different pex genes were

identified. Among those, Pex3, Pex16 and Pex19 are called 'early peroxins' since they are required in the first events leading to peroxisome biogenesis. Pex3 covers a critical role in the commitment of ER-budding vesicles to the peroxisomal fate and in the formation of the peroxisomal proteins importomer.

1.1.3.1 'Growth and division' peroxisome biogenesis pathway

Phospholipids building the peroxisomal membrane originate from the endoplasmic reticulum (Dimitrov et al. 2013; Agrawal & Subramani 2013). Peroxisomes are rather autonomous organelles, meaning that existing ones grow and divide under normal conditions. This growth is mediated by an increase of membrane surfaces through importing lipids and matrix proteins. The division process includes elongation, constriction and fission (Schrader et al. 2012; Schrader & Fahimi 2006a). Elongation and constriction are guided by Pex11 proteins (α, β and γ isoforms, in mammals), each of them having specific functions in the division pathway (Figure 5): Pex11α and Pex11β overexpression increase peroxisome quantity in mammalian cells, but that is not the case for Pex11γ (Li, X. et al. 2002). Pex11 genes are conserved across all the eukaryotes (Koch et al. 2010). Interestingly, proteins shared with mitochondrial fission process are taking part in peroxisome fission. These are DLP1/Drp1, Fis1, Mff and GDAP1 (Schrader et al. 2015; Schrader et al. 2013). DLP1/Drp1 is involved in various cellular membrane fission and fusion events and it is recruited and activated by Pex11β, oligomerize in ring-like structures, causing the constriction sites and, binding Fis1 and Mff, the scission of the daughter peroxisomes (Schrader et al. 2015; Williams et al. 2015). During cell division, like all the other organelles, peroxisomes are symmetrically segregated in daughter cells.

1.1.3.2 *De novo* peroxisome biogenesis pathway

In challenging situations (environmental or metabolic pressure), higher amounts of peroxisomes are needed, and they can be formed through alternative pathways. Peroxisomes are formed *de novo* and this can be demonstrated in cells devoid of any peroxisome or peroxisomal membrane, that are able to re-establish a peroxisome pool. Most probably, this *de novo* peroxisome biogenesis starts from pre-peroxisomal vesicles that originate from the ER (Dimitrov et al. 2013; Agrawal & Subramani 2013; Kim et al. 2006). Two peroxins in particular, Pex3 and Pex16, have indeed been found on the ER membrane and are described to have a specific role in the definition of 'pre-peroxisomal compartments'. Pex19 is assumed to be involved in the budding of pre-peroxisomal vesicles from the domains defined on the ER by

Pex3 and Pex16 (Fujiki et al. 2014). These pre-peroxisomal vesicles are then enriched with peroxisomal membrane proteins and peroxisomal matrix proteins, according the canonical pathways (Figure 5). The import of peroxisomal membrane proteins and matrix proteins is mediated by other members of the peroxin family.

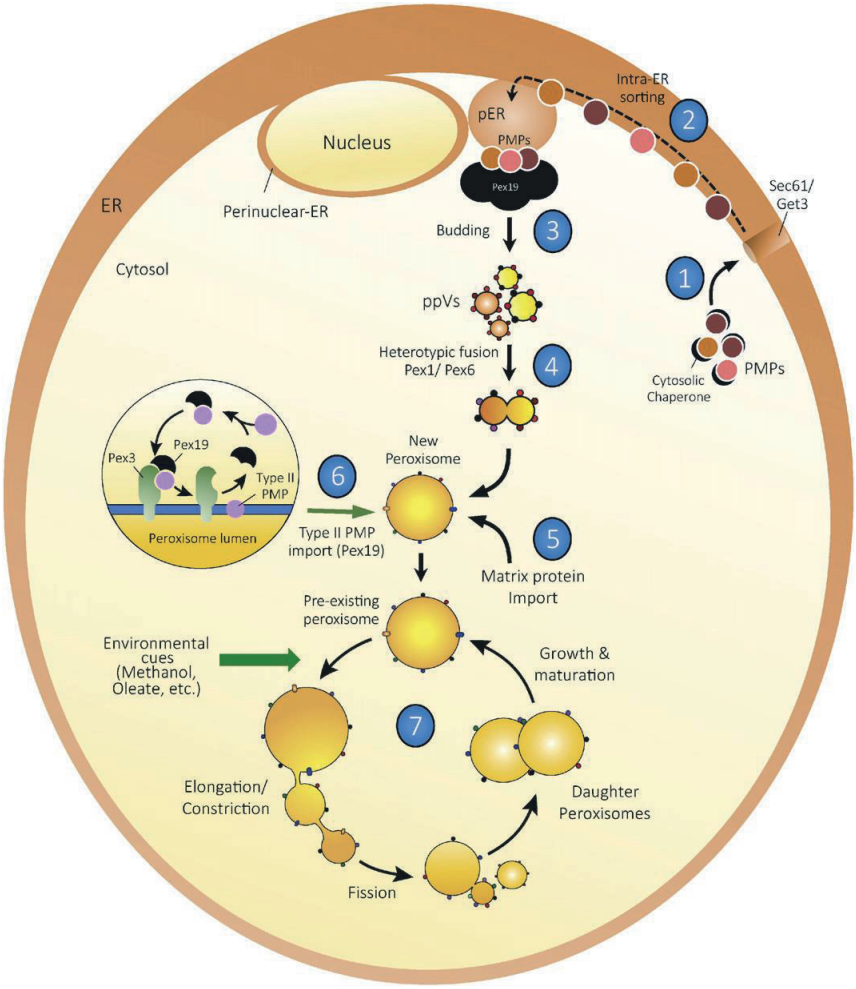

Figure 5 – Schematic representation of peroxisome biogenesis pathways. (**1**) Peroxisome membrane proteins (PMP) are either post-translationally or co-translationally incorporated in the ER membrane; in this step, the ER-translocon Sec61 may be required for the incorporation. (**2**) PMPs are sorted in the ER and they are targeted to specific subdomains (pER). (**3-4**) In a Pex19-dependent manner, PMPs are exported from the ER in vesicular carriers, that later fuse with other vesicles containing complementary sets of PMPs, among which Pex1 and Pex6. (**5-6**) The fusion of these vesicle carriers enable the forming peroxisome to import matrix proteins, with the assistance of Pex3 and Pex19, and become metabolically active. (**7**) Newly formed peroxisomes enrich the cellular peroxisome population, substituting the 'growth and division' pathway when it is blocked or impaired. (From Agrawal & Subramani 2016).

1.1.3.3 Peroxisomal membrane protein import

The embedding of membrane proteins and the import of matrix proteins is mediated by a complex machinery involving several Pex proteins, plus a set of accessory proteins required for Pex activity regulation, mainly via ubiquitination and deubiquitination (Hasan et al. 2013; Schluter et al. 2006b).

Peroxisomes do not possess their own genome, so the proteins dispatched to this compartment are encoded by nuclear genes, synthetized in free cytosolic ribosomes and transported to the peroxisomes. Pex3, Pex16 and Pex19 are the key peroxins for controlling Peroxisomal Membrane Proteins (PMPs) repertoire. Pex19 may be able to recognize PMPs and work as cytosolic chaperon (Rottensteiner et al. 2004). Pex3 is located in the peroxisomal membrane and it works as docking site for the Pex19-PMP cargo complex (Fang et al. 2004). Pex16 is not conserved across the eukaryotes, but in the species in which it is present, it was shown to be co-receptor for the Pex3-Pex19-PMP complex (Honsho et al. 2002). Once Pex19 is docked on the peroxisomal membrane with its cargo, Pex3 may induce a local remodelling of the membrane. The hydrophobic domains of the cargo protein may then come closer and hydrophobic forces would detach it from the chaperone, Pex19. Once this process is completed, Pex19 is released in the cytosol and can be recycled for the embedding of a new PMP (Figure 6). Some recent reports, based on research in yeast model, propose that PMPs are inserted in the membrane already at the ER, via a Sec61-dependent mechanism and they exit the ER already in pre-peroxisomal vesicles, that fuse with pre-existing peroxisomes (Thoms et al. 2012).

1.1.3.4 Peroxisomal matrix protein import

Proteins directed to the peroxisomal matrix must contain a peroxisomal targeting signal (PTS). Two PTSs were identified and characterized until now. The most common, PTS1 signal, is a C-terminal tripeptide with the consensus sequence serine-lysine-leucine (S-K-L) (Brocard & Hartig 2006), but conserved exchanges are accepted [(S/A/C)-(K/R/H)-(L/M)]. In rare cases, proteins may have a PTS2 signal, a nonapeptide at the N-terminus of the protein with consensus sequence (R/K)-(L/I/V)-X_5-(Q/H)-(L/I/V) (Subramani 1992). After the import into the matrix, PTS2 signal is cleaved off (Lazarow 2006). The import of matrix proteins into the lumen of peroxisomes requires a cytosolic receptor: Pex5 for PTS1-containing matrix proteins (Braverman 1998), or Pex7 for PTS2-containing matrix proteins (Dodt et al. 2001). Other peroxins, Pex13 and Pex14, form a gated pore onto which the matrix protein-receptor complex docks. With the assistance of Pex2, Pex10 and Pex12, the cargo is released inside the matrix and Pex1 and Pex6 allow the cytosolic receptor to be released for a new cycle or for proteasomal degradation (Dammai & Subramani 2001) (Figure 6). Proteins are usually transported through the membrane in the folded form and in oligomerized complexes, if required for the protein function (McNew 1994).

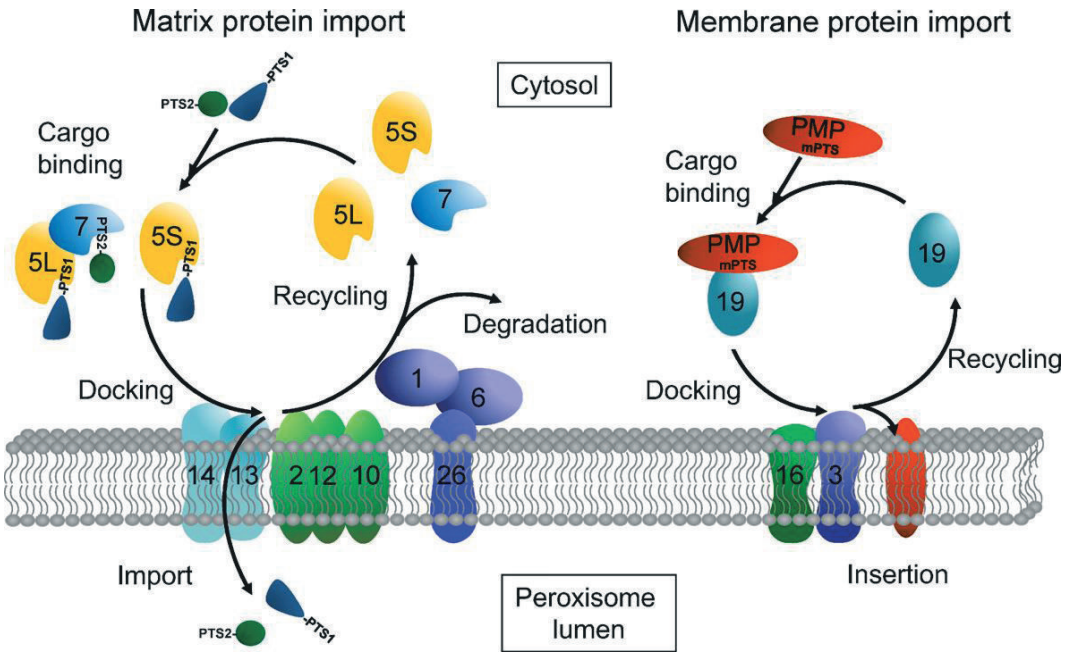

Figure 6 - Peroxisomal protein import. Peroxisomal membrane protein import depends on the Pex19 cytosolic chaperon and the Pex3 docking protein (with the facultative assistance of Pex16). On the other hand, peroxisomal matrix protein import depends on two different cytosolic chaperons (Pex5 for PTS1-containing proteins, Pex7 for PTS2-containing proteins) and several other peroxins at the peroxisomal membrane to allow the release of the cargo from the chaperon and the crossing of the membrane. (From Waterham et al. 2016).

1.1.4 **Pex3, key component of peroxisome biogenesis**

Pex3 is conserved across all the eukaryotes and it represents the key component of peroxisome biogenesis, orchestrating the interactions with other peroxins, mediating the successful sorting of membrane protein on peroxisome surface and providing lipid membrane supply for the organelle growth. Most of the studies describing Pex3 mode of actions were conducted in different yeast species (*S. cerevisiae*, *H. polymorpha*, *Y. lipolytica*), but in the last few years also mammalian cell lines or fibroblasts from patients affected by mutation in one of the PEX genes were used.

The first described Pex3 function is related to its role during peroxisomal membrane protein embedding. In fact, as previously mentioned, Pex3 acts as docking factor for the Pex19-cargo protein complex and it is able to locally remodel the membrane to facilitate the protein insertion (Fang et al. 2004; Fujiki et al. 2006). Pex3 is also found at the membrane of subdomains of the ER, which than evolve into pre-peroxisomal vesicles (Tam et al. 2005). Moreover, Pex3-containing vesicles do not necessarily progress to mature peroxisomes, but they might simply fuse to pre-existing ones, in order to supply lipids for membrane surface and volume growth (van der Zand et al. 2012). More recently, new roles were described,

connecting Pex3 to peroxisome inheritance during cell division, by means of interaction with Inp1 (Munck et al. 2009), and to the autophagic clearance of damaged peroxisomes (process also known as 'pexophagy') through ubiquitination and interaction with autophagy related proteins (Yamashita et al. 2014; Burnett et al. 2015).

Different studies carried out on yeast on murine Pex3 proteins clarified its three-dimensional structure and the nature of the interaction with other partner proteins (Sato et al. 2010; Schmidt et al. 2012a; Hattula et al. 2014). The cytosolic domain of Pex3 is described as a spheroid with a 'twisted six-helix bundle' fold. A hydrophobic surface located at the most distal part from the peroxisome membrane constitutes the interaction domain with a hydrophobic α-helix of Pex19, being responsible for the high affinity of these two proteins (Sato et al. 2008). Thus, Pex19 can be efficiently captured from the cytoplasm and its conformation can be changed to allow the release of the cargo protein. Another hydrophobic groove is located at the apex of the spheroid proximal to the peroxisome membrane and it is most probably required in post-translational membrane protein import (Schmidt et al. 2012b) (Figure 7). The interaction with Pex19 significantly stabilize Pex3, limiting its thermal mobility and possibly shielding hydrophobic residues, otherwise exposed to the aqueous environment (Schmidt et al. 2010).

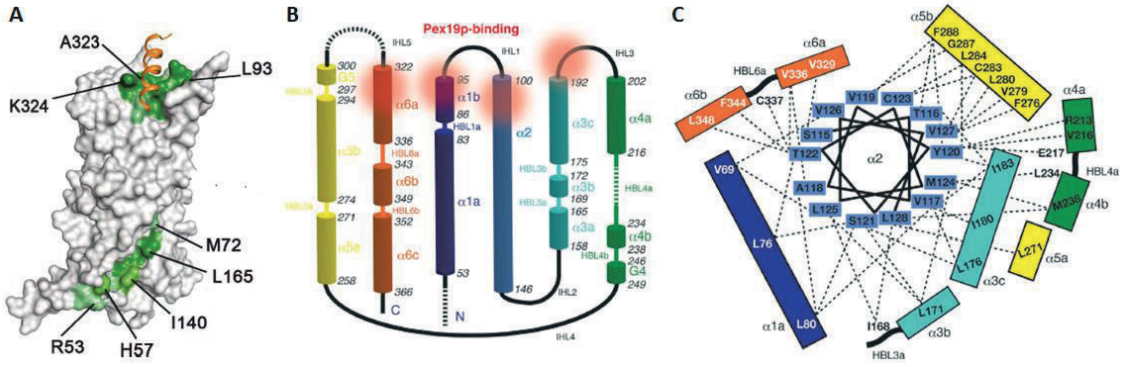

Figure 7 – Pex3 structure**.** (**A**) Surface representations of PEX3 with the bound PEX19-derived peptide depicted as an orange ribbon. A hydrophobic surface located at the most distal part from the peroxisome membrane (depicted in green) constitutes the interaction domain with a hydrophobic α-helix of Pex19. Another hydrophobic groove, necessary for Pex3 post-translational insertion into the membrane, is located at the opposite apex. Conserved amino acids are annotated. (Modified from Schmidt et al. 2012b) (**B**) Unfolded structure of the six cytoplasmic α-helices. Red shadings show the Pex19 binding regions (From Sato et al. 2010). (**C**) Scheme representing a view of Pex3 from the distal side. Boxes represent the different α-helices and amino acids which are interacting with Pex19 are annotated (From Sato et al. 2010).

1.1.5 Peroxisome related pathologies

Mutations in genes involved in peroxisome biogenesis, in any of the enzyme of the metabolic pathways or in any of the peroxisomal membrane metabolite transporter are causing severe pathologies in human. Since peroxisomes play a crucial role in human metabolism, these organelles are indispensable for normal life and their lack has detrimental effects and causes often lethality within the first years of age, in humans (Wanders 2014; Waterham & Ebberink 2012). The spectrum of diseases is rather heterogeneous and two main groups of pathologies can be identified: single Peroxisomal Enzyme Deficiencies (PEDs) and the Peroxisomal Biogenesis Disorders (PBDs). The estimated combined incidence of these two groups of disorders is of 1 in 5000 individuals with X-linked adrenoleukodystrophy as the most common (Kemp et al. 2012).

1.1.5.1 Peroxisomal enzyme deficiencies

PEDs are disorders caused by a defect of individual peroxisomal proteins involved in one specific catalysis step. Both peroxisomal matrix enzymes and peroxisomal membrane proteins involved in metabolite transport can be affected. The clinical and biochemical consequences are related to the specific function in peroxisomal metabolism of the mutated gene. Disorders can be caused by enzymes involved in peroxisomal β-oxidation (X-linked adrenoleukodystrophy, X-ALD, is the most frequently occurring - Engelen et al. 2014), peroxisomal α-oxidation (Refsum disease - Pagon et al. 1993), glyoxylate metabolism (primary hyperoxaluria type I), ether phospholipid biosynthesis (rhizomelic chondrodysplasia punctate, RCDP - Barth et al. 1996; Heymans et al. 1985), peroxisomal bile acid synthesis and peroxide metabolism (acatalasemia - Takahara 1952; Goth & Nagy 2013).

1.1.5.2 Peroxisomal biogenesis disorders

PBDs are caused by a heterogeneous group of autosomal recessive mutations affecting the assembly and the maintenance of functional peroxisomes. 13 different Pex genes have been identified until now to be causative of these pathologies. The affected Pex genes are mainly involved in the import of peroxisomal membrane or matrix proteins, but recently a few mutations in genes involved in peroxisome maintenance were described (Yik et al. 2009). The clinical presentation of PBD patients ranges from severe, early-lethal, multisystemic disorders to milder, late-onset progressive neurological diseases or even isolated visual or hearing problems. For this reason, PBDs are classified in Zellweger spectrum disorders (ZSDs),

rhizomelic chondrodysplasia punctate type 1 and type 5 and peroxisomal fission defects, according to the severity of the symptoms.

ZSDs include the three best characterized manifestation of PBDs, namely (from the most to the less severe) Zellweger syndrome (ZS), neonatal adrenoleukodystrophy (NALD), and infantile Refsum disease (IRD) (South et al. 2001). ZS patients display severe hypotonia, ocular abnormalities, seizures, renal cysts, hepatic dysfunction and craniofacial deformities (large anterior fontanel, prominent forehead, shallow orbital ridges, high arched palate and broad nasal bridge). In the plasma, increased levels of substrates normally handled by peroxisomes, such as VLCFAs, pristanic acid, phytanic acid, DHCA, THCA and pipecolic acid, and decreased levels of end products of peroxisomal metabolism, such as plasmalogens, cholic, chenodeoxycholic acid, and docosahexaenoic acid may be detected (Bootsma et al. 1999; Dacremont & Vincent 1995). These patients do not complete the first years of life (Figure 8).

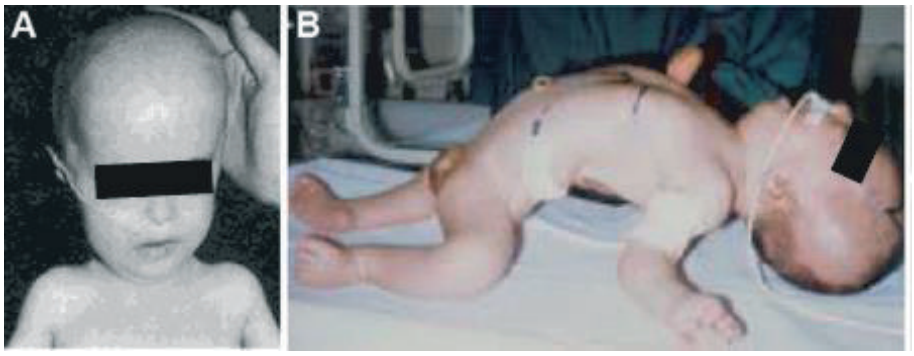

Figure 8 – Zellweger Syndrome patients. (**A**) In this patient the craniofacial deformities (prominent forehead, shallow orbital ridges) are particularly prominent. (**B**) Another Zellweger Syndrome patient shows severe hypotonia and other deformities. (Modified from Miller BF 2003).

NALD and IRD patients have highly variable clinical manifestations, all characterized by developmental delays, progressively worsening. They usually reach their teens or even adulthood (Berendse et al. 2016). Pex3, Pex16, and Pex19 mutations cause defects in the import of both peroxisomal matrix and membrane proteins, and no peroxisome-like structure can be detected anymore (Fujiki 2000); nevertheless, hypomorphic mutations in Pex3 and Pex16 genes were described and they cause less severe clinical presentations with cells having fewer but enlarged peroxisomes (Subramani 1992). Mutations in Pex1, Pex2, Pex5, Pex6, Pex10, Pex12, Pex13, Pex14, and Pex26 genes affect only the import of peroxisomal matrix proteins. Cells from PBD patients having mutations in one of these genes show peroxisomal membrane remnants that may contain peroxisomal membrane proteins, the so-called ‘ghost

peroxisomes'. The patients suffering of one of these mutations display only a few of the symptoms that are typically associated with ZSDs, with hardly recognizable biochemical defects.

Pex5L (encoding for the PTS1-protein receptor) cause RCDP type 5 (Baroy et al. 2015), while Pex7 mutations (encoding for the PTS2-protein receptor) cause RCDP type 1 (Braverman & Moser 2012); both have similar clinical symptoms: congenital contractures, cranial abnormalities, severe hypotonia, cataract, skeletal deformities, and stippled calcification of cartilage tissues.

Also peroxisome divisions can be affected by mutation in genes involved in the process: DLP1 (Waterham et al. 2007), Mff (Shamseldin et al. 2012), GDAP1 (Huber et al. 2013) and Pex11β (Ebberink et al. 2012). These mutations cause mitochondrial encephalopathy and cells display tubular peroxisomes. Since peroxisome fission machinery is partially shared with the mitochondria fission machinery, also mitochondria may be affected. Despite altered peroxisomal morphology in the analysed fibroblasts (so-called 'pearls-on-a-string' conformation), these patients do not display any biochemical parameters alterations.

1.1.5.3 Peroxisomal biogenesis disorder models

Due to the severity of PBDs, in order to gain further insight into their pathogenesis, biomedical research aimed to the generation of animal models. Mouse models deficient for Pex2, Pex5, Pex13 and Pex11b were generated (Baes & van Veldhoven 2006). All the clinical symptoms of the ZS phenotype are recapitulated in these mice. Similar to what happens in human, null models survive gestation, but die soon thereafter. Detailed analysis revealed changed brain morphology, with altered distribution of cortical neurons, altered neuronal migration and differentiation defects, extensive neuronal apoptosis (Pex5, Pex11b) and abnormal morphology of Purkinje cells in the cerebellum (Pex2) (Faust 2003). Pex11b mutant mice show only mild deficiencies in ß-oxidation and ether lipid biosynthesis and slight decrease of peroxisome amount (Li, Xiaoling et al. 2002). Pex5 null mutants show morphologically abnormal mitochondria with decreased respiratory chain complex activity, in liver, but no oxidative damage, possibly due to the increase of glycolysis and of mitochondrial proliferation (Dirkx et al. 2005). Pex5 conditional models for neural precursors or oligodendrocytes result in moderate cortical migration defects, with progressive degeneration of axonal integrity and maintenance of myelin, motor and cognitive impairment and premature death before 6 months of age (Baes & Aubourg 2009; Kassmann et al. 2007). Pex5 conditional knock-out in the hepatocytes results in postnatal arrest of neuron migration (Krysko et al. 2007).

Pex7 null mice recapitulate the RCDP phenotype (Braverman et al. 2010). The symptoms are pinpointed to altered plasmalogens biosynthesis and their requirement in cerebellar, lens and skeletal development, as well as spermatogenesis.

All the PBD mouse models were used to test potential therapeutic interventions, by means of dietary supplementation of missing metabolites, already during gestation. These strategies help to circumvent the lack of essential molecules for membrane formations, improving the phenotype, but they did not avoid the accumulation of other unprocessed, toxic metabolites (Braverman et al. 2013).

The attention is currently focused on peroxisome mosaicism in ZSD patient liver tissue and fibroblast cell lines, namely the conditions in which some cells are able to import peroxisomal proteins adjacent to others that show no import, in presence of a general Pex gene defect. The hypothesis is that microenvironmental factors (e.g. different body temperature) can influence peroxin activity (Steinberg et al. 2006).

Noteworthy, in parallel, also invertebrate models were generated. First publications in *C. elegans* date back to the early 2000s. Using an RNAi approach, different peroxin homologs and peroxisomal enzymes involved in α- and β-oxidation were inactivated, causing a developmental arrest at the L1 stage and the missing initiation of postembryonic cell divisions, similar to starvation-arrested larvae (Petriv et al. 2002; Thieringer 2003). More recently, also PBDs models in *D. melanogaster* were established. Pex mutants faithfully recapitulate several key features of human PBD, including impaired peroxisomal protein import, elevated VLCFA levels and growth retardation. Moreover, disruption of Pex function results in spermatogenesis defects (Chen et al. 2010). More in detail, Pex3 mutants are larval lethal, but in conditional knock-down, in which *Pex3* function is deleted in muscle, no peroxisome is detectable and this results in flightless animals, possibly by disrupting energy metabolism (Nakayama et al. 2011; Faust et al. 2014).

1.2 Zebrafish (*Danio rerio*)

1.2.1 Zebrafish in biomedical research

Zebrafish is the common name of *Danio rerio* (formerly classified as *Brachydanio rerio*), a member of the *Cyprinidae* family. Zebrafish is a freshwater fish originating from the sub-tropical regions in north-eastern India, northern Pakistan, Bangladesh, Bhutan and Nepal. Due to its robustness, it became globally available also for domestic aquariums.

In 1981 George Streisinger introduced zebrafish as genetic model to study vertebrate development. During the last few decades, zebrafish emerged as one of the most important, popular and potent experimental animal models in biomedical research (Figure 9). In fact, due to several advantages of zebrafish, research broadened to different fields, including neurobiology (Hughes 2013), cancer (Moore & Langenau 2016), cardiovascular development (Kessler et al. 2015), immune system disease (Galindo-Villegas 2016), infection models (Hall et al. 2016), tissue regeneration (Sehring et al. 2016), metabolic diseases (mainly diabetes and lipid-related diseases) (Den Broeder et al. 2015) and ciliopathies (Song et al. 2016).

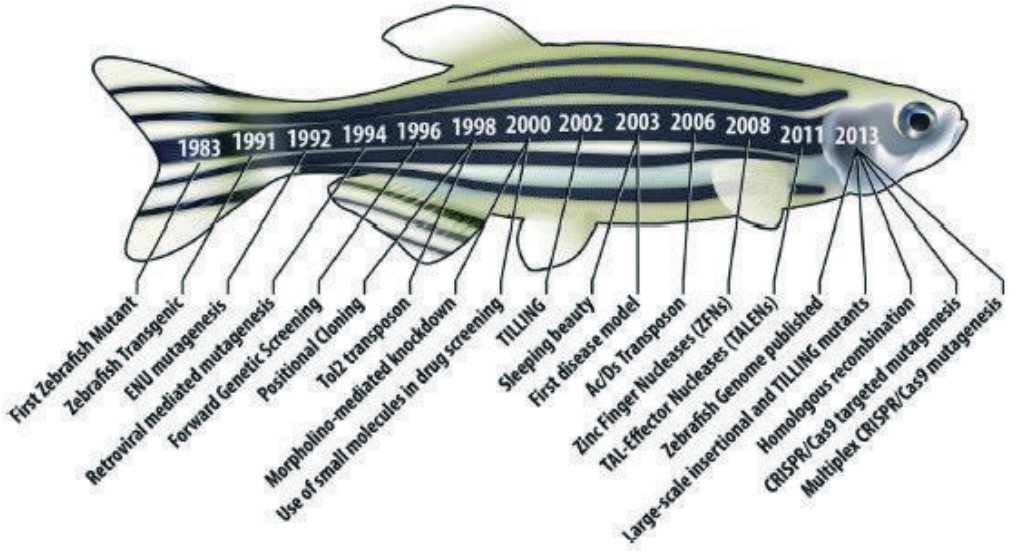

Figure 9 – Timeline of the most important technological milestones in zebrafish biomedical research. (From Varshney, Sood et al. 2015).

Despite being a relatively simple vertebrate animal, there is a considerable conservation of most of the human pathways in zebrafish. Embryonic development, biological functions, cellular biology, physiology and diseases are comparable to humans. Thus, despite teleost fish diverged from mammals during evolution more than 400 million years ago, zebrafish still share a considerable amount of genetic identity with humans, and several zebrafish organ systems are remarkably similar to those in humans.

1.2.2 **Zebrafish genome features**

In February 2001, the Wellcome Trust Sanger Institute initiated the zebrafish genome-sequencing project and since 2013 the fully sequenced genome is available (Howe et al. 2013a). The zebrafish genome is the result of approximately 340 million years evolution, with

additional rounds of whole-genome duplication, generating ohnologues genes (two copies of the same gene in the same genome) (Amores et al. 2011; Wolfe 2000). Because of the genome duplication, most of the time, ohnologues diverged to give two specialized paralogs (genes derived from the same ancestor sequence), with different expression patterns (spatial and/or temporal) and more restricted (less complex) functions. In some cases, only one copy maintained its function and the other degraded into a pseudogene. Zebrafish possess 26.206 protein-coding genes (Collins et al. 2012) with a higher number of species-specific genes in comparison to human or mouse (Kasahara et al. 2007). The zebrafish genome shares a great genetic identity with human, with 71,4% of human genes having at least one zebrafish orthologue (but only 47% have a one-to-one relationship), and 69% of zebrafish genes having at least one human orthologue (Vilella et al. 2009). Few notable human genes (interleukin 6 – IL-6, or leukaemia inhibitory factor – LIF) have no clearly identifiable zebrafish orthologue, even if the corresponding receptors were identified: most probably other genes, not recognized as orthologues, took over their function. 82% of the genes included in the Online Mendelian Inheritance in Man (OMIM) database can be related to at least one zebrafish orthologue.

1.2.3 **Zebrafish life cycle**

The main advantage of the zebrafish as animal model for biomedical research is its shorter life cycle in comparison to other models and the relatively high fecundity, with 100-1000 eggs produced per spawning (Kurtzman et al. 2010; Lawrence 2011). Eggs are spawned throughout the year (Clelland & Peng 2009) and best spawning performance is limited to a short period at dawn, with an optimal spawning frequency typically around 10 days (Niimi & LaHam 1974; Darrow & Harris 2004).

Spawned eggs immediately start to develop and the ideal incubation temperature is 28,0 to 28,5°C. Within the first 45 minutes, the first cell division takes place. 4 hours post fertilization (hpf) an embryo is composed of about one thousand cells that start to migrate over the yolk with extensive rearrangements. Afterwards, further cell movements and the differential activation of BMP, Wnt and Nodal signalling pathways in different areas, determine the formation of the three primary embryonic germ layers. At the end of the gastrulation process, 11 hpf, the basic vertebrate body plan is established and the first individual somites are formed in the anterior region, to progressively move to the posterior. At 18 hpf, 18 somite pairs are clearly visible; at 24 hpf a complete fish is recognizable, and the heartbeat and

associated blood flow can be observed. Within 48 hpf, embryogenesis is completed and larvae hatch during the third day post fertilization (dpf). Cell differentiation processes continue until 5 dpf, especially in the brain and in the gastrointestinal tract; only at this point all the organs have taken up their function and the mouth apparatus is completely formed, so that the larvae can start to feed independently (Kimmel et al. 1995).

Despite a quick embryonic and early larval stage, the remaining developing steps take longer. Larval stage lasts up to three weeks, when metamorphosis starts. Metamorphosis involves changes in a variety of traits: absorption of the larval fins, ventral drop of the gut tube, development of scales and of the pigmentation pattern (Ledent 2002). At 5 weeks of age, when metamorphosis in completed, larvae enter the juvenile stage, with an exponential growth, and reach puberty at 45 dpf in females. In captivity, reproductive maturity is reached at the completion of the third month of age (Chen & Ge 2013) (Figure 10).

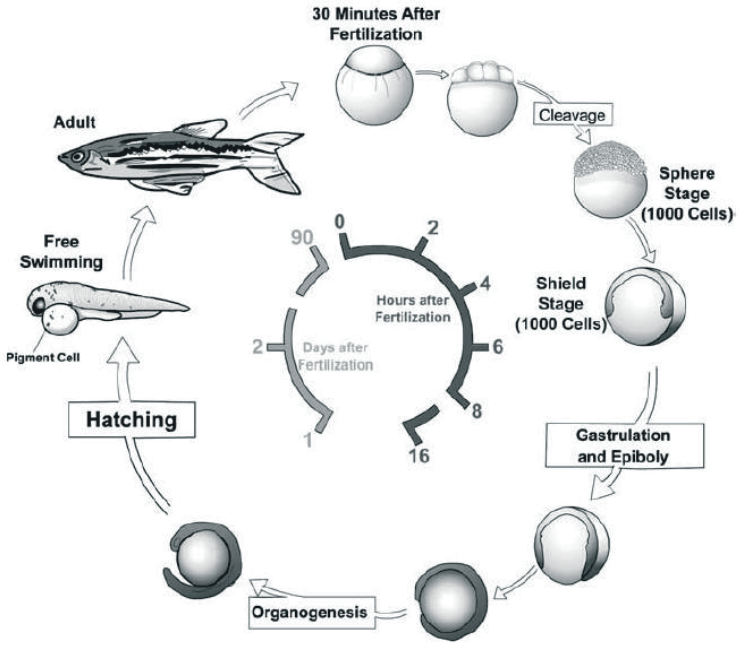

Figure 10 - Life cycle of zebrafish. Zebrafish develop rapidly from a one-cell zygote that sits on top of a large yolk cell. Cells divide every 30-45 minutes and within 6 hours the embryo is made of thousands of cells. Gastrulation begins approximately 6 hours post fertilization, and organogenesis starts immediately afterwards. At 2-3 days animals hatch as free-swimming larvae and they begin to feed at 5 days. Zebrafish reach sexual maturity around 3 months of age and can live for up to 5 years. (Modified from D'Costa & Shepherd 2009).

Adult zebrafish exhibits sexual growth dimorphism in favour of females. Adult animals can be distinguished based on differences in body size, shape and pigmentation: males are smaller, more elongated with gold and blue stripes, whereas females are bigger, more rounded, with silver and blue stripes and a whitish belly (Parichy et al. 2009; Brondolin et al. 2012). Under

laboratory conditions, zebrafish do not differ much from animals in wild populations (Spence et al. 2007): adult animals weight between 0,5 g and 0,9 g and are 22 mm to 38 mm long, with females being on average bigger than males (Lawrence et al. 2007). No difference between different zebrafish strains were reported, when kept in same housing conditions. Average lifespan is 36 months, but there are reports of zebrafish living until 62 months (Gerhard et al. 2002).

1.2.4 **Advantages of zebrafish as biomedical model**

The zebrafish combines several advantages, which made it a suitable model for biomedical research.

1 – Easiness to maintain: due to the small size of the adult animals, zebrafish can be kept in large numbers in a limited space; thus, zebrafish are relatively inexpensive to maintain. Moreover, it is possible to keep and analyse large populations, minimizing the effect of inter-individual variability.

2 – Easiness of breeding: each female can produce hundreds of embryos per spawning, throughout the whole year. This allows the possibility of making large genetic and pharmacological screens. Embryos undergo rapid development and organogenesis is completed within three days; it is possible to obtain a new generation after three months.

3 – *Ex utero* fertilization: embryos are fertilized and develop externally the body of the mother. Thus, embryos are immediately accessible, representing an ideal vertebrate model system for the study of the embryonic development.

4 – Transparency: During embryonic development, embryos are completely transparent; mutant lines unable to develop pigments are available, and the pigmentation process can be blocked or delayed using non-toxic chemical compounds. The translucent body of zebrafish embryos facilitates non-intrusive visualisation of organs and biological processes, allowing *in vivo* imaging and quantification.

5 - Size of embryos: embryos are sturdy and large enough (0,7 mm) to enable experimental manipulations, such as microinjections or transplantation of cells.

6 – Genomic manipulation: zebrafish are suitable both for ‘forward genetics’ and ‘reverse genetics’ studies. Large-scale forward genetics screens are possible; phenotypical defects are identified prior the mutation (spontaneous or induced) causing it (Driever et al. 1996). In recent years, also reverse genetics screens became common thanks to the availability of different genome manipulation techniques, enabling the generation of knock-down or knock-

out models. Transgenic lines can also be easily generated so that valuable tools are established and can be used for a more detailed analysis of biological processes. Newer transgenic techniques allow conditional gene activation or inactivation (Ni et al. 2012).

1.2.5 Gene manipulation in zebrafish

1.2.5.1 Antisense Morpholino Oligonucleotide knock-down

Gene expression can be transiently knocked-down using antisense morpholino oligonucleotides (AMOs) (Nasevicius & Ekker 2000). AMOs are 25-mer synthetic oligonucleotides, specifically designed to hybridize with mRNA molecules. AMOs can be injected in the cytoplasm of 1-cell stage embryo, without being rapidly degraded by nucleases and evocating immune response. Different strategies can be adopted: AMOs can be designed to anneal around the start codon of an mRNA, preventing protein translation initiation (Figure 11A); they can also be designed to bind a splicing site on the pre-mRNA molecule so that the protein cannot be properly spliced, leading to a frameshift, due to intron retaining or exon skipping (Figure 11, B' and B'').

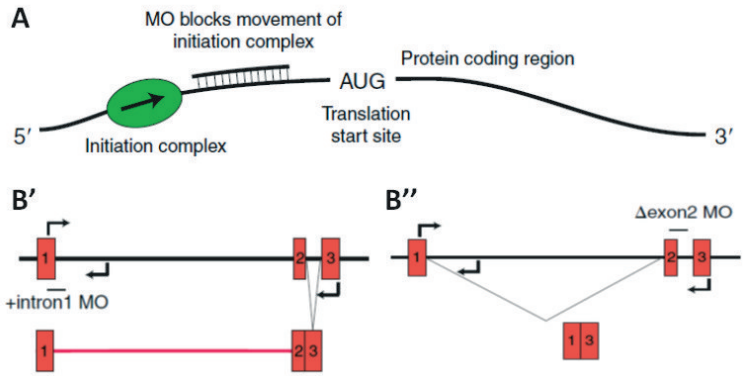

Figure 11 – Antisense morpholino oligonucleotide (AMO) knock-down modes of action. (**A**) The AMO can be designed to target the sequence 5' of the translation start site, inhibiting the progression of the initiation complex. (**B'-B''**) An AMO can be designed to be complementary to a splicing donor or acceptor site, so that the splicing machinery fails in its recognition, causing intron retaining (B') or exon skipping (B''). (Modified from Eisen & Smith 2008).

AMO knock-down allows rapid and effective study of gene function, even if this approach is limited to processes occurring during the first 5 days of development, since the AMO molecules are then degraded or diluted through the subsequent cell divisions.

Multiple genes can be knocked down at the same time, injecting AMO molecules targeting the different mRNAs. This can be useful to tackle redundant gene functions or to assess interaction

between proteins belonging to the same pathway. However, the AMO approach is prone to off target effects, due to sequence similarities in the genome.

1.2.5.2 Chemical mutagenesis screening

While developmental defects are evident during the first day after fertilization, mutations in genes regulating other processes may become apparent during the larval or the juvenile stage, when AMO action has vanished.

In the early 1990s, large-scale forward genetic screens were initiated in zebrafish to identify mutants with early embryonic developmental defects. The screens used an effective and efficient mutagen, N-Ethyl-N-NitrosUrea (ENU), able to transfer an ethyl group to nucleobases, especially to thymine, thus inducing point mutations (Davis & Justice 1998). Fish carrying gene-specific mutations can be identified by locus-specific PCR, positional cloning methods or by whole-exome sequencing (Henke et al. 2013). This approach was also adopted in reverse genetics screens, searching for mutations in genes of interest. The biggest of these projects is the Zebrafish Mutagenesis Project (ZMP) (https://www.sanger.ac.uk/resources/zebrafish/zmp/) aiming to generate a knock-out of every protein-coding gene in the zebrafish genome (Kettleborough et al. 2013). As of October 2016, ZMP has generated 36.296 alleles in 14.697 genes, roughly half of the zebrafish genome, and more than 80% of them have been made available to the scientific community.

1.2.5.3 Transcription Activator-Like Effector Nucleases (TALEN)

In 2010, the Transcription Activator-Like Effector Nucleases (TALENs) emerged as faster, cheaper and efficient way to introduce locus-specific double-strand breaks in the genome, generating disruptive mutations (Miller et al. 2011; Wood et al. 2011; Huang et al. 2011). Similar to Zinc Finger Nucleases (ZFNs) (Doyon et al. 2008), TALENs are fusion proteins, combining a DNA-binding domain and the endonuclease domain of FokI. The DNA-binding domain is inspired from the one of secreted proteins of the plant pathogenic bacteria of genus *Xanthomonas*. A TALEN DNA-binding domain combines 12 to 30 modules (usually 18). Each module is a repeated unit of 33 amino acids in which only two residues, at position 12 and 13, termed the Repeat Variable Di-residue (RVD), are variable and they give specificity for the single nucleotide that they recognize. Since the FokI nuclease is active only as a dimer, two TALEN arrays (left and right) need to be assembled to recognize the two different strands. The optimal spacer between the two recognition sites is recommended to be 14-20 bp (Ma et al.

2013; Reyon et al. 2012) (Figure 12). TALENs broadened the possible target sequence repertoire, basically without limitations, and provide high degree of specificity (Huang et al. 2011). Due to the multiple cloning steps required to assemble the TALEN arrays, the main effort was addressed to gain efficient processes in a shorter time. The most successful assembly methods are the Golden Gate, suitable for most zebrafish laboratories (Bedell et al. 2012), and the FLASH (Fast Ligation based Automatable Solid phase High throughput), suitable for laboratories aiming to perform large-scale targeted mutagenesis experiments (Cade et al. 2012). To date, only 20 different genes were successfully targeted with TALENs in zebrafish. Moreover, it was demonstrated that TALENs induce hotspots for homology recombination induction and that TALEN pairs targeting two sites can induce large genomic deletions (Gupta et al. 2013).

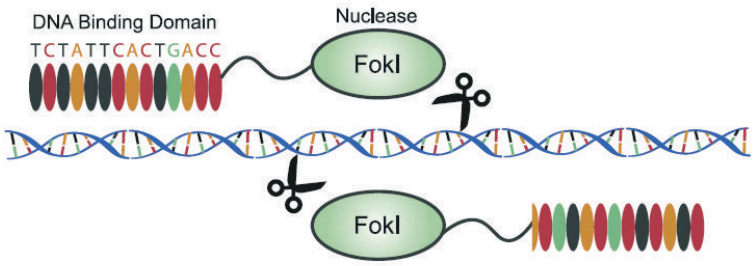

Figure 12 - Schematic representation of the assembly of Transcription Activator-Like Effector Nucleases at the genomic target site. Each monomer binds to opposite DNA strands; each motif of the DNA binding domains (fourteen for each TALEN, in the figure) recognize a single nucleotide. Two monomers of the FokI nuclease are brought in close proximity, so that they can be active and produce a double strand break on the DNA. (From Varshney, Sood et al. 2015).

1.2.5.4 Cluster of Regularly Interspaced Short Palindromic Repeats (CRISPR)/CRISPR-associated protein (Cas9)

The breakthrough in genome editing techniques came in 2013 with Cluster of Regularly Interspaced Short Palindromic Repeats (CRISPR)/CRISPR-associated protein (Cas9) (Hwang et al. 2013; Chang et al. 2013). CRISPR/Cas9 system is inspired by the adaptive immune system in archaea and bacteria; the most popular is the system derived from *S. piogenes* (Jinek et al. 2012). Cas9 is the effector RNA-guided endonuclease. It requires two RNAs, the programmable target specific CRISPR RNA (crRNA) and the transactivating RNA (tracrRNA). crRNA contains a 20 bp sequence complementary to the target, with the only requirements to have an protospacer adjacent motif (PAM), namely an invariable sequence, that in case of *S. piogenes*

Cas9 is NGG (less frequently, NAG) (Hsu et al. 2013). Once the crRNA binds the target sequence, it recruits the tracrRNA, which is necessary for the correct positioning and activation of Cas9.

To further simplify and strengthen the system, crRNA and tracrRNA binary system was replaced by a chimeric single-guide RNA (sgRNA) sequence, that is possible to synthetize using a 'cloning-free' assembly method (Gagnon et al. 2014; Varshney, Pei et al. 2015) (Figure 13). Moreover, a zebrafish codon optimized version of Cas9 (zCas9) was generated (Liu et al. 2014). Several tools were developed to predict target efficiency in inducing mutations and in transmission to the next generation, but no prediction turned out to be statistically significant (Moreno-Mateos et al. 2015). In parallel, mutated Cas9s able to recognize PAM sites other than NGG (or NAG) were developed to increase the targetable loci in zebrafish genome (Kleinstiver et al. 2015).

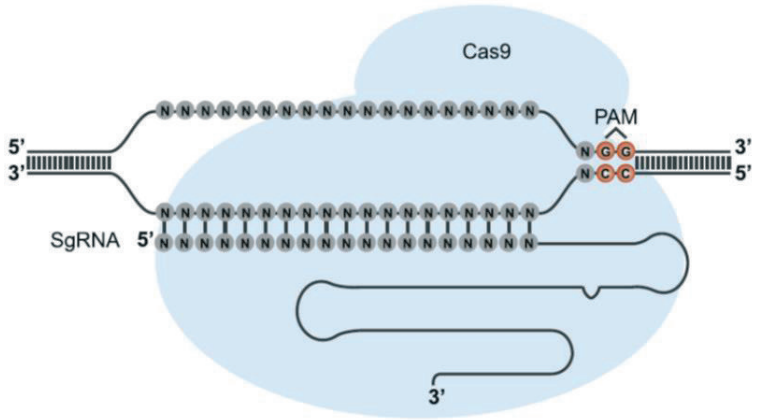

Figure 13 - Schematic representation of the assembly of Cluster of Regularly Interspaced Short Palindromic Repeats (CRISPR)/CRISPR-associated protein (Cas9) at the genomic target site. The target specific CRISPR RNA (crRNA), containing the 20bp target sequence upstream of the S. piogenes protospacer adjacent motif, 5'-NGG-3', and the transactivating RNA (tracrRNA) here are replaced by the chimeric single-guide RNA (sgRNA) sequence. The binding of the sgRNA to the target genome locus recruits and activates the Cas9 effector nuclease to produce a double strand break. (From Varshney, Sood et al. 2015).

Jao et al. demonstrated that it is possible to target multiple genes simultaneously (up to 10 with only a modest loss in efficiency) and this is especially convenient in presence of functional duplicates in zebrafish genome (Jao et al. 2013); this is called multiplexing mutagenesis. Heat-shock inducible and tissue-specific expression of Cas9, associated with GFP expression as transgenesis marker, allow now both temporal and spatial expression of the system, to obtain conditional knockouts (Yin et al. 2015; Ablain et al. 2015).

Even though CRISPR/Cas9 improved mutagenesis effectiveness, it also raised concerns related to specificity and off-target effects. Several studies addressed this point and they concluded that a low, but measurable rate of off-targets occurs (Varshney, Pei et al. 2015). However, given off-target mutations can easily be outcrossed away from the desired mutation in zebrafish, several strategies to lower or avoid off-targets were developed. These include: the generation of a mutant version of the Cas9, called “nickase”, that cleaves only one strand and need to work as a dimer to be effective (Ran et al. 2013); the use of truncated sgRNAs (tru sgRNAs) which are shorter by two or three nucleotides and have also shown to be more target-specific (Fu et al. 2014); the replacement of the catalytical domain of Cas9 with the FokI nuclease domain (Tsai et al. 2014).

1.2.5.5 Potentials of nuclease gene targeting

The principle common to all the strategies for specific gene targeting is the induction of a Double Strand Break (DSB) in the spacer sequence, in the case of ZFNs and TALEN, or in the target sequence, usually 3 bp upstream of the PAM sequence, in the case of CRISPR/Cas9 (Porteus & Carroll 2005). Thus, these nucleases can be imagined as custom restriction enzymes that recognize and cut at specific sequence sites in the genome (Pennisi 2013; Bogdanove & Voytas 2011). The break can be repaired either by Non-Homologous End Joining (NHEJ) or Homology-Directed Repair (HDR) (Symington & Gautier 2011) (Figure 14). NHEJ is preferred but imprecise and it is used to generate traditional gene knock-outs (Burma et al. 2006); the occurring insertion or deletion of one or more nucleotides in the open reading frame can cause a frameshift. HDR precisely repairs the DSB, but it requires a guide DNA template and it is used to create precise modifications in the genome; knock-in of specific sequences, desired transgenes, or dominant negative missense mutations are then available.

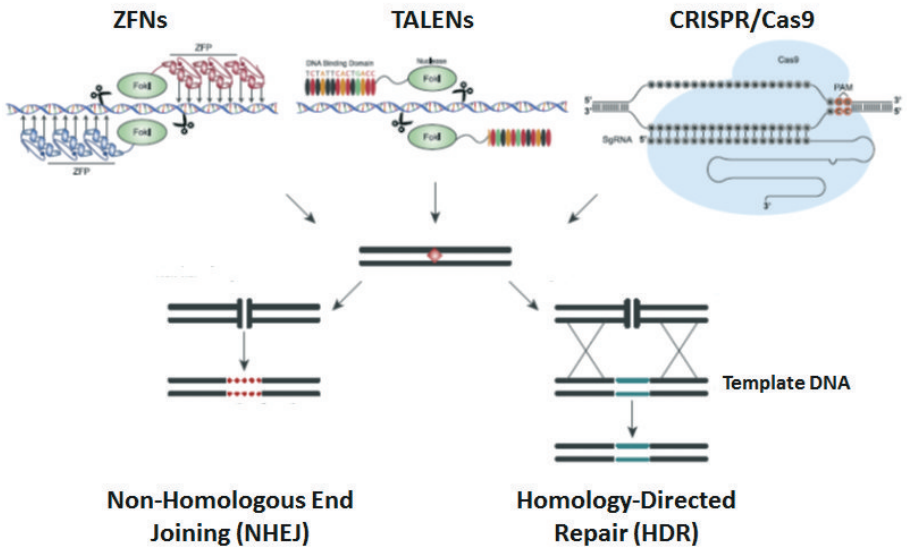

Figure 14 – Double strand break repair mechanisms**.** Independently from the used nuclease, the result is the generation of a double strand break (DSB) at the target site. The DSB can either be repaired by error-prone non-homologous end joining (NHEJ), which often leaves insertions or deletions, or if a donor template DNA is supplied, the DSB can be repaired (hopefully) perfectly by homology directed repair (HDR). (Modified from Varshney, Sood et al. 2015).

1.2.6 Study of metabolic disorders in zebrafish

Although relatively recent, zebrafish proved to be a suitable biomedical model for the study of metabolic disorders. In fact, it helps the comprehension of the biochemical, molecular and genetic basis of cell metabolism, as well as the understanding of the key molecular changes at the onset and during the progression of a disease. Pathologies can be easily studied at the level of the whole animal, but also in single tissues. The most important techniques for metabolism studies are all available in zebrafish: fluorescent reporter lines, transgenesis, imaging approaches, metabolomics, and isotope tracing (Santoro 2014). These findings may provide a solid platform to facilitate the identification of valid drug targets and to test new drug-based human therapies.

Zebrafish possess all the key organs required for metabolic control in human and their development and morphogenesis are accurately described. Appetite circuits that are present in the hypothalamus, the pancreas and the insulin-sensitive tissues are conserved between zebrafish and humans (Tiso et al. 2009; Kinkel & Prince 2009). Thus, models for diseases associated with different types of dyslipidaemia and diabetes can be generated and studied. Fluorescent lipid dies allow the application of imaging methods with subcellular resolution to a whole organism (Anderson et al. 2011).

Despite the several advantages, critical differences between zebrafish and mammals should be considered when studying metabolic phenotypes. For example, zebrafish and humans are exposed to different oxygen partial pressure levels. Zebrafish experience a more variable amount of dissolved oxygen and, to maintain blood oxygenation constant, it is not rare that zebrafish experience hypoxia (low oxygen levels) in some tissues. Thus, zebrafish developed a wider repertoire of strategies to protect the tissues from hypoxic conditions, which may produce ROS damaging nucleic acids, lipid membranes and proteins. For example, in zebrafish, there is a preference for glycolytic oxygen-independent production of ATP, rather than oxygen-dependent β-oxidation of fatty acids (Anastasiou et al. 2011; Malek et al. 2004; Tseng et al. 2011).

Another important difference is the temperature regulation. Zebrafish are ectothermic animals, meaning that the internal temperature control relies only for a small amount, if not at all, on internal physiological sources. Thus, zebrafish exposed to temperature fluctuations switch towards glycolysis, in order to gain high amount of heat in a short time (Shaklee et al. 1977).

Apart from intrinsic differences in the metabolism, other limitations in the use of zebrafish as a potent model to study metabolic disorders are represented by the size of the animals. Furthermore, the current techniques to measure food intake (Anderson et al. 2011) and energy expenditure (Makky et al. 2008) in the zebrafish model are not as sophisticated as those in rodents. Alternative methods to evaluate metabolic rate include acid production (van der Velden et al. 2011). Finally, high genetic diversity is common even in fish of the same strain and it might be appropriate to perform metabolic phenotyping in inbred lines (Guryev et al. 2006).

1.2.7 **Development of therapeutical approaches**

The generation of disease models in zebrafish made available valuable tools for innovative drug discovery strategies. Thus, new targets and metabolically active drugs can be identified and tested in an easily accessible *in vivo* model. This kind of drug screenings are reliable and low-cost during pre-regulatory phases, allowing also high-throughput screening of drug libraries (Ali et al. 2011; Lessman 2011). Zebrafish embryos can be exposed to different chemical compounds or to different concentrations and their development can be monitored with the aim of improving the zebrafish phenotype that mimics a specific human disease. Larvae remain available also after the exposure to the drug, so that further manipulations can be performed. High-throughput screenings identified positive hits for the treatment of a

plethora of diseases like cardiovascular defects, polycystic kidneys, cancer and obesity. Furthermore, zebrafish were used for testing psychotropic, antimicrobial and immunosuppressant drugs, for the identification of bioactive natural products and for toxicology studies (Mandrekar & Thakur 2009; Esch et al. 2012). Some drugs identified with this method are now in early clinical trials in cancer patients, whereas a drug boosting the production of blood stem cells has successfully concluded phase 1 of clinical trials (Callaway 2013).

1.3 Neural crest and its derived tissues

One of the main advantages of zebrafish as model of biomedical interest is the transparency of the embryos and the quick *ex utero* development, providing an important platform for the study of developmental biology. Thus, the dynamics underlying the formation of different cell populations and different tissues could be clarified and tools for the dissection of the cellular events were made available.

1.3.1 Neural crest during embryogenesis

During the embryonic development of all vertebrates, it is possible to identify a multipotent stem cell population, defined as neural crest (NC). It is the defining feature of the vertebrate phylum, indeed. This cell population emerges during neurulation at the neural plate border. Wnt, Fibroblast growth factor (Fgf), retinoic acid and Notch signalling jointly produced by ectoderm and mesoderm cooperate in the induction of this transient tissue (Milet & Monsoro-Burq 2012). The aforementioned signalling pathways activate a series of transcription factors (*Snail/slug, Foxd3, Sox9/10*) that define the NC territory and guide the next development steps (McKeown et al. 2013). Later, NC extensively migrates to colonize the peripheral tissues. When cells delaminate from the NC, they undergo an Epithelium-to-Mesenchyme Transition (EMT). During the migration, cell cooperation and cell guidance drive them to the final target tissues. It is currently not clear whether NC cells are predetermined or differentiate as a result of the signals that they encounter in their environment during migration (McKinney et al. 2013). Most likely, NC is composed of a heterogeneous cell population with different degrees of multipotency and plasticity.

During migration, NC cells maintain transient cell-cell contacts by expression of adhesion molecules. During this process, it is possible to assist to contact-inhibition of locomotion (CIL), a complex process during which migratory cells momentarily stop upon physical contact with

one another and subsequently repolarise in the opposite direction (Mayor & Carmona-Fontaine 2010). Nevertheless, NC cells migrate in large groups and they release chemoattractant molecules, establishing local gradients (Carmona-Fontaine et al. 2011). This chemotactic phenomenon allows collective NC cells migration in spite of low cell-cell adhesion. Negative and positive cues (fibronectin, laminins and collagens) subdivide the NC cells into different streams and establish their precise targeting to specific tissues (Sasselli et al. 2012).

Different cell populations derive from the neural crest and their identity depends on the positioning of the progenitor cells along the body axis of the embryo. Cephalic NC cells (CNC, spanning from the diencephalon to the third somite) mainly contribute to the craniofacial structures producing bones and cartilages of the face, teeth, blood vessels, eye and muscles and connective tissues of the ear, pigment cells, peripheral nervous system (Dupin et al. 2006; Le Douarin et al. 2012; Theveneau & Mayor 2011). Cardiac NC cells migrate to the heart and they are essential for septation. Trunk NC cells (TNC, spanning posteriorly the fourth somite) form pigments cells, the dorsal root and sympathetic ganglia of the peripheral nervous system, and endocrine cells of the adrenal gland; a subpopulation form the enteric peripheral nervous system, controlling the digestive track (Theveneau & Mayor 2011) (Figure 15).

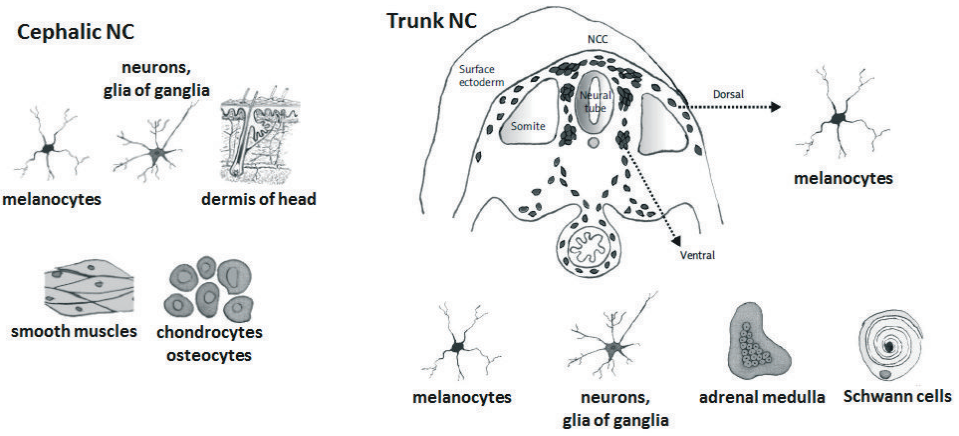

Figure 15 - Derivatives of the cephalic and the trunk neural crest cells (NC) and the basic pathways of the trunk NC cells migration during early embryonic time. Dorsally migrating trunk NC cells move between the surface ectoderm and somites, developing into melanocytes of the epidermis and hair. Ventrally migrating trunk NC cells move between the neural tube and somites, giving elements of the peripheral nervous system, medulla of the adrenal and melanocytes of the skin. (Modified from Cichorek et al. 2013).

1.3.2 **Pigment cell populations**

One of the main features of the zebrafish, *Danio rerio*, is the stereotyped pattern of four to five dark (blue) and four light (yellow) stripes along its body axis. This characteristic is the reason for its common name, zebrafish.

As mentioned, both the cranial and the trunk NC give rise to the pigment cells. While the cranial pigment population migrates directly to the target tissue, the pigment cells originating from the trunk NC follow a stereotyped path. They migrate dorso-laterally and the migration is controlled by endothelin and Eph/ephrin signalling, while the final targeting is controlled by Sdf1 (Belmadani et al. 2009).

Notably, there are some important differences between the pigmentation patterning establishment between mammals and fish. Mammals have only one pigment cell population, the melanocyte, and the final pigmentation pattern is determined by the ratio of two polymers, the eumelanin (brown to black) and the pheomelanin (yellow to red). Moreover, pigments produced in the melanocytes are then released and transferred to other dermis cell populations, like the keratinocytes (Wang et al. 2016).

In fish (but also in amphibians and reptiles), up to seven different pigment cell populations are represented. In zebrafish three pigment cell populations are the most common: xanthophores, containing pteridine and carotenoid-based yellow to red pigments; melanophores, containing melanin-based pigments; iridosomes, containing light-reflecting stacks of uniformly spaced membrane-bound guanine platelets (Bagnara & Taylor 1970; Bagnara et al. 2007). Other cell types are erytrophores, leucophores, cyanophores and erythro-iridophores. Each pigment-producing cell has a distinct shape (dendritic for the melanophores; compact roundish in the light stripes or stellate in the top layer of the dark stripes for xanthophores; oval or polygonal, more or less packed, for iridophores) and stores the pigments in specialized vesicular organelles, without transfer from these cells to others. The final pigmentation pattern is determined by the distribution and ratio of different pigment cells in several layers in the dermis. In particular, xanthophores cover the outermost layer, absorbing short-wave light; iridophores in the middle layer reflect the light while melanophores in the basal layer absorb the remaining light (Hirata et al. 2003; Bagnara et al. 1968).

1.3.3 **Pigmentation pattern formation in zebrafish**

In zebrafish, the pigmentation pattern is established according a periodicity along the dorso-ventral axis and develops following morphological landmarks (Svetic et al. 2007; McClure

1999). The larval and adult pigment patterns in zebrafish are regulated through different mechanisms.

During embryonic development, xanthophores uniformly cover the hypodermis of the flank. Melanophores migrate along the route determined by the peripheral neurons innervating the skin, first dorsally and anteriorly over the head (Knight et al. 2003), and later in the trunk, to form four distinct stripes (Kimmel et al. 1995; Milos et al. 1983):

1 - A dorsal stripe extending from two converging V-shaped stripes on the head region extending to the tail along the dorsal apex of the myotomes;

2 – A lateral stripe at the level of the horizontal myoseptum;

3 – A ventral band, extending from the head region between the eyes, over the dorsal yolk sac and to the top of the tail;

4 – A ventral band over the ventral surface of the yolk sac (Figure 16).

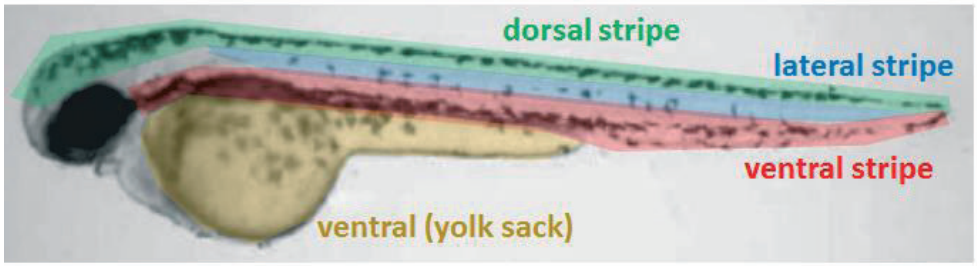

Figure 16 – Embryonic pigmentation pattern formation in zebrafish. The four embryonic melanophore stripes are highlighted with different colours: dorsal stripe in green, lateral stripe in blue, ventral stripe in red and melanophores of the yolk sack in yellow.

During this process, also other melanophores precursors, called melanoblasts, are generated and they localize in proximity of the dorsal root ganglia. These cells remain in a stem-like state, until they are reactivated, proliferate and migrate to the periphery, following the path determined by axons of peripheral motor neurons, to replace deteriorated melanophores. Melanophore progenitors enter the skin as melanoblasts predominantly over the dorsal and ventral myotomes and along the horizontal myoseptum (Dooley, Mongera, Walderich & Nusslein-Volhard 2013a; Budi et al. 2011).

The pattern generated during embryonic development persists during the whole larval stage. Afterwards, zebrafish larvae enter a metamorphosis stage, in which the four melanophore stripes evolve to the striped pigment pattern of the adult (Singh et al. 2014; Parichy et al. 2000). At the beginning of this process (18 dpf – 21 dpf) iridophores appear in the skin through the horizontal myoseptum, which serves as a morphological landmark that orients the stripe

pattern. This leads to the formation of a contiguous stripe of dense cells, constituting the first light stripe. Melanoblasts from the dorsal root ganglia migrate along the characteristic pathways and, after reaching the periphery, they stop to proliferate and start to melanise (Figure 17).

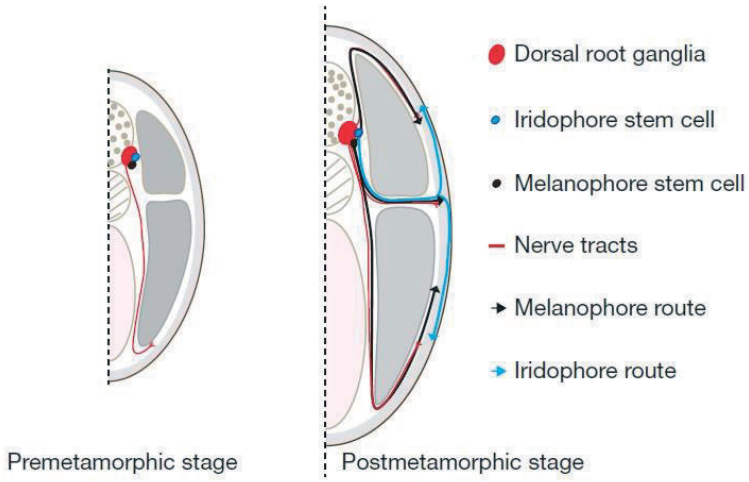

Figure 17 – Schematic showing the different origins and migration routes of melanophores and iridophores, both during the premetamorphic stage (larval development) and postmetamorphic stage. Melanophore progenitors migrate along the peripheral neurons innervating the skin, whereas iridophores migrate through the horizontal myoseptum and disperse dorsoventrally. (Modified from Singh et al. 2014).

Pigmented melanophores tend to align dorsally and ventrally the first iridophore light stripe, forming two “primary” dark stripes. Afterwards, they rarely divide and do not show extensive movements (Singh et al. 2014). In contrast to melanophores, iridophores keep on proliferating. Repulsion and clustering cues lead to the appearance of loose iridophores, which spread both dorsally and ventrally, to establish all the other iridophore light stripes at a given distance from the existing ones. Over the course of weeks, melanophores migrate from the dorsal root ganglia to the spaces between the light stripes, forming additional “secondary” dark stripes, for a total amount of 4-5 dark stripes detectable in adult zebrafish. Since melanophores do not proliferate in the dermis, they dramatically expand in size to completely fill the space between the light stripes (Hawkes 1974) (Figure 18). During this process, larval xanthophores persist and begin to proliferate and cover the entire dorsolateral skin, at the onset of metamorphosis. When covering iridophores, xanthophores acquire a flat shape with small cytoplasmic protrusion; in contrast, upon encountering melanophores, xanthophores acquire a dendritic shape, with long cytoplasmic protrusion and they show faint pigmentation (Mahalwar et al. 2014).

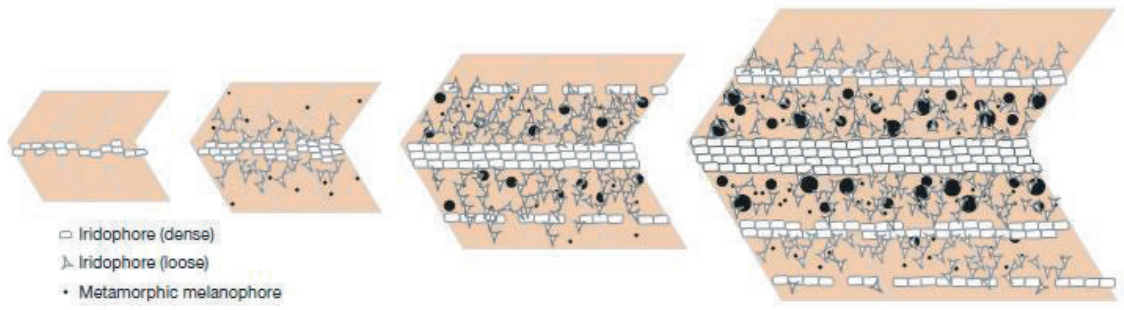

Figure 18 – Scheme showing the major developmental events leading to stripe pattern formation during metamorphosis. At the beginning, iridophores densely cluster along the anteroposterior axis, along the horizontal myoseptum, forming the first interstripe. Loose iridophores along the borders of the first interstripe start to disperse, while the first melanophores appear in the presumptive stripe region. Migrating loose iridophores aggregate into dense clusters and organize new interstripes at a given distance from the existing one, while melanophores grow in size. The repetition of these processes leads to the formation of an alternating pattern of stripes and interstripes. (Modified from Singh et al. 2014).

1.3.4 **Melanocytes**

The primary function of melanocytes is the production of the melanin pigment. Melanin is capable to absorb ultraviolet (UV) and visible light, protecting cell components, especially DNA, from radiation damage. Melanophores are able to proliferate and they adjust their pigmentation intensity and distribution in response to neural and hormonal cues. Melanosomes, the vesicular organelles synthetizing and containing melanin, can move along microtubules generating lighter shades when concentrated around the nucleus of the cell, or darker shades by dispersing in the cytoplasm (Logan et al. 2006). Many developmental markers for this lineage were identified, in particular enzymes for melanin synthesis. Melanocyte specific markers are dopachrome tautomerase (Dct, also known as tyrosinase related protein-2, Tyrp2), tyrosinase-related protein-1 (Tyrp1), tyrosinase (Tyr), premelanosomal protein 17 (Pmel17) and melanoma antigen recognized by T cells 1 (MART1).

1.3.4.1 **Melanocyte lineage establishment**

Melanophore differentiation from the NC is driven by transcriptional regulation of essential genes. Sox10 is required for proper development of all neural-crest derived tissues, including all three types of chromatophores in zebrafish (Dutton et al. 2001). The main transcription factor for this cell population is Microphthalmia associated Transcription Factor (Mitf) and its mutation influences normal specification and survival, with the result of reduced melanocyte number (Goding 2000; Hodgkinson et al. 1993). In zebrafish, two mammalian mitf homologs were identified, mitfa and mitfb, and they together recapitulate expression and function of the

single mammalian Mitf gene. Nevertheless, mitfb is not expressed in melanophores or their precursors, even if ectopic expression can rescue melanophore development in *mitfa* mutants. These findings suggest for a subfunctionalization of an ancestral locus occurred after gene duplication (Lister et al. 2001). Transcription of mitfa is regulated by extracellular factors, in particular the wnt signalling pathway, which stabilizes β-catenin and allows its translocation into the nucleus to interact with tcf/lef transcription factors (Dorsky et al. 2000). Moreover, mitfa expression is upregulated by sox10 and pax3, but repressed by foxd3, which binds the forkhead sites in the promoter region of mitfa (Ignatius et al. 2008). Kit signalling is required for establishment and survival of embryonic and early metamorphic melanophore progenitors. Kit also promotes melanoblast motility, independent of other morphogenetic effects, and in case of its mutation, melanophores are found principally near their sites of origin (Wehrle-Haller et al. 2001; Parichy et al. 1999; Dooley, Mongera, Walderich & Nusslein-Volhard 2013b). Mitf (especially mitfa, in zebrafish), can bind the promoter region of different genes involved in melanin synthesis, like Tyr, Tyrp1 and Dct (Bertolotto et al. 1998). These enzymes are synthetized on ribosomes of the rough ER and they are transported through the Golgi complex, where they undergo glycosylation, a process essential for their structure and function (Beermann et al. 1995).

1.3.5 **Melanosomes**

Melanosomes are organelle typical of melanin producing cells (melanophores or melanocytes). They are surrounded by a unique membrane, they can reach the size of 500 nm and it is the place where the melanin is synthetized and stored. They are used to eventually transport melanin in different regions of the cell (e.g. around the nucleus) or to neighbouring cells (e.g. melanosome to keratinocyte transfer in mammalian cells - Wu & Hammer 2014). Since melanosomes are the bioreactor where melanin synthesis take place, enzymes involved in its biosynthesis are included in this organelle.

1.3.5.1 Melanosome biogenesis

The origin of this organelle is still matter of debate, since different studies highlighted the presence of features that track back melanosomes either to lysosomes or to the endoplasmic reticulum. In fact, melanosomes contain enzymes and other proteins that are also present in lysosomes, like Lysosomal-Associated Membrane Proteins (LAMPs), participating in autophagy and regulation of intravesicular pH (Eskelinen 2006), or acid phosphatase (Hunziker & Geuze

1996). Some LAMPs are found exclusively in melanosomes and this lead to the formulation of the hypothesis that melanosomes belong to a separate lineage (Raposo et al. 2001); thus the endoplasmic reticulum is named as possible alternative origin of this organelle (Park et al. 2009). Most likely, pre-melanosomal vesicles derive both from multivesicular early endosome/lysosome structures and from the ER.

Melanosomes show a progressive maturation and four different stages are described. After the budding of the pre-melanosomal vesicles, it is possible to identify stage I melanosomes as round, small vesicles. They are characterized by an amorphous matrix and internal membrane invagination. Pmel17 is already present at this point (Kushimoto et al. 2001) and later it starts to organize in a fibrillary matrix. This one, along with the presence of tyrosinase, is a marker of stage II melanosomes. During stage III the synthesis of melanin starts and it is deposited on the fibrillary matrix; stage IV represents fully melanised compartments, in which the internal matrix is not recognizable anymore and tyrosinase activity decreases (Hearing 2005; Marles et al. 2003) (Figure 19).

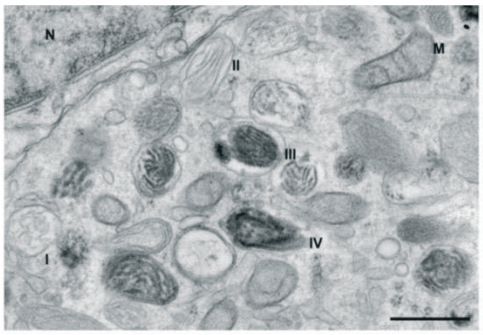

Melanosom features	Stage I	Stage II	Stage III	Stage IV
Shape	Spherical	Elongated	Elliptical, ellipsoidal	Elliptical, ellipsoidal
Internal structure	–	Matrix fibrils are visible	Matrix fibrils are visible	Matrix fibrils are covered by polymerized melanin
TYR	–	+	+	+
TYRP1	–	+	+	+
TYRP2	–	+	+	+
Melanin synthesis	–	–	Begins, settle on internal fibrils	Filled by melanin
Color			Brown	Dark brown to black

Figure 19 - Ultrastructural characterization of melanosomes. Electron microscopy analyses of MNT-1 human melanoma cells. The four stages of melanosome development (I-IV) are clearly distinguishable. M=mitochondria; N=nucleus. Scale bar: 0,5 µm. (Modified from Raposo & Marks 2007). Table describing the characteristics of the developmental stages of melanosomes during melanin synthesis. (Modified from Cichorek et al. 2013).

Functional melanosomes are required to modulate proliferation, differentiation and migration of melanophore cells (Wasmeier et al. 2008; Hirobe 2011; Hirobe & Terunuma 2012). They have an impact on Mitf transcription factor activity, modulating the transcription of genes influencing melanocyte survival (cyclin-dependent kinase 2 - Cdk2, p16INK4a, T-box transcription factor 2 - Tbx2 and p21 - CDKN1A), motility (Met), differentiation and apoptosis (Bcl2 and hypoxia-inducible factor 1a - Hif1a) (Chiaverini et al. 2008; Levy et al. 2006).

1.3.5.2 Melanin biosynthesis

Melanin synthesis in the melanocyte is a tightly regulated process. The main trigger initiating melanin synthesis is the activation of the melanocortin 1 receptor (MC1R) by its ligand, the α-melanocyte stimulating hormone (AMSH). AMSH is an endogenous peptide hormone generated by proteolytic cleavage of proopiomelanocortin (POMC), produced in the pituitary gland. Indeed, MC1R regulates also the balance of the production of two different forms of melanin, the eumelanin and the pheomelanin (Garcia-Borron et al. 2014). MC1R activation stimulates cAMP signalling pathway and the activation of Mitf. This transcription factor activates tyrosinase transcription stimulation as well as by posttranscriptional regulation mechanisms. MC1R is also required for the cAMP-dependent increase of the melanosomal pH (initially acidic) to near-neutral values, to enhance tyrosinase catalytic efficiency (Cheli et al. 2009)(Figure 20). In fact, on the membrane of the melanosomes V-ATPase, a proton pump, and several transporters of the solute carrier (*slc*) family were identified and proven to be essential for the pH regulation (Dooley, Schwarz et al. 2013; Basrur et al. 2003b).

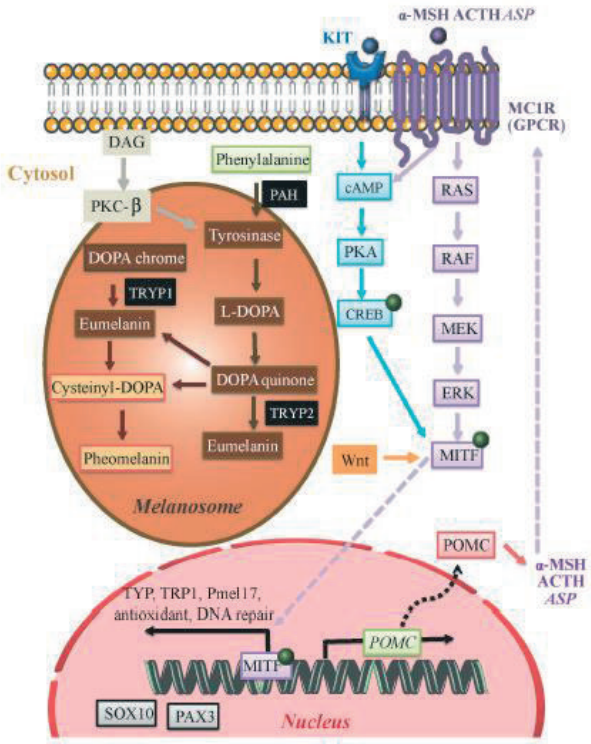

Figure 20 – Melanin biosynthesis is initiated by the activation of the melanocortin 1 receptor (MC1R) operated by α-melanocyte stimulating hormone (AMSH). Other alternative pathways can also influence melanocyte activation. The final event is the activation of Mitf transcription factor, which is responsible for the biosynthesis of those enzymes, catalysing melanin synthesis. Mitf transcription factor drives the expression of several genes including Sox10 and Pax3. (From D'Mello et al. 2016).

At the beginning of melanin synthesis, there is the tyrosinase-mediated oxidation of L-tyrosine to dopaquinone. This molecule undergoes a cascade of redox reaction giving at the end dopachrome and DiOxyPhenylAlanine (DOPA). Here the biosynthetic pathways producing either eumelanin or pheomelanin diverge: in the first case, dopachrome tautomerase catalyses the conversion of DOPA to 5,6-DiHydroxyIndole (DHI) and 5,6-DiHydroxyIndole-2-Carboxilic Acid (DHICA) which are oxidized and polymerize in eumelanin (Edge et al. 2006); in the second case, DOPA form adducts with sulfhydryl compounds (such as cysteine) which are oxidized and converted into pheomelanin (Ito & Prota 1977) (Figure 21). These reactions produce considerable amounts of highly reactive O-quinones, that may regulate sulfhydryl enzymes activity. The concentration of cysteine inside the melanosome may be the cue regulating the balance between eumelanin and pheomelanin (Land, E. J. et al. 2003).

Melanin is used to absorb light and to trap free radicals generated by radiations. Melanosomes can be transported to different regions of the cell along microtubules, facilitated by both dynein and kinesin motors (Seabra & Coudrier 2004).

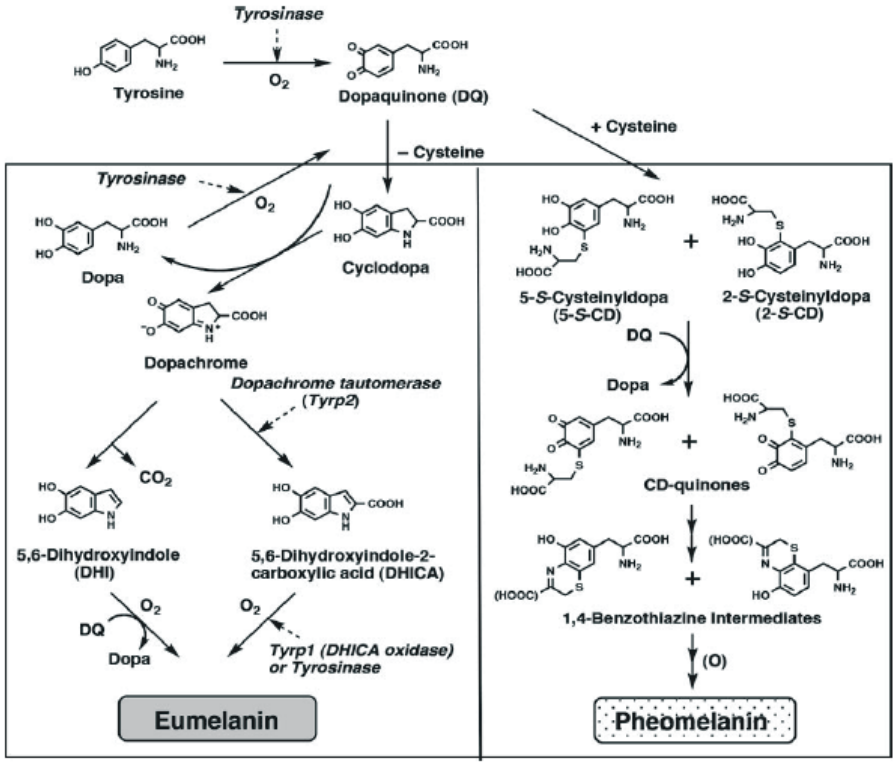

Figure 21 – Eumelanin and pheomelanin biosynthetic pathways. Tyrosinase, TYRP1, and TYRP2 are involved in the production of eumelanin, while only tyrosinase (and the amino acid cysteine) is necessary to produce pheomelanin. (From d'Ischia et al. 2015).

2 Aim of this thesis

Peroxisomal Biogenesis Disorders (PBDs) are a class of pathologies, affecting 1 every 5000 new-borns in the world population. The disease is caused by a heterogeneous group of autosomal recessive mutations affecting the peroxin genes, controlling the assembly and the maintenance of functional peroxisomes. Patients usually do not survive the first year of age due to the disrupted peroxisomal metabolism, leading to the accumulation of substrate and the lack of product molecules of enzymes localized in peroxisomes. As a consequence, patients suffer of brain disorders, progressive cognitive impairment, craniofacial dysmorphism and liver failure (Bootsma et al. 1999; Dacremont & Vincent 1995). Currently, no treatment for PBDs is available, except dietary palliative supplementation (Klouwer et al. 2015).

Previous efforts aimed to the generation of animal models impaired for peroxin controlling the dynamics of peroxisomal matrix proteins, reproducing the spectrum of PBDs (Baes & van Veldhoven 2006). Nevertheless, a vertebrate model deficient for one of the early peroxins (pex3, pex16 and pex19) still does not exist. Invertebrate models deficient for early peroxins did not help in filling the gap of knowledge in understanding the consequences of a total lack of peroxisome generation and maintenance (Petriv et al. 2002; Thieringer 2003; Nakayama et al. 2011; Faust et al. 2014).

The aim of this thesis is therefore to generate a zebrafish model for Peroxisomal Biogenesis Disorders, targeting the unique identified homolog of human *PEX3*. Preliminary experiments show that *pex3* expression in zebrafish recapitulate mammalian one. The generated model is characterized during organogenesis and development using genetic, cell biological, biochemical and immunohistochemical tools, taking advantage of zebrafish exclusive features (*ex utero* embryonic development, transparency throughout embryogenesis, large number of progenies).

3 Materials and Methods

3.1 Materials

3.1.1 Common materials

If not mentioned otherwise, all chemicals used were ordered from one of the following companies: Bio-Rad, Eppendorf, IDT, Invitrogen, Roche, Macheray-Nagel, Manzel-Gläser, Merck, Promega, Roth, Sigma-Aldrich, Stratagene or VWR.

3.1.2 Equipment

Name	Company
Artemia hatching cylinder	Tecniplast
Autoclaves	H+P Varioklav steam sterilizer EP-2 H+P Varioklav steam sterilizer Typ25 T
Bacterial incubator	Memmert 400
Binoculars	Olympus SZX16 with DP21-SAL CCD camera Olympus SZ40
Capillaries	WPI
Centrifuges	Eppendorf Centrifuge 5415R; Beckman Coulter Allegra X-15R; Beckman Coulter Avanti J-26 XP
Confocal microscope	Zeiss LSM 710
Fish Incubators	MIR-162 Sanyo Rumed E400
Fluorescence binocular	Olympus ZSX16
Gel documentation	Biozym, Alpha DigiDoc
Gel electrophoresis systems	Bio-Rad
Light microscope	Olympus AX70
Microinjector	Eppendorf FemtoJet
Micromanipulator	Narishige M-152
Micropipette puller	Flaming/Brown P97 Sutter Instrument Co.
Microwave	Panasonic NN-E235M
Multi-Linking WTU	Tecniplast
Multiplate reader	Tecan Infinite® 200 PRO
PCR cycler	Bio-Rad C1000™ Thermal Cycler Bio-Rad S1000™ Thermal Cycler
pH-meter	Mettler Toledo FiveEasy FE20
Power supply	Bio-Rad Power Pac 3000
Realtime PCR cycler	Bio-Rad C1000™ Thermal Cycler

	with CFX96™ Optical Reaction Module
Rocking platform shaker	Heidolph DuoMax 1030
Rotator	Snijders test tube rotator
Rotors	Beckman Coulter JA-10; Beckman coulter 70Ti; SW55Ti
Scales	Sartorius BL 1500 S Sartorius B 211 D
Slide Micrometer	ProSciTech Pty Ltd
Spectrophotometer	NanoDrop Peqlab Biotechnology GmbH, ThermoFisher Scientific
Thermo mixers	Eppendorf Thermo mixer comfort Thermo Mixer MHR13 HCL
Ultracentrifuge	Beckman Coulter Optima LE-80 K UZ
Ultracentrifuge tubes	Beckman Coulter g-max Kit, Quick-Seal®, Polypropylene, 13 x 25 mm
Vortexer	Vortex Genie2
Water Bath	Memmert VNB
ZebTec standalone	Tecniplast

3.1.3 Standards, Kits and Enzymes

Name	Company
2-log DNA ladder mix	NEB
4x Laemmli Sample Buffer	Bio-Rad
Ampicillin	Roth
Amplex® Red Hydrogen Peroxide/Peroxidase Assay Kit	Invitrogen
DIG RNA labelling Kit (SP6/T7)	Roche
DNA loading dye	NEB
DNaseI	Roche
GoTaq polymerase	Promega
Griess reagent Kit	ThermoFisher Scientific
iQ™ SYBR® Green Supermix 2x	Bio-Rad
Kanamycin	Roth
Lysozyme	Roth
NucleoSpin extract II Kit	Macherey-Nagel
NucleoSpin Plasmid AX-100 Kit	Macherey-Nagel
PCR Nucleotide mix	Roche
Penicillin-Streptomycin (10.000U/ml)	Invitrogen
Phenol Red	Sigma-Aldrich

Phusion High-Fidelity DNA polymerase	NEB
Pierce™ ECL Western Blotting Substrate	ThermoFisher Scientific
Precision Melt Supermix	Bio-Rad
Precision Plus Protein™ Unstained Standard	Bio-Rad
Proteinase K	Roth
PureLink® RNA Mini Kit	Ambion
QuantiTect reverse cDNA transcription Kit	Qiagen
Restriction endonucleases and buffers	NEB
RNA later®	ThermoFisher Scientific
RNAse A	Sigma-Aldrich
SP6 mMessage mMachine Kit	Ambion
SuperScript II Reverse Transcriptase Kit	Invitrogen
SybrSafe DNA gel stain	Invitrogen
T4 DNA ligase and buffer	NEB
T7 mMessage mMachine Kit	Ambion
TOPO TA cloning Kit	Invitrogen
TRIzol RNA isolation reagent	ThermoFisher Scientific
Tween-20	Sigma-Aldrich

3.1.4 Buffers and solutions

If not mentioned otherwise, all buffers and solutions are prepared using bidistilled autoclaved water. If a solution was prepared as stock solution, the dilution factor is mentioned. All buffers and solutions are stored at room temperature; if that is not the case, the storing temperature is mentioned.

Solution	Composition
100x Bafilomycin A1	10 µM Bafilomycin A1 in DMSO (-20°C)
10x SDS-running buffer	250 mM Tris-HCl pH 8,3, 1,9 M glycine, 1% SDS
10x TBST	200 mM Tris-HCl pH 7,5, 1,5 M NaCl, 1% Tween-20
10x Transfer buffer	250 mM Tris-HCl pH 8,3, 1,9M glycine
20x PBS	2.6 M NaCl, 140 mM Na_2HPO_4, 60 mM NaH_2PO_4; pH 7,4
20x SSC	175,3 g NaCl, 88,2 g citric acid trisodium; pH 7,0
250x Bezafibrate	5 mM 2-[4-[2-(4-Chlorobenzamido)ethyl]phenoxy]-2-methylpropanoic acid in 2% DMSO (4°C)
2x Coenzyme Q_2 (CoQ_2)	20 µg/ml Coenzyme Q_2 in 0,2 ml isopropanol and 0,8 ml sterile water (-20°C)

4-Amino-5-methylamino-2',7'-difluorofluorescein diacetate (DAF-FM diacetate) staining solution	5 µM 4-Amino-5-methylamino-2',7'-difluorofluorescein diacetate in embryo medium (4°C, protect from light)
50x Phenylthiourea (PTU) stock solution	0,15% w/v phenylthiourea in fish water
5-bromo-4-chloro-3-indolylphosphate (BCIP) stock	50 mg/ml in DMF (-20°C)
Alcian Blue staining solution	1% v/v concentrated HCl, 70% v/v ethanol, 0.1% w/v alcian blue in water (protect from light)
Alkaline Tris buffer	100 mM Tris-HCl, pH 9,5, 50 mM $MgCl_2$, 100 mM NaCl and 0,1% Tween-20 (4°C)
Ampicillin stock solution	50 µg/ml (-20°C)
Bleaching solution	0,4 ml 10% KOH, 0,15 ml 30% H_2O_2, 5 ml sterile water (prepare fresh)
Blocking buffer	2% v/v sheep serum, 2 mg/ml BSA in 1x PBT
Danieau's medium	17 mM NaCl, 2 mM KCl, 0,12 mM $MgSO_4$, 1,8 mM $Ca(NO_3)_2$, 1,5 mM HEPES pH 7,6
E3 Embryo medium	5 mM NaCl, 0,17 mM KCl, 0,33 mM $CaCl_2$, 0,33 mM $MgSO_4$
EDTA	0,5 M EDTA (pH 8,0)
Fixative solution	4% w/v formaldehyde (ultrapure, methanol free) in 1x PBS (4°C)
Hank's Stock Solution #1	80 g/l NaCl, 4 g/l KCl
Hank's Stock Solution #2	3,58 g/l Na_2HPO_4 anhydrous, 6 g/l KH_2PO_4
Hank's Stock Solution #4	14,4 g/l $CaCl_2$
Hank's Stock Solution #5	24,6 g/l $MgSO_4$
Hank's Stock Solution #6	35 g/l $NaHCO_3$ (-20°C)
Hybridization Mix	50% deionized formamide, 5x SSC, 0,1% Tween-20, 50 µg/µl heparin, 500 µg/ml RNAse-free tRNA; pH 6,0 (4°C)
Injection buffer	0,1 M KCl, 0,0625% Phenol red in 1X PBS
Instant Ocean stock	150 g of Instant Ocean salt mix in 1 l aqua bidest
Labelling solution	225 µl NBT stock solution and 175 µl BCIP stock solution in 50 ml alkaline Tris buffer + 2% PolyVinyl Alcohol (PVA)
Lysis buffer	25 mM NaOH, 0.2 mM EDTA; pH 12.0
Melanin extraction buffer	50 mM Tris-HCl pH 7,0, 0,5% SDS, 2 mg/ml pronase in 1x PBT
NCS-PBST	10% v/v sheep serum, 1% DMSO in 1x PBT
Neutralization buffer	40 mM Tris-HCl; pH 5.0
Nitro blue tetrazolium (NBT) stock	50 mg in 0,7 ml DMF and 0,3 ml sterile water (-

	20°C)
PBT	0,1% Tween-20 in 1x PBS
RIPA buffer	25 mM Tris-HCl pH 7,6, 150 mM NaCl, 1% v/v NP-40, 1% w/v sodium deoxycholate, 0.1% w/v SDS
Stop solution	1 mM EDTA, 0,1% Tween-20 in 1x PBS
Sucrose gradient stock	2 M sucrose in 20 mM HEPES (-20°C)
TAE	40 mM Tris acetate (pH 8,0), 20 mM acetic acid, 1 mM EDTA
TELT	50 mM Tris (pH 7,5), 62,5 mM EDTA, 2,5 M LiCl, 0,4% Tween-20 (-20°C)
Tricaine	400 mg tricaine in 100 ml fish water, pH 7,0 (4°C)
X-Gal	2% w/v 5-bromo-4-chloro-3-indolil-β-D-galactopyranoside stock solution in DMF (-20°C)

3.1.5 Fish lines

Name	Genotype	Source
AB	wildtype	Hammerschmidt lab (Köln) https://zfin.org/action/genotype/view/ZDB-GENO-960809-7
pex3^{CRIPSR}	pex3(231_232del)	This work
pex3^{sa11684}	pex3(1157+1G>A)	Zebrafish Mutation Project
pex3$^{TALEN10L+10R}$	pex3(13_20del)	This work
pex3^{ZMP} (or pex3^{sa17571})	pex3(106A>T)	Zebrafish Mutation Project
Tg[foxd3:GFP]	Tg[foxd3:GFP]	(Gilmour et al. 2002)
Tg[kita:mCherry]	Tg[kita:Gal4; UAS:mCherry]	(Distel et al. 2009)
Tg[mitfa:GFP]	Tg[mitfa:GFP]	(Curran et al. 2009)
Tg[sox10:mRFP]	Tg[sox10:mRFP]	(Mongera et al. 2013)

3.1.6 Standard fish food

23g of dried Great Salt Lake artemia cysts (brine shrimps) are soaked in 250 ml aqua bidest for 15 minutes at room temperature; afterwards, they are incubated in an artemia hatching cylinder in 4 l aqua bidest and 1,5 l Instant Ocean stock solution at 28°C for 24 hours, under gentle air reshuffling and constant illumination; before brine shrimps collection, unhatched cysts are discarded; hatched naupili are washed in aqua bidest and concentrated, before resuspension in a 1:1 solution in aqua bidest. Freshly prepared artemia solution is fed twice per day directly in fish tanks, at the amount of ~0,1 ml per adult fish.

Diet is daily supplemented with SDS dried food, according to the individual animals need, in terms of quantity and quality of the food.

Name	Company
SDS small granular food	Special Diet Services
SDS-100 powder food	Special Diet Services
SDS-200 powder food	Special Diet Services
SDS-300 powder food	Special Diet Services

3.1.7 Oligonucleotides

All primers were synthesized by Integrated DNA Technologies (IDT) in desalted or PAGE purified quality and shipped lyophilized. Primers were resuspended in aqua bidest to a final concentration of 100 μM.

Oligonucleotides for gene cloning		
	Forward (5'-3')	**Reverse (5'-3')**
pex3FL	TAAACCCGCTCTTGCTTCTC	TGCTGTACGGCATGAGAGAT
pex3ΔMTS	TAGGATCCTAAACCCGCTCTTGCTTCTC	TAGAATTCTCACTTCTGAAGAAAGTGGCTTGGAATTT
slc24a5	TAGAATTCCCGTCATCTGTGTTCTGC	TATCTAGATGTTATGTCGGGCATCTTGA
slc45a2	TAGGATCCTCTTACCATCCAGAACCATG	TATCTAGATTGAGGCTTATTCTGTACATCACAT

Oligonucleotides for CRISPR/Cas9 sgRNA cloning		
	Forward (5'-3')	**Reverse (5'-3')**
pex3 exon3 target	TAGGAATTTTTAGTCAACAGAA	AAACTTCTGTTGACTAAAAATT
pex3 intron1 target	TAGGTGATGGATGATTGCCTCT	AAACAGAGGCAATCATCCATCA

Oligonucleotides for High Resolution Melting Analysis (HRMA)		
	Forward (5'-3')	**Reverse (5'-3')**
$pex3^{CRISPR\text{-}exon3}$	TGTTATCAATGCTCCCCACTC	CACACACACGTGCATAACTCA
$pex3^{CRISPR\text{-}intron1}$	GGCATAGTCAAATCAAAGTTGAAA	TGATATGCTGCAAGCAAGAAC
$pex3^{ENU\text{-}sa11684}$	AGCGAAATTCCAAGCCACTT	AAACAGCCACACAGGAAGG
$pex3^{ENU\text{-}sa17571}$	GCAGGTGTTTATCTGCTTGGT	CTCCGAGCTTGAGCAATGTA
$pex3^{TALEN\text{-}target1and2}$	CCCGCTCTTGCTTCTCTTATT	ACAAACACCCCAGTGAAGATG
$pex3^{TALEN\text{-}target3}$	TCGGTGTCAAGTCTGTTAAAATG	GGTTCAGTTGCCCACGTTAG

Oligonucleotides for qRT-PCR		
	Forward (5'-3')	**Reverse (5'-3')**
amsh	ATCTGACACAGACTCACTGC	CCCAGATCCTCATCATAGGC
cdkn1a	CATCACAGATTTCTACCAAGCC	GAAGGTAGATGCAGGTCAAGAG
cebpa	AGCCAAGCAAGAATGAGACC	GTGTTGAGAGTGGTGGTAGG
cpt1a	GGGCTACACAGAAGATGGTC	ATAGTTTGGCACTCAGTTGGG
dct	TTATAATATGGTGCCCTTCTTCCC	TCTGTTGTCCAGTTCTTCGAG
elf1α	ATGACTCCACTGAGCCC	GGACGAAGGCAACACTG
foxd3	GAACTATAGGCAGCACTGGA	TACCTGTACTGAAAGCATTCCT
hmox1a	ATCTACAGCACAAAGATGGACTC	TGACGTGGCTGTCTTTAGTG
mc1r	GACCACTAGCATGAAGGGAG	GGACAGGTGAGAATTAGGATGAG
mitfa	ACAGCAATCATGCTCTTCCTC	GATGGAGTAACGGATAATTCCCT
nd-1 mt	GCCTACGCCGTACCAGTATT	GTTTCACGCCATCAGCTACTG
pex3	GAGAGGCAATCATCCATCAC	CTTTAGATCCTCCCAGATTTCAAG
polg1	GAGAGCGTCTATAAGGAGTAC	GAGCTCATCAGAAACAGGACT
pparaa	AACTGGAGTACGACAAGTGTG	AAACGAATAGCGTTGTGGGA
pparg	ACATCTACAGTAGTGCAGTC	TTAGTACAGGTCCCGCATGA
ppargc1a	GGATAGCTTTCTGGGAGGAC	CATCTATCTTCTCAAACAGGTTGG
rpl13	TCGTATTGCTCCAAGACCA	CCTCCAAGGTGAAGCCA
si.ch211-199	TCTCTAAAGCGACTGAAGAAACTC	CAGGAGTAAGTGGTTCCCAG
sox10	CCAATCGCATTACAAGAGCC	CTGTGACTCTGACCTGTAGC
tyr	TATTGACAGCATCTTTGAGCAG	CACCATGAAGTATCCGTCGT

3.1.8 Antisense Morpholino Oligonucleotides (AMOs)

All Antisense Morpholino Oligonucleotides (AMOs) were designed and synthesized by Gene Tools, LLC and shipped lyophilized. AMOs were resuspended in aqua bidest to a final concentration of 1 mM.

Oligonucleotides for gene knock-down		
	AMO (5'-3')	
foxd3	TGCTGCTGGAGCAACCCAAGGTAAG	(Lister et al. 2006)
pex11α	TCGTGAAGCTGATGAAAGTTTCCAT	
pex14	TGGAGGAATGCTATTAACTACCTGA	
pex16	GTTTCTCCATGTAGAGCACCGACAT	
pex19	TGCTCTGATGCTGACGCCATCTTGC	
pex3	ACTCAACATTTTAACAGACTTGACA	

3.1.9 Vectors

Name	Source	Link for vector map
pCMV-Sport6.1	Hoch lab	https://www.biocat.com/bc/data/IMAGE/lightbox.php?p=pCMV.SPORT6.1&cmd=map
pCRII-TOPO	Invitrogen	https://tools.thermofisher.com/content/sfs/manuals/topota_man.pdf
pCS2plus	Hoch lab	http://www.snapgene.com/resources/plasmid__files/image_consortium_plasmids/pCS2+/
pDR274	Addgene (Hwang et al. 2013)	https://www.addgene.org/42250/
pMLM3613	Addgene (Hwang et al. 2013)	https://www.addgene.org/42251/

3.1.10 Antibodies

Primary Antibodies	Antigen	Source	Obtained from	Dilution
α-pex3	pex3	rabbit	Aviva Systems Biology	1:200
α-tyr	tyrosinase	mouse	Invitrogen	1:200
α-cat	catalase	goat	ThermoFisher Scientific	1:200
1D4B	lysosome-associated membrane glycoprotein 1	rat	DSHB	1:150
H-69	endoplasmic reticulum, rough, glycoprotein	rat	DSHB	1:100
α-digoxygenin, Fab fragments, AP conjugated	Digoxygenin-UTP	sheep	Roche	1:10.000

Secondary Antibodies	Antigen	Source	Obtained from	Dilution
α-rabbit IgG^{647}	Rabbit Ig	donkey	Dianova	1:500
α-mouse IgG^{Cy3}	Mouse Ig	donkey	Dianova	1:500
α-rabbit IgG^{488}	Rabbit Ig	donkey	Dianova	1:500
α-goat IgG^{647}	Goat Ig	donkey	Dianova	1:500
α-rat IgG^{HRP}	Rat Ig	donkey	Santa Cruz	1:15.000
α-mouse IgG^{HRP}	Mouse Ig	donkey	Santa Cruz	1:15.000
α-rabbit IgG^{HRP}	Rabbit Ig	donkey	Santa Cruz	1:15.000

3.1.11 Microrganisms

Name	Genotype	Source
E. coli DH5α	fhuA2 Δ(argF-lacZ) U169 phoA glnV44 Φ80 Δ(lacZ) M15 gyrA96 recA1 relA1 endA1 thi-1 hsdR17	Stratagene
E. coli TOP10F'	F'(*lac*Iq*Tn*10(TetR)) *mcr*AΔ(*mrr-hsd*RMS-*mcr*BC) Φ80*lac*ZΔM15 Δ*lac*X74 *rec*A1 *ara*D139 Δ(*ara-leu*)7697 *gal*U*gal*K*rps*L*end*A1 *nup*G	Invitrogen

3.1.12 Cell lines

Name	Source	Link for information
Mus musculus skin melanoma B16-F0	Förster lab	https://www.lgcstandards-atcc.org/Products/All/CRL-6322.aspx
Mus musculus embryo fibroblasts NIH/3T3	Hoch lab	https://www.lgcstandards-atcc.org/Products/All/CRL-1658.aspx?geo_country=de

3.1.13 Bacterial culture media

LB: 10 g tryptone; 5 g yeast extract; 10 g NaCl; add 1 l aqua bidest; adjust to pH 7,0 and autoclave.

LB agar w/o antibiotic: 10 g tryptone; 5 g yeast extract; 10 g NaCl; 20g agar; add 1 l aqua bidest; adjust to pH 7,0 and autoclave; plate when cooled to 55°C; if required add antibiotics at proper concentration before plating bacteria.

3.1.14 Cell culture media

Dulbecco's Modified Eagle's Medium (DMEM), supplemented with 10% Fetal Calf Serum (FCS) and 1% Penicillin-Streptomycin (Invitrogen).

3.1.15 Softwares

Adobe Illustrator CS5
Adobe Photoshop CS5
Alpha DigiDoc
Bio-Rad CFX Manager 3.0
Bio-Rad Precision Melt Analysis Software 1.2
Chromas Lite 2.6
ImageJ
Microsoft Office 2011
PerlPrimer
ZEN Light 09 Zeiss

3.2 Methods

3.2.1 Fish work

3.2.1.1 Fish maintenance

Zebrafish (*Danio rerio*) were raised in Tecniplast ZebTec stand alone or Multi-Linking WTU systems, on a 14 h light/10 h dark cycle in standard condition (water temperature=28°C; pH=7,2; absent NH_3; [NO_2]<1mg/l; [NO_3]<50mg/l), according to Westerfield (Westerfield 2000). All the animals were reared in the LIMES Zebrafish Facility. All animal experiments were performed in accordance with Tierschutzgesetz §8 Abs.1, with European Union animal welfare Directive 2010/63/EU and with Tierversuchsvorhaben AZ 84-02.04.2013.A274 of the LANUV NRW.

3.2.1.2 Embryo collection and raising

Embryos were obtained from natural crossings. The evening before the experiment, after the regular feeding, a male and a female fish (around 6 to 12 months of age) of the desired genotype were selected and put in the same external 1 l-breeding tank, separated by a transparent plastic inlet. Breeding tanks were put in an external incubator at 28,5°C, with light/dark cycle adjusted to optimal experimental conditions. The morning of the experiment, breeding tanks were taken out of the incubator, still during the dark phase, exposed to light and the transparent plastic inlet was removed. Fish immediately started to spawn fertilized embryos, which sank to the bottom of the tank, through a net to prevent cannibalism from parental fish. Embryos were collected with a plastic pipette, washed with fish water, and used for experimental procedures.

After the experiment, embryos were transferred in Petri dishes containing 20 ml of freshly prepared embryo medium with 0,0005% w/v methylene blue (to prevent bacterial and algae proliferation) and, starting from 24 hpf, 1x PTU to prevent melanin synthesis, if required. Embryos were raised in an incubator at 28,5°C. Each Petri dish did not contain more than 50 embryos. Embryos were checked for survival every 12 hours and dead embryos were removed from the plate. Embryos were staged as previously described (Kimmel et al. 1995).

Embryos imported from external lab, were preventively subjected to bleaching procedure, to prevent pathogen import. 24 hpf embryos were rinsed twice in bleaching solution and afterwards twice in embryo medium and raised according to standard protocol; in case embryos did not hatch within 3 dpf, they were manually dechorionated.

3.2.1.3 Larvae collection and fixation

Before collection, embryos were staged (Kimmel et al. 1995) and synchronous ones were collected in Petri dishes containing embryo medium.

For early stage embryos (8 hpf or 12 hpf), Petri dish was coated with a thin layer of 1% agarose to prevent embryo disruption; embryos were exposed to proteinase K (200 µg/ml in embryo medium) for 5 minutes. At short intervals, Petri dish was gently swirled to allow chorion residuals to float away. As soon as most of the embryos were dechorionated, they were washed twice with embryo medium and collected in tubes with the lowest amount possible of embryo medium. For later stage embryos, if not hatched yet, chorion was removed using a

pair of fine-tip forceps. Embryos were then collected in tubes with the lowest amount possible of embryo medium.
For fixation, 1 ml of fixative solution was added and samples were stored overnight at 4°C under gentle shaking. Fixed samples were either used directly for downstream application, or washed once with methanol and then stored in methanol for several months at -20°C.

3.2.1.4 Scales isolation, fixation and bleaching

Adult fish of the desired genotype were anesthetized in tricaine and viewed under a stereobinocular. Scales were removed from the trunk region, from the side, gently pulling with fine forceps. Scales were immediately transferred to a tube containing fixative solution, whereas the fish was transferred to a separate tank and monitored in the next days for complete recovery.
Scales were incubated overnight at 4°C under gentle shaking in fixative solution. Fixed samples were washed twice in PBT for 5 minutes and then incubated in bleaching solution for 10 minutes at room temperature to remove melanin pigment which might interfere with following imaging. Bleached scales were then washed four time in PBT for 5 minutes and immediately used for downstream applications.

3.2.1.5 Adult organ preparation

Adult fish were sacrificed according to current legislation. All different tissues (brain, eyes, gill, heart, liver, kidney, intestine, ovary, testis and carcasses) were dissected according to standard protocol (Gupta & Mullins 2010). Organs were rapidly transferred into fresh tubes containing 250 µl of TRIzol RNA Isolation reagent and immediately homogenized with a pestle; additional 750 µl of TRIzol RNA Isolation reagent were added and samples were snap frozen in liquid nitrogen and stored at -80°C, until further processing.

3.2.1.6 TALENs-mediated mutant generation

pex3^{TALEN} mutant alleles were generated according to Huang et al. (Huang et al. 2011). Plasmid containing the coding sequences for the TALENs DNA-binding domains were obtained from the Hornung lab. DNA-binding domain coding sequences were in-frame sub-cloned in a new vector at the 5' of the FokI nuclease coding sequence. mRNAs were transcribed from the digested plasmid template using T7 mMessage mMachine (Ambion) as per manufacturer's protocol. All the mRNAs were resuspended in RNase-free water and stored at -80°C in aliquots.

3.2.1.7 CRISPR/Cas9-mediated mutant generation

pex3^{CRISPR} mutant alleles were generated according to Hwang et al. (Hwang et al. 2013). Cas9 mRNA was transcribed from PmeI-digested pMLM3613 plasmid template (purchased from Addgene) using T7 mMessage mMachine (Ambion) as per manufacturer's protocol. For sgRNAs generation, proper oligonucleotides (see Oligonucleotides) were purchased from Integrated DNA Technologies and cloned into pDR274 (purchased from Addgene www.addgene.org) according to Hwang et al. (Hwang et al. 2013). Transcription of sgRNAs was performed using the HindIII-digested sgRNA-containing vector as template and the MAXIscript T7 kit (Ambion)

as per manufacturer's protocol. Both the Cas9 mRNA and the sgRNAs were resuspended in RNase-free water and stored at -80°C in aliquots.

3.2.1.8 mRNA, Antisense Morpholino Oligonucleotides (AMOs) or chemicals injection

Microinjections were performed in freshly collected one-cell stage embryos of the appropriate genotype. For mutant generation, either with the TALENs of the CRISPR/Cas9 technique, embryos derived from AB strain crossed and raised in the LIMES Zebrafish Facility, previously sequenced for the genomic locus were used. mRNAs, AMOs or chemicals were dissolved in injection solution at the proper concentration. For mRNAs, the concentration is either indicated in the experimental description, or it is ~60 ng/µl for *pex3FL* or *pexΔMTS* mRNAs or ~120 ng/µl for *slc24a5* or *slc45a2* mRNA; for AMOs the concentrations are 250 µM for pex3 AMO, 250 µM for pex11α AMO, 333,3 µM for pex14 AMO, 250 µM for pex16 AMO or 200 µM for pex19 AMO; for chemicals, either CoQ_2 or CoQ_2H_2 were injected at the concentration of 10 µg/ml.

Embryos injected in parallel with only injection solution were used as negative control.

Embryos were arrayed on an acrylic slide with V-shaped drills fixed on the bottom of a Petri plate filled with embryo medium. Solutions were loaded in glass needles pulled from capillaries and the injected drop was adjusted to an optimal volume of ~1,5 nl, with the aid of a micrometer slide. Adjustments were obtained regulating injection pressures parameter on the FemtoJet microinjector (Eppendorf). Injections were controlled via a M-152 micromanipulator (Nasherige).

At the end of the injection procedure, embryos were moved to Petri dishes containing fresh embryo medium and checked for survival at 8 hpf and 24 hpf, discarding the dead ones.

3.2.1.9 Bafilomycin A1 exposure

At 24 hpf, embryo medium in Petri dishes was replaced with fresh embryo medium containing 100 nM Bafilomycin A1 in DMSO. At 48 hpf, embryos were washed twice with fresh embryo medium, and further incubated.

Embryos treated in parallel with DMSO only were used as negative control.

3.2.1.10 bezafibrate (PPARγ) activator exposure

At 12 hpf, embryo medium in Petri dishes was replaced with fresh embryo medium containing 20 µM Bezafibrate in 2% DMSO. Before the experiment end, embryos were washed twice with fresh embryo medium.

Embryos treated in parallel with 2% DMSO only were used as negative control.

3.2.1.11 Larval weight determination

For determination of larval weight, larvae of the desired developmental stage were transferred in embryo medium containing tricaine. As soon as the animals were not swimming anymore, they were delicately dried on a paper wipe for few seconds and moved on a weighing paper. Weight was determined in grams, on a fine scale, to the fourth decimal digit.

3.2.2 Histology

3.2.2.1 Immunofluorescence

For protein localization analysis in wildtype or mutant embryos, or in whole scales, antibody stainings were performed. If stored in methanol, fixed tissues were rehydrated through a methanol/PBT series, for 5 minutes each step, at room temperature, under gentle shaking. Tissues were permeabilized incubating them with proteinase K (10 µg/ml) for an appropriate time, adjusted to the embryonic developmental stage, or for the thickness of the tissue. Tissues were fixed again in fixative solution for 20 minutes at room temperature and washed four times for 5 minutes in PBT at room temperature. Samples were then washed in distilled water for one hour at room temperature and permeabilized in pre-cooled acetone for 7 minutes at -20°C. Samples were washed four times for 5 minutes in PBT at room temperature and blocked in NCS-PBT for one hour, prior to overnight incubation at 4°C with the primary antibody, diluted in PBT, as suggested.
Samples were washed four times for 5 minutes in PBT at room temperature and then incubated overnight at 4°C with the secondary antibody, diluted in PBT, as suggested. Samples were washed four times for 5 minutes in PBT and then soaked either in glycerol or Fluoromount+DAPI before mounting for imaging.

3.2.2.2 *In situ* hybridization

For *pex3* transcript localization analysis during embryogenesis, fixed wildtype zebrafish larvae of different stages were used in an *in situ* hybridization approach, according to standard protocol (Thisse & Thisse 2008), with minor modifications. Fixed embryos were placed in tubes and rehydrated through a methanol/PBT series for 5 minutes each step, at room temperature, under gentle shaking. Embryos were permeabilized incubating them with proteinase K (10 µg/ml) for an appropriate time, adjusted to the embryonic developmental stage (30 sec for 6-somite stage, 1 min for 24 hpf embryos, 3 min for 48 hpf embryos, and 7 min for 5 dpf embryos). Embryos were fixed again in fixative solution for 20 minutes at room temperature and washed four times for 5 minutes in PBT at room temperature. Samples were then pre-hybridized in hybridization mix for 4 hours at 70°C prior to overnight hybridization in 200 µl of hybridization mix containing 33,3 ng of antisense digoxygenin-labelled RNA probe at 68°C. Probes were denaturated at 80°C for 10 minutes and immediately stored on ice, before use.
The next day samples were transferred to PBT: first, through a hybridization mix (without tRNA and heparin)/2x SSC series for 10 minutes each step, at 68°C, under gentle shaking; then with two washings with 0,2x SSC for 30 minutes each, at 68°C, under gentle shaking; then through a new 0,2x SSC/PBT series for 10 minutes each step, at room temperature, under gentle shaking. Samples were blocked in blocking solution for 4 hours, prior to overnight incubation at 4°C with the α-digoxygenin, Fab fragments, AP conjugated, diluted as suggested in blocking solution. Samples were washed six times for 15 minutes in PBT and then three times for 5 minutes in alkaline Tris buffer. Embryos were then moved into plastic 24-well plates and stained in 800µl of labelling solution, as long as the desired staining intensity is reached. Staining was blocked washing the samples with stop solution for 5 minutes each step, at room temperature, under gentle shaking and then soaked in glycerol before mounting for imaging.
Sense digoxygenin-labelled RNA probes were used in parallel as negative control.

3.2.2.3 Alcyan Blue staining

Fixed embryos of the desired developmental stage were washed with PBT four times for 5 minutes under gentle shaking and then incubated in bleaching solution for 30 minutes at room temperature to remove melanin pigment which might interfere with following imaging. Samples were then rinsed twice with PBT and transferred into Alcian Blue staining solution overnight at room temperature. Embryos were washed four times for 5 minutes under gentle shaking in a solution of 1% v/v HCl-70% v/v ethanol in water and then rehydrated through a HCl-ethanol/PBT series for 5 minutes each step, at room temperature, under gentle shaking. Samples were finally soaked in glycerol before mounting for imaging.

3.2.2.4 DAF-FM staining

Larvae of the selected stage of development were transferred in DAF-FM diacetate staining solution and incubated for 2 h in the dark at 28°C. After incubation, larvae were rinsed with embryo medium twice and the tubes were then place in ice to euthanize the animals. Embryo medium was then replaced with glycerol before mounting the samples for imaging.

3.2.2.5 Imaging and quantification

For morphological parameter measurements (larval length, tail length/total length ratio, larva/yolk ratio) and for pigment intensity quantification, embryos or larvae of the desired developmental stage were transferred in embryo medium containing tricaine. In order to facilitate melanophore count, embryos or larvae were first treated with epinephrine for 5 min to contract the melanosomes, let them recover for 20 minutes in embryo medium until full melanophore contraction was reached and then placed in embryo medium containing tricaine. As soon as the animals were not swimming anymore, pictures of individual animals were taken at the Olympus SZX16 microscope, with the same parameter for all the experimental groups. Images were then processed and analysed using ImageJ or Photoshop CS6 software. Images were not adjusted for brightness and contrast, if not otherwise stated.

For melanophore lineage precursors count in transgenic animals, embryos of the desired developmental stage were sacrificed and fixed overnight as previously described (see Larvae collection and fixation). Embryos were then rinsed twice with PBT and soaked in Fluoromount+DAPI before mounting for imaging. Images were taken at the Zeiss LSM 710 confocal microscope. Images were the processed and analysed using Zeiss ZEN software. Images were not adjusted for brightness and contrast. Maximum intensity projections were obtained for each data set and the melanophore precursor cell clusters were counted afterwards.

3.2.3 Molecular work

3.2.3.1 PCR techniques

For amplification of polynucleotide sequences the following polymerases were used according to manufacturer's protocols: GoTaq (Promega) and Phusion High-Fidelity DNA Polymerase (NEB).

3.2.3.2 Isolation of plasmid DNA in analytical quality (Miniprep)

For testing colonies for successful transformation, 3vml of an *E. coli* overnight culture was centrifuged for 2 minutes at 13000 rpm and the pellet was resuspended in 200 µl TELT buffer with 10 mg/ml lysozyme. After 5 minutes of incubation at room temperature, cells were boiled (99°C) for 3 minutes in a termomixer. After cooling in ice for 5-10 minutes, samples were centrifuged at full speed for 20 minutes at 4°C. 200 µl of isopropanol were added to the supernatant. Plasmid DNA was precipitated by centrifugation at full speed for 30 minutes at 4°C. DNA was washed with 1 ml of 70% ethanol, precipitated again by centrifugation at 13000 rpm for 5 minutes at 4°C, air dried and resuspended in 50 µl aqua bidest.
For preparation of high amounts of pure plasmid DNA, Nucleospin Plasmid AX-100 Kit (Macherey-Nagel) was used according to manufacturer's instructions.

3.2.3.3 Gel electrophoresis and DNA clean-up

Agarose gels at the proper concentration (usually 1%, for smaller fragments 2%, in TAE buffer) were used for electrophoretic separation of DNA fragments. Gel fragments were detected using a UV-transilluminator (366 nm) and the desired fragment was excised with a clean scalpel. For clean-up of DNA fragments out of agarose gel pieces, NucleoSpin extract II Kit (Macherey-Nagel) was used according to manufacturer's instructions. The concentration of DNA was measured using a Nanodrop spectrophotometer (Peqlab Biotechnology GmbH, ThermoFisher Scientific).

3.2.3.4 Restriction digestion and ligation of DNA fragments

Enzymatic digestion of DNA was done using New England Biolabs (NEB) restriction endonucleases and appropriate buffers according to manufacturer's protocol. Ligation of DNA fragments into plasmid vectors was carried out overnight at 16°C in a total volume of 20 µl, including 2µl 10x ligation buffer and 1 U T4 DNA ligase (NEB).

3.2.3.5 mRNA *in vitro* synthesis

mRNAs were generated from plasmids containing the coding sequence of the desired gene under the control of either the SP6 or T7 promoter. Plasmids were linearized with a unique restriction endonuclease, cutting at the 3' of the coding sequence. Obtained linear template was run on an agarose gel, cleaned up (see Gel electrophoresis and DNA clean-up) and used as template for *in vitro* transcription with SP6 mMessage mMachine Kit (Ambion) or T7 mMessage mMachine Kit (Ambion) as per manufacturer's protocol. After precipitation, mRNAs were resuspended in RNase-free water and stored at -80°C in aliquots. The concentration of mRNAs was measured using a Nanodrop spectrophotometer (Peqlab Biotechnology GmbH, ThermoFisher Scientific).

3.2.3.6 Digoxygenin-labelled RNA probe synthesis

pex3 digoxygenin-labelled RNA probes were generated from pCRII-TOPO vector, containing the gene whole coding sequence and the two promoters SP6 and T7 on opposite ends. Plasmid was linearized with unique restriction endonucleases, cutting either at one or the other end of the coding sequence. Obtained linear templates were run on an agarose gel, cleaned up (see

Gel electrophoresis and DNA clean-up) and used as template for *in vitro* digoxygenin-labelled RNA probe synthesis with DIG RNA labelling Kit (SP6/T7) (Roche) as per manufacturer's protocol. After precipitation, digoxygenin-labelled RNA probes were resuspended in RNase-free water and stored at -80°C in aliquots, after the addition of RNA later® (ThermoFisher Scientific) and 0,5 M EDTA pH 8,0 at the final ratio of 20:9:1. The concentration of digoxygenin-labelled RNA probes was measured using a Nanodrop spectrophotometer (Peqlab Biotechnology GmbH, ThermoFisher Scientific).

3.2.3.7 Isolation of genomic DNA from tissues

Genomic DNA was isolated from whole embryos or from caudal fin sections according to the HotShot genomic DNA extraction protocol (Mosimann et al. 2013). Tissue was incubated in 50 µl alkaline lysis buffer at 95°C for one hour, cooled on ice for 5 minutes and an equal volume of neutralization buffer was added. Debris were removed by spinning down the samples at 5000 rpm for 15 minutes at 4°C and supernatant containing genomic DNA was transferred to fresh tubes. The concentration of DNA was measured using a Nanodrop spectrophotometer (Peqlab Biotechnology GmbH, ThermoFisher Scientific).

3.2.3.8 Isolation of total RNA from tissues

Total RNA was isolated either from pools (12-15) of whole embryos of the same stage, or from freshly dissected isolated adult organs. Tissue was homogenized with a pestle in 250 µl TRIzol RNA Isolation reagent; after homogenization, additional 750µl TRIzol RNA Isolation reagent were added. Samples were eventually stored at -80°C up to six months. Colourless total RNA-containing fraction was isolated according to manufacturer's protocol. Downstream cleaning was performed with RNA PureLink® RNA Mini Kit according to manufacturer's protocol. The concentration of RNA was measured using a Nanodrop spectrophotometer (Peqlab Biotechnology GmbH, ThermoFisher Scientific). Purified RNA was aliquoted and stored at -80°C.

3.2.3.9 Reverse transcription of RNA into cDNA

1 µg of total RNA was reverse transcribed into cDNA using QuantiTect reverse transcription kit (Qiagen) including DNase treatment. cDNA synthesis was carried out according to manufacturer's protocol, including a control reaction, which did not include the reverse transcriptase (-RT control). cDNA was stored at -20°C.

3.2.3.10 Quantitative RT-PCR

The C1000™ Thermal Cycler with CFX96™ Optical Reaction Module (Bio-Rad) was used to perform quantitative real-time PCR experiments. Amplification after each PCR cycle was detected via iQ™ SYBR® Green Supermix (Bio-Rad). cDNA probes of reverse transcribed total RNA served as template. All PCR reactions were done as technical triplicates in 96-well plates in a total volume of 15 µl. Data were analysed with CFX Manager 3.0 software (Bio-Rad). Expression is always shown relative to a control condition or sample and relative to two independent internal expression control, which were *rpl13* and *elf1α* in all experiments. Expression data were calculated according to the ΔΔCt method. Primers for qRT-PCR assays

were tested for efficiency before use and results were considered for corrected expression values. Primer dimers formation was excluded by melt curve analysis.

3.2.3.11 High Resolution Melting Analysis (HRMA)

The C1000™ Thermal Cycler with CFX96™ Optical Reaction Module (Bio-Rad) was used to perform High Resolution Melting Analysis (HRMA). Amplification after each PCR cycle and high resolution melting profile were detected via Precision Melt Supermix (Bio-Rad). Genomic DNA adjusted for concentration served as template. All PCR reactions were done as technical triplicates in 96-well plates in a total volume of 15 µl. Standard protocol was modified as follows: initial denaturation 3 min at 95°C; target amplification with denaturation 10 sec at 95°C, annealing 10 sec at 60°C and elongation 30 sec at 72°C repeated for 48 cycles; final elongation 5 min at 72°C; melting 2 min at 95°C and reannealing 5 min at 25°C repeated for 3 cycles; melting data acquisition from 75°C to 87°C, with 0.1°C incremental steps and 15 sec hold before fluorescence measurements. Data were analysed with Precision Melt Analysis software (Bio-Rad). Melting profiles were always compared with a wildtype sample, in all experiments, and with a homozygous mutated allele sample, if available. Automatic sample clustering was refined by manual analysis of normalized melting curves and melt peaks. Primers for HRMA were tested for uniqueness and identity of the amplified PCR product. Primer dimers formation was excluded by melt curve analysis.
For sequencing of the amplicon from HRMA experiments, either they were cloned into pCRII-TOPO vector (see TOPO TA cloning) and 4-8 positive clones were sent for sequencing or they were directly sent for sequencing (see DNA sequencing).

3.2.3.12 DNA sequencing

For sequence assessment, the desired polynucleotide sequence (either an isolated PCR- or HRMA-amplicon, or a vector) was sent to SeqLab, according to their instructions. For sequencing, either a primer contained in the vector sequence or the specific primer added to the reaction tube were used. In case of direct sequencing of HRMA amplicon, PCR product purification (removal of PCR primers and dNTPs) was requested and amplification primers were separately provided. Sequence results were individually validated through chromatogram analysis.

3.2.3.13 SDS-PAGE gel electrophoresis and Western Blot

SDS polyacrylamide gels at the proper concentration (12% running gel) were used for electrophoretic separation of proteins. Samples were run at 60 V until samples entered the running gel, then at 110 V in SDS-running buffer. Proteins were then transferred on methanol-activated PDVF membranes, blotting for 1 hour at 100 V at 4°C in Transfer Buffer. Membranes were blocked with 5% milk powder in TBTS and incubated with primary antibody overnight at 4°C under gentle shaking, at the indicated dilution. Membranes were then washed three times for 5 minutes in TBST at room temperature and decorated with secondary antibody for one hour at room temperature under gentle shaking. Membranes were washed again three times for 5 minutes in TBST and developed with Pierce™ ECL Western Blotting Substrate. Films were exposed as long as clear bands were appearing (usually between 1 minutes and 10 minutes).

3.2.4 Biochemical work

3.2.4.1 Melanosome separation

B16 murine skin melanoma cells were collected. Pellet was resuspended in 1 ml of 0,25 M sucrose in HEPES and sonicated (2 cycles) to disrupt cells. Cell lysate was layered on top of a discontinuous sucrose gradient (from 1,0 M to 2,0 M, with 0,2 M steps) and tubes were ultracentrifuged for one hour at 100.000xg at 4°C. At the end of the centrifugation step, the melanosomal fraction could be easily identified as a dark grey-black layer located at the interface between the 1,6 M and the 1,8 M sucrose gradient. This fraction was collected using a glass pipette, transferred into fresh tubes, centrifuged again for 30 minutes at 16.100xg at 4°C and resuspended in 500 µl 0,25M sucrose in HEPES. Samples were centrifuged again for 30 minutes at 16.100xg at 4°C and resuspended in 500 µl RIPA buffer. Melanosomal fraction was sonicated (2 cycles) to disrupt membranes and processed in SDS-PAGE gel electrophoresis.

3.2.4.2 CoQ_2 reduction

0,5 ml of CoQ_2 stock solution was pipetted into a tube and 25 µl of a 0,05 M solution of $NaBH_4$ in water was added. The mixture was vortex-mixed for 2 minutes and incubated at room temperature in the dark for 30 minutes. The resulting CoQ_2H_2 was extracted into 5 ml of hexane and the organic phase was washed three times with 1,5 ml of water. The hexane layer was separated and evaporated to dryness overnight and CoQ_2H_2 was resuspended in in 0,1 ml isopropanol and 0,4 ml sterile water. Success in reduction procedure and concentration were measured using a Nanodrop spectrophotometer (Peqlab Biotechnology GmbH, ThermoFisher Scientific): the main absorbance peak of CoQ_2 decreased in magnitude and shifted from 275 nm to 287 nm (CoQ_2H_2).

3.2.4.3 ROS/RNS quantification

Pools containing five embryos of the same developmental stage were collected in single tubes, embryo medium was removed as much as possible and 450 µl of PBT were added; embryos were homogenized on ice with a pestle. Tubes were centrifuged 30 minutes at full speed at 4°C and supernatant was used to perform either the reactive oxygen species (ROS) quantification via Amplex® Red Hydrogen Peroxide/Peroxidase Assay Kit or the reactive nitrogen species (RNS) quantification via the Griess reagent Kit assay, according to manufacturer's instruction. Each sample was measured in triplicates on a 96-well plate; for ROS quantification, absorbance was measured at 585 nm, whereas for RNS quantification, absorbance was measured at 548 nm.

3.2.4.4 Pigment Absorbance measurements

Pigment absorbance measurements were performed according to Dong et al. (Dong & Yao 2012), with minor modifications. Pools containing 5 to 10 embryos of the same developmental stage were collected in single tubes, embryo medium was removed as much as possible and 200 µl of melanin extraction buffer were added. Samples were incubated at 37°C for 4 hours and then centrifuged at 10.000xg for 30 minutes at 4°C. Pellets were resuspended in 0,9% NaCl and centrifuged again at 10.000xg for 30 minutes at 4°C; pellets were resuspended in 170µl of

8M urea/1M NaOH and centrifuged again at 10.700xg for 30 minutes at room temperature. Melanin containing surnatant was used for pigment absorbance measurement. The spectrum was measured in the range between 330 nm and 510 nm and the total pigmentation absorbance was calculated integrating the area under the absorbance curve in this range.

3.2.5 Microbiological work

3.2.5.1 Transformation of chemo-competent bacteria

For transformation of plasmid vectors into competent bacteria, cells were thawed on ice. 100 ng of plasmid DNA were added to 100 µl of bacterial suspension. After incubation on ice for 30 minutes, cells were heat-shocked at 42°C for 45 seconds and subsequently cooled on ice. 100 µl of LB medium without antibiotics were added and vials were incubated at 37°C in a shaking thermomixer for 1 hour. Bacteria were then plated onto LB agar plates with appropriate antibiotics.

3.2.5.2 TOPO TA cloning

After PCR amplification of the desired polynucleotide sequence, dATP overhangs were added in a GoTaq polymerase reaction, which was done at 72°C for 10 minutes. Cloning into pCRII-TOPO vector was performed according to manifacturer's (Invitrogen) protocol and transformation into TOP10F' bacteria according to the protocol described above (see Transformation of chemo-competent bacteria).

3.2.6 Bioinformatics

3.2.6.1 Oligonucleotides design

PerlPrimer software (Marshall 2004) was used to design optimal pairs of primers for PCR, qRT-PCR and HRMA applications. Primer size was restricted between 18 and 23 nucleotides; aligning temperature (Tm) should be comprised between 57°C and 62°C (with an optimal Tm of 60°C). For cloning purposes, restriction enzyme sites were added at the 5' end of the primers, when necessary. Primers were ordered and obtained from Integrated DNA Technologies.

For Antisense Morpholino Oligonucleotides, target gene sequences were provided to Gene Tools, LLC. They designed an optimal morpholino oligonucleotide satisfying the general requirements (i.e. 40-60% GC content without significant self-complementarity or stretches of 4 or more contiguous G, should form no more than 16 contiguous intrastrand hydrogen bonds).

3.2.6.2 Sequence alignments

The Basic Local Alignment Search Tool (BLAST) (Altschul et al. 1990) was used to align nucleotide or protein sequences retrieved from online databases. Results were ordered according to increasing E-values, parameter that describes the number of hits one can expect to see by chance when searching a database of a particular size. Other available parameters are the query cover (the percentage of the input sequence which is considered in the shown

result), similarity (only for protein sequences) and identity scores. The alignment of the sequence was also displayed.
Multiple alignment was performed using MUltiple Sequence Comparison by Log-Expectation (MUSCLE) algorithm (Edgar 2004). For visualization of multiple alignments, Jalview plugin was used (Waterhouse et al. 2009). Aligned amino acid sequences were edited for function conservation and residues consensus according to a BLOSUM62 similarity matrix (Thompson et al. 1994).

3.2.6.3 Protein domains prediction

Prediction of transmembrane domains and cytoplasmic α-helices was based on structural data obtained from murine pex3 crystal structure data (Schmidt et al. 2012b; Sato et al. 2010; Hattula et al. 2014), integrated with HMMTOP prediction based on the amino acid sequence (Tusnady & Simon 2001).

3.2.6.4 Transcription factors binding site prediction

Prediction of transcription factors binding sites in promoter regions of different genes was performed using JASPAR tool (Mathelier et al. 2016). This database collects transcription factor DNA-binding preferences, modelled as Position Weight Matrices, used for scanning genomic sequences. The desired matrix was selected from the list and the 2 kb region upstream of the transcription start of the desired gene was used as input; to increase specificity of the results, the threshold score was set at 92% (Wasserman & Sandelin 2004).

3.2.7 Statistics

3.2.7.1 Data analysis

For all the gene expression, ROS or RNS quantification and mitochondrial DNA quantification experiments, data were obtained by three independent samples; for demographic experiments, the starting population consisted of at least 100 embryos for each experimental group; for pigmentation intensity quantification or melanophore number determination experiments, between 20 and 25 embryos or juvenile larvae were analysed for each experimental group.
Data were analysed using either t-test or 2-way ANOVA and Bonferroni post hoc correction. All p-values are indicated in the figures (* 2p<0,05; ** 2p<0,005; *** 2p<0,001; n.s. not significant).

3.2.7.2 Average distance from stripe axis calculation

For determination of melanophore distribution during larval metamorphosis, migration of individual cells on the skin was translated on a bi-dimensional model (Luciani et al. 2011). Position of the cells belonging to the same stripe was described as xy coordinates. These coordinates were used for the calculation of a linear regression describing the mean position, namely the presumptive axis of the stripe. After that, we calculated the average distance of each pigment cell from the axis of the stripe and this was related to the wildtype positive control.

4 Results

PEX3 is recognized as the key component of peroxisome biogenesis. It is described to have multiple function in this process, interacting with other peroxins, mediating the successful sorting of membrane protein on peroxisome surface and supplying lipid membrane during the organelle growth. As described in the introduction, mutation affecting *PEX3* were characterized in human, being lethal within the first four weeks after birth. Due to the multiple roles in peroxisome biogenesis and homeostasis, PEX3 is an appropriate candidate gene to establish a Peroxisomal Biogenesis Disease model in vertebrates. Making use of the several advantages of zebrafish model organism, among which rapid *ex utero* embryonic development, transparency, and availability of large number of animals, it is possible to get a deeper knowledge of the molecular events underlying the progression of the disease (Santoro 2014; Seth et al. 2013).

4.1 Identification of the zebrafish homolog of the human PEX3

In order to support the following analysis, an *in silico* homology study of the human PEX3 in the genomes of mouse, fruit fly, and zebrafish was performed. HomoloGene (Group) and ENSEMBL Genome Browser (Gene: PEX3 - ENSG00000034693 - Summary - Homo sapiens - Ensembl genome browser 84 Ensembl release 85 – July 2016) databases annotate unique homologs for all the species. In zebrafish, the unique homolog, named pex3 (gene ID: ENSDARG00000013973), is located on chromosome 20. The predictions indicate two putative transcripts. The first one (transcript ID: ENSDART00000012826) consists of 1938 bp, containing the coding sequence for the full length pex3 protein. The predicted molecular weight of the protein is approximately 42kDa. The second unprocessed transcript (transcript ID: ENSDART00000153008) is composed of 783 bp, due to a cryptic splicing site after the eighth exon resulting in the retention of the following intron (Table 1).

	Gene name	Gene symbol	Gene ID	Chromosome location	Transcript ID	Length (bp)	Protein ID	Length (a.a.)
Human	PEX3	HGNC:8858	ENSG00000034693	Chromosome 6: 143,450,807-143,490,010 forward strand	ENST00000367591	1969	ENSP00000356563.4	373
					ENST00000367592	784	ENSP00000356564.1	182
					ENST00000585848	408		
Mouse	Pex3	MGI:1929646	ENSMUSG00000019809	Chromosome 10: 13,523,842-13,553,142 reverse strand	ENSMUST00000019945	2129	ENSMUSP00000019945.8	372
					ENSMUST00000105539	1961	ENSMUSP00000101178.1	306
					ENSMUST00000105541	1072	ENSMUSP00000101180.1	293
					ENSMUST00000170376	1381	ENSMUSP00000128512.1	359
					ENSMUST00000133332	2959		
					ENSMUST00000125207	771		
					ENSMUST00000145337	480		
Fruit fly	Pex3	CG6859	FBgn0036484	Chromosome 3L: 15,144,355-15,146,379 forward strand	FBtr0075640	1559	FBpp0075393	385
					FBtr0331830	1906	FBpp0304214	385
Zebrafish	pex3	ZDB-GENE-040426-979	ENSDARG00000013973	Chromosome 20: 37,857,614-37,866,424 forward strand	ENSDART00000012826	1938	ENSDARP00000023925.6	364
					ENSDART00000153008	783		

Table 1 – Identification of mouse, fruit fly and zebrafish homologs of human PEX3: description of genes IDs, genomic locations, transcripts and encoded proteins.

The presence of redundant genes cannot be excluded due to the fact that zebrafish underwent a number of duplication, followed by major genomic rearrangements, starting at the base of the teleost radiation, approximately 300–450 millions of years ago (Taylor et al. 2001). In fact, each duplicated gene can undergo neo-functionalization (novel functional properties) or sub-functionalization (subdivision of the original protein functions), in case of positive selection leading to the conservation of both copies, or can degenerate into pseudogenes, in case of accumulation of deleterious mutations (Holland et al. 1994; Postlethwait 2007). The identified *pex3* was subjected to a reverse analysis based on both the coding sequence, versus the whole zebrafish genome, and on the amino acids sequence, versus the whole zebrafish proteome.

At the genomic level, no similar sequence was found. Multiple results from different sources - amongst them NIH MGC Project (Strausberg et al. 2002) and the Welcome Trust Sanger Institute (Howe et al. 2013b) genome assemblies - show *pex3* itself as the only positive hit, hinting to the degeneration or loss of the duplicated copy of *pex3*. Similarly, at the protein level, only pex3 polypeptide emerged as hit with an E-value lower than the default threshold. Remarkably, the same search detected other proteins having a partial homology overlap, limited to amino acids strands spanning as much as 100 residues (Table 2). Most of the times, this could be due to a similar topology (i.e. similar composition in the tertiary structure of a particular region of the protein, for example). Nevertheless, these hits cannot be included in putative isoforms of the duplicated *pex3* gene, since they are associated with other domains absent in mammalian Pex3 or they lack other domains defining pex3 function. It is rather the case that the two genes may be derived from a common ancestor and independently evolved, still conserving partial features. Interestingly, one of the positive hits, apolipoprotein B-100, is involved in autophagy as regulator of lipids metabolism and it has the capability of binding lipid droplets, similar to what was described for pex3, in mammals (Zamani et al. 2016).

Description	Accession	Query cover	E-value	Identity
peroxisomal biogenesis factor 3	NP_956522.1	100%	2e-128	100%
PREDICTED: kinesin-like protein KIF21B	XP_009304054.2	42%	0,068	14%
PREDICTED: potassium voltage-gated channel subfamily G member 2-like	XP_690900.2	8%	1,2	21%
PREDICTED: serine/threonine-protein kinase pim-1-like	XP_009302304.2	47%	1,5	15%
potassium channel subfamily K member 15	NP_001104701.1	12%	1,5	11%
retinol dehydrogenase 13	NP_001038920.1	7%	3,8	24%
PREDICTED: apolipoprotein B-100	XP_694827.6	31%	4,7	12%

Table 2 – Identification of possible *pex3* paralogues in *Danio rerio* genome and annotation of genes having partial sequence homology (Identity>10%; query coverage>5%).

These data show that only one isoform of *pex3* gene is present in zebrafish and it can be excluded the existence of a second redundant homolog that may interfere with the following analysis.

4.2 Pex3 gene structural analysis

Further *in silico* analysis was performed determining the gene structure conservation across different model organisms. Gene assemblies were analyzed both at the level of exon-intron composition and at the level of gross genomic region organization.

In *Drosophila*, Pex3 is encoded by a single exon transcript; in all the other species analyzed in this work, zebrafish pex3 homologs are encoded by mRNAs derived from the splicing of twelve exons (Table 3). 5'-, 3'-UTR encoding exons and introns are rather heterogeneous and variable in length. In contrast, all the exons, except for exons 5 and 8, share the same length. Exon5 in zebrafish is 3 bp shorter (resulting in an in-frame shift in the ORF, leading to the absence of a single amino acid) when compared to human and murine ones. Exon 8 in mouse is 3 bp shorter and in zebrafish is 24 bp shorter when compared to the human one (resulting in an in-frame shift of the ORF, in both cases).

Exon	HS *PEX3*	MM *Pex3*	DR *pex3*
1	136	314	219
	7969	6344	372
2	132	132	132
	3699	3644	75
3	82	82	82
	5124	5149	172
4	44	44	44
	2795	1363	2307
5	125	125	122
	297	167	88
6	67	67	67
	107	99	111
7	55	55	55
	548	717	121
8	169	166	145
	2457	2261	1166
9	71	71	71
	4219	959	97
10	123	123	123
	5953	3420	2271
11	97	97	97
	3894	2772	93
12	868	853	781

Table 3 – Exon/intron structure comparison between *pex3* transcripts in human (HS), mouse (MM) and zebrafish (DR). Numbers represent the lenghts (in base pairs) of exons and introns. Alternating, there are exons (in yellow) and introns (in white). Exon containing the start codon is highlighted in green; exons containing the stop codon is highlighted in red.

The overall genomic region organization analysis showed no similarity between zebrafish genome and the one of the furthermost analyzed model, *D. melanogaster*. However, the genomic regions surrounding PEX3 in human and Pex3 in mouse include the adat2 (adenosine deaminase, tRNA specific, 2) in a head-to-head orientation at the 5'-end of the gene, similarly to what happens in zebrafish (Table 4; for further details, see Appendix).

	Gene 5'-end				Gene 3'-end			
Zebrafish			adat2	adenosine deaminase, tRNA-specific 2				
Human			ADAT2	adenosine deaminase, tRNA-specific 2	VDAC1P8	voltage-dependent anion channel 1 pseudogene 8	FUCA2	fucosidase, alpha-L- 2, plasma
Mouse			Adat2	adenosine deaminase, tRNA-specific 2			Fuca2	fucosidase, alpha-L- 2, plasma
Fruit fly	Pdi (P4HB)	prolyl 4-hydroxylase, beta polypeptide	CG32147 (PGPEP1)	pyroglutamyl-peptidase I	FucTA		Msh6	MSH6 mutS homolog 6

Table 4 – Evolutionary comparison of the genomic region surrounding *pex3* gene in different species in terms of conservation of the locus.

4.3 Prediction of pex3 functional domains

The predicted peptide sequences encoded by the identified homologs in the different species were then analyzed for similarity in amino acid composition. BLAST results show that zebrafish pex3 shares 74% of identical and 85% of similar residues when compared to the human homolog. Afterwards, topology analysis with secondary structure and transmembrane coils prediction tools (Chou & Fasman 1974; Tusnady & Simon 2001) was performed. Indeed, zebrafish pex3 is predicted to possess a short N-terminal transmembrane domain (residues 16-33) followed by six α-helices (amino acids 53-95, 100-146, 158-192, 202-240, 249-291, 313-357) (Figure 22). The N-terminus is predicted to be intra-luminal, whereas the C terminus cytoplasmic.

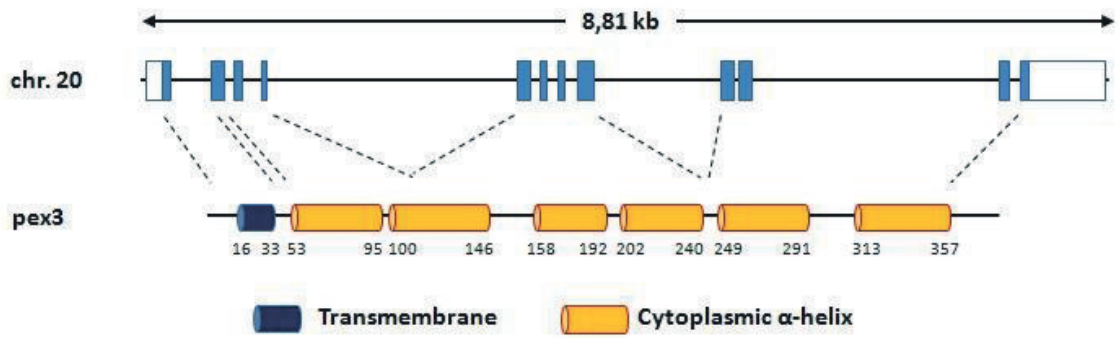

Figure 22 – Schematic representation of pex3 locus in zebrafish genome (full boxes are the coding sequence containing exons, whereas empty boxes are the 5'- and 3'-UnTranslated Regions [UTR]) and of the predicted secondary structure of the encoded peptide (in blue, the predicted transmembrane domain; in yellow, the predicted α-helices; numbers underneath indicate the corresponding amino acids positions in the primary polypeptide structure).

This prediction is in line with previous studies (Sato et al. 2010; Schmidt et al. 2012b) showing a similar topology of the protein after crystal structure determination. Multiple protein sequences alignment shows that the predicted transmembrane domain and α-helices align with the correspondent regions in the homologous proteins of other model organisms (Figure 23). These regions of the protein are demonstrated to be critical for the binding of the main interaction partner, pex19, and they are described to be necessary for the insertion of peroxisomal membrane proteins into the peroxisomal membrane (Sato et al. 2010). In fact, identity scores from the alignments of zebrafish pex3 with the correspondent regions of the human or murine homologs show even higher degree of conservation in comparison to full-length alignments (Table 5). The identity scores range between 87% and 100%, except for the fourth α-helix, which shows higher variability (Figure 22 and Table 3). The most heterogeneous regions lie on the coiled-coil strands linking the different α-helices, in particular the one between α-helix 5 and α-helix 6. These regions were not described to have a special function, other than allowing a certain flexibility of the remaining polypeptide chain in such a way to accommodate the interaction with other proteins.

	Transmem.		α-hel 1		α-hel 2		α-hel 3		α-hel 4		α-hel 5		α-hel 6	
	Id	**Sim**	**Id**	**Sim**	**Id**	**Sim**	**Id**	**Sim**	**Id**	**Sim**	**Id**	**Sim**	**Id**	**Sim**
HS PEX3	75%	88%	88%	95%	93%	87%	77%	91%	46%	55%	86%	93%	82%	93%
MM Pex3	75%	88%	88%	95%	96%	100%	83%	94%	49%	59%	86%	93%	82%	95%

Table 5 - Identitiy (Id) and similarity (Sim) scores for each of the predicted functional regions of zebrafish pex3 protein (see Figure 22) derived from multiple BLAST alignments with equivalent regions of the human (HS) or murine (MM) homologs.

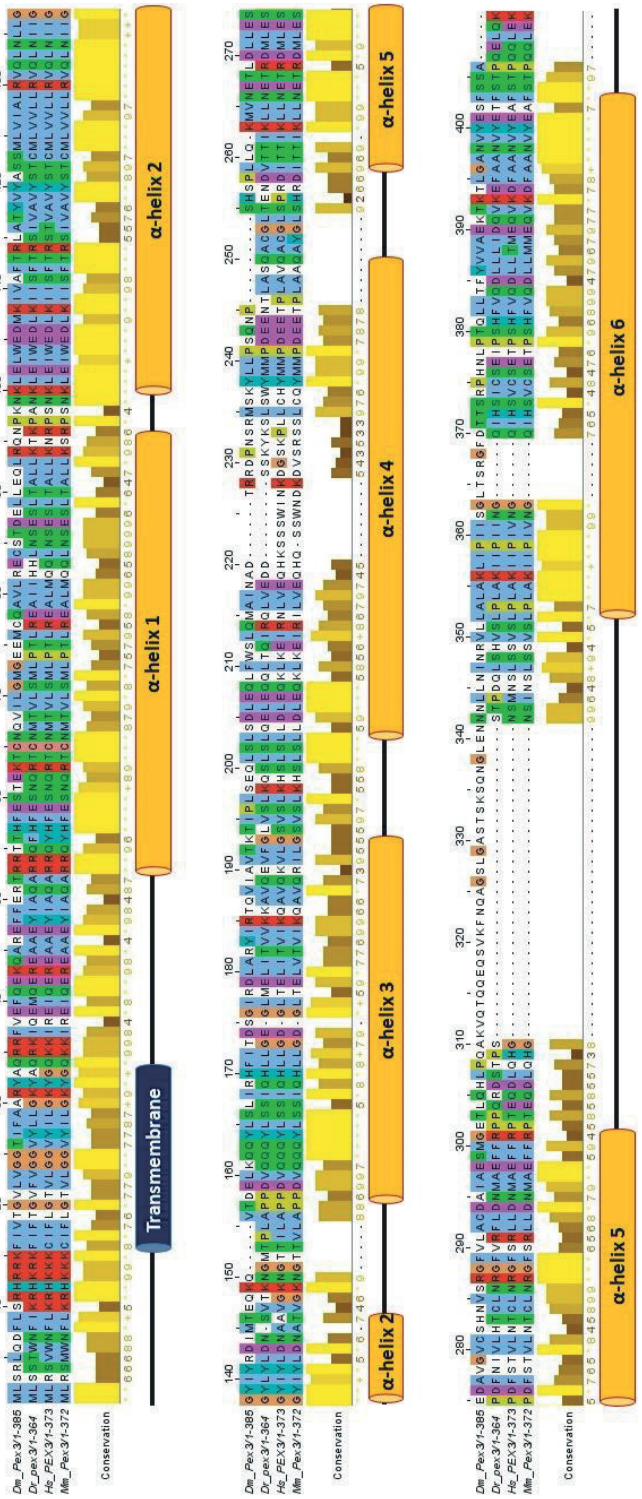

Figure 23 - Multiple alignment of fruit fly (Dm), zebrafish (Dr), human (Hs) and murine (Mm) pex3 proteins. The aligned amino acid sequences were edited for function conservation and residues consensus according to a BLOSUM62 similarity matrix. Colors shadowing indicates similar biochemical properties of the residues, whereas the height of the bars is proportional to the conservation of the region surrounding that specific residue. Predicted domains of pex3 proteins are depicted below the amino acid sequences (see Figure 22).

4.4 *pex3* expression in zebrafish

Following the identification and validation of a single *PEX3* homolog in zebrafish, the expression profile was determined with both an *in silico* and an experimental approach.

Queries to different databases collecting gene expression profiles were made to estimate zebrafish *pex3* expression at different time points, in different tissues or under different physio-pathological conditions or stimulations.

Expressed Sequence Tag (EST) profiles database (Group) shows approximate gene expression patterns as inferred from EST counts and cDNA library sources. According to EST annotation, *pex3* transcript is detected only at the pharyngula stage (24-48 hpf), but not in other stages during embryonic development (Table 6).

Developmental stage	Transcripts per million (TPM)	Gene EST/ Total EST
egg	0	0/3836
gastrula	0	0/6989
segmentation	0	0/11064
pharyngula	40	1/24767
hatching	0	0/42929
larval	0	0/19943
juvenile	0	0/7503

Table 6 – Summary of *pex3* expression pattern in different zebrafish developmental stages according to Expressed Sequence Tag (EST) database.

Experimental gene expression data from Gene Expression Omnibus (GEO) give a more comprehensive view of *pex3* expression. Indeed, *pex3* is detected already during the first cell divisions and its levels constantly increase in the following hours, until the end of embryogenesis. It is likely that the first detected transcripts are maternally derived - this kind of transcripts can be detected up to 5 hpf (Giraldez et al. 2006) – and they are afterwards replaced by embryonic expression, that increases.

As both EST counts and GEO expression profiles may be affected by false positive calls, due to limitation of the techniques, additional experimental approaches were adopted in order to gain a more detailed overview about *pex3* expression. In order to refine the spatio-temporal description of *pex3* expression, qRT-PCR (Figure 24) and *in situ* hybridization (Figure 25) were performed on whole embryos at different stages of the first five days of development. *pex3* transcript can be detected by qRT-PCR already at the earliest tested time point, 8 hpf, and its

levels stay constant also in the following developmental stages (12 hpf, 24 hpf and 48 hpf). Its transcription increased by 2,5-fold at 120 hpf.

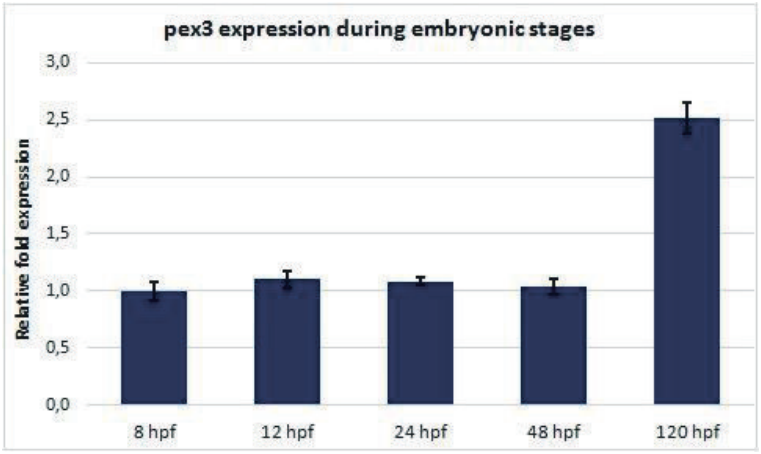

Figure 24 – *pex3* expression determined in different zebrafish embryonic stages *via* qRT-PCR. Expression normalized to the expression at 8 hpf.

While qRT-PCR data give a quantitative information about gene expression, *in situ* hybridization data suggest the spatial gene expression. At 12 hpf, *pex3* expression localizes in all the cells of the yolk syncytial layer, without a particular spatial restriction, meaning that a general requirement of peroxisomes exists, at this stage (Figure 25 A-A'). At 24 hpf, the expression is detectable in all the embryonic tissues, but it is particularly strong in the developing brain region, in the optic cups, and in a cell layer developing along the body axis, presumably the neural crest cells, in the trunk (Figure 25 B-B'). The same expression pattern is observed at 48 hpf. The highest expression localizes in the brain and in the medulla oblungata. Also the developing sensory organs, in particular the optic cup and the otic vesicles, display a strong *pex3* expression, as well as the residual neural crest cell layers (Figure 25 C-C'). *pex3* expression at 120 hpf is the most informative, because the development of the different organs in the zebrafish larva at this stage is completed and the size of the animal allows higher resolution in the pattern description. Once again, the central nervous system and the sensory organs are the areas where the expression of *pex3* is higher. In the central nervous system, telencephalon, medulla oblungata and olfactory epithelium are the most interested parts. In the eye, the expression is not spread anymore, as it was at earlier time points, but it is now restricted in three concentric cell population, namely, proceeding from the middle to the outside, the retinal perinuclear layer, the inner nuclear layer and the outer nuclear layer. Also the gills filaments show high *pex3* expression, whereas in the rest of the body the expression is quite weak. Interestingly, higher magnification of the more superficial epidermal layers shows

the presence of single cells, dispersed in the head regions, whereas in the trunk they line in a stripe on the dorsal part, and in two additional stripes in the lateral part (Figure 25 E-E’’’).

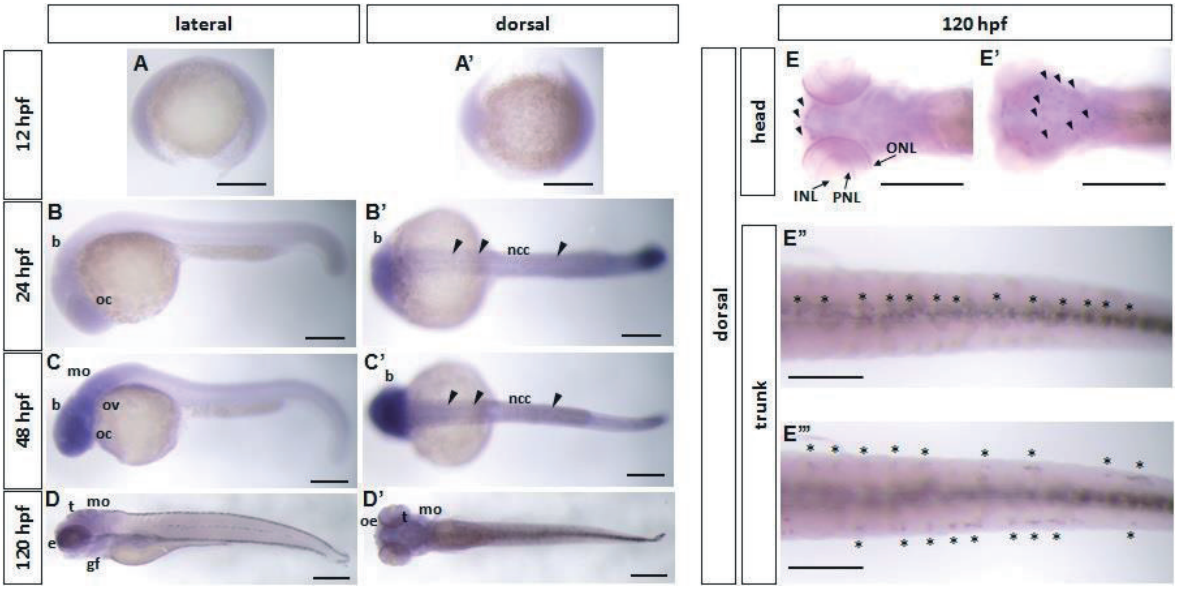

Figure 25 - pex3 expression determined in different zebrafish embryonic stages *via in situ* hybridization. (**A-A’**) 12 hpf. (**B-B’**) 24 hpf. Transcript presence is enhanced in brain (b), optic cup (oc) and neural crest cells (ncc – black arrowheads). (**C-C’**) 48 hpf. *pex3* highest expression localizes in brain (b), medulla oblungata (mo), optic cup (oc) otic vesicles (ov) and in residual neural crest cell layers (ncc – black arrowheads). (**D-D’**) 120 hpf. *pex3* is expressed in telencephalon (t), medulla oblungata (mo), eye (e), gills filaments (gf) and olfactory epithelium (oe). (**E-E’’’**) Higher magnification captures of previous samples show that in the eye, *pex3* expression is restricted in the perinuclear layer (PNL), the inner nuclear layer (INL) and the outer nuclear layer (ONL). Single cells are dispersed in the head regions (black arrowheads) and in the trunk (stars). Scale bars: 200 µm in panels A, A’, B, B’, C and C’; 1 mm in panels D, D’, E and E’; 500 µm in panels E’’ and E’’’.

Since transcription of a gene is not necessarily reflecting its translation into protein, the expression pattern of pex3 was analyzed also with immunofluorescence stainings. The results do not differ from the expression patterns detected with in situ hybridization or qRT-PCR methods. At 5 dpf, pex3 is present in the entire body. The area with the highest pex3 expression is the central nervous system (Figure 26 A): here it is possible to observe groups of cells with enhanced pex3 expression (Figure 26 A’). Interestingly, the protein presence and the expression determined with in situ hybridization mirror each other at the level of the eye, in the already described three concentric cell population: retinal perinuclear layer, the inner nuclear layer and the outer nuclear layer (Figure 26 A’’). In the trunk region it is possible to observe a broad pex3 expression, involving all the tissues. Remarkably, the inter-somite areas are enriched in pex3 protein (Figure 26 B). These areas accommodate the axons projecting from the spinal cord into the peripheral tissues and further along the same direction of the

muscular fascicle bundles. The observation of more superficial layers allows the detection of a group of cells enriched in pex3 protein expression. They line up in a stripe, similarly to what is observed at the transcriptional level with in situ hybridization (Figure 26 B').

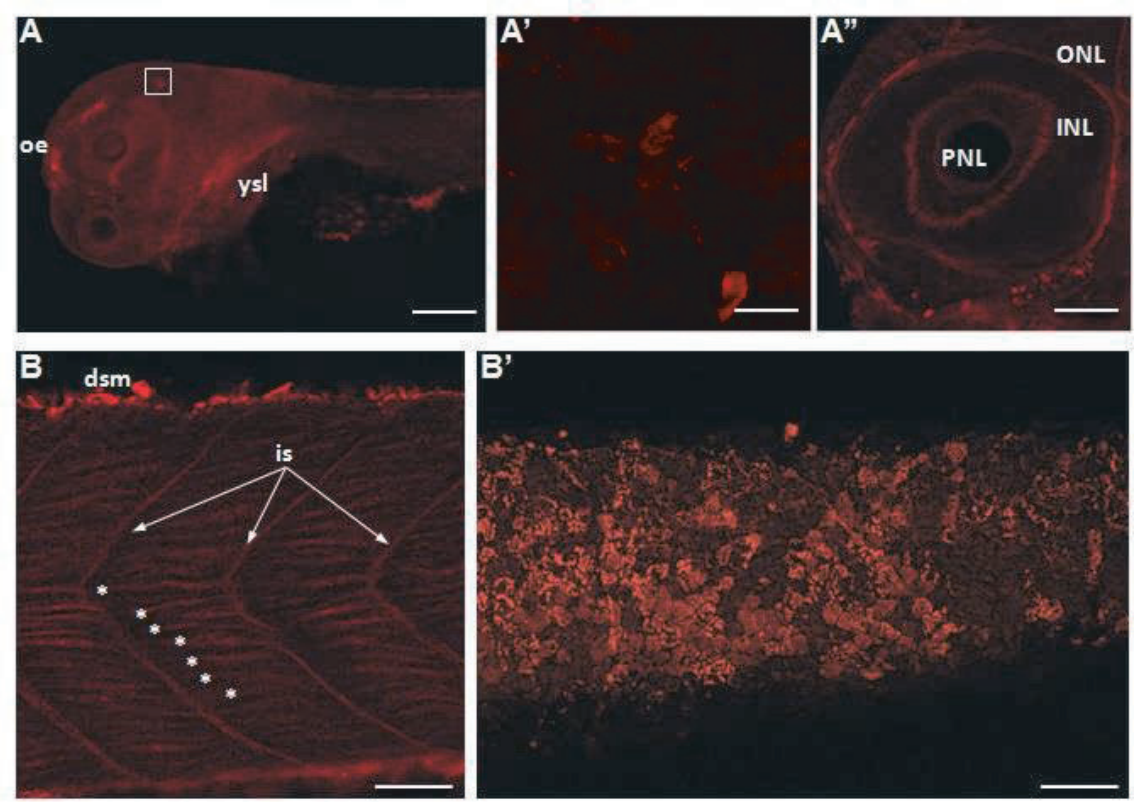

Figure 26 - *pex3* expression determined in 5 dpf zebrafish embryos via immunofluorescence stainings. (**A**) pex3 is enriched in the olfactory epithelium (oe) and in the yolk sack wall layer (ysl). (**A'**) pex3 presence is especially high in the central nervous system and in particular in a group of cells (picture corresponds to box in panel A) (**A''**) In the eye, the retinal perinuclear layer (PNL), the inner nuclear layer (INL) and the outer nuclear layer (ONL) are stained (**B-B'**) In the trunk region pex3 is enriched at the dorsal stripe melanocytes (DSM), in inter-somite areas (is), along the same direction of the muscular fascicle bundles (stars) and in a group of cells in the epidermal layer. Scale bars: 500 µm in panel A; 20 µm in panel B; 200 µm in panel C; 100 µm in panel D; 50 µm in panel E.

EST profiles database offers also expression data related to different organs at the adult stage (Table 7). *pex3* expression is remarkably elevated in the eye, heart, kidney, liver and reproductive system.

Adult organ	Transcripts per million (TPM)	Gene EST/ Total EST
bone	0	0/7413
brain	0	0/88205
eye	16	1/59653
fin	0	0/33258
gills	0	0/12723
heart	33	1/30017
intestine	0	9/4130
kidney	19	1/50205
liver	58	1/17174
lymphoreticular	0	0/1178
muscle	0	0/116351
olfactory rosettes	0	0/35226
reproductive system	22	4/179524
skin	0	0/9225

Table 7 – Summary of *pex3* expression pattern in different organs in zebrafish adult animals according to Expressed Sequence Tag (EST) database.

Similar to what was done for the different stages of embryonic developments, GEO database was queried. For adult zebrafish, pex3 expression data are referred to different physiological conditions or in response to different stimulations. Analysis restricted to specific organs shows that pex3 expression is remarkably elevated in the whole brain, and in particular in the pineal gland, without a specific tendency in relation with the night hours - pineal gland produces melatonin- and serotonin-derived hormones, modulating the circadian rhythm - the gender or the age of the fish (Toyama et al. 2009; Arslan-Ergul & Adams 2014).

qRT-PCR experiments performed on isolated organs from adult animals confirmed ubiquitous expression of pex3, but the highest expression was detected in brain (approximately 8-fold, when normalized to whole body) and in ovaries (approximately 8-fold). Other organs in which the transcript was detectable at relatively high levels were heart, kidneys and eyes (Figure 27).

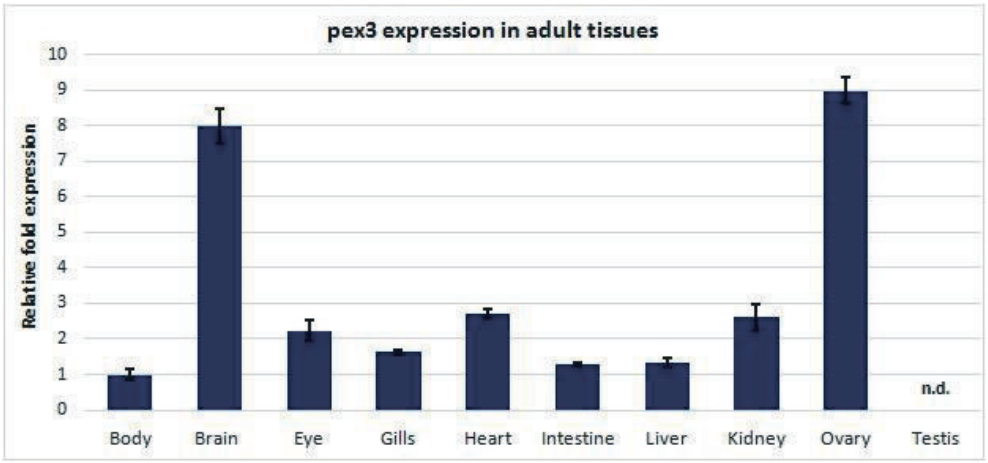

Figure 27 - *pex3* expression determined in different organs in zebrafish adult animals *via* qRT-PCR. Expression normalized to whole body (remaining carcasses). n.d. = not determined.

4.5 *Pex3* morphants do not show abnormal development

Due to the strong expression of the gene already during the first embryonic developmental stages, the possibility to obtain information about *pex3* function, knocking down the translation of the mRNA into protein using antisense morpholino oligonucleotides (AMOs) was explored. At least two different strategies can be designed for AMO-based experiments. They can either bind the mature mRNA molecules in proximity of the start codon, preventing the ribosome to dock and start the translation, or the pre-mRNA on a splicing site, causing the retention of an intron or the skip of an exon, statistically resulting in frameshift of the open reading frame in two out of three cases (Ekker 2000).

A *pex3* translational blocker morpholino (pex3 AMO TB) was used and the injected amount was titrated, in order to find the optimal quantity inducing a phenotype without toxicity. It was determined that zebrafish embryos tolerate up to 375 fmol of pex3 AMO TB, whereas higher amounts induced complete lethality within 8 hpf, hinting to an unspecific effect of the injected molecule. pex3 AMO-injected embryos were observed for lethality, development and behavioral defects (Figure 28).

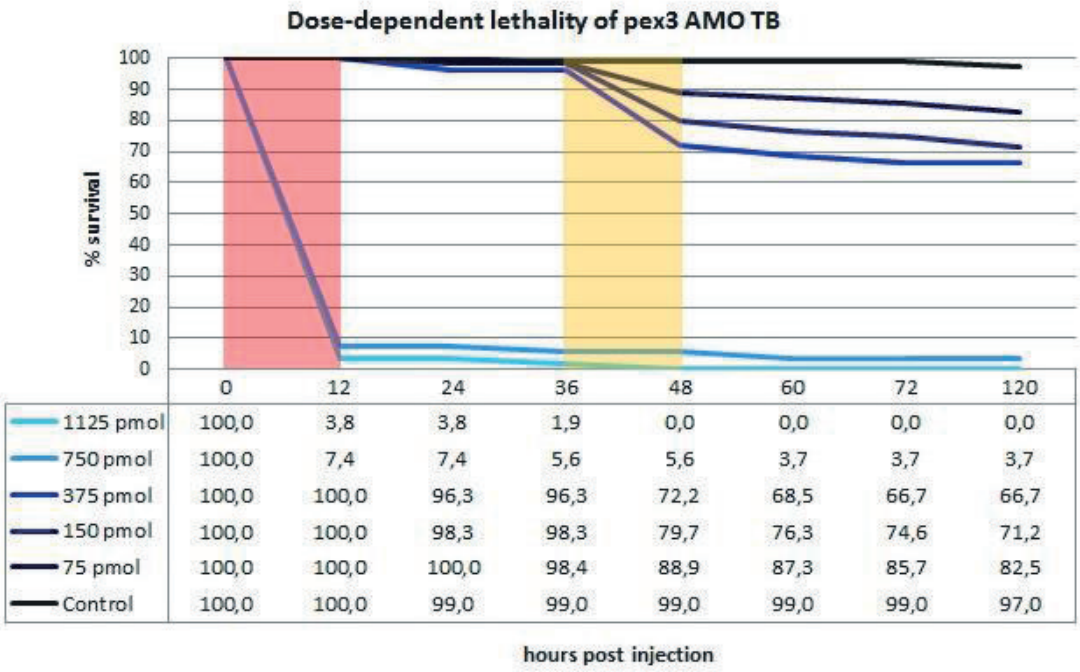

	0	12	24	36	48	60	72	120
1125 pmol	100,0	3,8	3,8	1,9	0,0	0,0	0,0	0,0
750 pmol	100,0	7,4	7,4	5,6	5,6	3,7	3,7	3,7
375 pmol	100,0	100,0	96,3	96,3	72,2	68,5	66,7	66,7
150 pmol	100,0	100,0	98,3	98,3	79,7	76,3	74,6	71,2
75 pmol	100,0	100,0	100,0	98,4	88,9	87,3	85,7	82,5
Control	100,0	100,0	99,0	99,0	99,0	99,0	99,0	97,0

Figure 28 – Dose-dependent lethality of pex3 translational blocker (TB) antisense morpholino oligonucleotide (AMO) monitored in the first 5 dpf. At high amounts (>750 pmol) pex3 AMO TB causes nearly complete lethality within 12 hpf (red box), whereas at lower amounts there is a dose-dependent lethality taking place between 36 hpf and 48 hpf (yellow box). Numbers represent percentage of survived injected embryos at each time point.

After injecting different quantities of pex3 AMO TB in one-cell stage embryos, a dose-dependent lethality of about 30% was observed between 36 hpf and 48 hpf, upon injection of the highest tolerated amount (Figure 28). After this stage and up to 5 dpf, there is no difference between the experimental groups in terms of survival rate. Surviving embryos do not show any phenotypical difference in comparison to control embryos and the swimming behavior is not altered. In light of this observation, it is possible to conclude that *pex3* knock down via AMO is able to induce a response which is specific and limited to a specific developmental time window (36 hpf – 48 hpf), but its efficiency is still not sufficient to allow an accessible phenotype analysis. Nevertheless, these preliminary results hint to a role of *pex3* during development, within 48 hpf.

4.6 Generation and validation of a *pex3* loss of function zebrafish model

As described, *pex3* ubiquitous expression starts early during zebrafish embryonic development, with already a strong maternal component and it greatly increases until the adulthood, with an enrichment in specific organs (brain, liver, kidney, reproductive system).

Based on phenotypical important effects of a *Pex3* mutation in yeast (Kiel et al. 1995; Hettema et al. 2000) or in fruit fly (Nakayama et al. 2011), main developmental defects were expected also in zebrafish embryos. Nevertheless, the antisense morpholino oligonucleotide approach proved to be limiting, due to the lack of an evident morphant phenotype.

To address these issues, different strategies were used with the goal of generating a *pex3* loss of function model in zebrafish. On one side, biased genome targeting technologies, such as TALENs or CRISPR/Cas9, were used to generate DNA double strand breaks in the *pex3* locus, to induce non homologous end joining (NHEJ)-mediated imprecise repairs. On the other, alleles from random ENU-induced mutagenesis screening were available and used for pex3 functional analysis.

4.6.1 TALENs-guided mutation generation

In order to generate a *pex3* loss of function model, the largely accessible TALENs were used, in first instance (Clark et al. 2011). Three TALEN pairs targeting the first exon, differing for targeting site or length of the spacer between the pairs, were generated. The three chosen sequences were verified for specificity using BLAST algorithm, searching for similar sequences in zebrafish genome and none of the hits could fully cover any target sequence, except for the *pex3* genomic sequence, with less than four mismatches (Table 8).

TALEN ID	Sequence	Gene	Identity	E-value
10L	TCTGTTAAAATGTTGAGTTC	transmembrane protein 251 (tmem251)	16/20	1,4
		heat shock transcription factor 1 (hsf1)	16/20	1,4
		zgc:171695	15/20	5,6
12L	TTTCATCAAACGCCATAAGA	uncharacterized LOC103909823	15/20	5,6
		si:ch1073-90m23.1	15/20	5,6
		phospholipid-transporting ATPase ID-like	15/20	5,6
		zgc:158296	15/20	5,6
10R	TTCCTCTTATGGCGTTTGAT	phospholipid-transporting ATPase ID-like	15/20	5,6
11R	TTTCCTCTTATGGCGTTTGA	phospholipid-transporting ATPase ID-like	15/20	5,6
12R	TTACCTCCAACAAACACCCC	solute carrier family 12 (sodium/chloride transporters), member 3	16/20	1,4
		family with sequence similarity 3, member C (fam3c)	16/20	1,4
		suppressor of variegation 3-9 homolog 1b (suv39h1b)	15/20	5,6
		uncharacterized LOC101882959	15/20	5,6
		protein arginine methyltransferase 9 (prmt9)	15/20	5,6
		cytoplasmic polyadenylation element binding protein 3 (cpeb3)	15/20	5,6
		family with sequence similarity 3, member A (fam3a)	15/20	5,6
		zgc:195220	15/20	5,6
		homeodomain interacting protein kinase 1a (hipk1a)	15/20	5,6

Table 8 – Identification of the possible off targets in the TALEN-based mutation generation approach. Each DNA binding sequence was verified and genes with less than five mismatches were anotated.

All constructs were validated in a cell culture system for cutting efficiency, as well as for efficacy in inducing frameshift mutations (see Appendix). According to the results of the preliminary test, TALEN pair 10L/10R is the most effective in generating a frameshift mutation. This pair was then chosen to produce mRNAs to be injected into zebrafish embryos. Different concentrations of the TALENs mRNA pair were tested to optimize the balance between efficient mutation induction and survival rate, and the best conditions were found to be the injection of a total amount of 200 pg of mRNA, with the two constructs at a 1:1 ratio.

4.6.2 CRISPR/Cas9-guided mutation generation

Alternative to TALENs, a CRISPR/Cas9-based targeting approach was used, since it promised higher efficiency and allows more flexibility in target design. With the help of ZiFiT targeter software package (Sander et al. 2010), two suitable target sites close to the 5'-end of *pex3* sequence were identified, one in intron 1 and the other in exon 3. The two identified candidate targets were screened for potential off targets using CRISPOR (Haeussler et al. 2016), an algorithm implementing eight other off target prediction tools, taking into account different parameters including efficiency score, guide activity and method of sgRNA production. Both targets possess a specificity score higher than the threshold, they have the highest predicted efficiency scores (Moreno-Mateos et al. 2015) and there is no locus in the genome with less than three mismatches in the seed sequence (12 bp adjacent to the PAM), ensuring low likelihood of off target binding (Table 9).

sgRNA ID	Sequence	Specificity score	Predicted efficiency	Gene	Off target sequence (mismatches)
Exon3	GGTGATGGATGATTGCCTCT	93	42	fynb	GATTATGGTTGATTTCCTCT * * * *
				ARHGEF12 (1 of 2)	GGAGTTGGATGATTTCCTCC * * * *
				klf3	GGCGATGGAGGACTGGCTCT * * * *
				cers4a	TGTGGTGGATGATTTGCTCT * * **
				si:ch211-79l20.4	GCTGATGGATGATGGCTTTT * * * *
Intron1	GGAATTTTTAGTCAACAGAA	65	25	CR391998.1	GGAATTTTTATTGAACACAG * * * *
				LTN1	GCAACTTTTATTCAACAAAA * * * *
				nop58	GGAGTGTTGAGTCACCAGAA * * * *
				SERBP1 (3 of 3)	CTAATGTTTAGTCGACAGAA ** * *
				si:ch211-229i14.2	GCCATTTTTGGTCAACAAAA ** * *
				slc35d1a	GTAATGTTTAATCTACAGAA * * * *
				slc6a2	GGATTTTGAAGTCATCAGAA * ** *

Table 9 – Specifity and efficiency prediction of the target sequences of the CRISPR/Cas9-based mutation generation approach and identification of the possible off targets. Specificity scores ranges from 0 to 100; scores above 50 are recommended (Hsu et al. 2013). Efficiency prediction according to (Moreno-Mateos et al. 2015). Each DNA binding sequence was verified for ff targets with CRISPOR (Haeussler et al. 2016) and genes with four mismatches in an exon or in a predicted regulatory region were anotated, including the off target sequence (stars show the mismatches).

The two constructs were validated directly in zebrafish embryos, injecting different amounts of sgRNA or Cas9 mRNA, at different ratios, in order to balance mutation induction efficacy with the toxic effects of injection of high quantities of nucleic acids. Both tested constructs effectively cut the targeted regions and induce frameshift mutations (see Appendix). For this reason, being desirable to induce a mutation in the protein coding sequence, only the exon3-targeting sgRNA was used to establish a mutant allele. Optimal conditions for efficiently induce mutation were found to be in the injection of 12,5 pg of sgRNA and 25 pg of Cas9 mRNA.

4.6.3 Commercial ENU-induced mutagenesis alleles

In the course of the generation of mutant *pex3* alleles with TALENs or CRISPR/Cas9 methods, the Wellcome Trust Sanger Institute made two additional alleles available. They were identified in the context of the Zebrafish Mutation Project (ZMP) (Kettleborough et al. 2013).
The allele *sa17571* carries an A>T missense mutation in the second exon and the resulting stop codon substitute amino acid 36, proximal to the C-terminus of the transmembrane segment, depriving the cytoplasmic protein interaction domain. The allele *sa11684* generates two different splicing variants due to a G>A mutation in the essential splicing site at the 5' of intron 11. The mutation causes the retention of the intron (Figure 29). According to bioinformatics predictions, it interrupts the natural protein sequence after amino acid residue 337, at the C-terminal part of the sixth α-helix, and introduces five more amino acids encoded by the intron, followed by a stop codon (see Appendix). Nevertheless, the mutation in the *sa11684* allele creates a cryptic splicing site, since in homozygous carriers it is still possible to detect the wildtype transcript, beside the one retaining intron 11, being then impossible to use this allele for the generation of a *pex3* loss of function model in zebrafish.

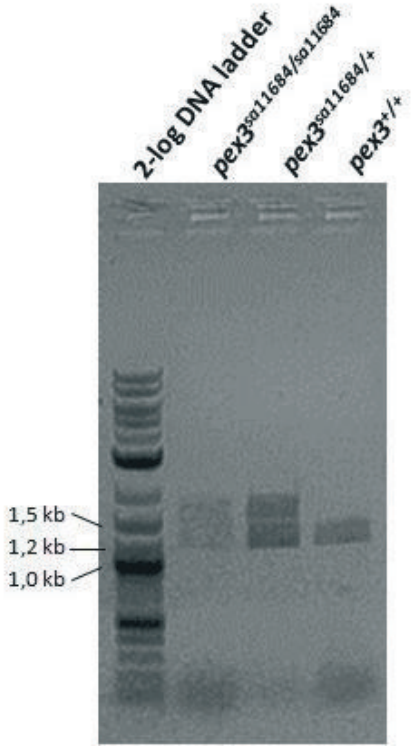

Figure 29 – Validation of the *pex3*^{sa11684} ENU allele. The mutation should affect a donor splicing site, causing the retention of the intron between exon 11 and exon 12. Wildtype sample shows a single band corresponding to *pex3* mRNA at around 1,2 kb; heterozygous sample shows an additional band for a longer mRNA; homozygous mutant sample shows the same pattern of the heterozygous, hinting to the fact that the mutation causes only a partial misplicing of the transcript (cryptic splicing site).

4.6.4 Establishing High Resolution Melting Analysis (HRMA) to validate mutant alleles

One of the biggest challenges in generating a new allele via genome editing methods is the identification of mutated alleles. In fact, the events at the targeted region vary from a single base pair exchange, without a change in the transcript size, to a single base pair insertion or deletion, to indels spanning a few dozen nucleotides. Because of this, conventional molecular biology methods (PCR or Southern Blot) are not suitable, since they are not able to discriminate different alleles. Different strategies were developed for the detection of these allele variants consisting in small variation, including Restriction Fragment Length Polymorphism (RFLP)(Cooper & Schmidtke 1984), T7 or surveyor endonuclease digestion (Vouillot et al. 2015) or methods based on different mobility of heteroduplexes (Cariello & Skopek 1993). In this work, a High Resolution Melting Analysis (HRMA) approach was adopted (Vossen et al. 2009). This strategy relies on the difference in melting profiles of short amplicons, monitored by the release of an intercalating fluorescent agent at the increase of

the temperature. The method allows the detection of small insertions or deletion or even single nucleotide exchanges. The presence of different alleles generated with genome editing techniques can be discriminated, given a high sensitivity of the detection instrument in terms of smallest temperature variation possible.

In the case of TALEN- or CRISPR/Cas9-generated mutant alleles, animals injected at the one-cell stage were analyzed for somatic mutations at the age of three months, using as specimen a caudal fin clip. It is known that there is a positive correlation between somatic mutations and germ line transmission (Bedell et al. 2012).

For the TALEN-based generation of a *pex3* mutant allele, twenty-four candidate fish were tested and two of them (2/24, 8%) displayed a melting profile of the amplicon deviating from that of wildtype reference sample (Figure 30). Positive hits were confirmed *via* sequencing of the HRMA amplicons. One of the candidate mutant alleles was a six-nucleotide deletion in the spacer region between the two DNA binding sequences, resulting in the deletion of amino acids at positions 5 and 6 (threonine and tryptophan). The other candidate was an eight-nucleotide deletion, predicted to produce a frameshift in the open reading frame with a premature stop codon after 9 amino acids (see Appendix). The fish somatically carrying the eight-nucleotide deletion was used to establish a mutant line by crossing it with wildtype breeder, and F1 progenies were screened for the mutation. Indeed, sequencing of the *pex3* locus in the F1 progeny highlighted that some of the animals were carrying the same mutation detected in the F0 parental fish (see Appendix).

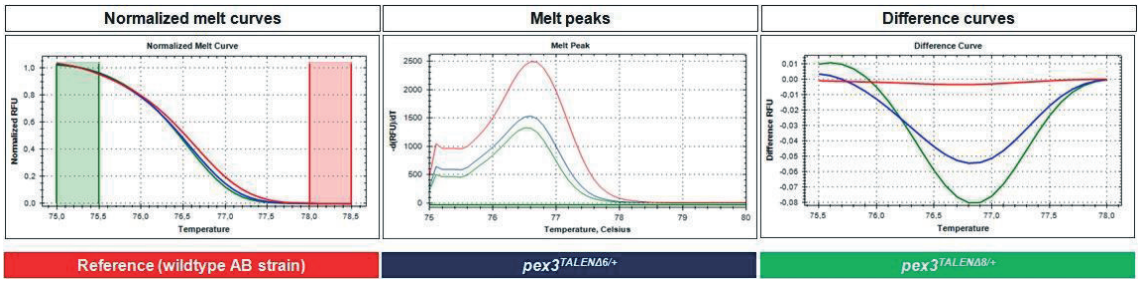

Figure 30 – HRMA identification of the TALEN-generated mutant *pex3* alleles. Normalized melt curves (fluorescence of the sample during the melting steps, normalized to the maximum set to 100%), melt peaks (first derivative graphs of the previous panels) and difference curves (difference of the curves in the first panel with the one set as reference, namely the wildtype sample) are represented. Only the wildtype reference (in red) and the positive candidates (six nucleotides deletion in blue and eight nucleotides deletion in green) are depicted in the panels.

Similarly, also the CRISPR/Cas9-injected fish were tested for the presence of somatic mutations in *pex3* locus. Five out of thirteen screened fish (5/13, 38%) displayed altered melting profiles

of the amplicon when compared to the wildtype reference sample (Figure 31). HRMA amplicons were sequenced to confirm the results. Two candidates revealed no difference in the sequence. Other three positive hits represented respectively a single nucleotide exchange, resulting in a predicted silent mutation, a three-nucleotide deletion, resulting in the deletion of amino acids in position 78 (glutamic acid), and a two-nucleotide deletion, predicted to produce a frameshift in the open reading frame with a premature stop codon after 94 amino acids (see Appendix). The fish carrying this last allele was crossed with a wildtype breeder and F1 progenies were screened for the mutation. Indeed, some F1 generation fish were carrying the mutated *pex3* allele identified in the F0 parental fish (see Appendix).

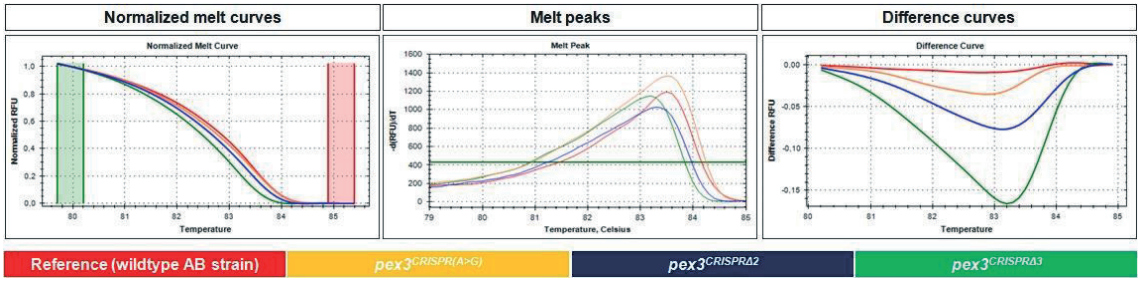

Figure 31 - HRMA identification of the CRISPR/Cas9-generated mutant *pex3* alleles. Normalized melt curves (fluorescence of the sample during the melting steps, normalized to the maximum set to 100%), melt peaks (first derivative graphs of the previous panels) and difference curves (difference of the curves in the first panel with the one set as reference, namely the wildtype sample) are represented. Only the wildtype reference (in red) and the positive candidates (point mutation in yellow, two nucleotides deletion in blue and three nucleotides deletion in green) are depicted in the panels.

Same validation process was used also for the identification of fish carrying the commercial allele sa17571 (Figure 32).

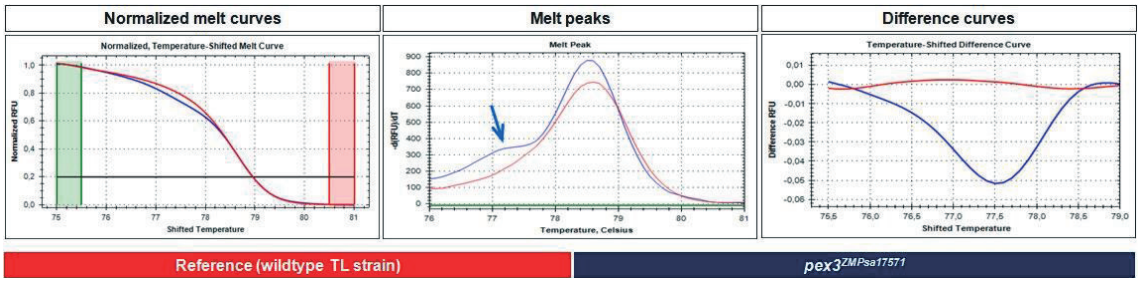

Figure 32 - HRMA identification of the commercial ENU-generated mutant *pex3*^{sa17571} allele. Normalized melt curves (fluorescence of the sample during the melting steps, normalized to the maximum set to 100%), melt peaks (first derivative graphs of the previous panels) and difference curves (difference of the curves in the first panel with the one set as reference, namely the wildtype sample) are represented. Wildtype reference (in red) and a positive heterozygous candidate (in blue) are depicted in the panels. In the melt peaks graph is possible to distinguish the classical 'shoulder' emerging in heterozygous samples (arrow).

All the above described methods for the generation of mutant alleles imply severe drawbacks, namely the possibility of off targets or secondary hits in other loci in the genome. In particular, TALENs DNA binding domain and CRISPR/Cas9 sgRNA could recognize other similar regions in the genome, since it is demonstrated for both methods that few mismatches are tolerated, allowing the binding and the activation of the effector endonucleases (Koo et al. 2015; Pattanayak et al. 2014). ENU mutagenesis generated alleles, however, could carry a second unscreened hit in another independent locus on the same chromosome, for example, and it may segregate with the mutated gene of interest, causing an unrelated phenotype. In this project, in order to rule out off target mutations in the CRISPR/Cas9-generated mutant *pex3* allele and potential secondary hits in the ENU-generated mutant, experiments were performed on trans-heterozygous CRISPR and *sa17571* carriers, hereafter named pex3$^{CRISPR/ZMP}$ (Figure 33).

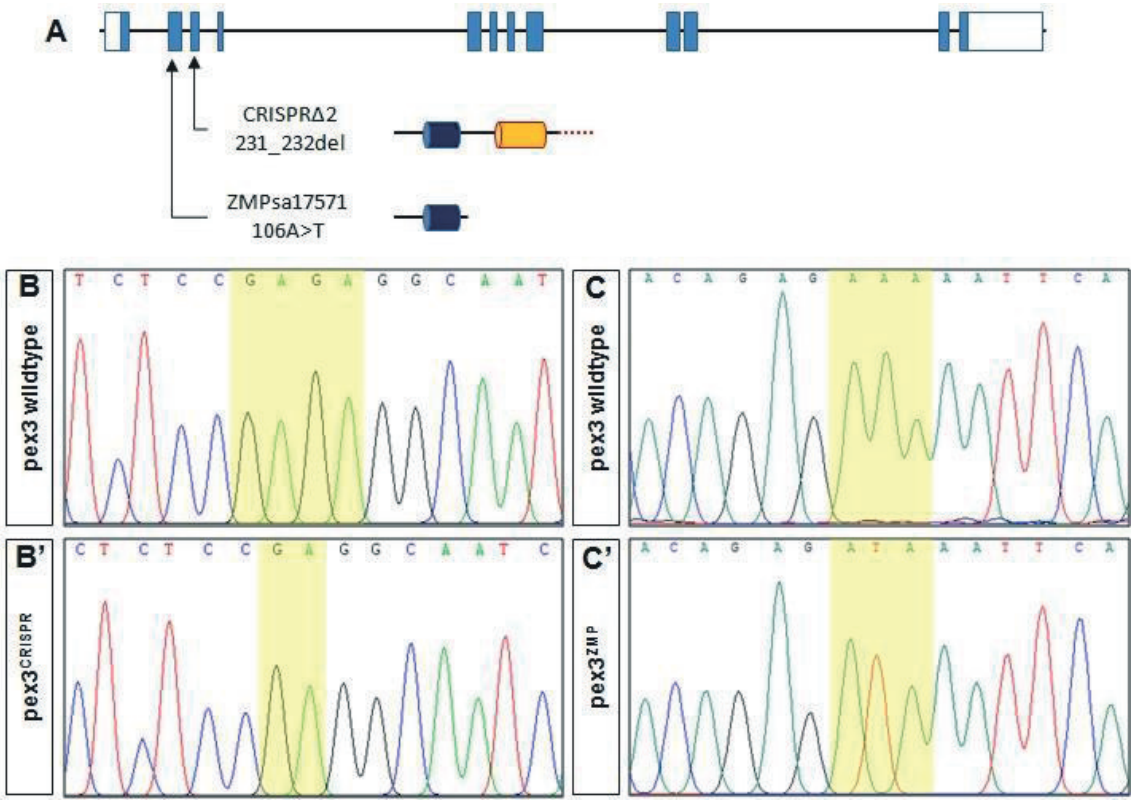

Figure 33 – Summary of the generated trans-heterozygous *pex3* mutant model. (**A**) The two regions targeted with CRISPR/Cas9 and by the Zebrafish Mutation Project approach respectively are indicated in the structure of zebrafish *pex3* gene. The resulting mutations and the predicted generated peptides are indicated (predicted transmembrane domain in blue, residual α-helix in yellow and frameshifted peptide in red dots). (**B-C'**) Sequencing validation of pex3^{CRISPR} (B') and the pex3^{ZMP} (C') mutant alleles; the yellow boxes highlight the mutation (in comparison to wildtype alleles, B and C).

4.7 In *pex3* mutants peroxisomal and mitochondrial metabolism is impaired, resulting in increased oxidative stress

Since pex3 is known to be one of the key regulator of peroxisome homeostasis in eukaryotic cells, a loss of function in this gene is expected to impair the peroxisome biogenesis process, with repercussion on the metabolic reactions catalyzed by enzymes residing in the organelle. Studies in other model organisms indicate that the detrimental effects of a pex3 mutation are principally caused by an altered metabolism. In *Y. lipolitica*, survival of Δpex3 cells is dependent on the energy source on which the yeast is grown and this is explained with the required presence of peroxisomes to process the substrate (Bascom et al. 2003). In *D. melanogaster*, the pex3 full knock out is larval lethal (Nakayama et al. 2011), whereas a tissue-specific knock out in muscles results in lethality at the pharate adult stage, impaired wing extension and decreased locomotion (Faust et al. 2014). This last phenotype is independent from neuronal activity, but it is related to fatty acid metabolism for energy production, with a toxic accumulation of long acyl chain lipids and ROS in the tissues, leading to mitochondrial damage. Surprisingly, pex3$^{CRISPR/ZMP}$ fish do not show any premature lethality: they complete the embryonic developmental stage and they survive until adulthood. With this background information, we focused our analysis on peroxisome and mitochondria function, trying to identify any detrimental consequence at the cell level.

4.7.1 In *pex3*$^{CRISPR/ZMP}$ zebrafish peroxisomal metabolism is impaired

4.7.1.1 Pex3 is essential for peroxisome biogenesis also in zebrafish

Pex3 is one of the key regulators of peroxisome homeostasis, being involved in the regulation of their size and number. The main function of pex3 lies in the *de novo* peroxisome biogenesis, where it defines pre-peroxisomal domains on the endoplasmic reticulum and it is the interaction partner of pex19, the cytosolic chaperon of peroxisomal membrane proteins. pex3 loss of function impairs peroxisome biogenesis. Indeed, in pex3$^{CRISPR/ZMP}$ embryos, there is no signal for pex3 protein, indicating that the protein is not produced. Even the predicted peptide derived from the translation of the CRISPR/Cas9-generated allele, that might be detected since the antibody epitope covers the amino acid residues 31-80 at the N-terminus of the protein, is not produced or is immediately degraded. Immunofluorescence staining for one of the proteins exclusively residing in the peroxisomes, catalase (cat), revealed an alteration of the distribution pattern, in absence of pex3 (

Figure **34**). This effect is the same observed in other models for Peroxisomal Biogenesis Disorders, in which peroxisomes are not competent for protein import anymore. Thus, peroxisomal enzymes remain soluble in the cytoplasm, they are misrouted to other cellular compartments such as endoplasmic reticulum or lysosomes, or they enter the degradation pathway (Shimozawa et al. 1999; Ghoneim et al. 2011).

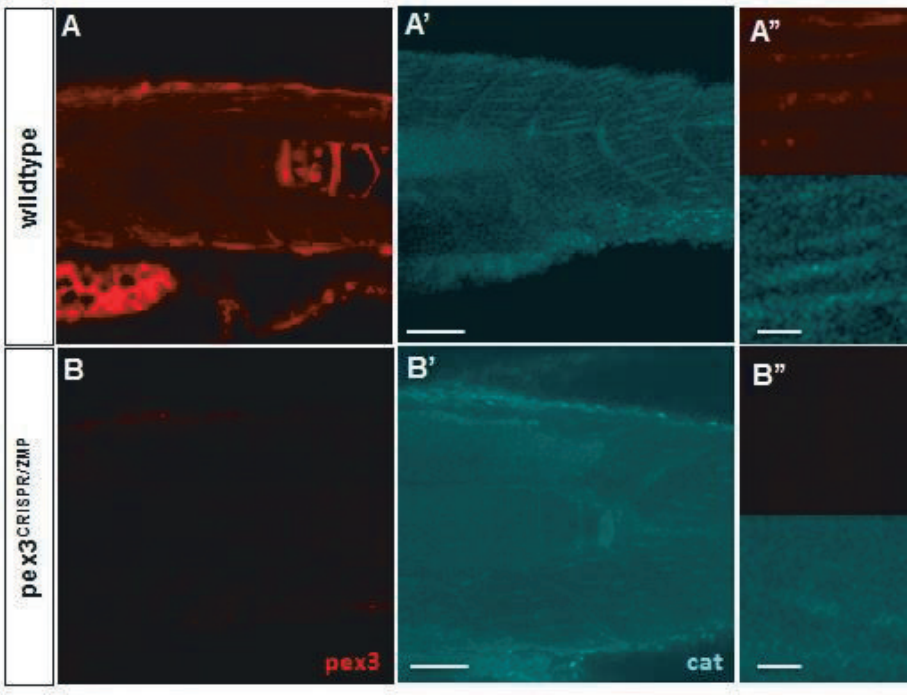

Figure 34 – Immunofluerescence staings for validation of pex3 knock out and assessment of peroxisomal function. (**A-B**) In trunk region of pex3$^{CRISPR/ZMP}$ embryos, no signal for pex3 protein is detectable (B), in comparison to wildtype (A) indicating that the protein is not produced. (**A'-B'**) In absence of pex3, the peroxisomal marker catalase lose the vesicular pattern resembling the one of pex3 (A') and the protein is rather diffuse and spread in the cell (B'). (**A''-B''**) Magnification of areas from previous panels. Scale bars: 200 µm in panels A, A', B and B'; 20 µm in panels A'' and B''.

4.7.1.2 Absence of peroxisomes lowers the energy status of zebrafish

Having verified that peroxisomes are missing in pex3$^{CRISPR/ZMP}$ embryos and that this defect is not lethal, it was investigated whether the mutation has an impact on cell biology and metabolism. In previous studies, the absence of peroxisome was described to cause the impossibility of processing fatty acids as energy substrates. They eventually accumulate in the organism, causing toxicity (Bascom et al. 2003; Faust et al. 2014). Due to the fact that missing peroxisome prevent the efficient use of a number of carbon sources and they do not only provide energy, but also building blocks for growth sustainment, peroxisome defects result in retarded growth. (Poirier et al. 2006; Fan et al. 1996). The development of pex3$^{CRISPR/ZMP}$, compared to wildtype siblings, was followed in the first 90 dpf, until the breeding adult stage.

Different body parameters were monitored, including wet weight, body length, tail length (compared to total body length) and body/yolk area ratio (Bagatto et al. 2001) (Figure 35).

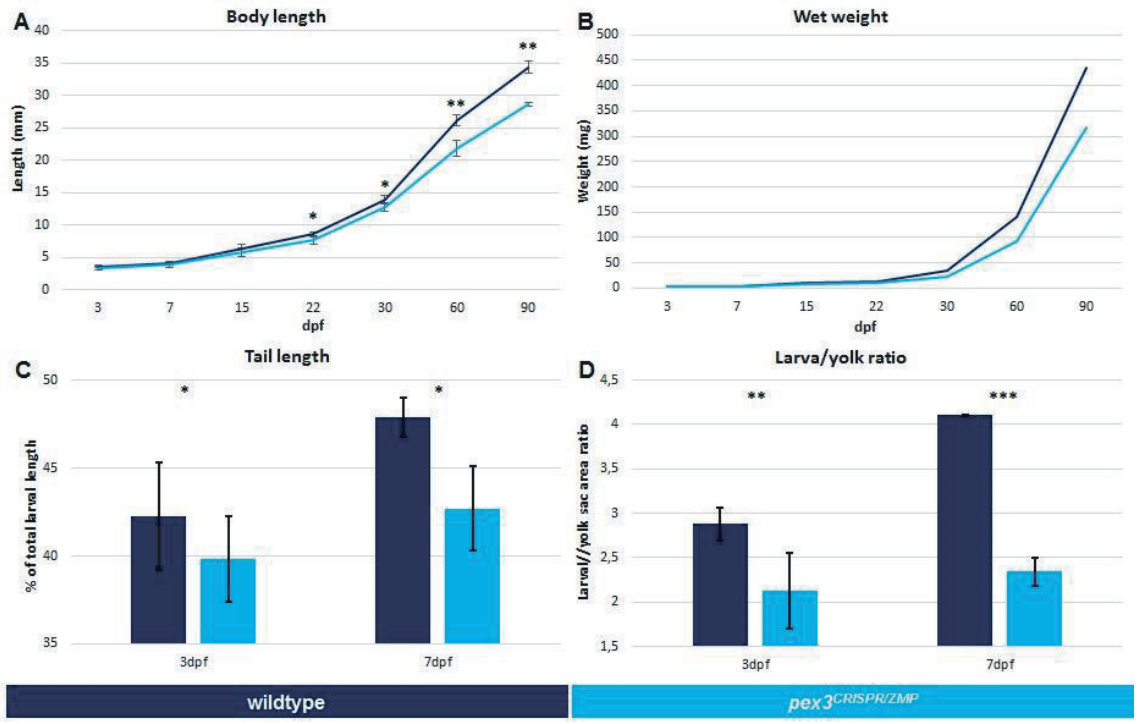

Figure 35 – Effects of the impaired peroxisome function on growth. (**A**) Zebrafish *pex3*$^{CRISPR/ZMP}$ are delayed in growth, when compared to wildtype siblings, especially after the feeding starts. (**B**) *pex3*$^{CRISPR/ZMP}$ mutants do not gain weight as fast as wildtype siblings, being on average approximately 27% lighter at 90 dpf. (**C-D**) Growth rate of *pex3*$^{CRISPR/ZMP}$ mutants is reduced during embryonic and early larval stages. At 7 dpf, there is a significant difference in tail length (compared to total body length) and in the larva/yolk sac area ratio, when compared to wildtype siblings. This values hints to a reduced absorption of the lipids from the yolk sac during the first developmental stages.

During the first 7 dpf both size and weight of the embryos of the two groups do not differ significantly (Figure 35 A-B), since larvae do not feed consistently during this stage (mouth apparatus opens only at 5 dpf - Kimmel et al. 1995). Nevertheless, at 7 dpf, the tail length is shorter and body/yolk area ratio is significantly lower in pex3$^{CRISPR/ZMP}$ larvae, indicating that the yolk consumption is reduced (Figure 35 C-D). In fact, during the first stages of zebrafish development, when the growth is not sustained by external diet, the only available feeding source are the lipids stored in the yolk sac, which are mobilized and processed by peroxisomes, particularly abundant in the yolk sac wall (Krysko et al. 2010). Later on, starting at 22 dpf, the body length profile of the two groups diverges, being significantly different, with pex3$^{CRISPR/ZMP}$ juvenile larvae approximately 17% shorter in comparison to wildtype control animals at 90 dpf.

Similarly, also the wet body weight was significantly decreased starting at 15 dpf and at the end of the experiment, pex3$^{CRISPR/ZMP}$ juvenile larvae are approximately 27% lighter. Further experiments would be aimed to determine whether the reduced growth rate is caused by a different feeding behavior of the two experimental groups or by a different way to metabolically process the diet components.

4.7.1.3 In pex3$^{CRISPR/ZMP}$ mutants oxidative stress is increased and mitochondrial activity is reduced

In case of defective peroxisome biogenesis, peroxisomal enzymatic activity is impaired. Thus, detoxification of peroxide compounds and peroxisomal β-oxidation of fatty acids are missing, with a number of effects at the cell level, ranging from gene regulation to biomolecules composition and regulation of cell cycle.

Detoxification of peroxide compounds in peroxisomes involves the action of catalase, transforming H_2O_2 in H_2O and O_2. If this process is impaired or not efficient, as it is in the case of missing peroxisomes, superoxide anion radicals ($O_2^{\cdot -}$) are produced and they react with nitric oxide ($NO^{\cdot}$) to give peroxynitrite ($OONO^-$). It results in an overall increase of the oxidative stress in the cell, with increasing peroxides and decreased amount of $NO^{\cdot}$ (Schrader & Fahimi 2006b). For these reasons, the relative amounts of these compounds in extracts of *pex3*$^{CRISPR/ZMP}$ and of wildtype embryos at 24 hpf and 48 hpf were measured (Figure 36). Levels of peroxides progressively increase by 2,5- to more than 4-folds in the first 48 hours in trans-heterozygous embryos and in parallel also the amounts of $NO^{\cdot}$ dramatically decrease and drop to approximately 20% relative to the wildtype animals.

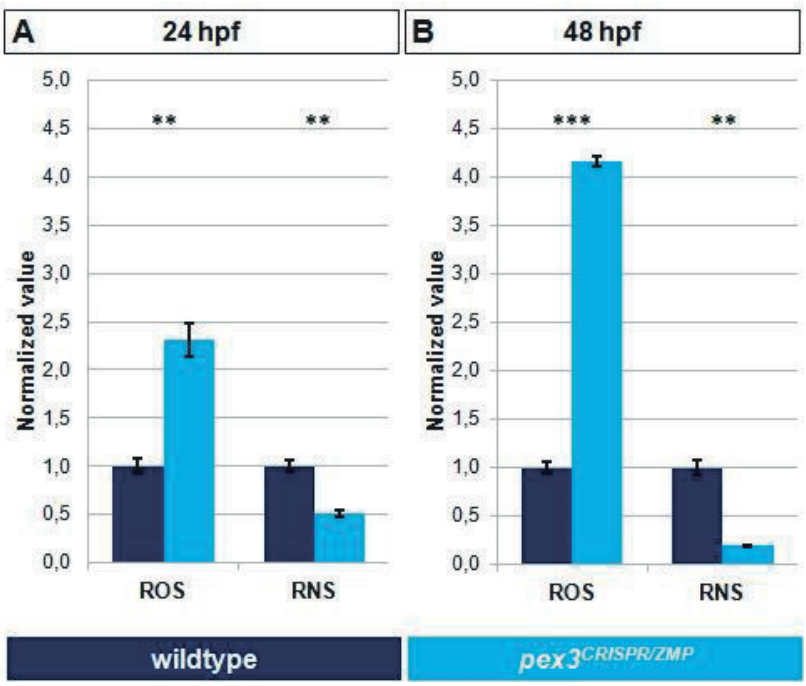

Figure 36 – The defective peroxisomal metabolism increases oxidative stress by increasing the free reactive oxygen species (ROS) and reducing the superoxide anion radicals' nitrogen acceptors (RNS) in a progressive way, between 24 hpf (**A**) and 48 hpf (**B**).

Additionally, to assess the significance of the data *in vivo*, a fluorescent dye for the detection of nitric oxide in cells, the DAF-FM diacetate (4-Amino-5-Methylamino-2',7'-Difluorofluorescein Diacetate) was used. This molecule is non-fluorescent until it reacts with $NO^{\cdot}$ to form a fluorescent benzotriazole, which is additionally trapped in the cell due to the hydrolysis of the diacetate esters (Lepiller et al. 2007). Both wildtype and *pex3*$^{CRISPR/ZMP}$ embryos were stained. Stained embryos highlight that in wildtype conditions, $NO^{\cdot}$ is present throughout the whole body and the concentration is particularly increased in the yolk region (Figure 37 B). In mutant embryos, instead, $NO^{\cdot}$ amount is remarkably reduced and the decrease in the yolk is evident, whereas the central nervous system remains the only area where $NO^{\cdot}$ is detectable (Figure 37 D). This is explained by the presence of a different non-peroxisomal isoform of nitric oxide synthase in neurons.

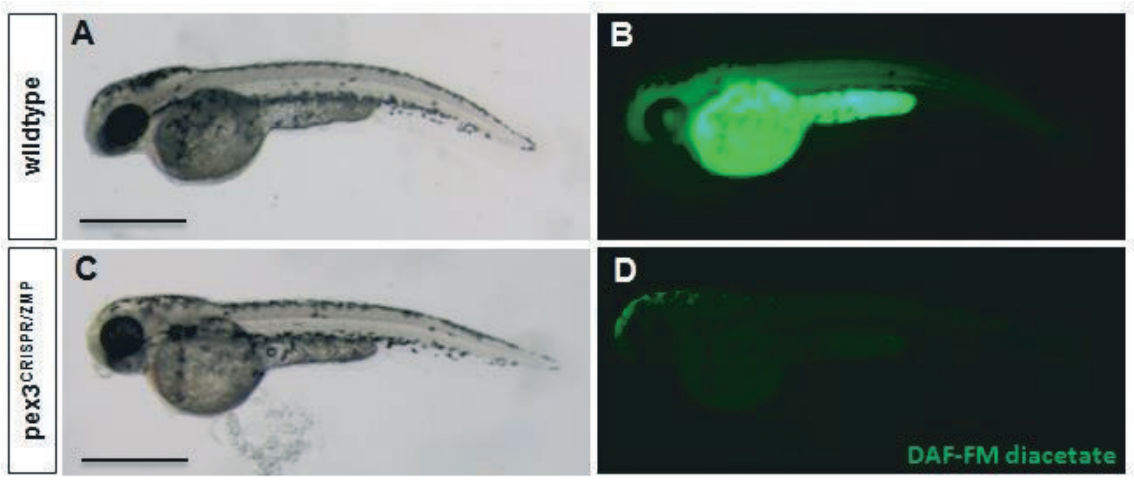

Figure 37 – In *pex3*$^{CRISPR/ZMP}$ mutants the pool of superoxide anion radicals' nitrogen acceptors is depleted. (**A-D**) The yolk sac, the region showing the highest staining intensity in wildtype animals (B), shows no fluorescence in the mutants; residual staining is present in the central nervous system (D). Of notice, *pex3*$^{CRISPR/ZMP}$ mutants develop pigmentation later in comparison to wildtype, but it clearly detectable at 3 dpf. Scale bars: 1 mm.

Increased levels of oxidative stress in the cell cause mitochondrial damage. Mitochondria might also act as a central hub that directly or indirectly controls a wide number of cellular processes including proliferation, ATP synthesis and cell death (Panieri & Santoro 2016). In light of the previous results, the average number of mitochondrial DNA copies per cell at 48 hpf was estimated, by calculating the ratio of the mitochondrial gene *mt-nd1* and the nuclear gene *polg1* (Figure 38) (Artuso et al. 2012). In *pex3* mutants, the amount of mitochondrial DNA copies is reduced to approximately one third, hinting to a reduced mitochondria number as a consequence of missing peroxisomes. Moreover, this would also better explain the previously observed reduced growth rate (Figure 35) as a consequence of reduced capability to process carbon sources for energy gaining.

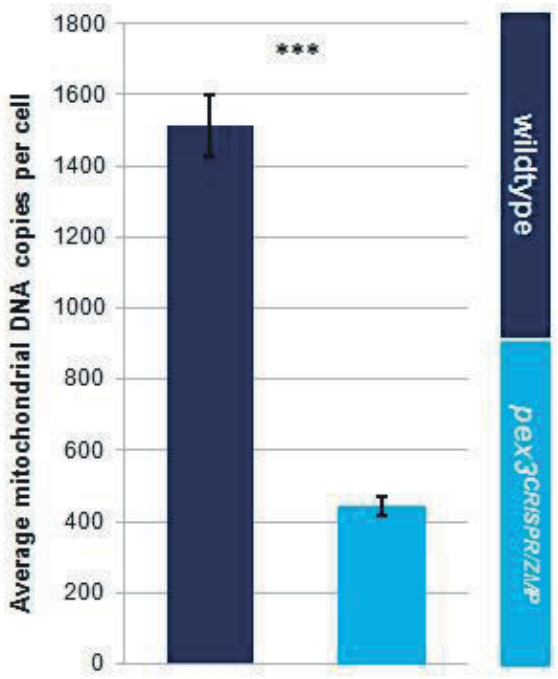

Figure 38 - Increased oxidative stress in the cell causes mitochondrial damage. At 48 hpf, the average number of mitochondrial DNA copies per cell is significantly decreased, justifying the previously observed reduced growth rate.

4.7.1.4 Oxidative stress induces pparγ-mediated mitochondria proliferation and peroxisomal activity

When the number of peroxisomes or mitochondria drops below a certain level and the intracellular signals indicate the need of a higher amount of these organelles, cells activate different mechanisms to stimulate their proliferation. In particular, there is the activation of nuclear receptors which drive the transcription of genes involved in the change of organelle number, structure and enzymes contained in the organelle matrix. In the last years, evidences of components shared by peroxisome and mitochondria proliferation processes increased, including in the list DLP1/Drp1, Fis1, Mff, and GDAP (Schrader et al. 2016). These events are mediated by a class of nuclear receptors, the peroxisome-proliferator activating receptors (PPARs). Thus, the upstream promoter regions of different peroxin genes for the presence of putative PPARs binding sites were analyzed (Figure 39). Indeed, pex genes, either involved in the *de novo* peroxisome biogenesis pathway or in the 'growth and division' are enriched in binding sites for pparγ.

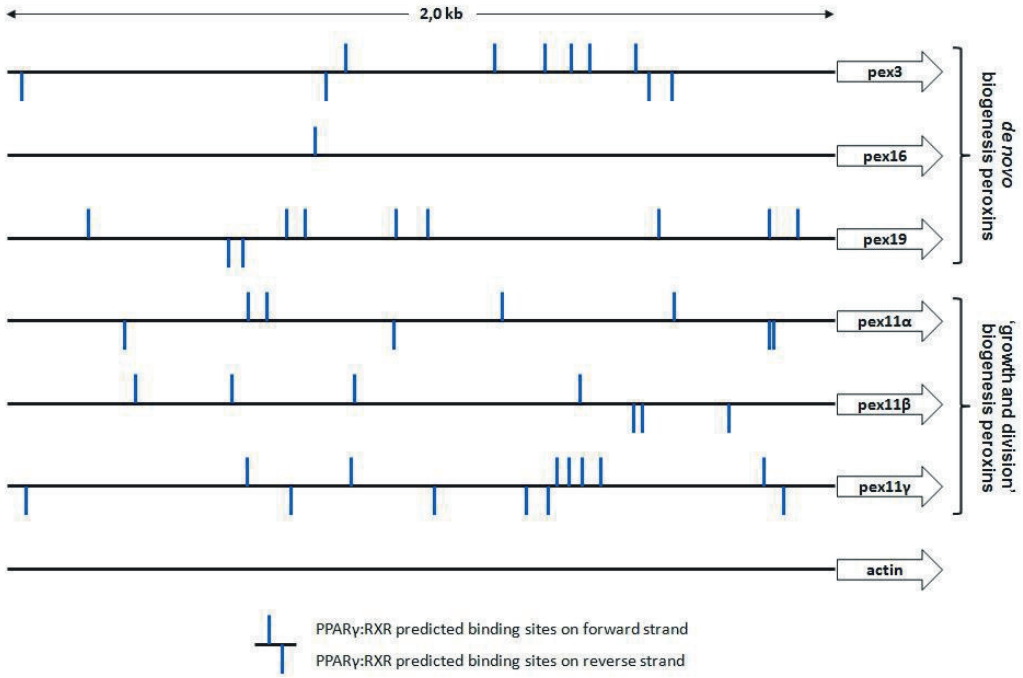

Figure 39 – Promoter region analysis for peroxin genes involved in the *de novo* biogenesis of peroxisomes (*pex3, pex16* and *pex19*) or in the 'growth and division' biogenesis (*pex11α*, *pex11β* and *pex11γ*). Predicted binding sites for PPARγ transcription factor (in association with RXR cofactor), either in the forward strand or in the reverse strand, are annotated. Actin promoter was used as control.

Interestingly, molecules sensing the oxidative status of the cell, like coenzyme Q (CoQ), were identified as modulators of the activation of these PPARs. The redox status of this molecule modulates its potency in activation of the nuclear receptor pparγ: only the reduced form of CoQ ($CoQH_2$) binds with high affinity pparγ, whereas the oxidized form not (Yan et al. 2006; Schmelzer et al. 2010). For this reason, *pex3*$^{CRISPR/ZMP}$ embryos were supplemented with a particular variant of CoQ, the Coenzyme Q_2 (CoQ_2), either in the reduced (CoQ_2H_2) or oxidized form, in order to investigate whether it would be able to activate pparγ and the transcription of genes rescuing peroxisome metabolic activity. The average count of mitochondrial DNA copies per cell and the transcription of pparγ target genes involved in peroxisome metabolism were analyzed (Figure 40). Upon CoQ_2H_2 injection in *pex3*$^{CRISPR/ZMP}$ embryos, the number of mitochondria is only partially rescued, with a significant increase similar to the one reached by exposing embryos to a control activator of pparγ, but not reaching the levels comparable to wildtype animal. When injecting the oxidized form of CoQ_2, no increase in the count of the average number of mitochondrial DNA copies per cell was observed (Figure 40 A). In parallel, the transcription levels of *pparγ* and known pparγ-controlled genes involved in lipid and xenobiotic metabolism (*cebp* and *cpt1a*), oxidative stress (*hmox1a* and *si.ch211-199*) and cell

cycle regulation (*cdkn1a*) (Semple et al. 2006; Sugden et al. 2010) were monitored at 24 hpf. In general, all these genes are downregulated at least 2-fold in *pex3*$^{CRISPR/ZMP}$ mutants, but expression levels are approaching wildtype expression when *pex3*$^{CRISPR/ZMP}$ embryos were injected with CoQ_2H_2 or stimulated with the pparγ activator, but not when injected with the oxidized form of CoQ_2 (Figure 40 B).

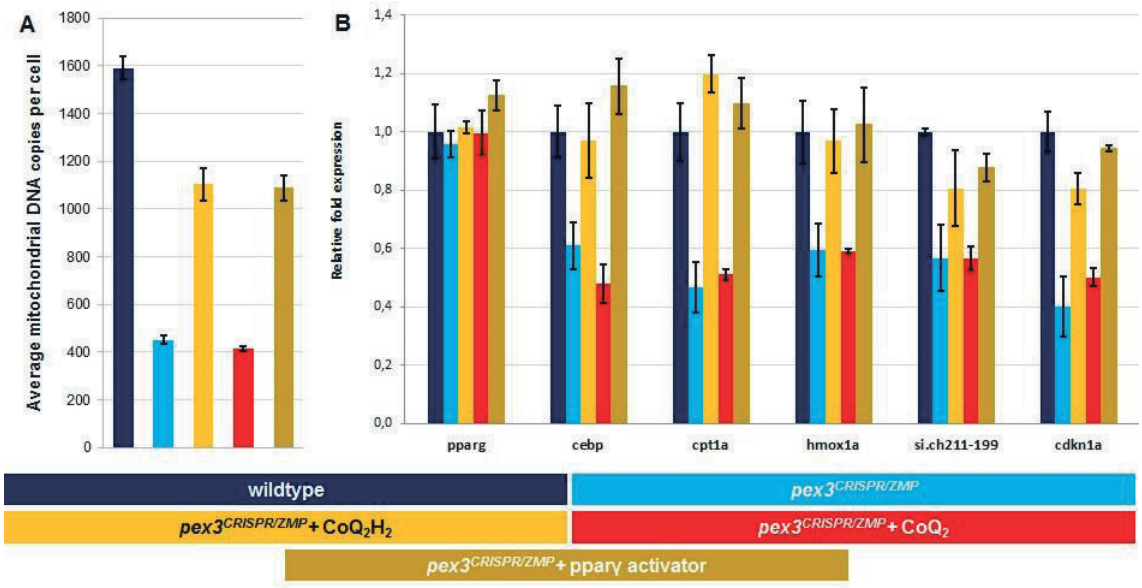

Figure 40 – Supplementation of the reduced ubiquinolic form of coenzyme Q_2 (CoQ_2H_2) rescues the metabolic activity in *pex3*$^{CRISPR/ZMP}$ embryos and modulates the activity of pparγ. (**A**) Upon CoQ_2H_2 injection in pex3$^{CRISPR/ZMP}$ embryos, the number of mitochondria is partially rescued, similarly to what happens when embryos of the same genotype are exposed to a pparγ activator. This does not happen when injecting the oxidized form of CoQ_2. (**B**) Transcription levels of pparγ are not altered, but pparγ-regulated genes involved in lipid and xenobiotic metabolism (*cebp* and *cpt1a*), oxidative stress (*hmox1a* and *si.ch211-199*) and cell cycle regulation (*cdkn1a*) at 24 hpf are restored to wildtype expression levels when *pex3*$^{CRISPR/ZMP}$ embryos are injected with CoQ_2H_2, but not when injected with the oxidized form of CoQ_2.

In light of these results, we could conclude that oxidative stress in *pex3*$^{CRISPR/ZMP}$ animals is able to induce the insurgence of protective mechanisms, including the proliferation of organelles re-equilibrating the redox status in the cell. In particular, we observed that the presence of a redox sensor molecule, namely CoQ_2 and its ratio between the oxidized and reduced forms, manages to modulate the activation of pparγ nuclear receptor which mediates the transcription of genes involved in the change of organelle number or structure.

4.8 *Pex3* mutation affects neural crest-derived tissues development

Mutant animals display morphological defects involving different tissues (Figure 41). In fact, the most evident phenotype is a different pigmentation pattern: in *pex3* trans-heterozygous mutants the typical dark light-reflecting stripes are less intensely pigmented, giving the appearance that they are missing. Moreover, the head shape is altered, due to altered formation of mandible structures. Remarkably, both of the mentioned tissues, pigment cell and cartilage-bone structures in the cranial region, originate from a common embryonic tissue, the neural crest (Dupin & Sommer 2012).

Figure 41 – Comparison of *pex3*$^{CRISPR/ZMP}$ mutants with wildtype siblings at 60 dpf. Wildtype animals develop the stereotyped pigmentation pattern alternating dark melanophore stripes and light-reflecting iridophore stripes, along the sagittal body axis. Mutant animals lack evident melanophore stripes and the mandibular structure is altered (red arrow head). Scale bar: 5 mm.

4.8.1 *Pex3* mutation affects proper melanophores migration and development

4.8.1.1 Pex3 mutation prevents the maturation of a fully pigmented melanophore stripe

As shown in Figure 41, the most characteristic trait of the trans-heterozygous animals is the absence of the typical striped pattern, giving the name to zebrafish. The final striped pattern is generated by the interaction of three different cell populations: melanophores, iridophores and xanthophores (Singh & Nusslein-Volhard 2015).

Mutant embryos are already distinguishable at 2 dpf due to the lower amount of dark melanophore cell which are detectable at this developmental stage (Figure 42). Wildtype

animals at this stage usually develop a stereotyped melanocyte distribution pattern. It consists of a V-shaped motif in the head region, six stripes in the trunk region (two dorsal, two lateral on both sides, two ventral at the border with the yolk sack elongation and further back on both sides) and a few dispersed cells around the yolk sac (Kimmel et al. 1995) (Figure 42 B). *pex3*$^{CRISPR/ZMP}$ embryos lack most melanophores, except for only a few ones that start to organize on the head region and along the dorsal stripe. Moreover, also pigmentation in the eye is remarkably reduced (Figure 42 B').

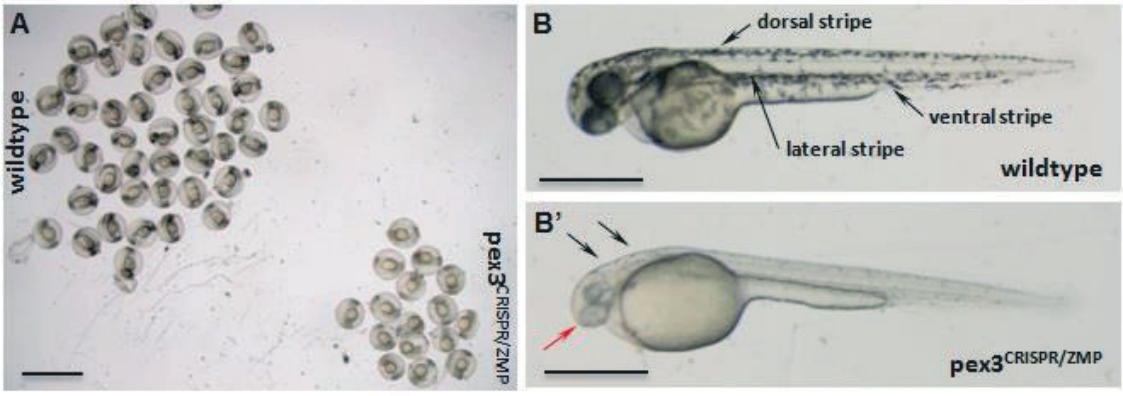

Figure 42 - Comparison of *pex3*$^{CRISPR/ZMP}$ mutants with wildtype siblings at 48 hpf. (**A**) Sibling embryos from a heterozygous crossing can be sorted for the genotype according pigmentation presence at this developmental stage. *pex3*$^{CRISPR/ZMP}$ embryos lack nearly completely any melanophore. (**B-B'**) Single embryos from the wildtype and the transheterozygous *pex3*$^{CRISPR/ZMP}$ groups. Wildtype animals develop the stereotyped pigmentation pattern with one dorsal, two lateral and two ventral stripes. Ate the same stage, *pex3*$^{CRISPR/ZMP}$ embryos develop few melanocytes in the anterior region (black arrows) and also the pigmentation in the eye is defective (red arrow). Scale bars: 500 µm in panel A; 1 mm in panels B and B'.

The phenotype transiently recovers during the following stages of embryonic development, since melanocytes become present and organize in stripes in the stereotyped pattern. At adult stage, mutant animals display again a major problem in pigmentation patterning (Figure 41). A closer analysis shows that melanophore stripes are indeed present in a regular size, number and shape, but the light-reflecting capability of each stripe is strongly impaired, giving the appearance that they are missing (Figure 43).

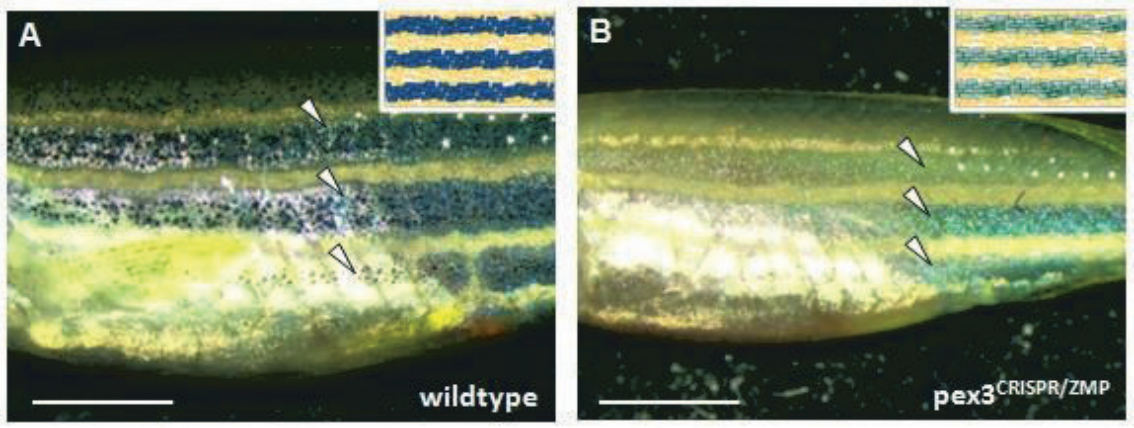

Figure 43 - Comparison of the pigmentation pattern in *pex3*$^{CRISPR/ZMP}$ adult mutants in comparison to wildtype siblings. (**A**) Wildtype animals shows alternating dark melanophore light-absorbing stripes (white arrowheads) and yellow-to-silver light-reflecting iridophore stripes (see scheme on the top right corner). (**B**) Mutant animals still have melanophore stripes (white arrows) but their melanin content is reduced, making them less contrasting to the iridophore stripes (see scheme on the top right corner). Scale bars: 2,5 mm.

Reduced amounts of melanin in each single melanocyte contribute to the reduced visibility of the stripe. Moreover, other overlying pigment cells, iridophores and xanthophores, dim the melanocyte stripes. The observed phenotype is similar to the one caused by other known mutations, for example *golden* and *albino*, which affect the genes *slc24a5* (Lamason et al. 2005) and *slc45a2* (Dooley, Schwarz et al. 2013) respectively. Both encode for antiporters localized at the membrane of the melanosomes, organelles designated for melanin synthesis typical of melanocytes. slc24a5 and slc45a2 regulate the pH of the melanosomal compartment, being responsible for the activation of tyrosine hydroxylase, an enzyme catalyzing the limiting step of melanin synthesis, namely the conversion of tyrosine in L-DOPA. Also *hdac1* mutation produces a similar phenotype by prolonging the expression of *foxd3* in the neural crest and preventing *mitfa* transcription. mitfa is the main transcription factor regulating the transcription of melanin synthesis enzyme genes and its lack results in absent melanophore stripes (Ignatius et al. 2008), similar to the defects seen in pex3$^{CRISPR/ZMP}$ mutants.

To verify that the phenotype is really caused by the absence of pex3, *in vitro* transcribed wildtype *pex3* mRNA was injected in *pex3*$^{CRISPR/ZMP}$ mutant embryos. Indeed, embryos were rescued for the pigmentation phenotype at 2 dpf (Figure 44 B). Similarly, also the injection of murine *Pex3* was able to rescue the pigmentation phenotype in most cases (Figure 44 C), confirming that a mutation in zebrafish *pex3* is responsible for the observed phenotype and that the gene function is conserved across different species.

Figure 44 - Rescue of mutant phenotype with the injection of *pex3* wildtype mRNAs. (**A-B**) Wildtype pigmentation pattern at 48 hpf (A) is completely rescued when injecting 100 ng of zebrafish full length wildtype *pex3* (Dr*pex3*) mRNA in transheterozygous pex3$^{CRISPR/ZMP}$ embryos (B). (**C**) The same effect can be obtained when animals of the same genotype are injected with the same amount of murine full length wildtype *Pex3* (Mm*pex3*) mRNA, even if there are still few exceptions in which there is no (dashed circles) or partial (red arrow) rescue. Scale bars: 500 µm in all panels.

In order to confirm the essential role of *pex3* in the melanocytes, a more detailed study of the gene expression was performed. As already observed in the *in situ* hybridization expression patterns, at 5 dpf single cells were positively stained in the more superficial epidermal layers of the head region and of the trunk (Figure 25 E''-E'''). In light of the observed mutant phenotype, these cells are assumed to be melanocytes, indeed. The original staining protocol prevents proper visualization of pigmentation as it includes a tyrosinase inhibitor, phenylthiourea (PTU) and a bleaching step through hydrogen peroxide to remove eventual melanin. Since pigmentation usually develops starting at 2 dpf and gene expression needs to be confirmed also at the protein level, protein expression in 3 dpf embryos was investigated. Transgenic indicator line Tg[kita:Gal4; UAS:mCherry] was used to mark melanocyte precursors (melanoblasts - Distel et al. 2009). Stainings against pex3 show that there is an accumulation of the protein in mCherry^{+} cells, confirming an enhanced pex3 expression in pigment cells also at the translational level.

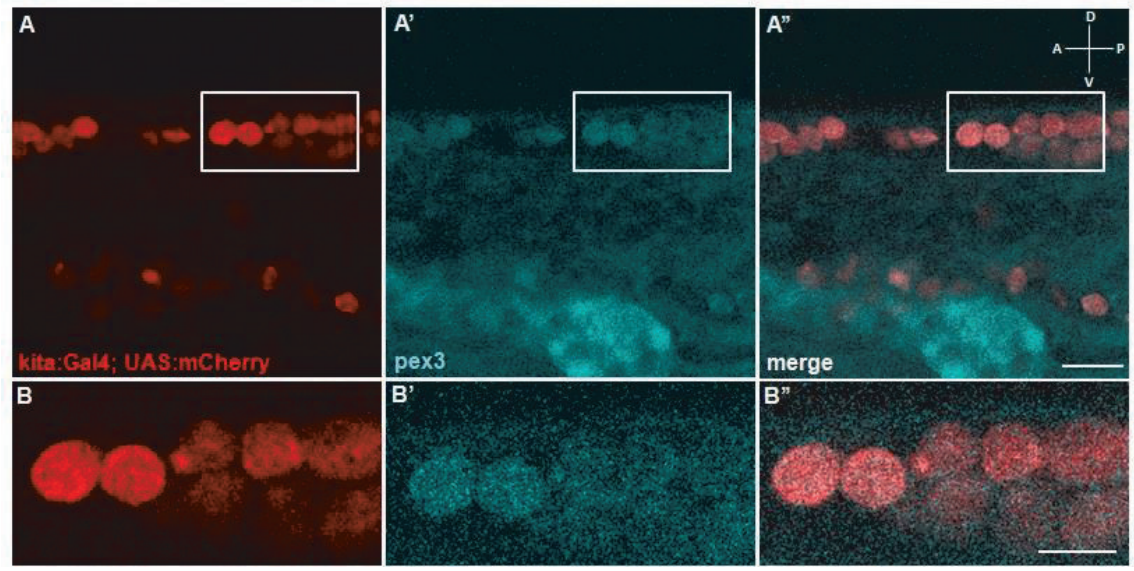

Figure 45 – Pex3 is enriched in the melanocytes already during embryonic development. (**A-A''**) Pex3 protein expression is compared to the expression of a transgene labelling the melanocyte precursors and the melanocytes themselves (Tg[kita:Gal4; UAS:mCherry expression]). (A) mCherry is expressed especially in two groups of cell corresponding to the dorsal and one of the lateral melanocyte stripes. (A') pex3 immunofluorescence stains the same group of cells and this can be verified by a substantial overlapping of the fluorescence signals at the level of the melanocyte stripes (A''). (**B-B''**) Details of the pictures from the previous panels, corresponding to the boxed areas. Scale bars: 20 µm in panels A, A' and A''; 10 µm in panels B, B' and B''.

4.8.1.2 The impaired melanocyte function in pex3$^{CRISPR/ZMP}$ embryos is independent from peroxisomes

Due to the observations that the pigmentation pattern of larval and adult zebrafish is altered upon a *pex3* loss of function and that *pex3* is usually highly expressed in zebrafish pigment cells, two different hypotheses can be formulated to explain the mechanism. On the one hand, the missing melanocytes can be justified as a secondary effect of the lack of the peroxisome, which can possibly provide signal molecules originating there. On the other hand, the phenotype may be pex3 exclusively related, independent from the peroxisome function. In order to test both these hypotheses, the phenotype produced by the injection of various antisense morpholino oligonucleotides (AMOs) blocking the translation of some pex genes, differently involved in peroxisome homeostasis, was screened. (Figure 46).

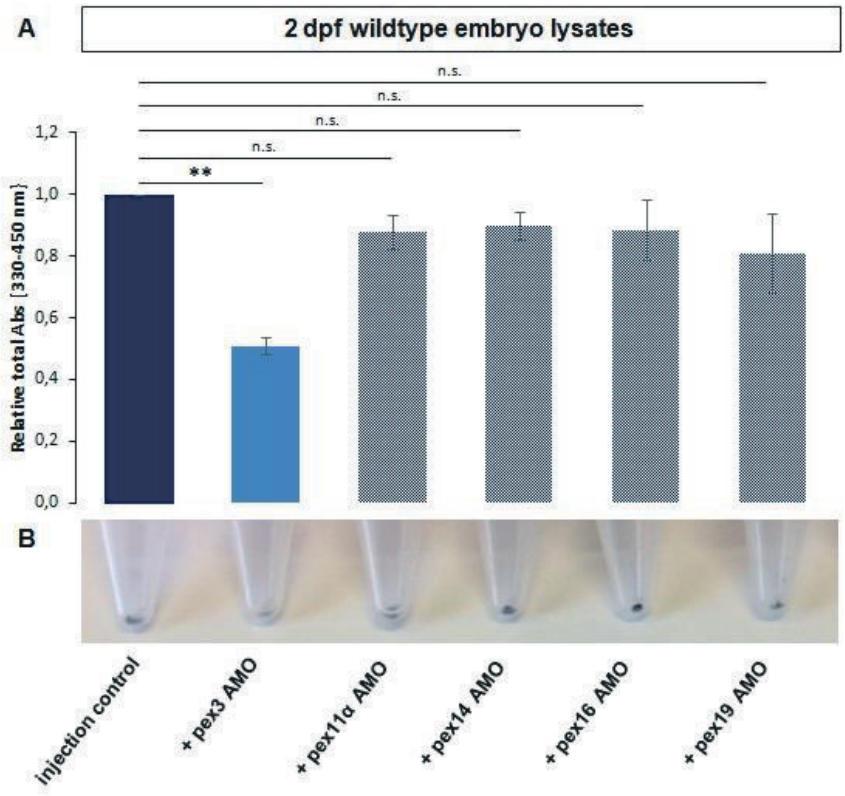

Figure 46 - pex3$^{CRISPR/ZMP}$ phenotype is specific for this peroxin (**A-B**) Embryos injected with pex3 AMO phenocopy pex3$^{CRISPR/ZMP}$ due to the reduced pigmentation absorbance at 2 dpf, while the injection of other AMOs targeting pex genes involved in peroxisome de novo biogenesis (*pex16* and *pex19*), in peroxisome growth and division (*pex11α*) or in the import of peroxisomal matrix proteins (*pex14*) cannot reduce the light absorption capability due to melanin (A). The effect is already evident at the macroscopic level in pelleted embryo lysates (B).

The only AMO which causes an altered pigmentation in the embryos is the pex3 AMO TB, recapitulating the phenotype already observed in mutant zebrafish. At 48 hpf, the light absorption capability of embryos injected with pex3 AMO TB is significantly reduced to only 50% to that of wildtype animals injected with control injection solution. Other AMOs for genes involved in peroxisomal homeostasis, either involved in peroxisome *de novo* biogenesis (*pex16* and *pex19*), or in the fission of existing peroxisomes (*pex11α*), or in the import of matrix protein into the lumen (*pex14*) were unable to produce a significant drop in embryo pigmentation intensity. Therefore, it is excluded that other peroxins has a direct impact on the observed impairment in melanocyte development in *pex3$^{CRISPR/ZMP}$* mutants.

4.8.1.3 Pex3 mutation is responsible of a foxd3-induced repression of melanocyte maturation

In order to further understand the relationship between the mutation in *pex3* and the reduced synthesis of melanin in the melanocytes, it was analyzed whether the enzymes of the melanin biosynthesis pathway are correctly synthetized and localized within the cell. Tyrosinase (tyr), the main enzymes regulating melanin synthesis, was chosen as marker for pigment cell functionality. Tyr localizes into the melanosomes and catalyzes three distinct reactions in the melanogenic pathway, transforming tyrosine in dihydroxyindol through intermediate molecules (Land, Edward J., Ramsden, Christopher A. & Riley, Patrick A. 2003). Immunofluorescence stainings highlight the presence of tyr in the melanocytes of the truncal stripes in wildtype 3 dpf larvae. On the contrary, in *pex3*$^{CRISPR/ZMP}$ mutants, melanocytes reveal a strong reduction in the same regions, making it difficult to pinpoint the single melanophore cells (Figure 47). Similarly, when looking at single melanocytes stained for tyrosinase in same age wildtype larvae, they display the typical melanosomal vesicular pattern, located perinuclearly, where they originate, as well as in the dendrite-like structures (Figure 47 A). In *pex3*$^{CRISPR/ZMP}$ mutants, the overall levels of tyrosinase are decreased by approximately 85%, the number of vesicles is remarkably reduced and located prevalently around the nucleus, without reaching the dendrite-like structures. Moreover, a pool of the protein does not localize on the vesicular structures, but it appears more diffuse (Figure 47 B).

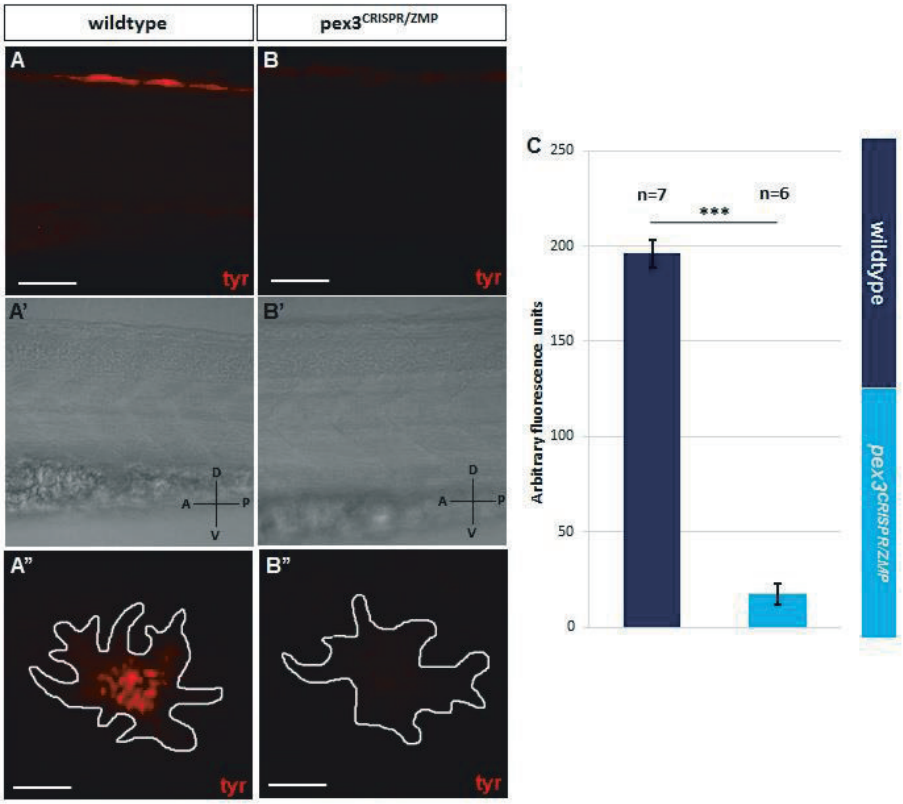

Figure 47 *(on previous page)* - pex3 is required for proper melanocytes function. (**A-B'**) Immunofluorescence stainings for tyrosinase on the medial plane sections in trunk region reveal the presence of tyr in the melanocytes of the dorsal stripe in wildtype 3 dpf larvae (A) but a strong reduction of tyr protein in visible in the same region of pex3$^{CRISPR/ZMP}$ mutants. Transmission light images (A' and B') are used as orientation reference. (**A''-B''**) Immunofluorescence stainings for tyrosinase at single melanocyte level. Wildtype melanocytes show a strong tyr signal in vesicular fashion, prevalently accumulated in the central region of the cell and extending to the dendrite-like structure (A''). Melanocytes in *pex3*$^{CRISPR/ZMP}$ mutants display a lower tyr signal, with a more diffuse distribution pattern (B''). (**C**) Quantification of tyrosinase content of single melanocytes in wildtype and transheterozygous *pex3*$^{CRISPR/ZMP}$ embryos at 3 dpf, based on immunofluorescence staining.

Since a variety of conditions may explain the absence of tyrosinase, it was first investigated whether the cause was a dysregulation at the transcriptional level (Mort et al. 2015). Transcription factors involved in the regulation of melanophore proliferation, maturation and function at 36 hpf were analyzed (Figure 48). This development stage was chosen because pigment cell fate is then being committed, and both embryonic transcription factors leading to pigment cell specification from the neural crest, as well as transcription factors specific for the initiation of melanocyte related enzymes are present (Cheung & Briscoe 2003). *Sox10*, an early transcription factor involved in determining the cell fate of neural crest, is not differentially expressed in trans-heterozygous animals, when compared to wildtype. Nevertheless, expression of *foxd3* is 10-fold higher in *pex3*$^{CRISPR/ZMP}$ mutants and *mitfa* is reduced to approximately half the amount.

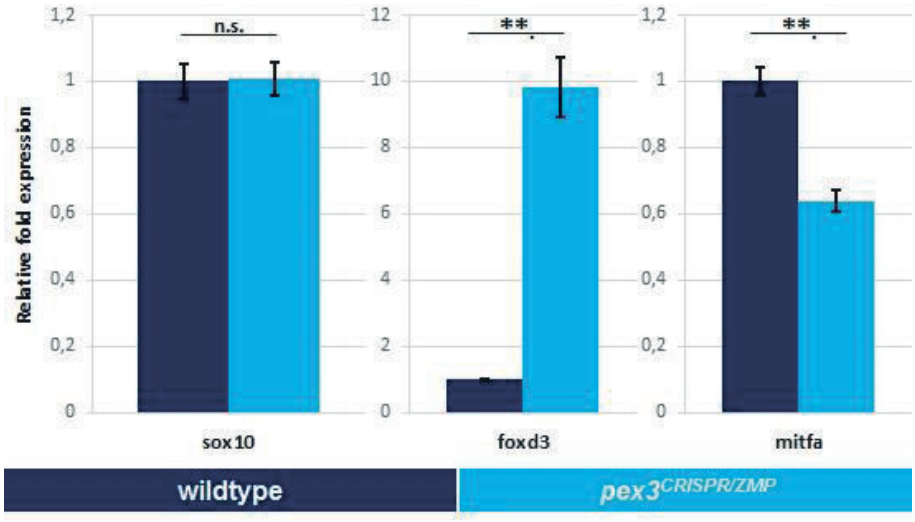

Figure 48 - Quantitative RT-PCR determination of melanocyte specific transcription factors activity at 36 hpf. The analysis reveals an increased expression of *foxd3* repressor with a consequent decrease in *mitfa* expression.

Since the effective translation into functional protein should reflect the differential gene expression, foxd3 and mitfa presence was visualized by making use of transgenic indicator lines for these two genes, Tg[foxd3:GFP] (Gilmour et al. 2002) and Tg[mitfa:GFP] (Curran et al. 2009). In order to reproduce the *pex3*$^{CRISPR/ZMP}$ mutant phenotype, the knock down strategy previously validated was adopted (Figure 46). In pex3 translational blocker AMO injected Tg[foxd3:GFP] embryos, a 1,4-fold increase in fluorescence at 36 hpf was observed, indicative of an increased activity of the gene promoter. This fact is mirrored by a parallel 0,7-fold decrease of fluorescence in pex3 translational blocker AMO injected Tg[mitfa3:GFP] embryos (Figure 49).

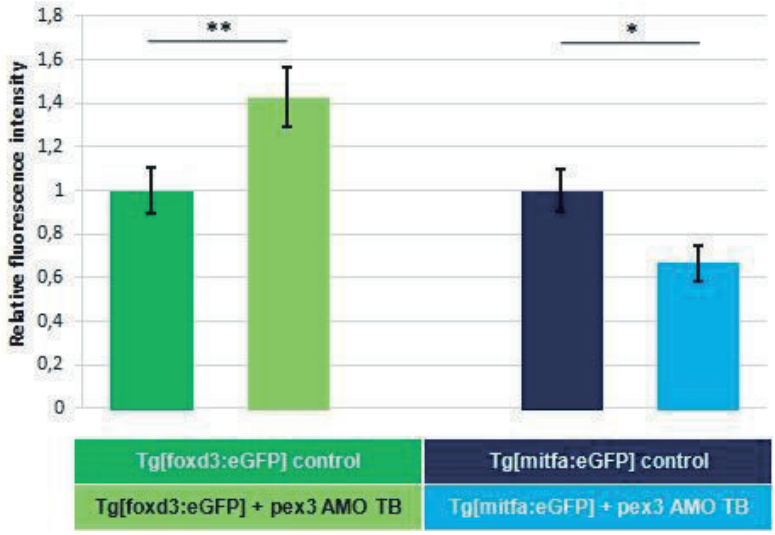

Figure 49 – The altered expression of *foxd3* and *mitfa* was verified also with transgenic reporter lines in a *pex3* morphant model. The experiments show that in the morphants, *foxd3:GFP* expression is increased and it translates into an increased fluorescence of the reporter protein, associated to a reduced expression of the *mitfa:GFP* expression, with consequent decreased fluorescence.

Indeed, foxd3 is a repressor of *mitfa*, the transcription factor driving the expression of enzymes controlling melanin synthesis, like tyrosinase, tyrosinase related proteins 1 (tyrp1) and dopachrome tautomerase (dct). In mutant embryos, *tyr* and *dct* expression is reduced as well, explaining the reduced amount of tyr previously described (Figure 50 A).

Melanocyte homeostasis is prevalently controlled by hormonal stimulation operated by melanocortins and their respective receptors, being part of the proopiomelanocortin signaling axis (Lerner 1993; Pawelek 1985; Pawelek et al. 1992). It was investigated whether pigment cell formation is properly stimulated, verifying the production of the *α-melanocyte stimulating*

hormone (amsh) and of the *melanocortin 1 receptor (mc1r)*, which determine the amount and distribution of dark pigments (Yale Journal of Biology and Medicine 1980). Both transcripts are significantly downregulated, with levels of both ligand and receptor reduced by approximately 80% (Figure 50 B). As a result, also the levels of the cytoplasmic effectors of the melanocyte stimulation signaling, *ppara*, *pparg* and *ppargc1a* (Mangelsdorf et al. 1995), are remarkably reduced (Figure 50 C).

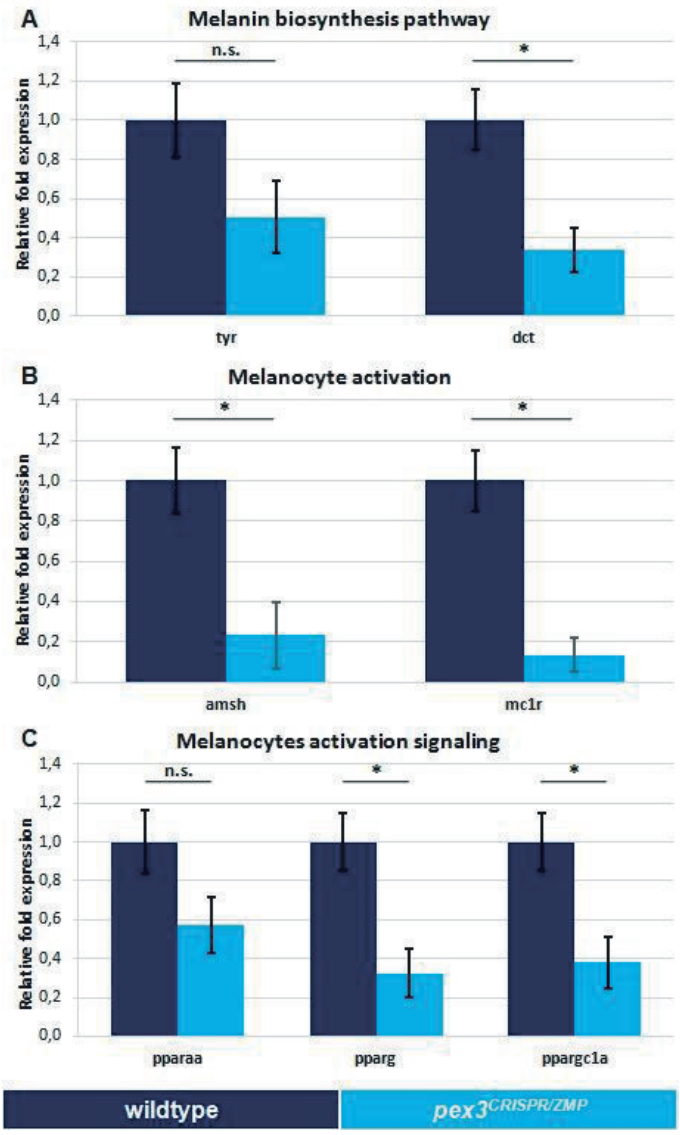

Figure 50 - Quantitative RT-PCR determination of melanocyte activation signaling and melanin synthesis activity at 36 hpf. (**A**) As already demonstrated at the protein level, due the reduction of *mitfa* expression, the transcription of *tyr* is reduced, as well as the one of dct. (**B-C**) Melanocytes activating factors are significantly downregulated (B) and, as a result, also the levels of the cytoplasmic effectors of the melanocyte stimulation signaling are remarkably reduced (C) in *pex3*$^{CRISPR/ZMP}$ mutants.

Thus, the delay and the reduced amount of pigmentation in trans-heterozygous *pex3* zebrafish mutants at 48 hpf is caused by an increased foxd3-mediated repression of melanocytes activation and development, resulting in a quantitative lack of melanin synthesis enzymes and their incorrect localization within the melanocytes.

4.8.1.4 Foxd3 knock down prevents the repression of mitfa transcription and rescues the pigmentation in pex3 mutant embryos

The previous observations highlighted that *pex3* loss of function has a primary impact on *foxd3*, which is upregulated. An attempt to recover the phenotype in *pex3*$^{CRISPR/ZMP}$ mutants, downstream of the upregulated *foxd3* transcription, would be its knock down by means of a translational blocker AMO (Lister et al. 2006). 150 fmol of the AMO were injected in mutant embryos and the effect on pigmentation development and on gene regulation was observed (Figure 51). While at 2 dpf, *pex3*$^{CRISPR/ZMP}$ embryos have a light absorbance capacity reduced by about 50% in comparison to wildtype animals of the same age, if *foxd3* is knocked down, total pigmentation intensity is rescued, without any significant difference with wildtype (Figure 51 A). In addition, the AMO injection itself reduces the transcription of *foxd3,* and at the same time *mitfa* levels are not significantly different in comparison to wildtype, indicating an arrest of the foxd3-operated repression. Consequently, also *tyr* and *dct* levels are restored (Figure 51 B-C).

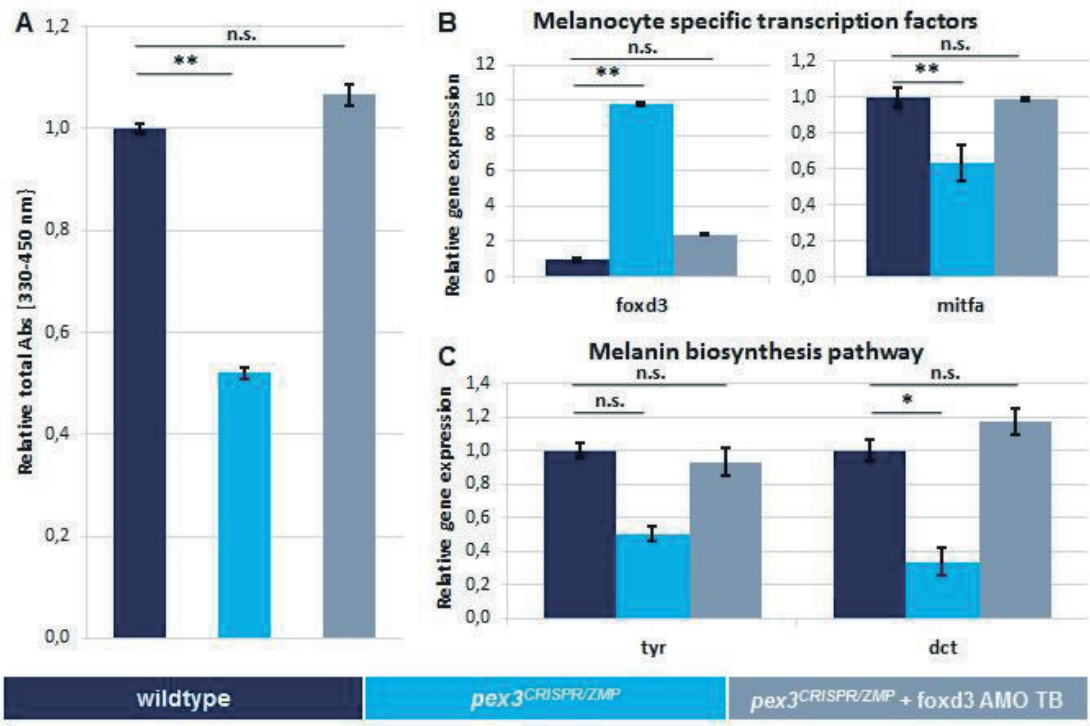

Figure 51 *(on previous page)* **–** Knock down of the transcript inhibits the foxd3-operated *mitfa* repression and restores the wildtypic phenotype. (**A**) At 2 dpf, *pex3* mutant embryos injected with foxd3 AMO develop pigmentation capable to absorb light in amounts comparable to wildtype, rescuing the reduced pigmentation absorbance of uninjected *pex3*$^{CRISPR/ZMP}$ embryos. (**B-C**) *foxd3* AMO injection in *pex3* transheterozygous embryos reduces the transcription of *foxd3*, and at the same time *mitfa* levels are restored, indicating an arrest of the foxd3-operated repression (B). This turns in normal levels of the melanin biosynthesis enzymes, tyr and dct (C).

4.8.1.5 Mitfa repression affects exclusively melanophores and not other developing organs

In mammals there is a single *mitfa* homolog, *MITF* in humans and *Mitf* in mice. In general, a mutation in *Mitf* gene is known to mediate not only pigmentation abnormalities due to altered melanocyte differentiation (Tachibana et al. 1996), but also profound deafness, and severe eye size reduction in homozygotes, with attenuated phenotypes already in the heterozygous condition (Hodgkinson et al. 1998). Since the two duplicated copies of the gene in zebrafish, *mitfa* and *mitfb*, show a conservation in the melanogenic potential, with overlapping expression pattern (Lister et al. 2001), it was verified whether the *pex3* mutation inducing a reduction in *mitfa* expression in zebrafish, has an impact in tissues other than the pigment cells. A possible further phenotype in the eye size or in the developing ear could be expected and for this reason the eye area was measured (Le et al. 2012) and the development of the ear by scoring the presence of the otoliths within a proper otic vesicle structure was verified (Yao et al. 2016) (Figure 52).

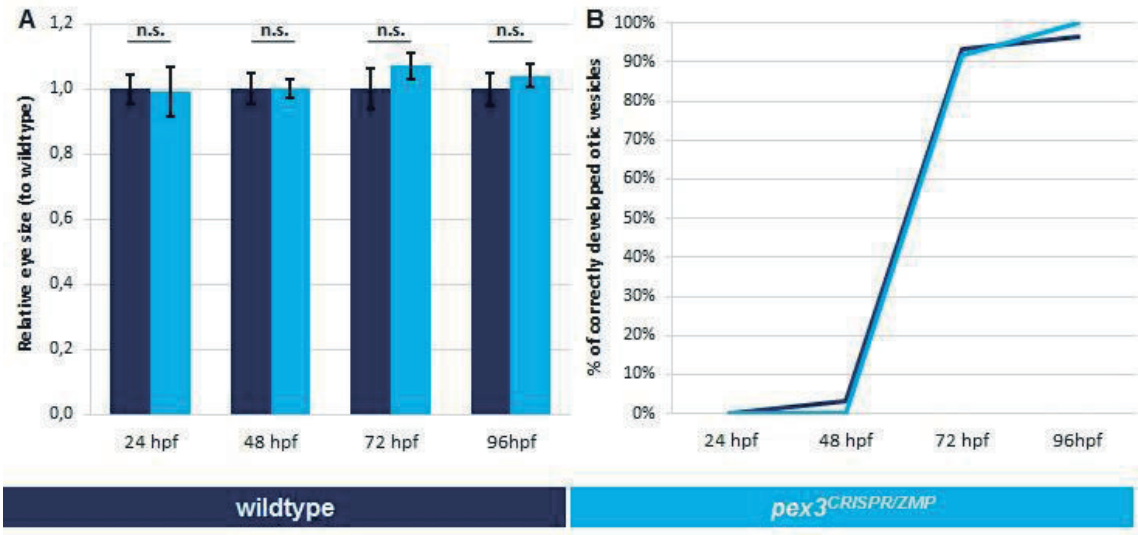

Figure 52 – *mitfa* altered expression in *pex3*$^{CRISPR/ZMP}$ mutants during embryonic development has no impact on eye size (**A**) and on otic vesicle development (**B**) in comparison to wildtype siblings, within 96 hpf.

None of the above mentioned parameters showed a significant difference when comparing wildtype animals and *pex3*$^{CRISPR/ZMP}$ mutants, with eyes being of the same size along the whole development between 24 hpf and 96 hpf and ear structures fully developing between 48 hpf and 72 hpf. Thus, a *pex3* loss of function in zebrafish affects primarily the melanocyte during embryogenesis, having a specific function in this cell population.

4.8.1.6 Pex3 possesses a melanosomal targeting signal driving the protein to melanosomes

Since it is possible to exclude that the *pex3* mutation causing a *mitfa* downregulation has a general wider function in the whole animal and that peroxisomes directly influence melanocytes homeostasis, the phenotype can be pinpointed to an intrinsic feature of pex3 protein in melanophore cell type.

Proteins that are post-translationally targeted to melanosomes possess a melanosomal targeting signal (MTSs) at the C-terminus, at a certain distance from transmembrane domains (Bonifacino & Traub 2003). In particular, for proteins that are either embedded in the melanosomal membrane or in the melanosomal lumen, a bipartite signal is described. It consists of a dileucine based sorting signal, surrounded by acidic amino acids, accompanied by a YXXΦ-type signal (with Φ being a bulky hydrophobic amino acid). pex3 C-terminus sequence was aligned with the C-terminus sequences of other known melanosomal proteins (tyr, tyrp1, dct, pmel17) from zebrafish, human and mouse (Table 10). Indeed, zebrafish pex3 shows the characteristic MTS following the last α-helix, with a dileucine motif surrounded by two aspartic acid residues, one immediately preceding and the other at a distance of two amino acids C-terminally, in addition to the YXXΦ-type signal, with Φ being a phenylalanine. In contrast, other peroxins necessary for the import of matrix protein into the lumen (pex14) or taking part in the *de novo* peroxisome biogenesis (pex16 and pex19), do not present any of the above mentioned features, reinforcing the hypothesis that the trans-heterozygous phenotype is exclusively due to a mutation in *pex3* and not a secondary effect of a peroxisomal disorder.

```
>HS_DCT      ---AFVLLLGLLAFLQYRRLRKG-----YAPLMETGLSSKRYTEEA
>MM_Dct      ---ALVGLFVLLAFLQYRRLRKG-----YTPLMETHLSSKRYTEEA
>DR_dct      LGLLLLLIVLVLYI-QQRR--KREFE----PLLNAEFTNTKYSGEA
>HS_PMEL17   CPIGENS--PLLSG-QQV-----------------------------
>MM_Pmel17   RGLGENS--PLLSG-QQV-----------------------------
>HS_TYRP1    -MDEANQ--PLLTD-QYQCY--AE---EYEKLQNPNQSVV------
>MM_Tyrp1    -KNEANQ--PLLTD-HYQRY--AE---DYEELPNPNHSMV------
>DR_tyrp1a   FGTETRQ--PLLGD-QYQRY--DE---QHKT-----QSVV------
>DR_tyrp1b   RSAEGLE--PLLGE-QFRRY--SE---DERHAS---QSVV------
>MM_Tyr      -PQEERQ--PLLMD-KD-D---------YHSLL-YQSHL-------
>HS_TYR      -LPEEKQ--PLLME-KE-D---------YHSL--YQSHL-------
>DR_tyr      LSYGERQ--PLLNS-SEEE---GSAS--------YQTTL-------
>DR_pex3     IPSHFVQ--DLLLI-DQVKEFAAN---VYETFSTPQELQK------
>DR_pex14    EKKADDEEE-------EDEEDDDDVTHVDEEDHLNV--QTE--...
>DR_pex16    ERAEMRRRAFLLLYYLLRSPFYDR----YSETKILFLLRFLAD...
>DR_pex19    FEKD--------------EDKDS----AFENI-LELMQKLQD...
```

Table 10 - Alignment of C-terminal regions of melanosomal residing proteins (tyrosinase – tyr, dopachrome tautomerase – dct, tyrosinase related protein – tyrp, premelanosome protein 17 – pmel17) from human (HS), mouse (MM) or zebrafish (DR), with different zebrafish pex proteins. Only pex3 possesses a non-canonical melanosomal targeting signal, composed of a degenerate dileucine-based sorting signal (red box, with leucine residues in red) and a YXXΦ-type signal (blue box, with tyrosine residues in blue).

The previous analysis revealed the presence of a MTS in the pex3 sequence. Its *in vivo* requirement, namely whether it is able to target the protein to the melanosome, was assessed. The presence of pex3 on the membrane of melanosome was checked with the help of melanosomal marker, tyr (Figure 53). Immunofluorescence co-stainings in 2 dpf embryo melanocytes show that tyr accumulates in a vesicular pattern and most of these vesicles are enriched in pex3 (Figure 53 A''). Nevertheless, only part of the pex3^{+} vesicles do co-localize with tyr^{+} vesicles, hinting the fact that only a pool of the cellular pex3 protein is required to exert the function at the melanosome, while the rest is required at other cellular compartments.

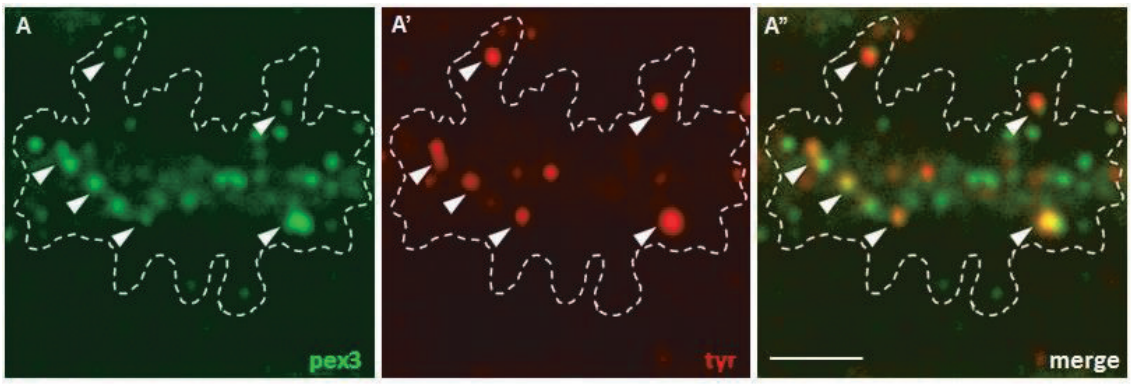

Figure 53 *(on previous page)* – In melanocytes of 2 dpf wildtype zebrafish embryos, the identified melanosomal targeting signal in pex3 protein sequence indeed targets the protein to the melanosomes (**A**) since it co-localizes with the melanosomal marker tyr (**A'-A''**, white arrows). Scale bar: 5 µm.

The same kind of experiments was also performed on isolated single scales from adult animals. In this tissue, melanocytes accumulate at the exposed distal part, whereas they are absent in the proximal part, covered by the neighboring scale. In scales from wildtype animals, the distribution of pex3 and tyr was similar to that observed in embryonic melanocytes, where most of the tyr^+ vesicles are also enriched in pex3 (Figure 54 A-A''). Instead, in scales from *pex3*$^{CRISPR/ZMP}$ mutants the tyrosinase vesicles are reduced in number and size, consistently with what already described. The staining is not localized exclusively in the vesicles anymore, but it spreads in the cytoplasm. This observation is in line with previous studies showing that, whenever tyrosinase cannot be correctly delivered to melanosomes, due to their lack or to the absence of carrier proteins, it is misrouted to other cell compartments or degraded (Chen et al. 2002; Costin et al. 2003; Toyofuku et al. 2002).

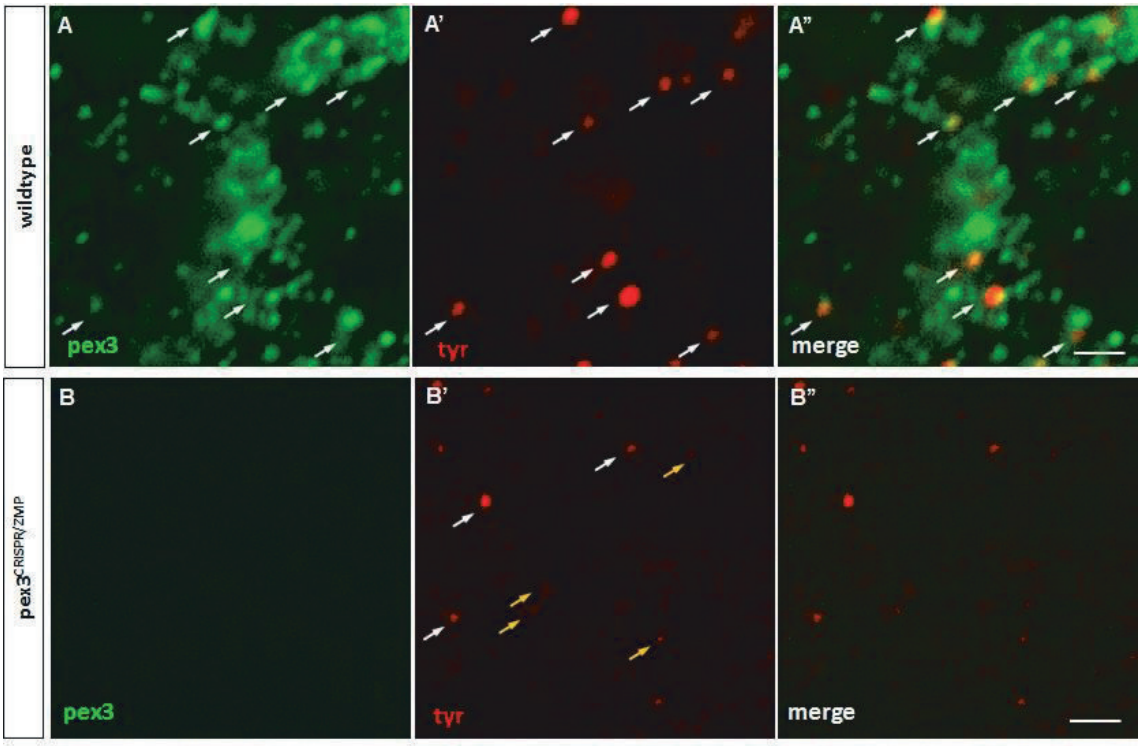

Figure 54 - (**A-A''**) At protein level, pex3 co-localizes with melanosome marker tyr also in scales from wildtype adult animals, indicated by white arrows (**B-B''**) In scales from transheterozygous *pex3*$^{CRISPR/ZMP}$ adult animals, due to the missing pex3 protein (B), tyr^+ vesicles (B') are smaller (white arrows) and less intensively stained (white arrows). Scale bars: 2 µm in all panels.

4.8.1.7 Pex3 is functionally required in melanosomes

pex3 localizes at the melanosomes in pigment cells and in the protein sequence there is a MTS. Thus, it makes sense to further explore its biological function and its impact on the organelle homeostasis. To this end, the role of pex3 was dissected by using a construct in which the stop codon was shifted in front of the newly identified MTS. Both *pex3* full-length (FL) or the *pex3* without the MTS (ΔMTS) were injected in *pex3*$^{CRISPR/ZMP}$ mutant embryos and the rescues of peroxisomal or melanosomal function, detectable by the presence of their respective markers cat and tyr, were followed (Figure 55). In trans-heterozygous embryos injected with *pex3FL* mRNA, both the peroxisomal and the melanosomal functions are brought back in melanocytes (Figure 55 C-D''). The injection of pex*3ΔMTS* mRNA restores only the peroxisomal function, but not the melanosomal one (Figure 55 E-F'').

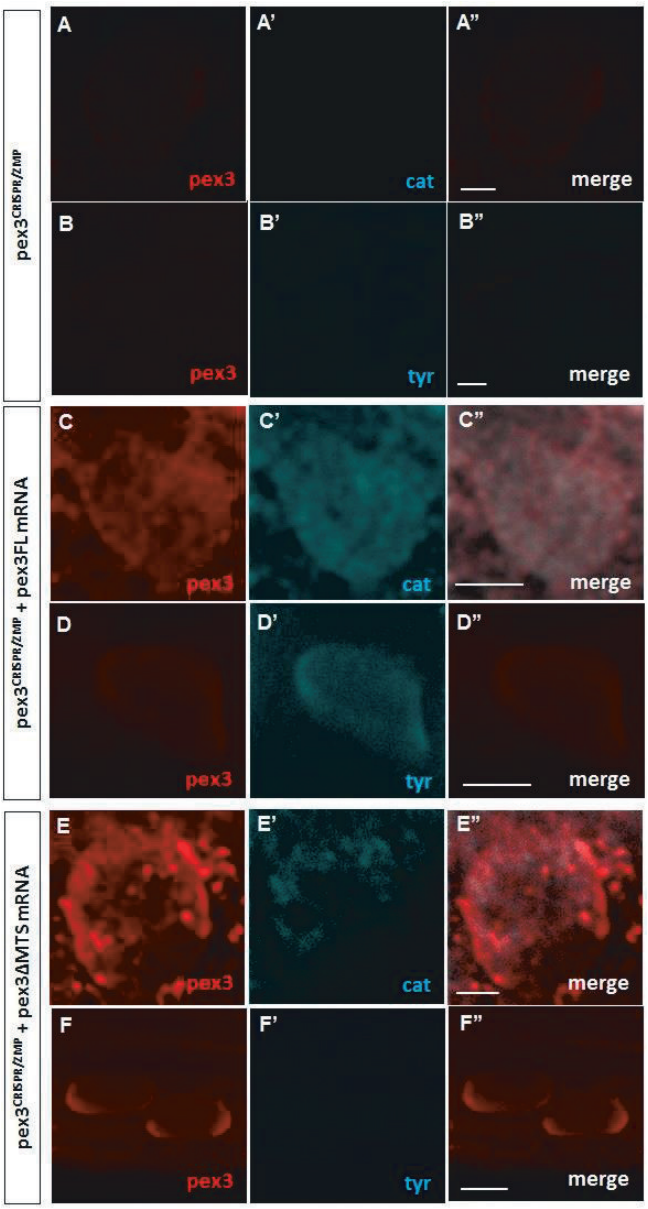

Figure 55 – The identified melanosomal targeting signal in pex3 protein sequence has a biological function in melanosome homeostasis. Immunofluorescence stainings for the peroxisomal marker catalase (cat) and the melanosomal marker tyrosinase (tyr). In transheterozygous pex3$^{CRISPR/ZMP}$ mutants, both the peroxisomal (**A-A''**) and the melanosomal (**B-B''**) functions are impaired, since no staining for both the markers is detectable. Upon *pex3FL* mRNA injection, both functions are restored (**C-D''**); on the other hand, upon *pex3ΔMTS* mRNA the melanosomal function is not restored since the tyrosinase staining is still missing, even if pex3 is detectable (**F-F''**) and the peroxisomal function is restored as well (**E-E''**). Scale bars: 2 µm in panels A-A'', B-B'', C-C'' and E-E''; 5 µm in panels D-D'' and F-F''.

The development of the pigmentation pattern in the first 2 dpf was verified (Figure 56). As already showed in Figure 44, upon injection of *pex3FL* mRNA, the pigmentation phenotype in trans-heterozygous embryos is rescued. The count of melanocytes in the three stripes in the

truncal region of interest is similar to the count in wildtype animals, if not even slightly increased. Similarly, the total light absorption value of these melanocytes is possibly higher than the wildtype. These results can be explained by the fact that the amount of pex3 produced after injection of *pex3* mRNA is likely to be higher than the endogenous wildtype amount, inducing the cellular machinery to be even more efficient in regulating the melanocyte homeostasis events and the melanin production. Injection of *pex3ΔMTS* mRNA is only able to rescue the count of the melanocytes on the dorsal stripe, but not in the lateral and in the ventral ones, and also the total light absorbance in embryo lysates is only partially improved, but still significantly reduced in comparison to wildtype embryos.

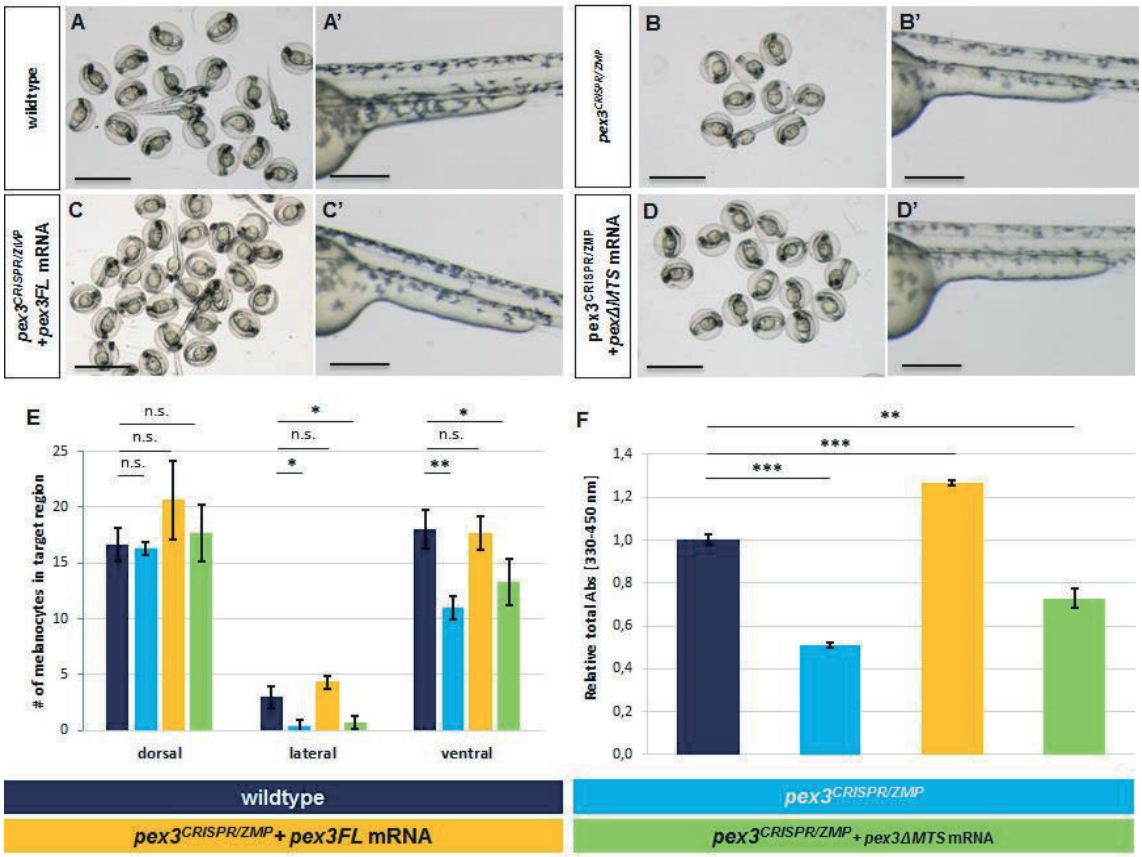

Figure 56 - pex3 requires the melanosomal targeting signal to support the generation of functional melanosomes during embryogenesis. (**A-D**) Batches of 2 dpf wildtype embryos, as positive control (A), transheterozygous *pex3*$^{CRISPR/ZMP}$ embryos uninjected (B) or injected with either *pex3FL* mRNA (C) or *pex3ΔMTS* mRNA (D). (**A'-D'**) Magnifications of the trunk region of single dechorionated embryos from previous panels show differences in the count and pigmentation intensity of the melanocytes in the different stripes in the region of interest. Count of melanocytes on the dorsal, lateral and ventral stripes in the region of interest (**E**) and total pigmentation intensity from embryos lysates (**F**) at 2 dpf under different conditions. *pex3ΔMTS* mRNA is not able to rescue the total pigmentation intensity and the melanocyte count as effectively as *pex3FL* mRNA, when injected in *pex3*$^{CRISPR/ZMP}$ embryos. Scale bars: 5 mm in panels A, B, C and D; 1 mm in panels A', B', C' and D'.

According to those last results, the identified MTS is necessary for full restoration of melanocyte function. In zebrafish melanocytes pex3 is differently targeted to peroxisomes or melanosomes. This could be based on a different accessibility of the targeting signals or on the presence of different protein pools which are interacting with pex3.

4.8.1.8 In pex3$^{CRISPR/ZMP}$ mutants, melanosome pH is dysregulated affecting their function

In order to further support the theory that pex3 is required for proper melanosome development and that in absence of this protein on the organelle membrane melanosome activity is impaired, Bafilomycin A1, an inhibitor of the V1 proton pump portion of the V-ATPase complex was used (Dooley, Schwarz et al. 2013). In such a way melanosome functionality should be restored by regulating the inner pH. Bafilomycin A1 was applied to 24 hpf developing *pex3$^{CRISPR/ZMP}$* embryos and the effect on pigmentation development was monitored (Figure 57).

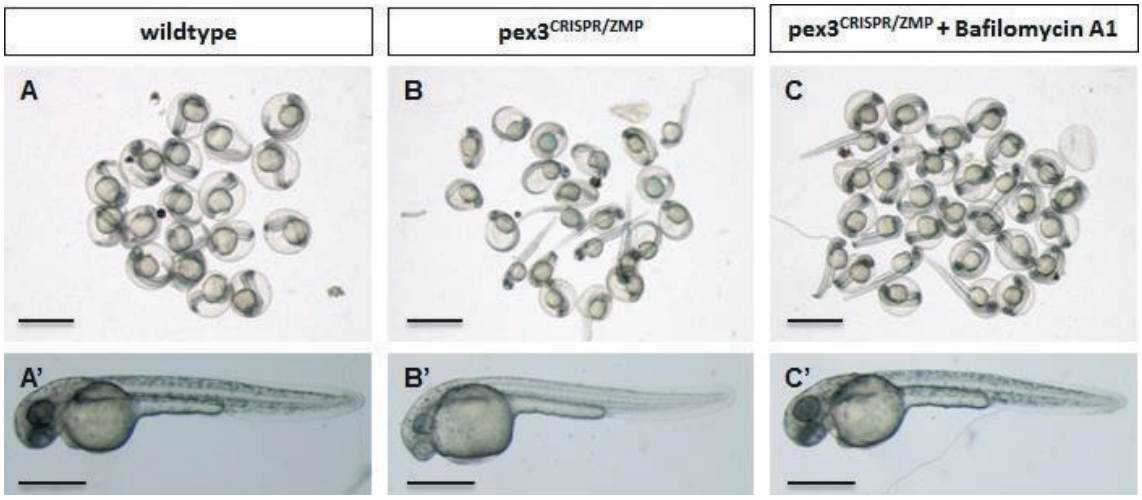

Figure 57 – Inhibition of the V1 proton pump portion of the V-ATPase complex with Bafilomycin A1 restore the optimal melanosomal pH and allows melanin production. *pex3$^{CRISPR/ZMP}$* embryos treated with 50 µM Bafilomycin A1 for 8 hours at 24 hpf (**C-C'**), but not with control medium (1% DMSO, **B-B'**) develop pigmentation similarly to wildtype embryos (**A-A'**) at 48 hpf. Scale bars: 5 mm in panels A, B and C; 1 mm in panels A', B' and C'.

Indeed, the treatment with Bafilomycin A1 improved the activity of melanosomes in trans-heterozygous *pex3$^{CRISPR/ZMP}$* embryos and melanocytes could be distinctly observed in those animals at 48 hpf. Thus, the absence of pex3 in melanocytes prevents the activity of the enzymes involved in melanin synthesis, through a modulation of the luminal pH. By increasing

the pH of the melanosome using Bafilomycin A1, the optimal pH for tyrosinase is restored and melanin production is resumed.

4.8.1.9 pex3 has the same molecular function on melanosomes as on peroxisomes

On the melanosomes, pex3 might exert a function similar to the one on the peroxisomes, namely cooperating in the insertion of membrane protein defining specific domain on the lipid bilayer. In order to test this hypothesis, mRNAs for *slc24a5* of *slc45a2* were generated. *slc24a5* and *slc45a2* encode for melanosomal transmembrane antiporters, regulating the pH of the organelle during different stages of its maturation and controlling the activation of melanin synthesis enzymes (Dooley, Schwarz et al. 2013; Lamason et al. 2005). Should pex3 have the same molecular function (import of membrane protein) on melanosomes as on peroxisomes and be required to integrate transmembrane proteins into the organelles, then simple overexpression of these antiporters should not rescue the pex3$^{CRISPR/ZMP}$ mutant pigmentation phenotype. In fact, after injection of *slc24a5* or *slc45a2* mRNA in trans-heterozygous embryos, only a partial rescue of the pigmentation at 2 dpf was observed, with few melanocytes developing in the head region and along the dorsal part of the trunk, with an intensity of pigments remarkably reduced in comparison to wildtype animals (Figure 58).

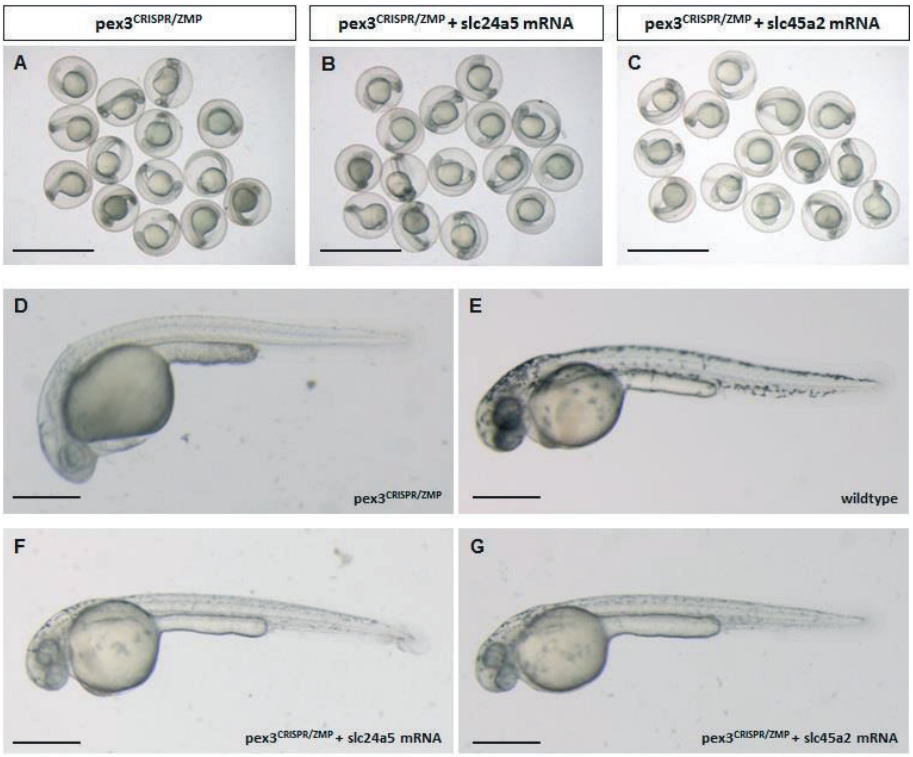

Figure 58 *(on previous page)* - *golden* (*slc24a5*) and *albino* (*slc45a5*) need pex3 to be functional. (**A-C**) Batches of *pex3*$^{CRISPR/ZMP}$ mutant embryos at 2 dpf uninjected (A) or injected with *slc24a5* mRNA (B) or *slc45a2* mRNA (C). (**D-G**) Single dechorionated embryos from the previous panels (D, F and G) and a same stage wildtype embryo (E) for comparison. Injection of either *golden* mRNA or *albino* mRNA does not completely rescue the pigmentation phenotype; few fully pigmented cells are present in the head region and around the yolk, but the typical stripes are still totally missing in the trunk region. Scale bars: 5 mm in panels A, B and C; 1 mm in panels D, E, F and G.

4.8.1.10 Pex3 affects melanoblasts proliferation and melanocytes migration

The functionality of melanosomes in the melanocytes is required for them to be able to modulate proliferation, differentiation and migration (Wasmeier et al. 2008; Hirobe 2011; Hirobe & Terunuma 2012). Since in absence of pex3 the melanosomal function is impaired, it is necessary to get a deeper insight into the detailed process leading to this defect. In particular, melanocyte biogenesis is a well characterized process and different regulatory elements are described (Mort et al. 2015; Singh & Nusslein-Volhard 2015). One of the advantages of zebrafish is its transparency during the embryonic development, which takes place *ex utero*; moreover, different indicator lines for the regulatory elements in melanocyte homeostasis were previously generated, giving the possibility to follow these processes *in vivo*. Different indicator lines were used, allowing to follow the expression of transcription factors or receptors involved in melanoblasts development:

- Tg[sox10:mRFP] (Mongera et al. 2013), is expressed in the branchial arch region, in the dorsal neural tube, around the otic vesicles and along the walls of the dorsal aorta and the ventral notochord;
- Tg[foxd3:GFP] (Gilmour et al. 2002), is expressed in neural crest-derived glial and pigment cell precursors and in glial cells associated with axons of the lateral line system; foxd3 acts as repressor of mitfa transcription;
- Tg[mitfa:GFP] (Curran et al. 2009), is expressed in lateral stripes along the dorsal aspect of the hindbrain and trunk region; mitfa drives the expression of enzymes that are part of the melanin biosynthesis pathway;
- Tg[kita:Gal4; UAS:mCherry] (Distel et al. 2009), is expressed in migrating melanocytes and in quiescent melanoblasts precursors localizing at the dorsal root ganglia; kita expression is necessary for the melanoblasts survival during migration and for their retention in an undifferentiated state.

For each of the above-mentioned indicator lines, a morphant model was established by injecting pex3 translational blocker AMO, which proved to phenocopy the trans-heterozygous model in terms of pigmentation development (Figure 46). The number of cell clusters positive

for the marker in the region of interest was determined at 2 dpf, with the only exception of Tg[kita:Gal4; UAS:mCherry] indicator line, for which the time point was shifted to the earliest detectable time point, namely 3 dpf. In such a way, cell differentiation and proliferation could be monitored and it was possible to resolve at which point of the melanoblast development the process is impaired due to the *pex3* loss of function (Figure 59).

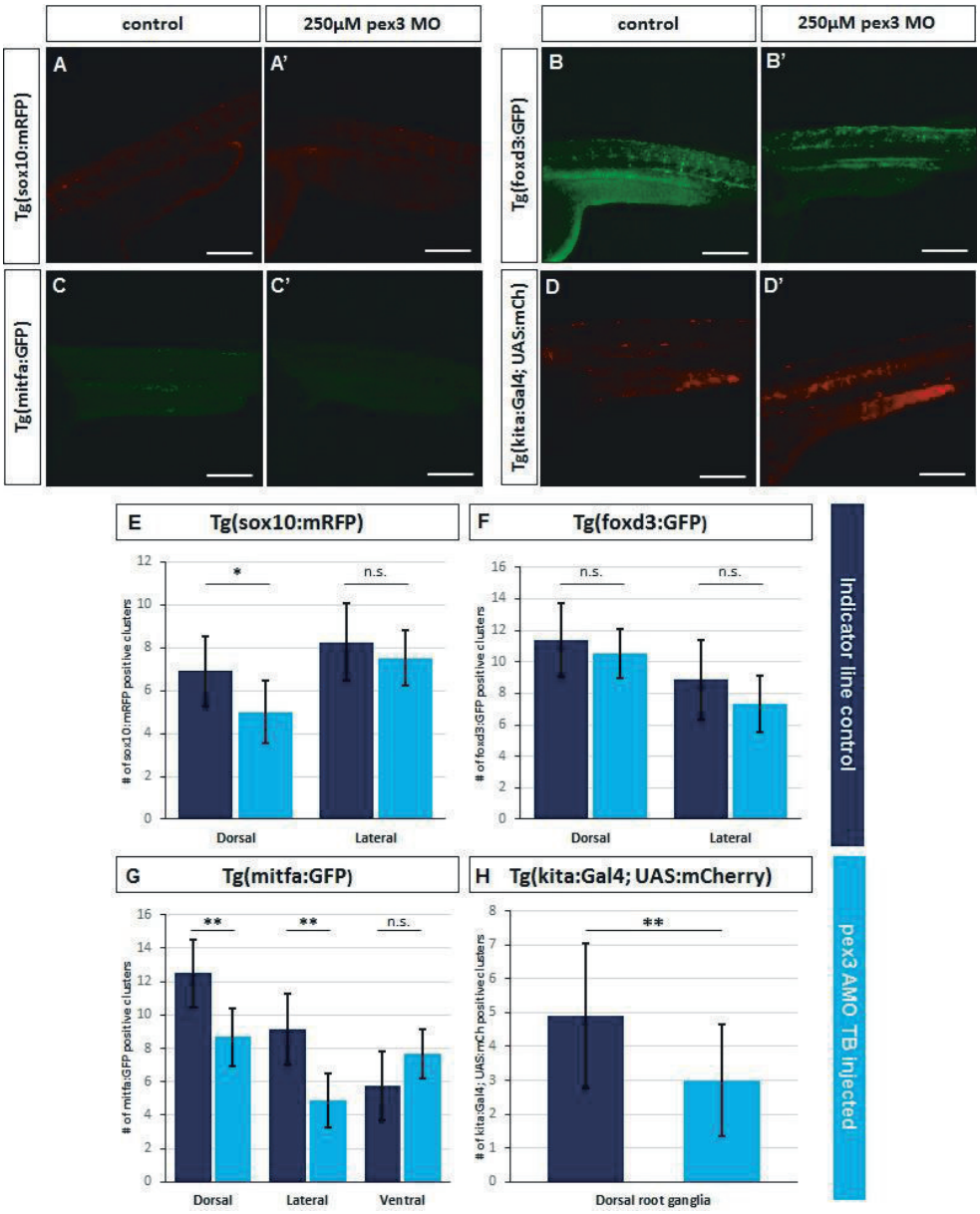

Figure 59 - *pex3* is not necessary for the initiation but for the proper melanoblasts proliferation and differentiation. (**A-C'**) Sample pictures for the count of cell clusters on different melanophores stripes at different points of their ontogenesis in Tg[sox10:mRFP] (A-A'), Tg[foxd3:GFP] (B-B') or Tg[mitfa:GFP] (C-C') at 2 dpf either injected with control injection solution (left panels) or containing 250 µM pex3 AMO (right panels). (**D-D'**) Sample pictures for the count of dorsal root ganglia clusters in Tg[kita:Gal4; UAS:mCherry] at 3 dpf either injected with control injection solution (left panel) or containing 250 µM pex3 AMO (right panel). (**E-G**) Count of cell clusters on different melanophores stripes at different points

of their ontogenesis in Tg[sox10:mRFP] (E), Tg[foxd3:GFP] (F) or Tg[mitfa:GFP] (G) at 2 dpf. (H) Count of dorsal root ganglia clusters in Tg[kita:Gal4; UAS:mCherry] at 3 dpf. In the morphant model, the count is reduced in comparison to the control samples, especially for the late *mitfa* and the melanoblast *kita* markers. Scale bars: 50 µm. (Experiment perform in collaboration with Verena Monika Juchems).

sox10 or *foxd3,* marking the first stages of pigment cell development from the neural crest, are only partially affected, since the number of cell clusters expressing the fluorescent indicator is only slightly dysregulated in comparison to injected control embryos (Figure 59 A-A', B-B', E-F). The effect is eventually limited to the dorsal stripe, whereas it is not possible to count the number of the cell clusters in the ventral region, since they did not emerge at this stage, yet. For later stages in the melanocyte development, GFP expression under control of the *mitfa* promoter indicates that there is a reduced number of expressing cell clusters, in both the dorsal and the lateral stripes in morphant larvae (Figure 59 C-C', G). Also *kita* promoter derived expression is detected in a significantly lower number of cluster at the dorsal root ganglia, indicating a lower proliferation of quiescent stem-like progenitors and lower potential for further melanophore replacement (Figure 59 D-D', H). These results point to an impaired melanoblasts development upon *pex3* loss of function, with a lower number of cells reaching the fully mature stage, a lower number of generated precursor cells which can replace other melanocytes and a delay in the migration progression, especially related to the dorsal and lateral stripes.

4.8.1.11 Embryonic melanoblasts development influences melanocyte proliferation until the metamorphic phase

Melanocyte precursors emerging during embryonic development are recruited to replace dying melanophores during the whole life cycle. In zebrafish, a rearrangement in the pigment cell distribution is happening and the adult stripe pattern is determined during metamorphic phase (21-35 dpf) (Singh & Nusslein-Volhard 2015). Since in *pex3* mutants a lower number of melanophore precursors is generated during embryogenesis, it was assessed whether this has an impact on later events. *pex3*$^{CRISPR/ZMP}$ embryos were injected with either *pex3FL* or p*ex3ΔMTS* mRNAs and the number of melanocytes and pigmentation intensity of the different stripes were quantified in the region of interest between 5 dpf and 30 dpf (Figure 60).

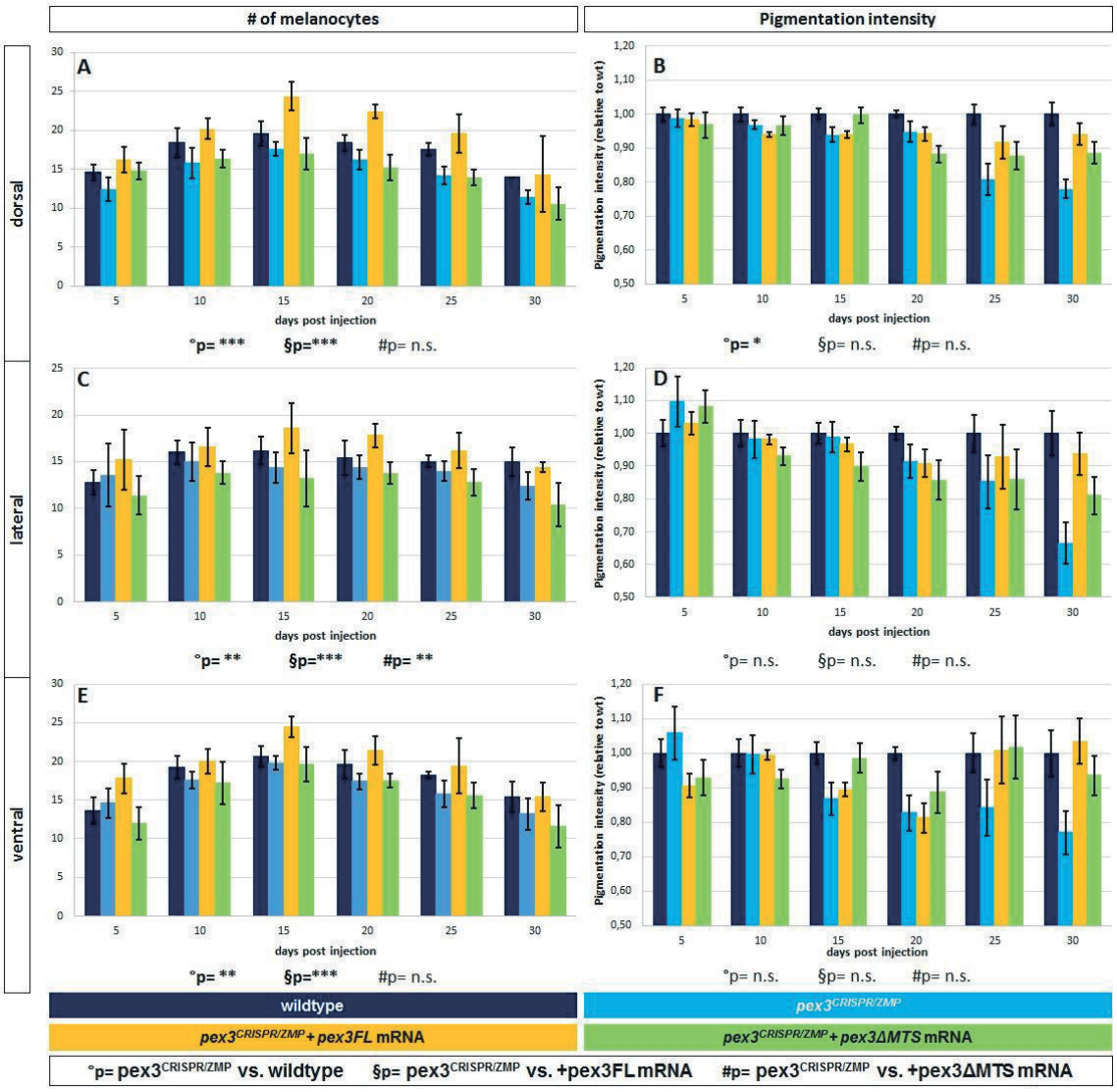

Figure 60 - Melanoblast defects caused by *pex3* loss of function have an impact on the post metamorphic development of pigmentation. Number of melanocytes on dorsal (**A**), lateral (**C**) and ventral (**E**) melanophore stripes between 5 dpf and 30 dpf. Relative pigmentation intensity of the dorsal (**B**), lateral (**D**) and ventral (**F**) stripes between 5 dpf and 30 dpf. Both values are reduced when comparing transheterozygous *pex3*$^{CRISPR/ZMP}$ to wildtype; they are restored after injection of *pex3FL* mRNA, but not upon *pex3ΔMTS* mRNA injection. All p values refer to the whole time series; each dataset is tested for significant difference in comparison *pex3*$^{CRISPR/ZMP}$ sample.

When comparing both the cell count and the pigmentation intensity values for the transheterozygous *pex3*$^{CRISPR/ZMP}$ injected embryos in comparison to wildtype controls, they are significantly reduced for all stripes. In particular, the pigmentation intensity values in the single stripes start to divert from the wildtype after 15 dpf, indicating that at this point a new wave of events, additional to those observed during embryogenesis, is producing the phenotype observed in the adult animals. Injection of *pex3FL* mRNA restores both cell count and pigmentation intensity, occasionally in a measure even higher than in wildtype animals. This

indicates that pex3 protein produced after injection of the full-length version of the coding sequence stimulates the cellular machinery even more efficiently than the normal protein dose. This is sufficient to also rescue the initiation of metamorphic events, even if the protein is likely not to be present anymore. In *pex3ΔMTS* mRNAs injected *pex3*$^{CRISPR/ZMP}$ mutants, the values trend is similar to the untreated *pex3*$^{CRISPR/ZMP}$ embryos, hinting to the fact that the construct cannot rescue. Considering that no effect should be expected beyond 5 dpf, due to the degradation of the injected mRNAs after this period (Fink et al. 2006), the post-metamorphic development of pigmentation, with a reduced number of melanocytes and a reduced light absorption, is caused by the lower amount of mature melanophores arising few days post-fertilization and by the lower amount of quiescent melanocyte precursors.

4.8.1.12 Pex3 is responsible for the post-metamorphic melanocyte migration and distribution

The final analysis focused on the post-metamorphic pigmentation pattern in juvenile animals (30 dpf). In particular, it was determined how pex3 dysfunction could affect the melanocyte distribution, with regard to the function of the newly identified MTS in the pex3 protein sequence. For this reason, animals from the previous analysis were further screened (Figure 61).

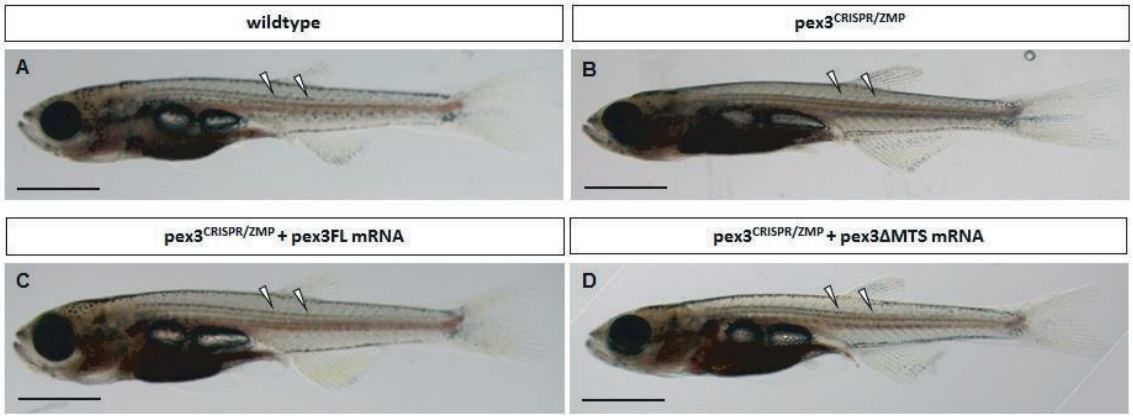

Figure 61 - Macroscopic pigment distribution seems unaffected in *pex3*$^{CRISPR/ZMP}$ mutants after the metamorphosis stage. 30 dpf juvenile animals, wildtype (**A**) as control, transheterozygous *pex3*$^{CRISPR/ZMP}$ (**B**) or transheterozygous *pex3*$^{CRISPR/ZMP}$ injected with either pex3FL mRNA (**C**) or pex3ΔMTS mRNA (**D**). Macroscopic observation of the larvae does not highlight any major alteration of the standard pigmentation pattern, especially in the melanocyte distribution in the trunk region (white arrowheads). Scale bars: 2 mm.

The mere macroscopic observation of the juvenile fish does not show any major alteration in the distribution of the melanocytes. Nevertheless, in the trunk region there is a different dispersion of the melanocytes both dorsally and ventrally of the first iridophores interstripe, which emerges along the myoseptum (see arrows in Figure 61). Normally, soon after the beginning of the metamorphic stage, melanophores line up in two stripes, and only then they start to increase in size, keeping the number unaltered (Kimmel et al. 1995; Singh & Nusslein-Volhard 2015). These events can be observed only in wildtype and in *pex3*$^{CRISPR/ZMP}$ larvae injected with *pex3FL* mRNA (Figure 62 A-A''), but not in *pex3*$^{CRISPR/ZMP}$ mutant larvae, even if injected with *pex3ΔMTS* mRNA (Figure 62 A'-A'''). The migration of melanophore on the skin of larvae was translated on a bi-dimensional model and a linear regression was calculated to describe the mean position, along the axis of the stripe (Luciani et al. 2011). After that, the average distance of each pigment cell from the axis of the stripe was calculated (Figure 62 B-B''', C). In *pex3*$^{CRISPR/ZMP}$ juvenile fish, the average distance is approximately ten times higher when compared to wildtype animals, and these values can be reduced to approximately one third when *pex3*$^{CRISPR/ZMP}$ embryos are injected with *pex3FL* mRNA, but not with *pex3ΔMTS* mRNA. Taken together, these results demonstrate that the impaired early proliferation, maturation and migration events in the chromophore cell lineage have an influence on the fate of this cell population at a later time point, during metamorphosis. This results in inappropriate timing and aspect of the stereotyped striped pattern of adult zebrafish.

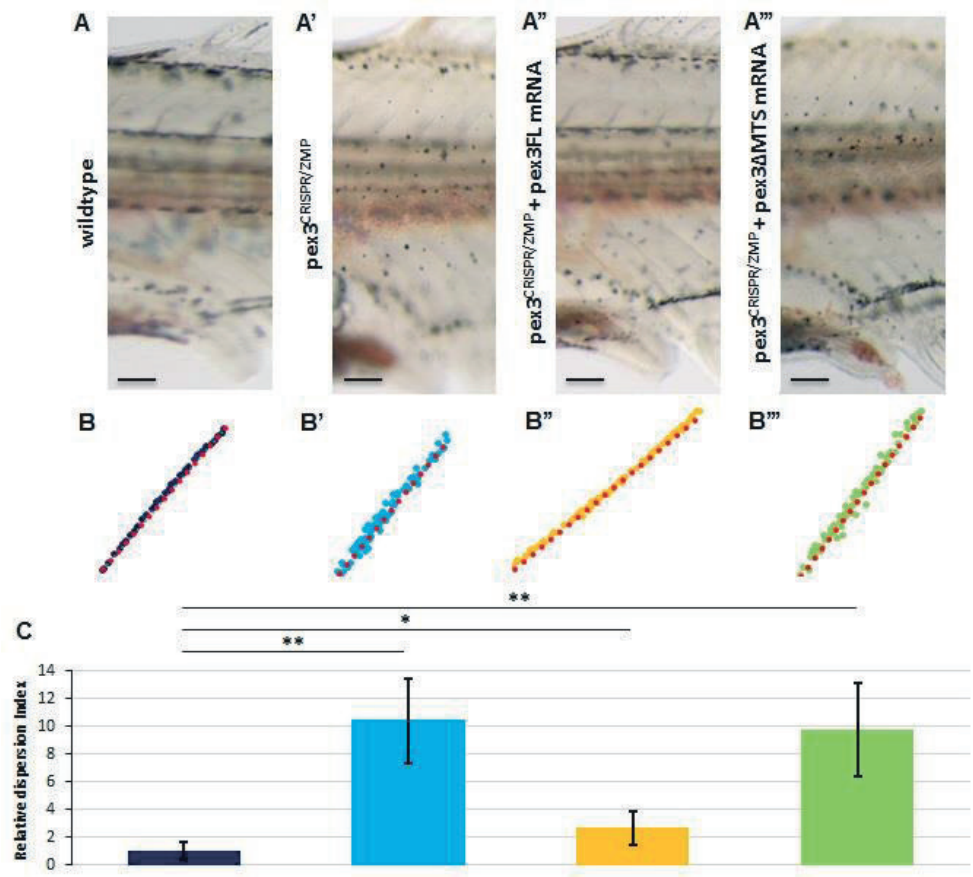

Figure 62 - (**A-A'''**) Melanocyte distribution in the trunk region of juvenile animals (30 dpf), wildtype (A), control pex3$^{CRISPR/ZMP}$ (A') or pex3$^{CRISPR/ZMP}$ injected with either *pex3FL* mRNA (A'') or *pex3ΔMTS* mRNA (A'''). (**B-B'''**) Graph of a representative regression model for each of the analyzed conditions. Each dot represents a single melanocyte, while the red dotted line represents the mean position in the sample. In wildtype (B) and pex3$^{CRISPR/ZMP}$ samples injected with *pex3FL* mRNA (B'') the single melanocytes are closer to the average position in comparison to control pex3$^{CRISPR/ZMP}$ (B') or pex3$^{CRISPR/ZMP}$ injected with *pex3ΔMTS* mRNA (B'''). (**C**) Quantification of the relative average distance from the first interstripe, measured on the same samples. *pex3FL* mRNA, but not *pex3ΔMTS* mRNA injection reduces the dispersion in *pex3$^{CRISPR/ZMP}$* to levels comparable to wildtype animals. Scale bars: 200 µm in panels A, A', A'' and A'''.

4.8.1.13 A possible conserved role of pex3 in mammalian melanocytes

Pex3 loss of function in zebrafish is responsible for the altered pigmentation phenotype, and the pex3 localization can be restricted to a C-terminal melanosomal targeting signal which drives the protein on the membrane of the melanosome. In light of these results, it was investigated whether the mechanism and function could also potentially be conserved in other species, in particular in human and mouse. Alignment of the C-terminal sequence of zebrafish, human and murine pex3 proteins shows that the bipartite signal identified in zebrafish is

conserved, with the dileucine motif surrounded by two aspartic acid residues and the YXXΦ-type signal (Table 11).

```
>HS_PEX3    TPSHFVQDLLTMEQVKDFAANVYEAFSTPQQLEK
>MM_Pex3    TPSHFVQDLLMMEQVKDFAANVYEAFSTPQQLEK
>DR_pex3    IPSHFVQDLLLIDQVKEFAANVYETFSTPQELQK
            ********* ::***:********:*****:*:*
```

Table 11 - Alignment of C-terminal regions of pex3 proteins from human (HS), mouse (MM) or zebrafish (DR). They all possess the identified non-canonical melanosomal targeting signal. Degenerate dileucine-based sorting signal (red box, with leucine residues in red) and a YXXΦ-type signal (blue box, with tyrosine residues in blue) are highlighted.

This result hints to a possible conserved mechanism targeting pex3 on the membrane of melanosomes also in other species, having there a function. A cell culture system based on B16 mouse melanoma cell line was used (Overwijk & Restifo 2001). Immunofluorescence co-stainings in B16 cells do not show a strong co-localization of pex3 with the melanosomal marker tyr. Nevertheless, the melanosomal fraction could be isolated by ultracentrifugation of cell lysate (Kushimoto et al. 2001; Basrur et al. 2003a) and an enrichment of pex3 was found in tyr-positive melanosomal fraction. At the same time, the presence of other compartments which could contribute to melanosome biogenesis like endoplasmic reticulum or early endosomes (Schiaffino 2010) are either absent or remarkably reduced (Figure 63).

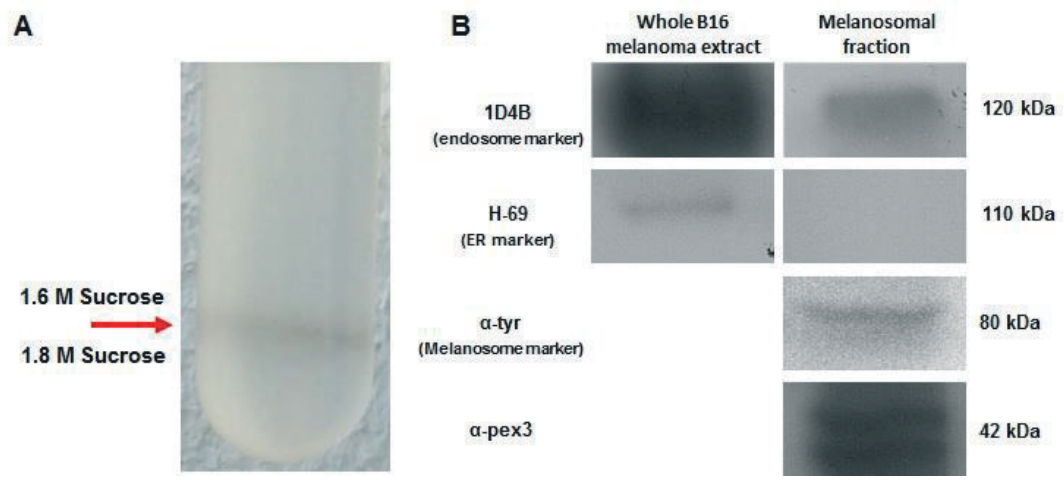

Figure 63 *(on previous page)* **–** The purified melanosomal fraction from mammalian melanoma cells is enriched in pex3 protein. (**A**) Sucrose gradient ultracentrifugation of a cell lysate of B16 mouse melanoma cells. At the end of the procedure it is possible to detect a band at the interface between the 1,6 M and the 1,8 M sucrose gradient (red arrow) enriched in melanosomes, visible because of the presence of melanin. (**B**) Western blot analysis of the purified melanosomal fraction shows the absence of endoplasmic reticulum contamination and a strong reduction of endosome contribution, still showing the presence of the melanosomal marker and an enrichment in pex3 content.

In summary, the observations hint to the fact that pex3 might have a conserved role in controlling and regulating melanosome biogenesis homeostasis also in mammalian melanocytes, through a mechanism similar to the one just described for zebrafish.

5 Discussion

The fundamental role of metabolism in health and disease opened the need for a deeper comprehension of the mechanisms controlling it. In order to easily and thoroughly study the impact of metabolism on organ development and tissue homeostasis, the generation of experimental models is needed (Vander Heiden et al. 2009; Suhre & Gieger 2012). In particular, the recent availability of new biochemical technologies and the establishment of animal systems helped to find answers to open questions in cellular metabolism.

Peroxisomes have a key role in cell metabolism. In this organelle, there are more than one hundred enzymes involved in a multiplicity of biosynthetic pathways. They are responsible of the catalysis of several enzymatic reactions related to lipid metabolism (detoxification of reactive oxygen species, oxidation of fatty acids, ether phospholipids synthesis) and the impairment of any of those has an impact on cell homeostasis. Impaired β-oxidation of very long chain fatty acids or β- and α-oxidation of methyl-branched fatty acids results in the lack of proper substrates for energy production in the mitochondria and the accumulation of toxic molecules in the cell. Missing ether phospholipid biosynthesis causes abnormal membrane composition, whereas missing peroxide detoxification increases oxidative stress (Klouwer et al. 2015). Due to the cell high metabolic requirements, peroxisomes are highly dynamic organelles and the cell can promptly react to different environmental and metabolic stress conditions, to adjust their number, their size and their enzymatic content. The cell can start this adjustment process from already existing peroxisomes, in the so-called 'growth and division' pathway. If this is not sufficient, the cell can generate brand-new peroxisomes from vesicles budding from the endoplasmic reticulum following the *de novo* biogenesis pathway (Agrawal & Subramani 2016; Schrader et al. 2016). These so-called 'pre-peroxisomal' vesicles are then enriched with peroxisomal membrane proteins which are necessary for the import of the peroxisomal matrix proteins, synthetized in the cytoplasm.

A class of genes, called peroxins (*pex*), regulates peroxisome homeostasis. Peroxins control membrane dynamics during fission and growth in size. Moreover, they control the import of peroxisomal matrix enzymes in the peroxisomal matrix. One of the most important peroxins is pex3, defining the pre-peroxisomal compartment on the endoplasmic reticulum in the *de novo* peroxisome formation (Agrawal et al. 2011), controlling the embedding of peroxisomal membrane proteins (Fujiki et al. 2006), regulating the subdivision of existing peroxisomes into daughter cells during mitosis (Knoblach et al. 2013) and being the target of ubiquitination during the autophagic clearing of nonfunctional peroxisomes (Motley et al. 2012).

In this study, expression pattern of *pex3* in zebrafish is described. The first vertebrate model for this gene loss of function is generated and characterized. Peroxisomal and mitochondrial metabolism are impaired causing oxidative stress and reduction of mitochondria amount. pparγ activation and transcription of genes involved in lipid metabolism or oxidative stress reduction can rescue the phenotype. Moreover, *pex3* mutation causes lack of most melanophores in embryos and reduced pigmentation in adult melanocytes. This phenotype is independent of peroxisome; indeed, it has to be attributed to the melanosomal targeting signal (MTS) identified at the C-terminus of pex3. If pex3 is not addressed to melanosomes, they do not mature properly; moreover, foxd3-induced repression of the transcription of genes involved in the melanin biosynthesis pathway is prolonged. Zebrafish melanophores are then delayed in proliferation and migration and this has an impact also during metamorphosis, altering the pigment cell distribution, necessary for stripes formation.

5.1 In zebrafish developing embryos, *pex3* is expressed also in developing sensory organs, gill filaments and melanophores

Distribution pattern of peroxisomes in zebrafish embryos and in adults were previously described, based on *in situ* hybridization experiments and on cytochemical procedures to reveal catalase activity (Krysko et al. 2010). Krysko et al. evaluated the expression of peroxisome markers *pex14* and *catalase* with an *in situ* hybridization approach during early embryonic stages (24 hpf and 48 hpf). They described a ubiquitous expression, enhanced in the head region. Moreover, functional peroxisomes were detected in the wall of the yolk sack, in liver parenchymal cells, in the epithelium of the proximal renal tubules and in the intestinal epithelium at 96 hpf. These data closely resemble the well-established pattern of peroxisome distribution in mammals and human (Baes & van Veldhoven 2006).

The present study focused on a single peroxin gene, *pex3*, and its expression at different developmental stages and in each adult organ. Due to the presence of peroxisomes in all cell types and to the key role of pex3 in peroxisome biogenesis, it was expected to find a broad expression of this gene. The data confirmed ubiquitous *pex3* expression and refined published expression patterns. *pex3* expression is detected already at 8 hpf without interruption with the maternally supplied mRNAs (Giraldez et al. 2006), and progressively increases till 120 hpf. During embryonic development, from a spatially non-restricted expression pattern, *pex3* becomes increasingly enriched in the central nervous system. pex3 presence is enhanced in specific CNS regions, both at the mRNA and at the protein level. *pex3* higher expression might

correlate with an increased requirement of peroxisomes, due to particularly high metabolic activity in those areas, or with a specific function exerted by peroxisomes in terms of synthesis of molecules having a role in signaling or metabolism modulation. Besides this observation, new domains not previously described for *pex3* expression were identified during zebrafish embryogenesis. *pex3* was found in the developing sensory organs (optic cup, otic vesicles and olfactory epithelium), the gill filaments and in clusters of cells in the epidermis, identified as melanocytes. This outstanding expression might be connected to a particular necessity of pex3, restricted to those organs or to a specific stage in their development.

The different methods adopted to determine *pex3* expression in zebrafish (*in situ* hybridization, qRT-PCR and immunofluorescence) gave partially different results. In fact, the present study detected expression in organs which were not previously reported, such as specific regions of the brain and melanophore cells in the skin. The fact that the automated transcript analysis did not detect transcript in some organs may depend on the relative abundance of *pex3* transcript in comparison to others or to biological variation in the samples (Glaus et al. 2012; Trapnell et al. 2013).

Furthermore, the analysis complements data obtained in mammals. For example, the International Mouse Phenotyping Consortium made available *Pex3* expression patterns based on a conditional approach, in which the coding sequence of the LacZ gene was inserted into the gene ORF (Koscielny et al. 2014, release 4.3). Here, similarly to zebrafish, the brain is one of the most intensively stained organs, especially in the cortical part. Interestingly also the pineal gland displays a staining for *pex3* expression (Figure 64 A-A'). Other tissues which are positively stained are the adrenal medulla (Figure 64 B), the fibrocartilaginous intervertebral discs and other cartilage structures of the rib cage (Figure 64 C-C') and, similarly to zebrafish, groups of cells in the dermis layer of the skin (Figure 64 C''). Thus, the *pex3* expression data obtained in zebrafish mirror the mouse expression data and prepare the ground for knowledge transfer between different model organisms.

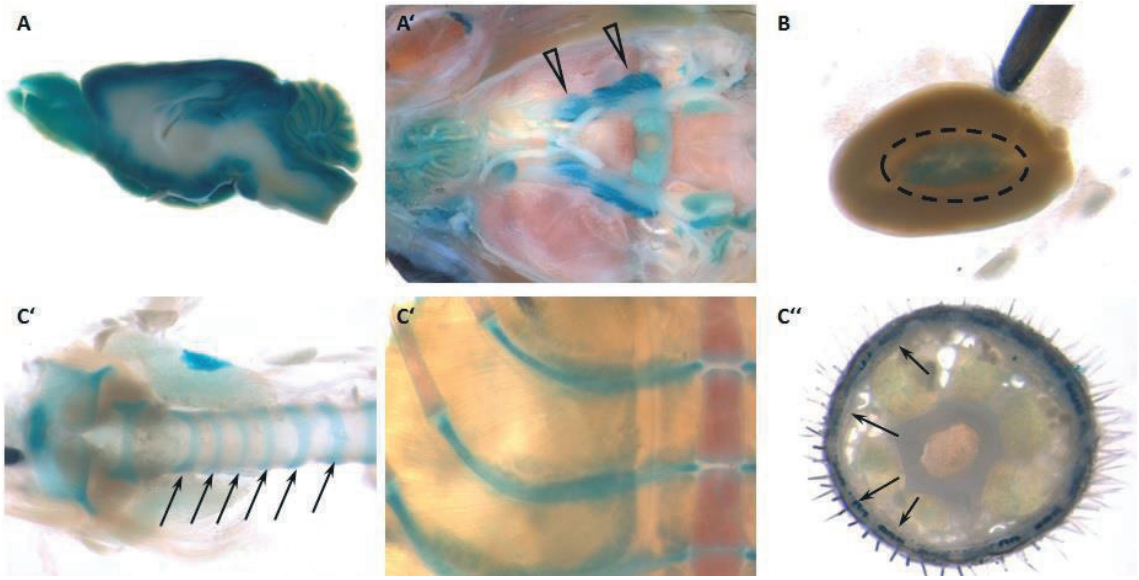

Figure 64 – Pex3 expression pattern in mouse. (**A-A'**) LacZ staining in the brain shows particularly high expression in the cortical part and in the pineal gland (arrowheads). (**B**) Also the adrenal gland is one of the tissues in which high *Pex3* expression can be detected, especially in the medulla portion (dashed circle). (**C-C''**) Fibrocartilaginous intervertebral discs (arrows in panel C) cartilage structures of the rib cage (C') and groups of cells in the dermis layer of the skin (arrows in panel C'') are also positive for *Pex3* expression. (Modified from http://www.mousephenotype.org/data/genes/MGI:1929646).

5.2 *Pex3* mutant alleles are responsible for mild forms of Peroxisomal Biogenesis Disorders

In contrast to the lethal or severely impairing effects in other established *pex3* loss of function models (yeast - Kragt et al. 2005 and fruit fly - Nakayama et al. 2011), the observed phenotype in the zebrafish *pex3* loss of function is not dramatic. First of all, the knock down models showed that lethality occurred only at high amounts of injected pex3 AMO TB and it seems to be a toxic effect of the nucleic acid, rather than a specific phenotype. A dose-dependent lethality is observed at lower amounts of injected AMO between 36 hpf and 48 hpf, but the effect is not penetrant enough to allow a comprehensive analysis of the onset of the phenotype. In the *pex3*$^{CRISPR/ZMP}$ mutants, no lethality could be observed in zebrafish at the embryonic and larval stage, despite studies describing at least three different mutations in human *PEX3* which causes lethality within the first four months after birth (Ghaedi et al. 2000; Shimozawa et al. 2000; Muntau et al. 2000). Recently, additional *PEX3* mutations were described in humans. In the first case, residue 347, rather at the C-terminus of the protein, is mutated from aspartic acid to tyrosine. The male patient was not diagnosed until the age of 30 and he reached the age of 36. He suffered of a mild form of Peroxisomal Biogenesis Disorder, the Infantile Refsum Disease (IRD), and the main symptoms were psychomotor regression,

late-onset leukodystrophy, peripheral neuropathy, hearing impairment, renal cysts, and renal hypertension. Fibroblasts contained peroxisomal structures positive for catalase (Matsui et al. 2013). In the second case, two novel compound heterozygous mutations were identified in a 9-year-old boy. The mother-inherited allele encodes for a truncated PEX3 version, after amino acid at position 300; the allele inherited from the father shows a change of the amino acid in position 331, from glycine to arginine. The patient suffers from mild biochemical abnormalities, with accumulation of VLCFA and reduction of plasmalogens. Cultured fibroblasts display abnormal peroxisomal mosaic pattern, with cells with import-competent peroxisomes and cells without (Maxit et al. 2016). Thus, *PEX3* mutant alleles might exist in the population, without giving any clinical symptom, or developing into disease at relatively late stage. They might not be identified, due to a possible residual activity or to a non-obligate PEX3 role in peroxisome biogenesis, in human. The few mutations classified as early lethal might be encoding for a mutated version of PEX3 protein, that only when present in homozygosity might negatively affect the cellular processes and the functionality of other interacting proteins. Nevertheless, it has to be excluded a dominant negative effect of these early lethal mutations, since a mutation giving clinical symptoms in heterozygosity was never described.

5.3 Metabolic differences between zebrafish and human account for dissimilarities in phenotypes

Some differences between zebrafish and human metabolism exist. First of all, zebrafish and humans are exposed to different oxygen partial pressure levels; zebrafish experience a more variable amount of dissolved oxygen, depending on depth, turbulence and chemicals. Despite the optimal standardized breeding condition in any facility and the physiological and molecular strategies to maintain constant blood oxygenation, it is not rare that zebrafish experience hypoxia (low oxygen levels). Thus, zebrafish depend much more on glycolytic production of ATP, preferring it to β-oxidation of fatty acids. The higher usage of anaerobic reactions induced the development of a variety of efficient ways to detoxify ROS, in comparison to humans, and this different oxidative status might have an impact on metabolic pathways (Anastasiou et al. 2011; Malek et al. 2004; Tseng et al. 2011). Another important difference is the temperature regulation. Zebrafish are ectothermic animals, meaning that the internal temperature control relies only for a small amount, if not at all, on internal physiological sources. Thus, zebrafish

exposed to temperature fluctuations switch towards glycolysis, in order to gain high amount of heat in a short time (Shaklee et al. 1977).

Moreover, peroxisome assembly is a temperature-sensitive process. This means that catalase-positive vesicle cannot be detected in fibroblasts from patients suffering of Peroxisomal Biogenesis Disorders that are cultured at 37°C, but in some cases, prevalently associated with mutations in *PEX2* gene, they do gain functional peroxisomes when cultured at 30°C (Moser et al. 1995; Osumi et al. 2000). Authors speculated that patients may be a mosaic for peroxisome occurrence from cell to cell, due to the different body temperatures (Giros et al. 1996). Finally, it has to be considered that the temperature range in which zebrafish could live in the wild is really broad, as low as 6°C in winter to over 38°C in summer (Spence et al. 2008), and the standard temperature kept in the LIMES Zebrafish facility is 28°C.

These considerations invite for a cautious interpretation of findings in zebrafish related to metabolism, since they might not completely reflect the cellular and tissue physiology in mammals.

5.4 *pex3* facilitates peroxisome interaction with other organelles

In the last years, several studies addressed the intracellular localization of peroxisomes and there are strong evidences that they interact with other organelles like mitochondria (Mattiazzi Usaj et al. 2015; Schrader et al. 2013), lysosomes (Kim et al. 2016; Chu et al. 2015; Jin et al. 2015) and lipid droplets (Zehmer et al. 2009). The importance of these interactions are not clear, yet, but they are usually associated with economy strategies in sharing proteins and metabolite required for the same function in different organelles (Dixit et al. 2010; Jin et al. 2015). In most cases, these interactions involve membrane-anchored proteins having a domain able to bind specific classes of lipids part of the membrane of the counterpart organelles (Chu et al. 2015; Binns et al. 2006).

Thus, peroxisomes should not be thought of as isolated organelles in the cytoplasm, communicating and exchanging metabolites exclusively by simple passive diffusion, but they are rather part of dynamic networks (Daniele & Schiaffino 2016).

Interestingly, the sequence analysis of pex3 highlighted the presence of regions which are highly conserved with proteins, such as Apolipoprotein B 100, which are known to bind lipids and have the task to sort lipids within and between cells. Moreover, lipid binding ability was demonstrated also for pex3 protein, both in association with lipoproteins and with liposomes (Pinto et al. 2009). This lipid binding activity is also associated with the local perturbation of

lipid bilayer structure in order to embed peroxisomal membrane proteins. Considering these observations, in the described *pex3*$^{CRISPR/ZMP}$ zebrafish model, missing peroxisomes might have an impact on other organelles. In fact, mitochondria are also affected by pex3 mutation: their metabolic activity and their number are remarkably reduced, most probably because of the reduced flux of substrate for fatty acid oxidation or increased oxidative stress (Figure 38). This would explain the observed reduced growth rate as a consequence of an energy deficit due to a reduced capability to process carbon sources. Moreover, the resulting oxidative stress in *pex3*$^{CRISPR/ZMP}$ animals should be able to induce the activation of protective mechanisms, including the proliferation of organelles re-equilibrating the redox status in the cell. In particular, the presence of a redox sensor molecule, namely CoQ_2, manages to modulate the activation of pparγ nuclear receptor. Its ratio between the oxidized and reduced forms mediates the transcription of genes involved in the change of organelle number or structure (Figure 40).

pex3 would not only be a structural component on the membrane of peroxisomes, but it might be able to guide and establish contacts with other cell compartments, through the recognition of specific lipids which are bound by cytoplasmic domains. With this study, the effect of interaction of peroxisomes with other organelles, especially with mitochondria, are defined at the cellular level. This means that loss of *pex3* is not only responsible of the impairment of peroxisomal metabolism, but it also affects mitochondria function, leading to increased oxidative stress. This is most likely the result of a loss of peroxisome-mitochondria liaison, in which peroxisomes seem to be a crucial factor. Furthermore, the effect of missing peroxisomes disrupting contacts with other organelles was explored at a higher level, namely in the embryonic development of zebrafish, with a range of cell populations in need of different hormonal and metabolic requirements.

Melanosome biogenesis is matter of long debate and a clear model describing this process is still missing. The most accepted model describes melanosomes originating from early endosomal compartments (Raposo et al. 2001). Later, these compartments undergo different maturation stages, distinguishable by morphology, enzymatic content and melanin content (Marks & Seabra 2001; Yamaguchi et al. 2007). However, recent evidences highlight a much more complex dynamic regulating melanosome biogenesis, with a multitude of membrane contact sites which involve different cellular compartments at different time points. Melanosome-mitochondrion contacts might control the quality of the maturing melanosomes, in order to ensure a proper membrane trafficking (Daniele et al. 2014). In the *pex3*$^{CRISPR/ZMP}$ zebrafish model both a reduced mitochondria average count and a defective melanosome

maturation were observed. Considering these information, the observed peroxisomal defect might have an impact on melanosome biogenesis. Future experiments should prove whether altered peroxisomal biogenesis has a direct impact on melanosome biogenesis, or rather due to the influence of mitochondrial function. To this end, the injection of the *pex3FL* or *pex3ΔMTS* mRNA in *pex3*$^{CRISPR/ZMP}$ mutant background and the measurement of mitochondrial abundance will clarify this aspect. Moreover, it is now recognized that melanosomal protein trafficking includes an endoplasmic reticulum transit step (Theos et al. 2006) and an involvement of the peroxin complex to assist the targeting and embedding of the proteins to specific domains cannot be excluded, similarly to what is described for proteins directed to lipid droplets (Schrul & Kopito 2016).

The same reasoning can be extended to other cell types in which peroxisomes turned out to exert a characteristic function. Chondrocyte migration is also affected in *pex3* transheterozygous zebrafish. Recently, it was demonstrated that altered peroxisomal proliferation has a negative impact on chondrocyte activity, recapitulating an osteoarthritis model (Kim et al. 2016). They link the phenotype with mitochondrial damage. Peroxisome and mitochondria dysfunctions activate the expression of several miRNAs with predicted functions in lysosome regulation, preventing the autophagy and degradation of the damaged cellular components (Levine & Kroemer 2008; Okamoto 2014).

5.5 Melanosomes and melanin synthesis are affected by cellular metabolism

Melanogenesis is a process regulated at different levels. Both the lack and the excess of melanin production are deleterious for the cell because, in one case, there would be a lack of DNA protection from UV-light mediated damage and, in the opposite case, the hyperactivation of the system can cause inflammatory responses or even malignant melanoma (Slominski et al. 2004). Melanogenesis is under the influence of modifying agents acting in a multidimensional network. Signaling pathways activated by receptor-dependent and -independent mechanisms contribute to induce the synthesis of melanin and they can influence the equilibrium to one or the other isoforms of the different biopolymers. The presence of metabolites in the melanosomal compartment can also promote or arrest the melanin synthesis, by limiting the substrate concentration, as in the case of dopaquinone to be transformed in dopachrome and dihydroxyindole carboxylic acid (Prota 1995), or the enzymatic activity, as in the case of H_2O_2 that is a potent inhibitor of tyrosinase (Schallreuter & Wood 1989). Also nitric oxide has

melanogenic activity, *via* stimulation of guanylate cyclase which produces cGMP as second messenger in the signal pathway (Romero-Graillet et al. 1996).

Melanosomes are metabolically active organelles and they could detect the effect of impaired peroxisomal metabolism (Slominski et al. 1993). In fact, melanosomes can sequester the host cell metabolism, switching to the most convenient mechanism according to the actual energy status, either activating oxidative catabolism or anaerobic glycolysis (Scislowski et al. 1984) and altering the intracellular availability of NAD/NADH and NADP/NADPH (Scislowski & Slominski 1983). The ratio in eumelanin rather than pheomelanin synthesis is determined by the redox potential inside the melanosome. A reducing environment with abundance of cysteine and/or glutathione in fully reduced thiolate state, both actively transported through the melanosomal membrane, stimulates eumelanin production; an oxidizing environment shifts the synthesis towards pheomelanin production (Hearing 2000; Potterf et al. 1999; Prota 1995). Therefore, the actual activity of antioxidant enzymes such as catalase, superoxide dismutase, glutathione peroxidase, glutathione reductase and thioredoxin reductase/thioredoxin supports the melanogenic pathway (Schallreuter et al. 1994).

Recent studies reported that in cells actively producing melanin, it is necessary the presence of the NAD(P)H:quinone oxidoreductase-1 (NQO1) enzymes and its expression positively correlates with that of tyrosinase (Choi et al. 2010; Yamaguchi et al. 2010). NQO1 is a flavoenzyme that exerts its role in the cellular defense mechanism against oxidative stress and catalyzes the reduction of quinones in hydroquinones, without an intermediate semiquinone. Thus, the differential phenotype rescue of *pex3*$^{CRIPSR/ZMP}$ embryos supplemented with either the oxidized or the reduced form of CoQ_2, may involve a direct induction of tyr expression, bypassing an eventual peroxisome homeostasis genes induction. Moreover, pparγ might have a direct role in pigmentation stimulation, by stimulating Tyr activity and the expression of Tyr and Mitf, in the melanocytes (Grabacka et al. 2008; Lee et al. 2007).

In light of this information, a mutation in *pex3* might play a fundamental role in melanogenesis at different levels, both considering the known role in peroxisome biogenesis homeostasis, and a putative novel function specific for the melanosomes. In first instance, *pex3*$^{CRIPSR/ZMP}$ zebrafish are devoid of functional peroxisomes, inferred by the loss of the catalase vesicular pattern in the cell. Absence of peroxisomes may affect all the other peroxisome-residing enzymes, including several antioxidant enzymes which lose their metabolic activity (Waterham et al. 2016), thus altering the cell redox status and the synthesis of different melanin isoforms.

5.6 pex3 is targeted also to melanosomes and exert its function on their membrane

In this study, a melanosomal targeting signal needed for pex3 localization to the melanosome membrane was identified. At the melanosome pex3 might cooperate with other proteins in the insertion of melanosomal proteins onto the membrane of the organelle. This feature is characteristic of pex3 and does not involve other peroxins (Table 10). In fact, other peroxins necessary for the import of matrix protein into the lumen (pex14) or taking part in the *de novo* peroxisome biogenesis (pex16 and pex19) seem not taking part in melanosome homeostasis, since their knock-down did not produce any effect in pigmentation intensity, in 2 dpf embryo lysates. Moreover, the fact that *pex3ΔMTS* mRNA construct was able to rescue the peroxisomal function, but not the proper proliferation and maturation of melanoblasts, reinforces the hypothesis that the trans-heterozygous phenotype is not a secondary effect of a peroxisomal disorder, but it is caused by an intrinsic property of pex3 (Figure 60). Thus, pex3 would be exerting a role in the regulation of the homeostasis of an organelle different than peroxisomes.

slc24a5 (Lamason et al. 2005) and *slc45a2* (Dooley, Schwarz et al. 2013) are genes encoding for antiporters present on the membrane of zebrafish melanosomes. They regulate the ion flux through the membrane, in order to keep the proper intra-luminal pH, necessary for the activity of enzymes involved in melanin biosynthesis. A mutation in either one of the genes causes a phenotype similar to *pex3*$^{CRISPR/ZMP}$ animals, with lower melanophore amounts at embryonic stage and poorly pigmented stripes at adult stage. In absence of pex3, even if overexpressed, *slc24a5* and *slc45a2* can barely rescue the embryonic *pex3*$^{CRISPR/ZMP}$ pigmentation phenotype. Only few melanosomes develop in the anterior region of the animals (Figure 58). This hints to the impossibility for slc24a5 and slc45a2 to exert their function on the melanosomes. According to this experiments, it is possible to propose a model in which pex3 would have the same molecular function on melanosomes as on peroxisomes. This means that pex3 protein would be anchored at the membrane of the melanosome and pex3 would act as docking receptor to facilitate the insertion of melanosomal proteins onto the membrane. If this is the case, this model would add a new player in the poorly understood process of protein delivery to melanosomes in pigment cells (Sitaram & Marks 2012; Toyofuku et al. 2002; Chen et al. 2002). Moreover, also other transporters or channels found on the melanosome membrane might not be correctly localized in *pex3*$^{CRISPR/ZMP}$ animals, preventing the trafficking of molecules between the cytoplasm and the lumen and vice versa. Melanin synthesis is under the control

of different stimuli such as concentrations of cysteine and glutathione, which are actively transported through the membrane. Thus, an incorrect concentration of these molecule prevents melanin synthesis and correct pigmentation pattern development.

The proposed model is partially in accordance with what was recently published by Schrul and Kopito (Schrul & Kopito 2016). In mammalian cells, they observed that a PEX3-farnesylated PEX19 complex is necessary for the insertion of newly synthetized UBXD8 in specific endoplasmic reticulum subdomains. UBXD8 is a protein present especially in the membrane of lipid droplets and requires a non-canonical insertion pathway through endoplasmic reticulum. In the model they propose, peroxins are part of a shared targeting machinery, having the endoplasmic reticulum as hub for mutual control of delivery of metabolic enzymes to their specific target organelle involved in lipid storage and consumption.

5.7 pex3 influences melanin synthesis sensing mechanism in melanophores

So far, the molecular function of pex3 protein was described. However, the phenotypical description of *pex3*$^{CRIPSR/ZMP}$ zebrafish embryos includes a broader range of events, which influence the whole cell homeostasis. In fact, the mutation has consequences also on the proliferation and migration of melanophores. The observed pigmentation phenotype hints to a pex3 function specific for the melanophore cell population, independent of the peroxisome. Several studies addressed the maturation of melanoblasts and melanocytes in relation to the melanin synthesis and there is a consensus that defective melanosomes prevent cells to proceed with cell cycle (Falletta et al. 2014; Choi et al. 2014; Hirobe 2011). The way the melanophores sense the incorrect function of melanosomes is still partially unexplored. Nevertheless, several studies show that this mechanism might include tyrosinase localization. In fact, tyrosinase mislocalizes in a variety of other pathological conditions, in which melanosomal function is impaired (Manga et al. 2001; Sprong et al. 2001; Sone & Orlow 2007). Indeed, also in *pex3*$^{CRIPSR/ZMP}$ melanophores, tyrosinase is not targeted to melanosome only anymore, with a strong reduction of the number and the size of tyr^{+} vesicles in immunofluorescence stainings.

The results show that pex3 action on melanosome proliferation is necessary and sufficient in the first developmental stages, when the melanophore cell population is specified and delaminates from the neural cell crest, and the melanoblast precursors are established and migrate to the dorsal root ganglia. In *pex3*$^{CRISPR/ENU}$ mutants, melanophores could not

proliferate in the proper number, preventing the establishment of the proper pigmentation pattern. Nevertheless, the rescue of *pex3* expression in the first developmental days through the injection of *pex3FL* mRNA, is sufficient to restore the pigment cell number. The rescue goes beyond the actual action of the injected mRNA, since it lasts through the metamorphosis stage, preserving pigment cell count and pigmentation intensity and it allows a convergence of the pigment cells to the final lateral stripe position nearly comparable to the one in wildtype animals.

5.8 Defective pex3 localization impairs proliferation and migration of specific cell populations

The key findings of this study are the defective proliferation and migration of the melanoblasts, when *pex3* is mutated in zebrafish. Melanocytes are affected also when the protein is only lacking the C-terminal melanosomal targeting signal, preventing its localization at the melanosome. Moreover, in the described *pex3*$^{CRISPR/ZMP}$ zebrafish model, *foxd3* is upregulated, leading to *mitfa* repression and dysregulation of the enzymes involved in melanin synthesis and of the genes involved in the melanocyte stimulation pathway.

When describing the pigmentation phenotype, there is a similarity with other published zebrafish mutants, e.g. *colgate*. In this mutant, *histone deacetylase 1* (*hdac1*) gene is affected. In mutant *hdac1* embryos, neural crest derived melanophores and their precursor are delayed in differentiation and migration. This comes as result of increased and prolonged expression of *foxd3* which represses *mitfa*, directly interacting at the promoter region (Ignatius et al. 2008). Interestingly, *hdac1* expression pattern is ubiquitous during the first embryonic stages, but it restricts at 36 hpf-48 hpf to the branchial arches, fin bud mesenchyme, hindbrain and otic vesicle, covering partially *pex3* expression domains (Pillai et al. 2004; He et al. 2016). The same gene was also previously described to be involved in the regulation of other neural crest-derived tissues during zebrafish embryonic stages, even if with different spatial and temporal requirements (Ignatius et al. 2013). Since the gene regulation in *colgate* and *pex3* mutants is rather similar, gene expression domains are mainly overlapping and affected tissues (melanophores and neural crest-derived tissues) are the same, it is possible to speculate that the two genes might be genetically interacting in the same pathway, producing the phenotype. Further experiments should be addressed in clarifying whether this is true and the possible mechanism linking the peroxin to intranuclear gene regulation. A hint is offered by previously published work, describing the bifunctional activity of a different peroxin, *PEX14* (also known

as *NF-E2 associated polypeptide-2 – NAPP2*), acting both as a polypeptide transport modulator and transcriptional corepressor (Gavva et al. 2002). In this last function, in human erythroid K562 cell line, PEX14 would interact with HDAC1, but not with other HDACs, regulating the accessibility to the promoter region of certain genes. Considering all this information, pex3 might be able to regulate gene expression, by modification of trans-acting elements on the genome.

Interestingly, the pineal gland is a region in which *pex3* expression was detected with *in situ* hybridization experiments and *foxd3* transgenic reporter is clearly visible in zebrafish (Curran et al. 2009). The same observations hold true also in mammals (Ge et al. 2005; Thorrez et al. 2008) (Figure 64 A'). The expression of the two genes in the same domain of the brain might put those in close correlation, with a possible regulation of *foxd3* operated by pex3 by means of a not yet identified mechanism. Interestingly, in *pex3*$^{CRISPR/ZMP}$ mutants, *foxd3* is nearly 10-fold upregulated and by knocking it down, the mutant phenotype is rescued, with total pigmentation intensity and enzymes involved in the melanin biosynthesis pathway similar to wildtype (Figure 51). This information becomes even more relevant if it is considered that the pineal gland is an endocrine gland located in the brain in which several hormones are produced. One of those is the α-melanocyte stimulating hormone, responsible for the stimulation of melanin production in the periphery (D'Agostino & Diano 2010) which was shown to be down-regulated in the presented *pex3*$^{CRISPR/ZMP}$ zebrafish model. Thus, future studies should address the question whether the expression of *pex3* (or *foxd3* knock out or knock down) in the pineal gland in *pex3*$^{CRISPR/ZMP}$ embryos is sufficient to rescue the pigmentation phenotype, through a specific gene regulation in that organ. Tools like transgenic lines used in this study for the quantification and migration of melanocyte precursors would help to carry on a transcriptomic analysis in a uniformed sample and to obtain a homogeneous picture of the gene regulation events.

5.9 Other tissues and cell population depending on melanin production could be affected in *pex3* zebrafish mutants

According to the results of this study, due to the ubiquitous expression of *pex3* (Figure 25 and Figure 27) and the presence of the protein on the membrane of the melanosomes (Figure 53 and Figure 54), all the cell types producing and storing melanin would be affected in the *pex3*$^{CRIPSR/ZMP}$ zebrafish model. Due to defective melanosomes also these other would suffer different kind of dysfunctions. Indeed, melanophores are not the only cell type having

melanosomes; they were detected also in the cochlea and in the inner ear, in the brain, in the eye, in the heart, in the adipose tissue and in the lung. Their function in the different tissues can vary, but it is mainly associated to UV-light protection and reactive oxygen species scavenging and protection (Plonka et al. 2009).

The most curious function of melanin is the one associated to certain regions of the brain, in which melanosomes and the melanin herein produced might have a neuroprotective and neuroendocrine function (Zucca et al. 2004). A brain region producing a particular form of melanin, the neuromelanin, is the substantia nigra. It controls motor activity and the circadian rhythm (Zucca et al. 2014). Future studies could address whether *pex3* mutation might have an impact on the endocrine activity of this part of the brain and whether pathological conditions similar to the human Parkinson's disease or schizophrenia might develop in the long term (Shibata et al. 2008; Dawson & Dawson 2003).

5.10 *pex3*$^{CRISPR/ENU}$ mutants stand out as disease model for pharmacological screenings

In this work, the first vertebrate model for a Peroxisomal Biogenesis Disorder based on the loss of function of *pex3* was generated. Previous attempts of treating patients suffering from PBDs are addressed to alleviate symptoms, rather than curative therapies (Klouwer et al. 2015). Supportive interventions consist in dietary supplementation of those intermediate metabolites which cannot be synthetized, due to the absence of peroxisomes, like docosahexaenoic acid (DHA; C22:6ω3), glyceryl trioleate and glyceryl trierucate (the 4:1 mixture of those is also known as Lorenzo's oil), cholic acid (first treatment officially approved by the American Food and Drug Administration), plasmogen precursors or citrate. Among the most technologically advanced, but invasive, approaches there are attempts of tissue-specific gene therapy (Hiebler et al. 2014), orthotopic liver transplantation (van Maldergem et al. 2005) and bone marrow transplantation, especially for the syndromes in which leukodystrophy develops in infancy (Aubourg et al. 1990). Because the PBDs spectrum is quite wide and that symptoms are rather heterogeneous, with higher variance in terms of morbidity and mortality, there is no univocal treatment.

Nevertheless, zebrafish cannot be considered a suitable animal model to perform metabolic studies, due to the problems connected to the control of food intake and to the peculiar way to breed animals in the laboratories. Moreover, in contrast to the human disease, in which mutations in almost all the peroxins cause early lethality, the mutation of *pex3* is not lethal and

this can be and much milder. This can be attributed to differences in metabolism, making zebrafish less dependent on peroxisomes (see Metabolic differences between zebrafish and human account for dissimilarities in phenotypes). A possible pharmacological intervention to modulate the metabolic phenotype consists in the activation of peroxisome proliferation through ppar-family transcription factors. Several molecules (thiazolidinediones, pioglitazone, rosiglitazone and fibrates, for example) are already on the market as ppar agonists for the treatment of dyslipidemia and type 2 diabetes mellitus. Even if they are specific in the ppar binding, if assumed for long periods they have important side effects, including genotoxicity, reduction of bone mass and resistance, edema because of fluid retention, heart failure and myocardial ischemia (Bortolini et al. 2013; Home 2011). Thus, this kind of treatment might not be suitable for the cure of genetic conditions. An alternative may derive from the data showing that only the reduced form of CoQ_2 (CoQ_2H_2) is able to activate pparγ-dependent transcription of target genes. In fact, since CoQ_2 is extremely lipophilic, its scaffold may be used for the generation of an optimized molecule for the distribution (by reducing the length of the isoprenyl units or by substituting hydrophilic groups on the benzoquinone ring). Once delivered in the oxidized (ubiquinone) form to the cell, the molecule should be able to sense the internal redox status, switching to the reduced (ubiquinol) form and being active, only in case of necessity.

The idea to interfere with melanosome biogenesis in *pex3*$^{CRISPR/ZMP}$ mutant is more intriguing. In fact, the availability of this new zebrafish model offers a new tool to tackle the need of a robust drug treatment. Due to the availability of large numbers of animals, their quick embryonic development and the early onset of the disease-related phenotype, zebrafish *pex3* mutant model carries several advantages to progress pharmaceutical research into the advanced preclinical phase. The phenotype caused by the *pex3* loss of function develops within the first 2 dpf and it can be easily scored with multiple parameters (count of melanophores in different region of interest, spectrophotometric measurements on different specimens). Thus, a quantitative analysis is easily accessible and possible in a relatively quick time, while this is not possible with other vertebrate models.

In this study, a potential mechanism is outlined, in which pex3 positively controls melanosome formation. Since it is difficult to envision a rescuing approach, in which a chemical compound substitutes pex3 protein function, it is easier to aim to a blockage of pex3 interaction with other proteins, to prevent the generation of functional or hyperactive melanosomes. This approach is particularly advantageous in several pigmentation disorders, where there is an

excess of melanin production or it is uncontrolled, such as melasma, age spots, acanthosis nigricans or melanoma (Stollery 2015; Pillaiyar et al. 2015; Que et al. 2015).

The role of pex3 and its localization might be conserved also in mammals, as observed in the murine melanoma B16 cell line. Interestingly, a metanalysis of numerous published gene expression datasets highlighted a potential therapeutic approach for the treatment of melanoma. Pex3 expression during melanoblast differentiation and migration to mature melanocyte, the first stages of transformation into *in situ* and invasive metastatic melanoma was analyzed (Figure 65). During the differentiation phase, there is an increasing expression of *Pex3* reaching its maximum when the cell needs to produce melanin into functional melanocytes. Later, *Pex3* expression maintains constant levels, also in the initial transforming phase, but a drop is detectable when the cells acquire invasive and metastatic properties, which is in line with the reduced pigmentation of certain types of metastatic melanomas (Brożyna et al. 2016).

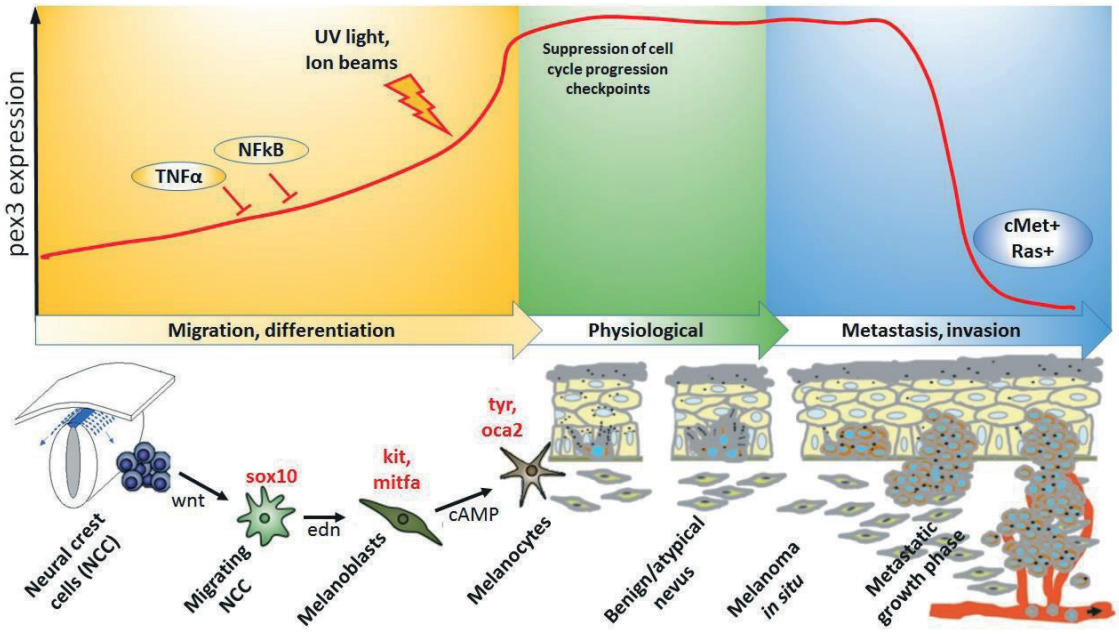

Figure 65 – Summary of the results of a metanalysis of numerous published murine gene expression datasets related to melanocyte lineage. During the differentiation phase, there is an increasing expression of Pex3, going along with the appearance of cell specific markers and the activation of different signaling pathways. Different physical and biological factors may induce variation in the Pex3 expression, resulting in an alteration of the proliferation profile. Pex3 peak expression is reached when the cell needs functional melanocytes for melanin production. Later, Pex3 expression levels remain constant, also in the initial transforming phase; but a drop is detectable when the cells acquire invasive and metastatic properties, associated to the expression of oncogene markers associated to cell proliferation.

When the association between pex3 expression and pigmentation is confirmed and pex3 would prove a possible predictor to foresee the outcome of melanoma in the clinical practice, pex3 might be a suitable target for therapeutic purposes, either directly to inhibit the protein interactions promoting melanogenesis, or as an anchor to address cytotoxic drugs.

Since the protein structure and the domains interacting with other proteins are well characterized (Sato et al. 2010; Hattula et al. 2014), by means of drug design molecular modelling it is possible to project different lead compounds, to further be tested in zebrafish, after the enrichment of the chemical space with different covalently bound moieties.

6 Conclusions

This study aimed to describe the consequences of *pex3* loss-of-function in the zebrafish vertebrate model. According to the results of the experiments, a model in which pex3 has a dual role can be proposed: a general one referred to the already known regulation of peroxisome homeostasis, present in all cell populations, and the other referred to the control of melanosome biogenesis, specific of melanophore cells.

As expected, in *pex3*$^{CRISPR/ZMP}$ mutants there is an impairment in peroxisomal function and metabolism. In details, the absence of pex3 prevents the import of peroxisomal enzymes, such as catalase or those involved in very long chain fatty acid oxidation, in the organelle matrix. This results in reduced peroxisomal function: energy sources cannot effectively be used, causing reduced growth rate, and ROS detoxification is impaired, with a parallel decrease of RNS concentrations. Thus, also the average number of mitochondria per cell is reduced. Activation of peroxisome biogenesis can be induced by providing a redox sensor molecule, namely Coenzyme Q. It can induce pparγ-mediated expression of genes of the lipid metabolism or oxidative stress reduction pathways, only when present in the reduced form.

This study provided important elements in defining a novel function of pex3 in a specific cell population, the melanophores. In fact, *pex3*$^{CRISPR/ZMP}$ mutants display an altered pigmentation pattern already during embryogenesis and then later, at adult stage. Indeed, pex3 was found to be present on the melanosomes, organelles required for melanin synthesis. The route bringing pex3 on the melanosome remains unclear. In absence of pex3 - either because it is totally missing or not targeted to the organelle due to the lack of the MTS – melanosome function is impaired and melanophore lineage cannot generate the correct striped pattern, typical of zebrafish. This mechanism is independent from peroxisomes, since it was observed that the injection of a truncated form of pex3, lacking the C-terminal MTS, can rescue peroxisome biogenesis in *pex3*$^{CRISPR/ZMP}$ embryos. The final phenotype is also mediated by an upregulation of *foxd3*, a repressor of *mitfa*, factor activating the transcription of enzymes involved in the melanin biosynthetic pathway. A defective establishment of the melanophore lineage precursors during embryogenesis affects the development of the proper adult striped pattern, in zebrafish. pex3 presence during the first days of embryonic development is sufficient to rescue not only the embryonic pigmentation pattern, but also partially the post metamorphosis one, in *pex3*$^{CRISPR/ZMP}$ mutants.

Preliminary data hint to a conserved similar function also in mammals.

Thus, pex3 is proposed to have the same molecular function on melanosomes as on peroxisomes, in mediating the import of membrane and matrix proteins on these two organelles, in order to ensure their function. It means that, beside of the well-established function on the peroxisome membrane, on the melanosomes pex3 acts as component of the importomer complex, cooperating with a pool of other proteins in the import of melanosomal proteins. A defective import mechanism prevents proper melanosome maturation, which impacts on melanophore lineage cells migration and proliferation. Whenever the melanophore lineage establishment during embryogenesis is rescued in *pex3*$^{CRISPR/ZMP}$ animals, this is sufficient to support the following metamorphosis stripe pattern determination.

Moreover, this study offers a valuable model for the study of pigmentation disorders. It opens new possibilities for the pharmaceutical research and for the discovery of new drug treatments.

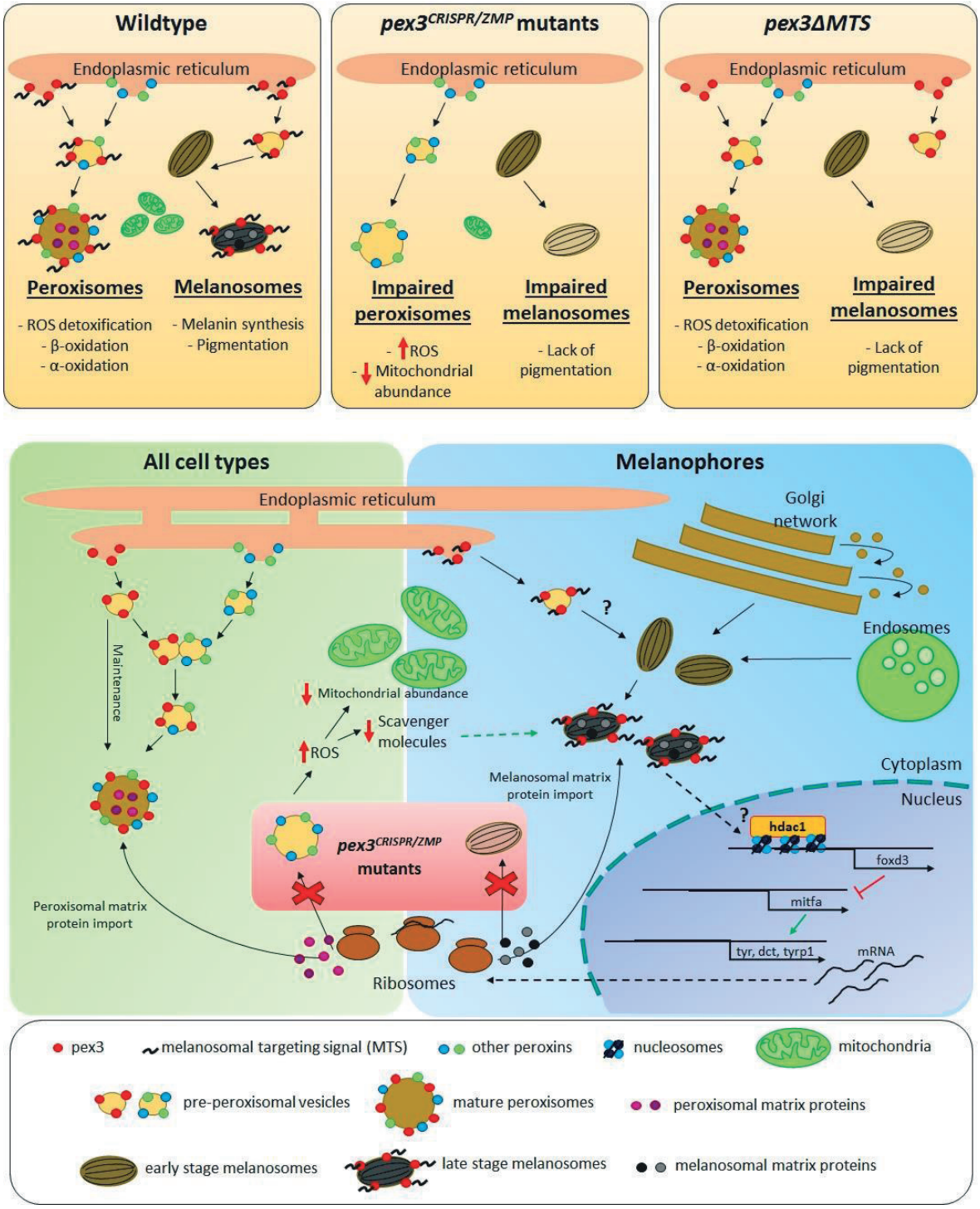

Figure 66 – Model summarizing the main findings of the present study. In zebrafish, pex3 has a dual role: a general one, linked to peroxisome homeostasis, in all cell types, and a second one linked to melanosome biogenesis, in melanophore cells lineage. The discriminant factor is the melanosomal targeting signal, newly identified at the C-terminus of the protein sequence.

7 Summary

Previous efforts aimed to understand the consequences of a dysregulated control of peroxisome biogenesis and of the dynamics of peroxisomal matrix proteins. Nevertheless, previous publications did not fill the existing gap in understanding the molecular events underlying the progression of Peroxisomal Biogenesis Disorders at systemic level. In particular, a vertebrate model deficient for one of the early peroxins (Pex3, Pex16 and Pex19) was never generated (Baes & van Veldhoven 2006).

In this work, the generation and characterization of a zebrafish model for Peroxisomal Biogenesis Disorders (PBDs) is described. The unique homolog of human *PEX3* was identified and its expression pattern was determined querying different online databases and with experimental techniques (*in situ* hybridization, qRT-PCR, immunofluorescence), during embryogenesis and at adult stage. This helped to identify new domains in which *pex3* is expressed and that were not previously described in mammals: specific regions in the brain, developing sensory organs (optic cup, otic vesicles and olfactory epithelium), gill filaments and clusters of cells in the epidermis, identified as melanocytes. Different genome editing methods (TALENs, CRISPR/Cas9) were successfully applied to generate a loss-of-function model (*pex3*$^{CRISPR/ZMP}$).

Different from what observed in *C. elegans* (Petriv et al. 2002) or *D. melanogaster* (Nakayama et al. 2011), zebrafish *pex3*$^{CRISPR/ZMP}$ mutants do not show any premature lethality and they survive to adulthood, even if they lack functional peroxisomes. Nevertheless, their peroxisomal and mitochondrial metabolism are impaired, lowering the energy status, increasing the oxidative stress and reducing the mitochondria abundance. This phenotype can be rescued through the activation of pparγ nuclear receptor, that induces the transcription of genes involved in lipid and xenobiotic metabolism, oxidative stress reduction and cell cycle regulation.

Surprisingly, zebrafish *pex3*$^{CRISPR/ZMP}$ embryos display additional major defects in the neural crest derived tissues, like pigment cell and cartilage-bone structures in the cranial region. In *pex3*$^{CRISPR/ZMP}$ mutants, embryos lack most melanophores, whereas melanophores are poorly pigmented at adult stage. In these animals, there is a prolonged foxd3-induced repression of the transcription of genes involved in the melanin biosynthesis. The phenotype develops independent of peroxisome and the discriminant factor is the identified C-terminal melanosomal targeting signal (MTS) driving pex3 on the melanosomes. In absence of this MTS, pex3 does not localize to melanosomes, whereas peroxisomes do not suffer any dysfunction.

Therefore, melanosomes do not mature properly, inducing a delay in the proliferation and migration of zebrafish embryo melanophores. This has an impact also later, during metamorphosis, for establishing of the correct pigmentation stripes pattern. Thus, pex3 presence on melanosome during embryogenesis is necessary for correct proliferation, maturation and migration events, in melanophore cell lineage.

The results of this study offer a model in which pex3 has the same molecular function on melanosomes and on peroxisomes. pex3 mediates the import of membrane and matrix proteins on these two organelles, in order to ensure their function. To achieve this role of importomer complex component on different organelles, pex3 might interact and cooperate with different pools of proteins. When pex3 is missing from the melanosome - either because it is mutated or not targeted due to the lack of the MTS – melanosome function is impaired and melanophore lineage cannot generate the correct striped pattern, typical of zebrafish. Preliminary data hint to a conserved similar function also in mammals.

Moreover, this study offers a valuable animal model for the study of pigmentation disorders. It opens new possibilities for the pharmaceutical research and for the discovery of new drug treatments.

8 Appendix

8.1 *Pex3* mutation reduces chondroblast differentiation and migration

In *pex3* loss of function zebrafish, the head shape is altered, due to defective formation of mandible structures. In order to verify the dynamics leading to the development of this morphological abnormality, an alcian blue staining in developing embryos at 72 hpf was performed (Figure 67). Alcian blue is an anionic dye able to stain acidic polysaccharides such as glycosaminoglycan in cartilages and sialoglycan in chondrocytes (Walker & Kimmel 2007). Indeed, when comparing wildtype and pex3$^{CRISPR/ZMP}$ stained embryos, it is possible to detect differences in the pattern. In mutants, first, the global staining of cartilage structures is much less intense, especially in the region of the mandibular and the developing gill arches. It can be detected both from a dorsal view (Figure 67 A-B) and from a lateral view (Figure 67 C-D). The stereotypic hyosymplectic, palatoquadrat and Meckel's cartilages are barely detectable. Moreover, during this developmental stage, cells which are involved in the deposition of the cartilage proteoglycan matrix, the chondrocytes, migrate from the neural crest to reach the periphery (Yan et al. 2002). These cells are similarly stained with alcian blue. In trans-heterozygous *pex3* mutants, the number of detectable peripheral chondroblasts is markedly reduced in comparison to wildtype (Figure 67).

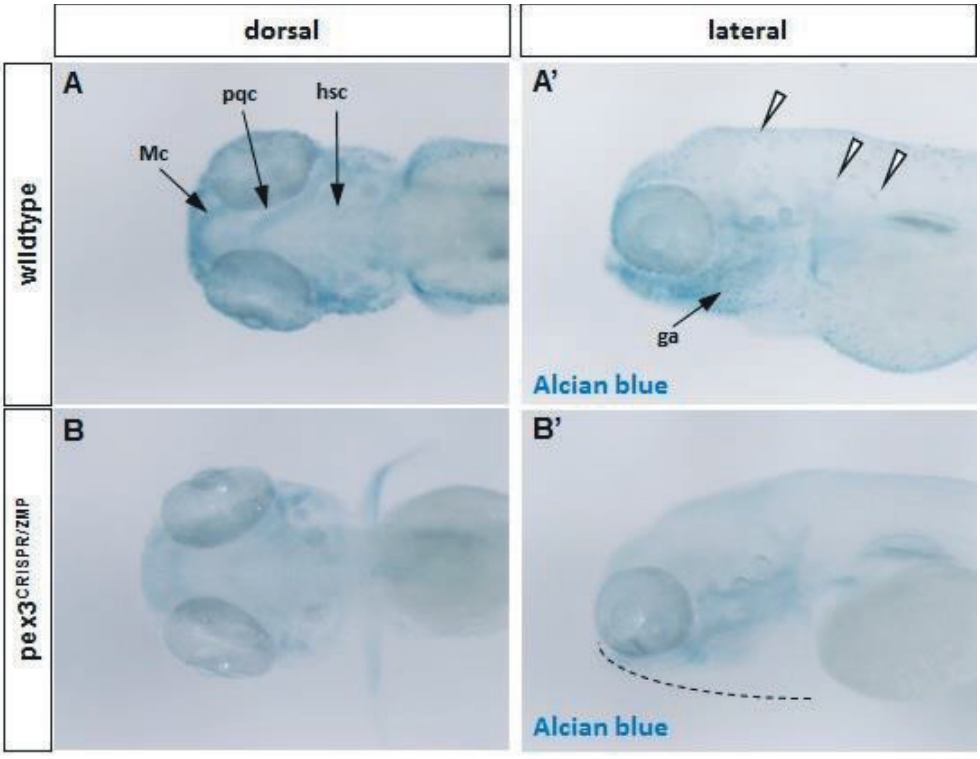

Figure 67 *(on previous page)* **–** Alcian blue staining reveals altered morphogenesis of the cranial cartilage structures and distribution of the migrating chondrocytes in *pex3*$^{CRISPR/ZMP}$ embryos at 2 dpf. (**A-A'**) At this stage the Meckel's cartilage (Mc) the palatoquadrat cartilage (pqc), the hyosymplectic cartilage (hsc) and the gills arches (ga) are clearly distinguishable in wildtype embryos. Moreover, single chondrocytes migrating from the neural crest to reach the periphery are clearly detectable (white arrowheads). (**B-B'**) In *pex3*$^{CRISPR/ZMP}$ mutants, the mentioned cartilage structures are barely visible and it is not possible to detect any migrating chondrocyte. This results in an altered facial cranial morphology, with the mandibular part not extending (dashed line in panel B' represent the projection of the wildtype sample in panel A').

These results show that, in addition to the described effect influencing proliferation, maturation and migration of precursors of pigment cells, in *pex3*$^{CRISPR/ZMP}$ embryos, the migration and function of another neural crest-derived cell type, the chondrocyte, is impaired. In this case, it was not possible to further characterize this phenotypical aspect, to determine whether it is connected to the lack of peroxisomes in the cells, or to some other unknown mechanism.

8.2 Additional data

8.2.1 Zebrafish *pex3* genomic sequence

AGACTCTATCTGTTATCTGCAGTTAGCCTGTCTGCAGCTAACATGAGAACTTATT 5'UTR Exon 1
GCCATGTAGCATTGTGCTAGCTAGTGAGTTACGTCTAAACCCGCTCTTGCTTCTC
TTATTTCTTTTCATTTTCGGTGTCAAGTCTGTTAAA**ATG**TTGAGTTCTACATGGA **ORF start**
ATTTCATCAAACGCCATAAGAGGAAATTCATCTTCACTGGGGTGTTTGTTGGAGG
TAACTAACGTGGGCAACTGAACCTCATCCATGCATACATATCAGTGACTGTTCAC
TAGCTGTAACTATTTCTTGTTTTTAATAAAATACTTGTAGCTATAGCATGTTAAT
ATGATGTGATGTGTAGTTTAGCGTGTTATTACAGTGTTGACAACCATTATATATT
TTTTCCACATTCAGCCCTTCAATCTCAGTTCACCTGTCACCTAGTTTTTCTATTG
GCATAGTCAAATCAAAGTTGAAATGGACTTTACCCTGGAATTTTTAGTCAACAGA
AAGGCTTTATTTAACTGAATAGTTCTTGCTTGCAGCATATCACTTTGTTAACATG
GATGCTATACTATATTGTAATCTCAAACTTTTTATTTGCAGGTGTTTATCTGCTT Exon 2
GGTAAATATGCACAGAGAAAAATTCAGGAGATGCAGGAGCGAGAGGCAGCTGAAT
ACATTGCTCAAGCTCGGAGACAGTTTCATTTTGAAAGCAACCAAAGGACATGCAA
CATGACAGGTAAACTAAATACCGCCATAACTGATGTTTATGTTGTTATAATTATT
TATGGAGTATGTAATTTGTTTTTTGTAGTGTTATCAATGCTCCCCACTCTCCGAG Exon 3
AGGCAATCATCCATCACCTGAACTCAGAGAGTCTCACTGCTTTGCTGAAGACTAA
GTGAGTTATGCACGTGTGTGTGTGTGTGTGTGTTTGTGTGTGTGTGTGTGTGTGT
GTGTGTGTGTGTGTGTGTGTGTGTGTGTGTGTGTGTGTGTGTGTGTTGTAGAAGC
TTAACTACATTATAAATGTAAAAGAATATAAATGACGCAAGTGATCATGTCTTTC
TCTACAGGCCAGCAAATAAACTTGAAATCTGGGAGGATCTAAAGATTATAAGTGA Exon 4
GATTATTTCTCATTTTTATGTAGTTTGTCATATATTGTTTTTTTCATTCATTCAT
TTTCTTTTCGGCTTAGTCTCTTTATTAATTAGAGGTTGCCCCAGCAGAATGAACC
GCCAACTTATCCAGCATATGTTTTACACAGTGGATGCCCTTCCGACTGCAACCCA
AGACTGGAAAACATCCATACATCCTCATTCACTAGATACACTATGGCCAATTTAG
TTTATGCAATCTTGCTACCCACTGCACCACTGTGTCGCCTATTGGTTTTTTTTTT
TTTCATTCAGTCATTTTCTTTCAGCTTAGTCCCTTTATTAATCAGGGGTTGGCCC
AGCGGAATGAACCGCCAACTTATCCAGCATATGTTTTACGCTGAGGATGCCCTTT
CAGCAGGCAACTTAGTACTTGAAAACACTCATCATACACTCTGACATGCACACAT
ACACTACAGCCAATTTAATTTATTCAATTCACCTATAGCACATGTCTTTAGATTG
TGGGGGAAACTGGAGCACCCTGAGGAAACCCACGAGAACATGAGGAGAACATGCA
AACTACACACAGAAATGCCAACTTACCCAGCCAGGGCTCGAATCCTCAACCTTCT
TGCTGTGAGGCGATCATGCTACCCACTGCGCCACTGTGATGCCCTATTGTTTTTA
TTGAGAATAAATATTTTGTATATAGCAATTGAATTTATTTTGTTTATGAACAGTA
AAATTACAGTAAAAATGTTGACATTTCAATTCACTCATTCCTTTTAAAATTTAAT
ATAATTGAATATTTTTTTTTATTTTACAGAATTTCCTTTTTAACATTCTCAATCA
AAAAATCTTAAAAATAATAAATAACTTTTTTTCAAAGAAATTGAATATCAGAGTG
AGCTAAATTGTCAATTGTATTCAAGTAGTAAACAGTTGTAGTAATAATTGAAACT
TTTTTTTTTAAGTACAATGTAGCAAATTCCACTGACATCATGTGGGTTATTAAAA
AATGACTAATAGATATTAAAGCATTGTCTAGGCTCAATTCTACTATGAAACACCC
ACTATTGACAATCAGAATAATTCACACCCTACAATTCTGGGAATCTTCTGTTTTA
CAATACATCACATTCAAGAATTAAAATACGTCATGACCAGAAATTCTGCTGAAAT
CTCAACCATGCCTTTTAGCAATGTTTAAGCTTAATTTGCACAAACAATTCCAGGA
GGATAGGTTCTGCTATTGTTTTCAATTAATTAATTAAAGCGTGGTGTTGGAATAT
TTAATCAATTCCATGCGTGTTCAATAAAAAAGGTTAGGTTTTTCTTTAAGGTTTA
ACATATTAGCAATTTAATGCATACAACTGAATAATTTGATTTACAGAATTCTGTT

ATCCTCAATGCAATGCAAAAATTACATTCAGGATGTGCGCACAGGTTTCATTTCC
TGACTTCAACTTATATAGGCAGCTGATATTAACAGGTGGAGTTTAATGGAATTTT
TCACTTGTCAATCATTCTCCAGTCCTCCAATTTTAGACTATCAGGCCTGTGCTTC
ATCTACTTCTGCAAAAATGTTTTATTGGTATGCAAAGCAAATCACACTCATAAAA
AAGTTCAGGTAATATTTGACCTTTAAGCAATACAAATACAATTGTTTAATGAAAA
GAAAAAAAAGGCAAAAATGTTTACAATTTTTCCCAGACAGTATCCATACTCTCAT
CTTTTATAAGTTGAAGAGAAGTTGATTCATTAATGTATTGCAAAATTAAGTGTAA
CAACTTGTAACGGGGTGGCAATGTGGCTCAGTGGTTAGCACTGTCGCCTCATAGC
AAGAAGTTTGCTGGTTTGAGTCACGGCTGGGCCAGTTGGCATTTCTGTGTGGAGT
TTGCATGTTCTCCCTGTGTTTGCATGGGTTTCCTCCAGATCCTCCGGTTTCCCCA
ACAGTCCAAAGACATGCACTATAGATGAACTGAATAAGCTAAAATAGCTGTAGTG
TATGTGTATGAATGGGTGTATGGCTGTTTCCCAGAACTGGGTTTCAGCTGGAAGG
GCATCCGCTACGTAAAACATGTTGGAATAGTTGGCAGTTCATTCCGCTGTGGTGA
CCCCTGTGAAATAAGGGACTAAGCCGAATTAATGGATAAACTTGTAATGGCCACC
TTTAGACCGCTTCTCATTGCCACTTTTGACTTTTAAAAATAGCCAATATTAGGCC
TAGGTTCAGTCGTTTTAACAACACTAAGACTGAAATCCAATAATTATGACATTTC
GGAATGCTGCTCCATTCCTTTTTCTAAAACACCCATCTCTGTGTTCAGGTTTTAC Exon 5
CCGCAGCATTGTAGCCGTTTACAGCACCTGCATGCTGGTTGTGTTACTCAGAGTT
CAGCTCAACATAATCGGTGGATATCTGTACCTAGATAACTCTGTGACGAAAAATG
GAATGGTACGTCAGTTTTTTTAACAGCATAGCAATCCGATTTTATCATGTTGAAG
CACATGAACATTTAATTTCTCTCATGCTCCAATTTTAGACCCCCTTAGCACCACC Exon 6
TGATGTTCAACAACAGTATCTTTCCAGTATCCAACATCTTCTTGGAGAAGGTGAG
GACAATGTCAGATCTGTATAAGAGCGTATAATCTGTACTACAGGTTAATCCTCTG
TTTGCACATATCCCCTGTAGCTGACACTGATGTTTGTTTTGTGTTTTTTAGGGCT Exon 7
CATGGAACTGATAACTGTGGTCAAGAAAGCTGTTCAGGAAGTTTTTGGACTGTAT
GTTGAGTAATTGATTTGAGAATTAATTTGAATCTACTCTATTGGCGAGTGCAGCC
ATCATGTGGTGACAAAATTGTATGTTTATCAAGAGAGAAAACTACTGTCCGTGTC
TCCTCAGGGTGTCTCTGAAGCAGAGTTTGTCTCTACAAGAGCTGGAGCAACAGTT Exon 8
GACACAGATCAGACAGTTAGTGGAGGACGACTCCTCTAAATACAAAAGTCTTTCC
TGGTACATGATGCCTGATGAAGAGAACACACTTGCCTCACAGGTAGATATATATG
ATATAATTTATACATAATTTCTTAATTGCATACAGTTGAAGTCAAAATATTTTTT
TTAACAGAGCAAGAAATTTTTCATATATTTCTTATACATATAGAGATTTTTTTTT
TCTGGAGAAAGTCTTATTTGTTTTATTTATTACCCTAACTTGCCTATTTAAACTA
ATTAGTCTAGTTGAGCCTTTAAATTGCACTTTAGGCTGAATATGTACTGTCATCA
TGGCAAAGATAAAATAAATCAGTTATTACAAATTAGTTATTAATCTAATGTTTAG
AAATTATGTTTATTATATTAAATTAATAAATTATGTTTAGAAATGTGTTGATTTT
TTTCTCCATTAAACAGAAATTGGGGGAAAAATATACAGGGGGGCTAATAATTCAG
GAAAGCTTCAACTGTATATAATGCATTCATTCATTTTGTTTCTGGGTCAAAGCTG
TTTGATTTTGTAATCCATGTATAATTACAATAAAAAAATGACCAATTTAAATGTA
ATATATACAGGAAGCATATTAAATGCAAGTAAGAGCTTTACTTAAATGTTTCTTT
GATGGTGTCTACTTAAATGTCTCCAATAATTTTTGTAAAACTAAAATGTCATTGG
GTAAAATAATATTCTATTGTCATTTAGCCTAACAGATGTATTTATTAATCCCTCC
AGGATTTTGCAGTGATTTATTTTCTTTTTATATCTGCAACCTAAAATTAATGGTT
TTGTGATTGTAATTCAAAAAAAGTCTTAAGCATTATTTCCTTTAATATGTGTGTT
TTGCTGTGAAAATATACACAAATGTTTTATTTTTTATTACATTTATTTTTCTTTT
TTGATCTCAAGAACCACTGGATCTCAAAATCCTGAATGCACTGATTTGTGTAAAA
ATAAAACGATATTATTGTTCTGACCATTACTGATTACAATGTATTATATACAGTA
TATATATATATATATATATATATATATATATATATATATATATATATATATATAT
ATATATATATATATATATATATATATTGTAATCATTGAGCATCAAATTGGCACAT
TAGTGTAATTTCCGAATGATCGTATAACACTAAAAACTGTATTGATGATAAAAAT
GACATTTTATGTTTCTCTGTTTATTTATTCCTGTATAATGACATTTTTTCTAGGC Exon 9
CTGTGGTCTCACAGAGAATGATGTCACAACGATAAAGCTACTAAATGAAACCAGA

GATATGCTGGAAAGGTGAGGAAAAGGAGTACTTGCACTAATCAGAGATCACTAAA
ACAATCTTTTGAGCACCAGGTACTAATTGCTCCACAACTTCTACTTCTTTTTTCA
GTCCAGACTTCAATATTGTTCTTCACACTTGCTTGAATCGAGGATTTGTCAGATT Exon 10
TCTAGACAACATGGCAGAGTTTTTCCGACCCCCGCAGAGAGACTCCACTCCCTCC
AGCACACCTGACCAGTCAGTGGACATGCTTTTCATTTCATTGAGAAAAATGACTG
AGTGGACATGGTTAATAATAATAATAATTATTGGGGCACTTAAAAGGTTTATTTA
CAAAGGTTTCAGGGAACAACATAAGCTTAAGTAAATAAATTGTAAACATTTAAAG
GTAATTCTGGCTTCTCTCATAATTCTGGATTGTGAGAAAAAACATCATTACATTG
TGAAAACAATTACAAGTTAGAAGCTCAAGCTTTAATTGTGCCATGCAGAATTTAC
ATTTCACATTTTTATTCTTTATCATTTCATTTTTAACTTCACACAGTCTTGGTTC
TGAATTCTGAATTTGCATCTCAATTCTGACTTATTTTATTTTACACAGATCAGAT
TTTTTCCGTAATTCTGAATTTACATCTCACATTATCCCATAAAAGGATTGGTCAG
CCATAAATTCTGTCATTATTTACTGACTGTTTACTTGTTCCAAACCTGTTTGAGA
TTGTATTTGTTGTGTTGAACACAAAAAAAAAGATTTTTTGAAGAATGTTAAAAAC
CTGTAACTATTTACTTCCATAGTATTTGTTTTTCCTACTATGGAAGTCAACAGTT
ACAGGATTTTAGGGTGCTTTCACACCTACACTTTTGTTTCGTAACGTGTCTCGTT
TGCCCAGTTACCGCGGTTCGTTTGGCATATGTGAACAGGGCAATCACGCTCTGTT
CCGCGCCAAAGTAATCGCTCCGTGATCGCTTGAATGAGGTGGTCTCGGCTCGATT
GAAACGAACCCTGGAGCGGTTCAATTACAGTGAGAAAGCGATTCGATCTGAGCGC
GGTTTTATCACAGTGTTTTATGGATATGTAATAGGCATACGGCGATATGAAGAGA
GAATTATGAGTATGGCGGGAAGTTTCCCGAGTCTCCGGATGCCCGCAAACGAGTG
ATGATCTCCCGGTAATCTTGCATCTCCCTCCCTGTCCTCAAATAGGCTACATCGC
GCACCCTTCTCACCCCTCCCCACTGCATCTCTCCTCAGACACATCGCGCGCGCAC
CCTGTCAATCACCACCAAACCCCCACCTCTCCTGACAGCTGAGCGGGACGCTGCA
AAATAAACCCTGACACTCTGACCAATGTAAGGAGAGTTTACTCGCACGTGACTTG
TTTTAGCTCTTTTGGTCTGATTAGAAACTTTGCAATGTGAAAGTGAACCGCTCCA
AGAGCAAAGAGCAACAATGTAACAATTGTAATCTCTGTTTCGGAACAACTGAATC
GATTCACAGGTGTGAAAGCACCCTTAAACTTTCTTAAAAATATTTTTGTGTTCAA
CAGAATAGAGAAACTCAGAGGTTGAAACCATTTGAGGATGAGTAAATTATTAGTT
TTGAGTGAATTATCCCTTTAACTGTACGTTCACACTGAAGGCGGCAAGAGCGTCA
AAGTACTGGAAGTCATTCATTTTCAATGGGAGCCGGCGACGGCTTCATCAGTGTG
AGTGTTGAGAAGAGTTGAAATCAAGTCAACTTTATAGTAATGAGGTATGACGCGG
TTCAGCGGCAAGCAATTGGTATGTAGAAGTCAACCGCTTGAGAGGAGTCCAGAGA
ACACAGCCCTATGAACATTGGTTCTGACCAGAGTTCCCAAAGTTTTGATTATTGC
GGTCACTGGAGTTCCAATTATTTACAATGTTTTCTTACAGGGACTTAAATATAAA
AAAAGTTACTGGCGAGTTGCTGATGTGCATTAATGTTATATATGTTTTTTTTAAA
TGGGAATCTTATGCTAACTAATGACAGTACAAAAAAGTATAGCTGCTTCAGAATA
TTTCAGACATATGGACATATTGGATATAGTCTATTTCTATGTATAGTTTAGCAAA
GCCACAGCACTCGCAACAACAGGATCTTCCGTATAGGTAAATCAATTTCATAAAA
GATGCGCAACACTTTCACACTAAAAAGCACATTTTTATGCAGAAATGTTAGTGAT
TTGCTGATGTGCTGCAACGGCTCCTTTAAATACAAGATCAATGTAGCAAATTTTG
ATGCTCTCACTGCCGGTGTGGACGCAATTTAGTTCTAAATTTAGGTCTCATATTT
CTGATCTTTTTCTTTAAAATTTTCACCTCACATTTGACTTTTTCCTAAAGATTTC
TTAATTTAAATCTCACATTAATTCTTAGTTTACATCCCACAATTTTTACCTTGTT
TTCTCTACATTTTGACCTTACATGTTAACAGTTCATTTATTAATCTGTTTTTAAA
TGACTGAAAACTGTTGTTTTATCCCTCCAGACTATCGCATGTAAGCCTCCCACTA Exon 11
GCCAAAATCATTCCCATTATCAACGGACAGATTCATTCAATATGCAGCGAAATTC
CAAGCCACTTTGTTCAGGTGAGCACCTTCATATAAACTGACTCTTTTTCATTTAA
ATCATATATAAGCTTCCCATACACAACTTGTTCCTTCCTGTGTGGCTGTTTTTAG
GATCTCCTGTTGATAGACCAGGTAAAAGAATTTGCCGCCAACGTATACGAAACCT Exon 12
TCAGCACCCCTCAGGAACTTCAGAAG**TGA**GCAAGACATAAAAGCAAAACTCCTAG **ORF end**
AAATCTCTCATGCCGTACAGCACAGAATTGCTCTCCTCACGCGCCAAAAAAATCA 3'UTR

ACCTGGAGTGAAAAAAAAAACTTGAATCAAGTTCTAAGTGTGTGTTAAAGGAGTT
CAGATTCACTGTTGTTAGTAGGCATTCAGTTTGGAGTAGCTTTAGCTGACCCCTC
TGTATGCTGTGACCCTCTTAACATTGTCCAGGGCATGCCAAGGTTTGTAGTCTAT
AATAAACTGTAGCACATTATTTATTTATATTTTAATAAAACAAACCCCTTTAGCA
TAACATTGTCATTAATATCACAAATAAAAAGGAAAACAACTTGTTCACCGGACTC
AATTCTGACAGCCTTACATCTGCAGTATGGACTTAAATGGGTGAATTGTGGTCAT
TTTGTATATTATATCAATATTATACCTGAGGTTGCAGCTTCTGGACCAAAACTCA
CCTTTGCACCAATAAACTGCTAAGCACATGGATATTTGGGAGCATTTTTGTTTGT
ATCGACTTTCATTTTGAACGGCTCTACTACTAACTGATGGGAATCATTTGCAAAA
TGGTACAGTTCGTAGTATGCTCTTCTGTTTTTTTTGTAAAATGACCCATGAATGT
TAATGAATAATAATGTGAGTAATATTATCGGAACTATTCATTAAAAT

8.2.2 pex3 *t*ranscripts coding sequence

Exons are indicated in alternate colors.

ATGTTGAGTTCTACATGGAATTTCATCAAACGCCATAAGAGGAAATTCATCTTCACTGGGGTGTTTGTTG
GAGGTGTTTATCTGCTTGGTAAATATGCACAGAGAAAAATTCAGGAGATGCAGGAGCGAGAGGCAGCTGA
ATACATTGCTCAAGCTCGGAGACAGTTTCATTTTGAAAGCAACCAAAGGACATGCAACATGACAGTGTTA
TCAATGCTCCCCACTCTCCGAGAGGCAATCATCCATCACCTGAACTCAGAGAGTCTCACTGCTTTGCTGA
AGACTAAGCCAGCAAATAAACTTGAAATCTGGGAGGATCTAAAGATTATAAGTTTTACCCGCAGCATTGT
AGCCGTTTACAGCACCTGCATGCTGGTTGTGTTACTCAGAGTTCAGCTCAACATAATCGGTGGATATCTG
TACCTAGATAACTCTGTGACGAAAAATGGAATGACCCCCTTAGCACCACCTGATGTTCAACAACAGTATC
TTTCCAGTATCCAACATCTTCTTGGAGAAGGGCTCATGGAACTGATAACTGTGGTCAAGAAAGCTGTTCA
GGAAGTTTTTGGACTGGTGTCTCTGAAGCAGAGTTTGTCTCTACAAGAGCTGGAGCAACAGTTGACACAG
ATCAGACAGTTAGTGGAGGACGACTCCTCTAAATACAAAAGTCTTTCCTGGTACATGATGCCTGATGAAG
AGAACACACTTGCCTCACAGGCCTGTGGTCTCACAGAGAATGATGTCACAACGATAAAGCTACTAAATGA
AACCAGAGATATGCTGGAAAGTCCAGACTTCAATATTGTTCTTCACACTTGCTTGAATCGAGGATTTGTC
AGATTTCTAGACAACATGGCAGAGTTTTTCCGACCCCCGCAGAGAGACTCCACTCCCTCCAGCACACCTG
ACCAACTATCGCATGTAAGCCTCCCACTAGCCAAAATCATTCCCATTATCAACGGACAGATTCATTCAAT
ATGCAGCGAAATTCCAAGCCACTTTGTTCAGGATCTCCTGTTGATAGACCAGGTAAAAGAATTTGCCGCC
AACGTATACGAAACCTTCAGCACCCCTCAGGAACTTCAGAAGTGA

8.2.3 Predicted pex3 amino acid sequence

MLSSTWNFIKRHKRKFIFTGVFVGGVYLLGKYAQRKIQEMQEREAAEYIAQARRQFHFESNQRTCNMTVL
SMLPTLREAIIHHLNSESLTALLKTKPANKLEIWEDLKIISFTRSIVAVYSTCMLVVLLRVQLNIIGGYL
YLDNSVTKNGMTPLAPPDVQQQYLSSIQHLLGEGLMELITVVKKAVQEVFGLVSLKQSLSLQELEQQLTQ
IRQLVEDDSSKYKSLSWYMMPDEENTLASQACGLTENDVTTIKLLNETRDMLESPDFNIVLHTCLNRGFV
RFLDNMAEFFRPPQRDSTPSSTPDQLSHVSLPLAKIIPIINGQIHSICSEIPSHFVQDLLLIDQVKEFAA
NVYETFSTPQELQK

8.2.4 Pex3 genomic loci syntheny analysis

Zebrafish (chr. 20; 37.857.614-37.866.424)

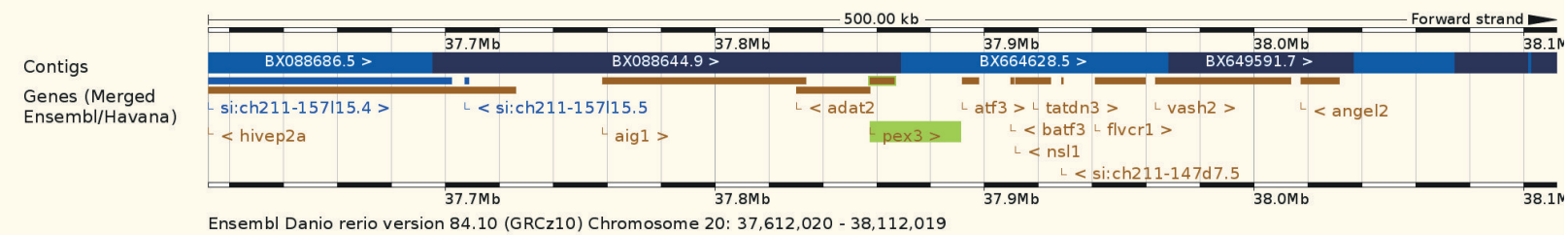

Human (chr. 6; 143.450.807-143.490.010)

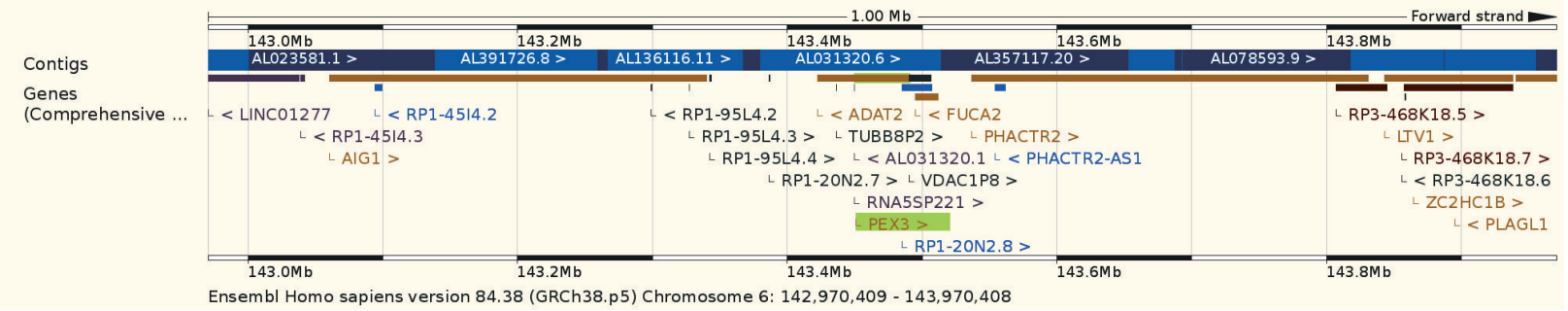

Mouse (chr. 10; 13.523.842-13.553.142)

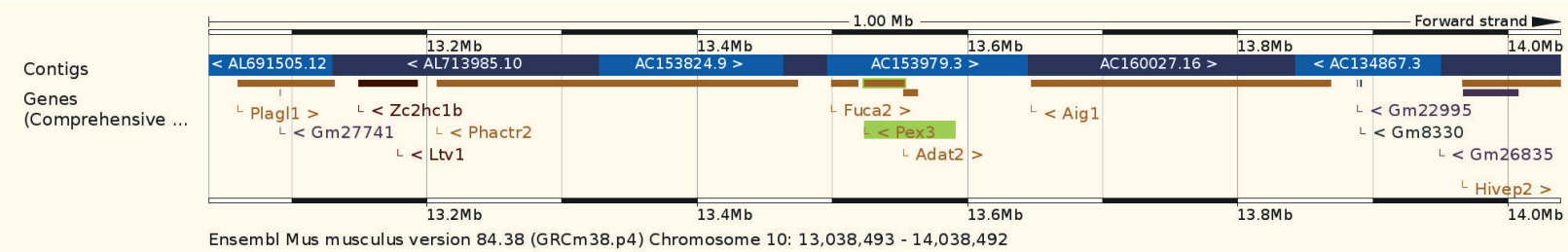

Fruit fly (chr. 3L; 15.144.355-15.146.379)

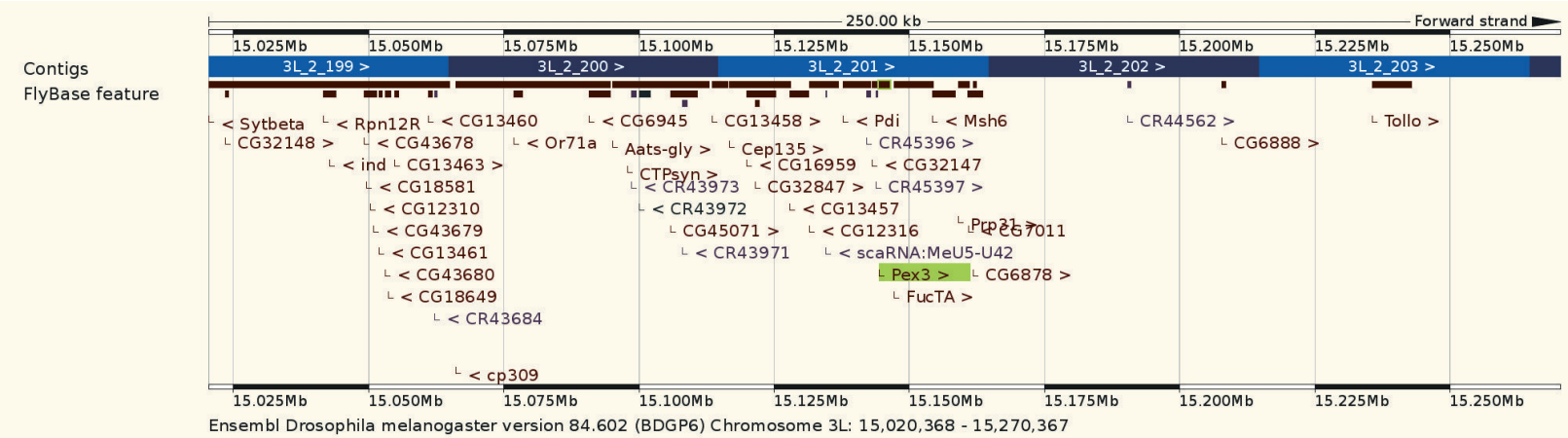

8.2.5 TALENs binding sites

All TALENs were targeting the first exon (here depicted in red; ORF start highlighted in yellow). DNA binding sites are underlined.

8.2.5.1 TALENs 10L + 10R

```
            TALEN 10L                          TALEN 10R
TGTCAAGTCTGTTAAAATGTTGAGTTCTACATGGAATTTCATCAAACGCCATAAGAGGAAATTCAT
```

8.2.5.2 TALENs 10L + 11R

```
            TALEN 10L                           TALEN 11R
TGTCAAGTCTGTTAAAATGTTGAGTTCTACATGGAATTTCATCAAACGCCATAAGAGGAAATTCAT
```

8.2.5.3 TALENs 12L + 12R

```
                                                          TALEN 12L
CTTTTCATTTTCGGTGTCAAGTCTGTTAAAATGTTGAGTTCTACATGGAATTTCATCAAACGCCAT

                              TALEN 12R
AAGAGGAAATTCATCTTCACTGGGGTGTTTGTTGGAGGTAACTAACGTGGGCAACTGAACCTCATC
```

8.2.6 CRISPR/Cas9 sgRNAs binding sites

8.2.6.1 sgRNA targeting intron 1

The whole sequence of zebrafish *pex3* intron 1 is here annotated; sgRNA binding site is underlined.

```
GTAACTAACGTGGGCAACTGAACCTCATCCATGCATACATATCAGTGACTGTTCACTAGCTGTAACTATT
TCTTGTTTTTAATAAAATACTTGTAGCTATAGCATGTTAATATGATGTGATGTGTAGTTTAGCGTGTTAT
TACAGTGTTGACAACCATTATATATTTTTTCCACATTCAGCCCTTCAATCTCAGTTCACCTGTCACCTAG
TTTTTCTATTGGCATAGTCAAATCAAAGTTGAAATGGACTTTACCCTGGAATTTTTAGTCAACAGAAAGG
CTTTATTTAACTGAATAGTTCTTGCTTGCAGCATATCACTTTGTTAACATGGATGCTATACTATATTGTA
ATCTCAAACTTTTTATTTGCAG
```

8.2.6.2 sgRNA targeting exon 3

The whole sequence of zebrafish pex3 exon3 is here annotated; sgRNA binding site is underlined.

```
TGTTATCAATGCTCCCCACTCTCCGAGAGGCAATCATCCATCACCTGAACTCAGAGAGTCTCACTGCTTT
GCTGAAGACTAA
```

8.2.7 Commercial ENU-induced mutagenesis alleles

8.2.7.1 Allele sa17571

ENU-induced mutation is highlighted in yellow; other mismatches are annotated SNPs naturally occurring in zebrafish population, or due to differences between strains. Below, the predicted coding sequence (with exons in alternate colors) and the predicted translation into protein are indicated.

```
wt      TTGGTAAATATGCACAGAGAAAAATTCAGGAGATGCAGGAG
sa17571 TTGGTAAATATGCACAGAGATAAATTCMGGAGATGCAGGAG
        ******************** ****** *************

ATGTTGAGTTCTACATGGAATTTCATCAAACGCCATAAGAGGAAATTCATCTTCACTGGGGTGTTTGTT
GGAGGTGTTTATCTGCTTGGTAAATATGCACAGAGATAA

MLSSTWNFIKRHKRKFIFTGVFVGGVYLLGKYAQR
```

8.2.7.2 Allele sa11684

ENU-induced mutation is highlighted in yellow; other mismatches are annotated SNPs naturally occurring in zebrafish population, or due to differences between strains. Below, the predicted coding sequence (with exons in alternate colors and the predicted retained intron, in green) and the predicted translation into protein (with newly inserted amino acids at the C-terminus in red) are indicated.

```
wt      TTCCAAGCCACTTTGTTCAGGTGAGCACCTTCATATAAACT
sa11684 TTCCAAGCCACTTTGTTCAGATGAGCACCTTCATATAAACY
        ******************** ********************

ATGTTGAGTTCTACATGGAATTTCATCAAACGCCATAAGAGGAAATTCATCTTCACTGGGGTGTTTGTTG
GAGGTGTTTATCTGCTTGGTAAATATGCACAGAGAAAAATTCAGGAGATGCAGGAGCGAGAGGCAGCTGA
ATACATTGCTCAAGCTCGGAGACAGTTTCATTTTGAAAGCAACCAAAGGACATGCAACATGACAGTGTTA
TCAATGCTCCCCACTCTCCGAGAGGCAATCATCCATCACCTGAACTCAGAGAGTCTCACTGCTTTGCTGA
AGACTAAGCCAGCAAATAAACTTGAAATCTGGGAGGATCTAAAGATTATAAGTTTTACCCGCAGCATTGT
AGCCGTTTACAGCACCTGCATGCTGGTTGTGTTACTCAGAGTTCAGCTCAACATAATCGGTGGATATCTG
TACCTAGATAACTCTGTGACGAAAAATGGAATGACCCCCTTAGCACCACCTGATGTTCAACAACAGTATC
TTTCCAGTATCCAACATCTTCTTGGAGAAGGGCTCATGGAACTGATAACTGTGGTCAAGAAAGCTGTTCA
GGAAGTTTTTGGACTGGTGTCTCTGAAGCAGAGTTTGTCTCTACAAGAGCTGGAGCAACAGTTGACACAG
ATCAGACAGTTAGTGGAGGACGACTCCTCTAAATACAAAAGTCTTTCCTGGTACATGATGCCTGATGAAG
AGAACACACTTGCCTCACAGGCCTGTGGTCTCACAGAGAATGATGTCACAACGATAAAGCTACTAAATGA
AACCAGAGATATGCTGGAAAGTCCAGACTTCAATATTGTTCTTCACACTTGCTTGAATCGAGGATTTGTC
AGATTTCTAGACAACATGGCAGAGTTTTTCCGACCCCCGCAGAGAGACTCCACTCCCTCCAGCACACCTG
ACCAACTATCGCATGTAAGCCTCCCACTAGCCAAAATCATTCCCATTATCAACGGACAGATTCATTCAAT
ATGCAGCGAAATTCCAAGCCACTTTGTTCAGGTGAGCACCTTCATATAA

MLSSTWNFIKRHKRKFIFTGVFVGGVYLLGKYAQRKIQEMQEREAAEYIAQARRQFHFESNQRTCNMTVL
SMLPTLREAIIHHLNSESLTALLKTKPANKLEIWEDLKIISFTRSIVAVYSTCMLVVLLRVQLNIIGGYL
YLDNSVTKNGMTPLAPPDVQQQYLSSIQHLLGEGLMELITVVKKAVQEVFGLVSLKQSLSLQELEQQLTQ
IRQLVEDDSSKYKSLSWYMMPDEENTLASQACGLTENDVTTIKLLNETRDMLESPDFNIVLHTCLNRGFV
RFLDNMAEFFRPPQRDSTPSSTPDQLSHVSLPLAKIIPIINGQIHSICSEIPSHFVQVSTFI
```

8.2.8 HRMA amplicons

Forward and reverse primers are underlined in the sequence. Exons are indicated in red, introns in black, ORF start is highlighted in yellow.

>pex3CRISPR-exon3
TGTTATCAATGCTCCCCACTCTCCGAGAGGCAATCATCCATCACCTGAACTCAGAGAGTCTCACTGCTTT
GCTGAAGACTAAGTGAGTTATGCACGTGTGTGTG

>pex3CRISPR-intron1
GGCATAGTCAAATCAAAGTTGAAATGGACTTTACCCTGGAATTTTTAGTCAACAGAAAGGCTTTATTTAA
CTGAATAGTTCTTGCTTGCAGCATATCA

>pex3TALEN-target1and2
CCCGCTCTTGCTTCTCTTATTTCTTTTCATTTTCGGTGTCAAGTCTGTTAAAATGTTGAGTTCTACATGG
AATTTCATCAAACGCCATAAGAGGAAATTCATCTTCACTGGGGTGTTTGT

>pex3TALEN-target3
TCGGTGTCAAGTCTGTTAAAATGTTGAGTTCTACATGGAATTTCATCAAACGCCATAAGAGGAAATTCAT
CTTCACTGGGGTGTTTGTTGGAGGTAACTAACGTGGGCAACTGAACC

>pex3ENU-sa17571
GCAGGTGTTTATCTGCTTGGTAAATATGCACAGAGAAAAATTCAGGAGATGCAGGAGCGAGAGGCAGCTG
AATACATTGCTCAAGCTCGGAG

>pex3ENU-sa11684
AGCGAAATTCCAAGCCACTTTGTTCAGGTGAGCACCTTCATATAAACTGACTCTTTTTCATTTAAATCAT
ATATAAGCTTCCCATACACAACTTGTTCCTTCCTGTGTGGCTGTTT

8.2.9 TALENs preliminary efficiency tests

In order to validate the efficacy of different TALENs pairs in inducing frameshift mutations, a cell culture system was used. For each combination of TALENs pair, four wells of a 24-well plate seeded with NIH 3T3 cells were transfected with plasmids containing zebrafish pex3 coding sequence and the two TALENs, in the right combination. 24 hours post transfection, plasmid DNA was collected from each well and the target region was amplified in a HRMA experiments, in triplicates. Amplicons from each experimental group were sent for sequencing.

```
                        TALEN 10L                          TALEN 10R
wt    TTTCGGTGTCAAGTCTGTTAAAATGTTGAGTTCTACATGGAATTTCATCAAACGCCATAAGAGGAA
A3.1  --TCGGTGTCAAGTCTGTTAAAATGTTGAGTTCTACATGGAATTTCATCAAACGCCATAAGAGGAA
A4.1  ----GGTGTCAAGTCTGTTAAAATGTTGAGTTCTACATG--ATTTCATCAAACGCCATAAGAGGAA
A2.1  TTTCGGTGTCAAGTCTGTTAAAATGTTGAGTTCTACATG-AATTTCATCAAACGCCATAAGAGGAA
A1.1  ------TGTCAAGTCTGTTAAAATGTTGAGTTCTAC-----ATTTCATCAAACGCCATAAGAGGAA
            ******************************     ************************
```

```
                      TALEN 10L                          TALEN 11R
wt   TTTCGGTGTCAAGTCTGTTAAAATGTTGAGTTCTACATGGAATTTCATCAAACGCCATAAGAGGAAA
B1.1 ----GGTGTCAAGTCTGTTAAAATGTTGAGTTCTACATGGAATTTCATCAAACGCCATAAGAGGAAA
B3.1 --TCGGTGTCAAGTCTGTTAAAATGTTGAGTTCTACATGGAATTTCATCAAACGCCATAAGAGGAAA
B4.1 TTTCGGTGTCAAGTCTGTTAAAATGTTGAGTTCTACATGGAATTTCATCAAACGCCATAAGAGGAAA
B2.1 -TTCGGTGTCAAGTCTGTTAAAATGTTGAGTTCTACATGG-ATTTCATCAAACGCCATAAGAGGAAA
         *********************************** *************************

                    TALEN 12L                          TALEN 12R
wt   CTACATGGAATTTCATCAAACGCCATAAGAGGAAATTCATCTTCACTGGGGTGTTTGTTGGAGGTAA
C2.1 CTACATGGAATTTCATCAAACGCCATAAGAGGAAATTCATCTTCACTGGGGTGTTTGTTGGAGGTAA
C3.1 CTACATGGAATTTCATCAAACGCCATAAGAGGAAATTCATCTTCACTGGGGTGTTTGTTGGAGGTAA
C4.1 --ACATGGAATTTCATCAAACGCCATAAGAGGAAATTCATCTTCACTGGGGTGTTTGTTGGAGGTAA
C1.1 -----TGGAATTTCATCAAACGCCATAAGAGGAAA------TTCACTGGGGTGTTTGTTGGAGGTAA
          ******************************      *************************
```

8.2.10 CRISPR/Cas9 preliminary efficiency tests

In order to validate the efficacy of different sgRNA constructs in inducing frameshift mutations, sgRNA and Cas9 mRNA were injected directly in zebrafish embryos in different amounts and at different ratios. For each experimental setup, a pool of randomly picked 10 embryos was collected, genomic DNA was extracted and used as template for target region amplification in a HRMA experiments, in triplicates. Amplicons from each experimental group were sent for sequencing.

S. piogenes Cas9 PAM is highlighted in yellow.

```
             sgRNA intron1
wt1   CCCTGGAATTTTTAGTCAACAGAAAGGCTTTATTTAACTGAATAGTTCTTGCTTGCAGCA
Pool2 -CCTGGAATTTTTAGTCAACAGAAAGGCTTTATTTAACTGAATAGTTCTTGCTTGCAGCA
Pool4 CCCTGGAATTTTTAGTCAACAGAAAGGCTTTATTTAACTGAATAGTTCTTGCTTGCAGCA
Pool1 --CTGGAATTTTTAGTC-ACAGAAAGGCTTTATTTAACTGAATAGTTCTTGCTTGCAGCA
Pool3 --CTGGAATTTTTAGT-----GAAAGGCTTTATTTAACTGAATAGTTCTTGCTTGCAGCA
         **************     ************************************
```

S. piogenes Cas9 PAM is highlighted in yellow (to be read on the antisense strand).

```
                                  sgRNA exon3
wt    TGTTATCAATGCTCCCCACTCTCCGAGAGGCAATCATCCATCACCTGAACTCAGAGAGTC
Pool4 TGTTATCAATGCTCCCCACTCTCCGAGA----ATCATCCATCACCTGAACTCAGAG----
Pool2 TGTTATCAATGCTCCCCACTCTCCGAGAGGC-ATCATCCATCACCTGAACTCAGAGAG--
Pool1 TGTTATCAATGCTCCCCACTCTCCGAGG--CAATCATCCATCACCTGAACTCAG------
Pool3 TGTTATCAATGCTCCCCACTCTCCG-------ATCATCCATCACCTGAACTCAGAGAGTC
      *************************       **********************
```

8.2.11 TALENs-induced somatic mutations and germ line transmission

```
                          TALEN 10L                          TALEN 10R
wt      TTTCGGTGTCAAGTCTGTTAAAATGTTGAGTTCTACATGGAATTTCATCAAACGCCATAAGAGGAA
Fish12  TTTCGGTGTCAAGTCTGTTAAAATGTTGAGTTCTACAT--------ATCAAACGCCATAAGAGGAA
Fish7   TTTCGGTGTCAAGTCTGTTAAAATGTTGAGTTCTA------ATTTCATCAAACGCCATAAGAGGAA
        ***********************************           **************
```

The fish somatically carrying the eight-nucleotide deletion (fish 12) was used for the mutant line establishment, crossing it with wildtype breeder, and F1 progeny embryos were screened for the mutation. Below, the predicted coding sequence and the predicted translation into protein (with newly inserted amino acids after the frameshift, in red) are indicated.

```
wt       TTTCGGTGTCAAGTCTGTTAAAATGTTGAGTTCTACATGGAATTTCATCAAACGCCATAAGAGGAA
Fish12   TTTCGGTGTCAAGTCTGTTAAAATGTTGAGTTCTACAT--------ATCAAACGCCATAAGAGGAA
Embryo2  ---CGGTGTCAAGTCTGTTAAAATGTTGAGTTCTACATGGAATTTCATCAAACGCCATAAGAGGAA
Embryo3  ---CGGTGTCAAGTCTGTTAAAATGTTGAGTTCTACATGGAATTTCATCAAACGCCATAAGAGGAA
Embryo6  -TTCGGTGTCAAGTCTGTTAAAATGTTGAGTTCTACATGGAATTTCATCAAACGCCATAAGAGGAA
Embryo7  TTTCGGTGTCAAGTCTGTTAAAATGTTGAGTTCTACATGGAATTTCATCAAACGCCATAAGAGGAA
Embryo1  --TCGGTGTCAAGTCTGTTAAAATGTTGAGTTCTACAT--------ATCAAACGCCATAAGAGGAA
Embryo4  ---CGGTGTCAAGTCTGTTAAAATGTTGAGTTCTACAT--------ATCAAACGCCATAAGAGGAA
Embryo5  -TTCGGTGTCAAGTCTGTTAAAATGTTGAGTTCTACAT--------ATCAAACGCCATAAGAGGAA
Embryo8  TTTCGGTGTCAAGTCTGTTAAAATGTTGAGTTCTACAT--------ATCAAACGCCATAAGAGGAA
           ***********************************         ********************


ATGTTGAGTTCTACATATCAAACGCCATAA

MLSSTYQTP
```

8.2.12 CRISPR-Cas9-induced somatic mutations and germ line transmission

```
                                    sgRNA exon3
wt      TGTTATCAATGCTCCCCACTCTCCGAGAGGCAATCATCCATCACCTGAACTCAGAGAGTC
Fish8   -GTTATCAATGCTCCCCACTCTCCGAGAGGCAATCATCCATCACCTGAACTCAGAGAGTC
Fish1   ---TATCAATGCTCCCCACTCTCCGAGAGGCAATCATCCATCACCTGAACTCAGAGAGTC
Fish13  TGTTATCAATGCTCCCCACTCTCCGA--GGCAATCATCCATCACCTGAACTCAGAGAGTC
Fish7   ----ATCAATGCTCCCCACTCTCCGA---GCAATCATCCATCACCTGAACTCAGAGAGTC
Fish5   -GTTATCAATGCTCCCCACTCTCCGAGGGGCAATCATCCATCACCTGAACTCAGAGAGTC
            **********************   ********************************
```

The fish somatically carrying the two-nucleotide deletion (fish 13) was used for the mutant line establishment, crossing it with wildtype breeder, and F1 progeny embryos were screened for the mutation. Below, the predicted coding sequence (with exons in alternate colors) and the predicted translation into protein (with newly inserted amino acids after the frameshift, in red) are indicated.

```
wt       TGTTATCAATGCTCCCCACTCTCCGAGAGGCAATCATCCATCACCTGAACTCAGAGAGTC
Fish13   TGTTATCAATGCTCCCCACTCTCC--GAGGCAATCATCCATCACCTGAACTCAGAGAGTC
Embryo4  TGTTATCAATGCTCCCCACTCTCCGAGAGGCAATCATCCATCACCTGAACTCAGAGAGTC
Embryo5  TGTTATCAATGCTCCCCACTCTCCGAGAGGCAATCATCCATCACCTGAACTCAGAGAGTC
Embryo7  TGTTATCAATGCTCCCCACTCTCCGAGAGGCAATCATCCATCACCTGAACTCAGAGAGTC
Embryo1  TGTTATCAATGCTCCCCACTCTCCGAGAGGCAATCATCCATCACCTGAACTCAGAGAGTC
Embryo2  TGTTATCAATGCTCCCCACTCTCC--GAGGCAATCATCCATCACCTGAACTCAGAGAGTC
Embryo3  TGTTATCAATGCTCCCCACTCTCC--GAGGCAATCATCCATCACCTGAACTCAGAGAGTC
Embryo6  TGTTATCAATGCTCCCCACTCTCC--GAGGCAATCATCCATCACCTGAACTCAGAGAGTC
Embryo8  TGTTATCAATGCTCCCCACTCTCC--GAGGCAATCATCCATCACCTGAACTCAGAGAGTC
         ************************  **********************************
```

```
ATGTTGAGTTCTACATGGAATTTCATCAAACGCCATAAGAGGAAATTCATCTTCACTGGGGTGTTTGTTG
GAGGTGTTTATCTGCTTGGTAAATATGCACAGAGAAAAATTCAGGAGATGCAGGAGCGAGAGGCAGCTGA
ATACATTGCTCAAGCTCGGAGACAGTTTCATTTTGAAAGCAACCAAAGGACATGCAACATGACAGTGTTA
TCAATGCTCCCCACTCTCCGAGGCAATCATCCATCACCTGAACTCAGAGAGTCTCACTGCTTTGCTGAAG
ACTAA
```

```
MLSSTWNFIKRHKRKFIFTGVFVGGVYLLGKYAQRKIQEMQEREAAEYIAQARRQFHFESNQRTCNMTVL
SMLPTLRGNHPSPELRESHCFAED
```

8.2.13 Accession number list

Accession numbers of the genes used for the identification of the non-canonical melanosomal targeting signal in zebrafish pex3. Tyrosinase – tyr, dopachrome tautomerase – dct, tyrosinase related protein – tyrp, premelanosome protein 17 – pmel17 and peroxins - pex from human (HS), mouse (MM) or zebrafish (DR).

Gene designation	Gene ID
DR_dct	ENSDARG00000006008
DR_pex14	ENSDARG00000028322
DR_pex16	ENSDARG00000058202
DR_pex19	ENSDARG00000004891
DR_pex3	ENSDARG00000013973
DR_tyr	ENSDARG00000039077
DR_tyrpa1a	ENSDARG00000029204
DR_tyrpa1b	ENSDARG00000056151
HS_DCT	ENSG00000080166
HS_PMEL17	ENSG00000185664
HS_TYR	ENSG00000077498
HS_TYRP1	ENSG00000107165
MM_Dct	ENSMUSG00000022129
MM_Pmel17	ENSMUSG00000025359
MM_Tyr	ENSMUSG00000004651
MM_Tyrp1	ENSMUSG00000005994
MM_Pex3	ENSMUSG00000019809
HS_PEX3	ENSG00000034693

9 References

Ablain, Julien; Durand, Ellen M.; Yang, Song; Zhou, Yi; Zon, Leonard I. (2015): A CRISPR/Cas9 vector system for tissue-specific gene disruption in zebrafish. In: *Developmental cell* n. 6, 32, pp. 756–764. DOI: 10.1016/j.devcel.2015.01.032.

Agrawal, Gaurav; Joshi, Saurabh; Subramani, Suresh (2011): Cell-free sorting of peroxisomal membrane proteins from the endoplasmic reticulum. In: *Proceedings of the National Academy of Sciences of the United States of America* n. 22, 108, pp. 9113–9118. DOI: 10.1073/pnas.1018749108.

Agrawal, Gaurav; Subramani, Suresh (2013): Emerging role of the endoplasmic reticulum in peroxisome biogenesis. In: *Frontiers in physiology,* 4, p. 286. DOI: 10.3389/fphys.2013.00286.

Agrawal, Gaurav; Subramani, Suresh (2016): De novo peroxisome biogenesis: Evolving concepts and conundrums. In: *Biochimica et biophysica acta* n. 5, 1863, pp. 892–901. DOI: 10.1016/j.bbamcr.2015.09.014.

Ali, Shaukat; Champagne, Danielle L.; Spaink, Herman P.; Richardson, Michael K. (2011): Zebrafish embryos and larvae: a new generation of disease models and drug screens. In: *Birth defects research. Part C, Embryo today : reviews* n. 2, 93, pp. 115–133. DOI: 10.1002/bdrc.20206.

Altschul, S. F.; Gish, W.; Miller, W.; Myers, E. W.; Lipman, D. J. (1990): Basic local alignment search tool. In: *Journal of molecular biology* n. 3, 215, pp. 403–410. DOI: 10.1016/S0022-2836(05)80360-2.

Amores, Angel; Catchen, Julian; Ferrara, Allyse; Fontenot, Quenton; Postlethwait, John H. (2011): Genome evolution and meiotic maps by massively parallel DNA sequencing: spotted gar, an outgroup for the teleost genome duplication. In: *Genetics* n. 4, 188, pp. 799–808. DOI: 10.1534/genetics.111.127324.

Anastasiou, Dimitrios; Poulogiannis, George; Asara, John M.; Boxer, Matthew B.; Jiang, Jian-kang; Shen, Min et al. (2011): Inhibition of pyruvate kinase M2 by reactive oxygen species contributes to cellular antioxidant responses. In: *Science (New York, N.Y.)* n. 6060, 334, pp. 1278–1283. DOI: 10.1126/science.1211485.

Anderson, Jennifer L.; Carten, Juliana D.; Farber, Steven A. (2011): Zebrafish lipid metabolism: from mediating early patterning to the metabolism of dietary fat and cholesterol. In: *Methods in cell biology,* 101, pp. 111–141. DOI: 10.1016/B978-0-12-387036-0.00005-0.

Antonenkov, Vasily D.; Grunau, Silke; Ohlmeier, Steffen; Hiltunen, J. Kalervo (2010): Peroxisomes are oxidative organelles. In: *Antioxidants & redox signaling* n. 4, 13, pp. 525–537. DOI: 10.1089/ars.2009.2996.

Arslan-Ergul, Ayca; Adams, Michelle M. (2014): Gene expression changes in aging zebrafish (Danio rerio) brains are sexually dimorphic. In: *BMC neuroscience,* 15, p. 29. DOI: 10.1186/1471-2202-15-29.

Artuso, Lucia; Romano, Alessandro; Verri, Tiziano; Domenichini, Alice; Argenton, Francesco; Santorelli, Filippo Maria; Petruzzella, Vittoria (2012): Mitochondrial DNA metabolism in early development of zebrafish (Danio rerio). In: *Biochimica et biophysica acta* n. 7, 1817, pp. 1002–1011. DOI: 10.1016/j.bbabio.2012.03.019.

Aubourg, P.; Blanche, S.; Jambaque, I.; Rocchiccioli, F.; Kalifa, G.; Naud-Saudreau, C. et al. (1990): Reversal of early neurologic and neuroradiologic manifestations of X-linked adrenoleukodystrophy by bone marrow transplantation. In: *The New England journal of medicine* n. 26, 322, pp. 1860–1866. DOI: 10.1056/NEJM199006283222607.

Ayala, Antonio; Munoz, Mario F.; Arguelles, Sandro (2014): Lipid peroxidation: production, metabolism, and signaling mechanisms of malondialdehyde and 4-hydroxy-2-nonenal. In: *Oxidative medicine and cellular longevity,* 2014, p. 360438. DOI: 10.1155/2014/360438.

Baes, Myriam; Aubourg, Patrick (2009): Peroxisomes, myelination, and axonal integrity in the CNS. In: *The Neuroscientist : a review journal bringing neurobiology, neurology and psychiatry* n. 4, 15, pp. 367–379. DOI: 10.1177/1073858409336297.

Baes, Myriam; van Veldhoven, Paul P. (2006): Generalised and conditional inactivation of Pex genes in mice. In: *Biochimica et biophysica acta* n. 12, 1763, pp. 1785–1793. DOI: 10.1016/j.bbamcr.2006.08.018.

Bagatto, B.; Pelster, B.; Burggren, W. W. (2001): Growth and metabolism of larval zebrafish: effects of swim training. In: *The Journal of experimental biology* n. Pt 24, 204, pp. 4335–4343.

Bagnara, J. T.; Taylor, J. D. (1970): Differences in pigment-containing organelles between color forms of the red-backed salamander, Plethodon cinereus. In: *Zeitschrift fur Zellforschung und mikroskopische Anatomie (Vienna, Austria : 1948)* n. 3, 106, pp. 412–417.

Bagnara, J. T.; Taylor, J. D.; Hadley, M. E. (1968): The dermal chromatophore unit. In: *The Journal of cell biology* n. 1, 38, pp. 67–79.

Bagnara, Joseph T.; Fernandez, Philip J.; Fujii, Royozo (2007): On the blue coloration of vertebrates. In: *Pigment cell research / sponsored by the European Society for Pigment Cell Research and the International Pigment Cell Society* n. 1, 20, pp. 14–26. DOI: 10.1111/j.1600-0749.2006.00360.x.

Baker, Alison; Graham, Ian A.; Holdsworth, Michael; Smith, Steven M.; Theodoulou, Frederica L. (2006): Chewing the fat: beta-oxidation in signalling and development. In: *Trends in plant science* n. 3, 11, pp. 124–132. DOI: 10.1016/j.tplants.2006.01.005.

Baroy, Tuva; Koster, Janet; Stromme, Petter; Ebberink, Merel S.; Misceo, Doriana; Ferdinandusse, Sacha et al. (2015): A novel type of rhizomelic chondrodysplasia punctata, RCDP5, is caused by loss of the PEX5 long isoform. In: *Human molecular genetics* n. 20, 24, pp. 5845–5854. DOI: 10.1093/hmg/ddv305.

Barth, P. G.; Wanders, R. J.; Schutgens, R. B.; Staalman, C. R. (1996): Variant rhizomelic chondrodysplasia punctata (RCDP) with normal plasma phytanic acid: clinico-biochemical delineation of a subtype and complementation studies. In: *American journal of medical genetics* n. 2, 62, pp. 164–168. DOI: 10.1002/(SICI)1096-8628(19960315)62:2<164::AID-AJMG9>3.0.CO;2-W.

Bartoszewska, Magdalena; Opalinski, Lukasz; Veenhuis, Marten; van der Klei, Ida J. (2011): The significance of peroxisomes in secondary metabolite biosynthesis in filamentous fungi. In: *Biotechnology letters* n. 10, 33, pp. 1921–1931. DOI: 10.1007/s10529-011-0664-y.

Bascom, Roger A.; Chan, Honey; Rachubinski, Richard A. (2003): Peroxisome biogenesis occurs in an unsynchronized manner in close association with the endoplasmic reticulum in temperature-sensitive Yarrowia lipolytica Pex3p mutants. In: *Molecular biology of the cell* n. 3, 14, pp. 939–957. DOI: 10.1091/mbc.E02-10-0633.

Basrur, Venkatesha; Yang, Feng; Kushimoto, Tsuneto; Higashimoto, Youichiro; Yasumoto, Ken-ichi; Valencia, Julio et al. (2003a): Proteomic Analysis of Early Melanosomes. Identification of Novel Melanosomal Proteins. In: *J. Proteome Res.* n. 1, 2, pp. 69–79. DOI: 10.1021/pr025562r.

Bedell, Victoria M.; Wang, Ying; Campbell, Jarryd M.; Poshusta, Tanya L.; Starker, Colby G.; Krug, Randall G. 2nd et al. (2012): In vivo genome editing using a high-efficiency TALEN system. In: *Nature* n. 7422, 491, pp. 114–118. DOI: 10.1038/nature11537.

Beermann, F.; Orlow, S. J.; Boissy, R. E.; Schmidt, A.; Boissy, Y. L.; Lamoreux, M. L. (1995): Misrouting of tyrosinase with a truncated cytoplasmic tail as a result of the murine platinum (cp) mutation. In: *Experimental eye research* n. 5, 61, pp. 599–607.

Belmadani, Abdelhak; Jung, Hosung; Ren, Dongjun; Miller, Richard J. (2009): The chemokine SDF-1/CXCL12 regulates the migration of melanocyte progenitors in mouse hair follicles. In: *Differentiation; research in biological diversity* n. 4, 77, pp. 395–411. DOI: 10.1016/j.diff.2008.10.015.

Berendse, Kevin; Engelen, Marc; Ferdinandusse, Sacha; Majoie, Charles B. L. M.; Waterham, Hans R.; Vaz, Frederic M. et al. (2016): Zellweger spectrum disorders: clinical manifestations in patients surviving into adulthood. In: *Journal of inherited metabolic disease* n. 1, 39, pp. 93–106. DOI: 10.1007/s10545-015-9880-2.

Berg, Jeremy M.; Stryer, Lubert; Timoczko, John L.; Gatto, Gregory J. (2012): Biochemistry. New York: W. H. Freeman.

Berridge, Michael J. (2014): Module 2. Cell Signalling Pathways. In: *Cell Signalling Biology,* 6, csb0001002. DOI: 10.1042/csb0001002.

Bertolotto, C.; Busca, R.; Abbe, P.; Bille, K.; Aberdam, E.; Ortonne, J. P.; Ballotti, R. (1998): Different cis-acting elements are involved in the regulation of TRP1 and TRP2 promoter activities by cyclic AMP: pivotal role of M boxes (GTCATGTGCT) and of microphthalmia. In: *Molecular and cellular biology* n. 2, 18, pp. 694–702.

Binns, Derk; Januszewski, Tom; Chen, Yue; Hill, Justin; Markin, Vladislav S.; Zhao, Yingming et al. (2006): An intimate collaboration between peroxisomes and lipid bodies. In: *The Journal of cell biology* n. 5, 173, pp. 719–731. DOI: 10.1083/jcb.200511125.

Bogdanove, Adam J.; Voytas, Daniel F. (2011): TAL effectors: customizable proteins for DNA targeting. In: *Science (New York, N.Y.)* n. 6051, 333, pp. 1843–1846. DOI: 10.1126/science.1204094.

Bonekamp, Nina A.; Volkl, Alfred; Fahimi, H. Dariush; Schrader, Michael (2009): Reactive oxygen species and peroxisomes: struggling for balance. In: *BioFactors (Oxford, England)* n. 4, 35, pp. 346–355. DOI: 10.1002/biof.48.

Bonifacino, Juan S.; Traub, Linton M. (2003): Signals for sorting of transmembrane proteins to endosomes and lysosomes. In: *Annual review of biochemistry,* 72, pp. 395–447. DOI: 10.1146/annurev.biochem.72.121801.161800.

Bootsma, A. H.; Overmars, H.; van Rooij, A.; van Lint, A. E.; Wanders, R. J.; van Gennip, A. H.; Vreken, P. (1999): Rapid analysis of conjugated bile acids in plasma using electrospray tandem mass spectrometry: application for selective screening of peroxisomal disorders. In: *Journal of inherited metabolic disease* n. 3, 22, pp. 307–310.

Bortolini, Michele; Wright, Matthew B.; Bopst, Martin; Balas, Bogdana (2013): Examining the safety of PPAR agonists - current trends and future prospects. In: *Expert opinion on drug safety* n. 1, 12, pp. 65–79. DOI: 10.1517/14740338.2013.741585.

Braverman, N. (1998): An isoform of pex5p, the human PTS1 receptor, is required for the import of PTS2 proteins into peroxisomes. In: *Human molecular genetics* n. 8, 7, pp. 1195–1205. DOI: 10.1093/hmg/7.8.1195.

Braverman, Nancy; Zhang, Rui; Chen, Li; Nimmo, Graeme; Scheper, Sarah; Tran, Tammy et al. (2010): A Pex7 hypomorphic mouse model for plasmalogen deficiency affecting the lens and skeleton. In: *Molecular genetics and metabolism* n. 4, 99, pp. 408–416. DOI: 10.1016/j.ymgme.2009.12.005.

Braverman, Nancy E.; D'Agostino, Maria Daniela; Maclean, Gillian E. (2013): Peroxisome biogenesis disorders: Biological, clinical and pathophysiological perspectives. In: *Developmental disabilities research reviews* n. 3, 17, pp. 187–196. DOI: 10.1002/ddrr.1113.

Braverman, Nancy E.; Moser, Ann B. (2012): Functions of plasmalogen lipids in health and disease. In: *Biochimica et biophysica acta* n. 9, 1822, pp. 1442–1452. DOI: 10.1016/j.bbadis.2012.05.008.

Breidenbach, R. W.; Beevers, H. (1967): Association of the glyoxylate cycle enzymes in a novel subcellular particle from castor bean endosperm. In: *Biochemical and biophysical research communications* n. 4, 27, pp. 462–469.

Brocard, Cecile; Hartig, Andreas (2006): Peroxisome targeting signal 1: is it really a simple tripeptide? In: *Biochimica et biophysica acta* n. 12, 1763, pp. 1565–1573. DOI: 10.1016/j.bbamcr.2006.08.022.

Brondolin, M.; Völzmann, A.; Hahn, I. (2012): Straight forward approach to sort fish by gender. In: *LIMES Klaaf* n. 6, p. 42.

Brożyna, Anna A.; Jóźwicki, Wojciech; Roszkowski, Krzysztof; Filipiak, Jan; Slominski, Andrzej T. (2016): Melanin content in melanoma metastases affects the outcome of radiotherapy. In: *Oncotarget* n. 14, 7, pp. 17844–17853. Available online in http://www.impactjournals.com/oncotarget/index.php?journal=oncotarget&page=article&op=download&path%5B%5D=7528&path%5B%5D=21732.

Buchert, Rebecca; Tawamie, Hasan; Smith, Christopher; Uebe, Steffen; Innes, A. Micheil; Al Hallak, Bassam et al. (2014): A peroxisomal disorder of severe intellectual disability, epilepsy, and cataracts due to fatty acyl-CoA reductase 1 deficiency. In: *American journal of human genetics* n. 5, 95, pp. 602–610. DOI: 10.1016/j.ajhg.2014.10.003.

Budi, Erine H.; Patterson, Larissa B.; Parichy, David M. (2011): Post-embryonic nerve-associated precursors to adult pigment cells: genetic requirements and dynamics of morphogenesis and differentiation. In: *PLoS genetics* n. 5, 7, e1002044. DOI: 10.1371/journal.pgen.1002044.

Burgoyne, Joseph R.; Mongue-Din, Heloise; Eaton, Philip; Shah, Ajay M. (2012): Redox signaling in cardiac physiology and pathology. In: *Circulation research* n. 8, 111, pp. 1091–1106. DOI: 10.1161/CIRCRESAHA.111.255216.

Burma, Sandeep; Chen, Benjamin P. C.; Chen, David J. (2006): Role of non-homologous end joining (NHEJ) in maintaining genomic integrity. In: *DNA repair* n. 9-10, 5, pp. 1042–1048. DOI: 10.1016/j.dnarep.2006.05.026.

Burnett, Sarah F.; Farre, Jean-Claude; Nazarko, Taras Y.; Subramani, Suresh (2015): Peroxisomal Pex3 activates selective autophagy of peroxisomes via interaction with the pexophagy receptor Atg30. In: *The Journal of biological chemistry* n. 13, 290, pp. 8623–8631. DOI: 10.1074/jbc.M114.619338.

Cade, Lindsay; Reyon, Deepak; Hwang, Woong Y.; Tsai, Shengdar Q.; Patel, Samir; Khayter, Cyd et al. (2012): Highly efficient generation of heritable zebrafish gene mutations using homo- and heterodimeric TALENs. In: *Nucleic acids research* n. 16, 40, pp. 8001–8010. DOI: 10.1093/nar/gks518.

Callaway, Ewen (2013): Zebrafish genome helps in hunt for treatments. In: *Nature. DOI:* 10.1038/nature.2013.12821.

Cariello, N. F.; Skopek, T. R. (1993): Mutational analysis using denaturing gradient gel electrophoresis and PCR. In: *Mutation research* n. 1, 288, pp. 103–112.

Carmona-Fontaine, Carlos; Theveneau, Eric; Tzekou, Apostolia; Tada, Masazumi; Woods, Mae; Page, Karen M. et al. (2011): Complement fragment C3a controls mutual cell attraction during collective cell migration. In: *Developmental cell* n. 6, 21, pp. 1026–1037. DOI: 10.1016/j.devcel.2011.10.012.

Chang, Nannan; Sun, Changhong; Gao, Lu; Zhu, Dan; Xu, Xiufei; Zhu, Xiaojun et al. (2013): Genome editing with RNA-guided Cas9 nuclease in zebrafish embryos. In: *Cell research* n. 4, 23, pp. 465–472. DOI: 10.1038/cr.2013.45.

Cheli, Yann; Luciani, Flavie; Khaled, Mehdi; Beuret, Laurent; Bille, Karine; Gounon, Pierre et al. (2009): {alpha}MSH and Cyclic AMP elevating agents control melanosome pH through a protein kinase A-independent mechanism. In: *The Journal of biological chemistry* n. 28, 284, pp. 18699–18706. DOI: 10.1074/jbc.M109.005819.

Chen, Haiyang; Liu, Zhonghua; Huang, Xun (2010): Drosophila models of peroxisomal biogenesis disorder: peroxins are required for spermatogenesis and very-long-chain fatty acid metabolism. In: *Human molecular genetics* n. 3, 19, pp. 494–505. DOI: 10.1093/hmg/ddp518.

Chen, Kun; Manga, Prashiela; Orlow, Seth J. (2002): Pink-eyed dilution protein controls the processing of tyrosinase. In: *Molecular biology of the cell* n. 6, 13, pp. 1953–1964. DOI: 10.1091/mbc.02-02-0022.

Chen, Weiting; Ge, Wei (2013): Gonad differentiation and puberty onset in the zebrafish: evidence for the dependence of puberty onset on body growth but not age in females. In: *Molecular reproduction and development* n. 5, 80, pp. 384–392. DOI: 10.1002/mrd.22172.

Cheung, Martin; Briscoe, James (2003): Neural crest development is regulated by the transcription factor Sox9. In: *Development (Cambridge, England)* n. 23, 130, pp. 5681–5693. DOI: 10.1242/dev.00808.

Chiaverini, Christine; Beuret, Laurent; Flori, Enrica; Busca, Roser; Abbe, Patricia; Bille, Karine et al. (2008): Microphthalmia-associated transcription factor regulates RAB27A gene expression and controls melanosome transport. In: *The Journal of biological chemistry* n. 18, 283, pp. 12635–12642. DOI: 10.1074/jbc.M800130200.

Choi, Hye-In; Sohn, Kyung-Cheol; Hong, Dong-Kyun; Lee, Young; Kim, Chang Deok; Yoon, Tae-Jin et al. (2014): Melanosome uptake is associated with the proliferation and differentiation of keratinocytes. In: *Archives of dermatological research* n. 1, 306, pp. 59–66. DOI: 10.1007/s00403-013-1422-x.

Choi, Tae-Young; Sohn, Kyung-Cheol; Kim, Jin-Hwa; Kim, Seong-Min; Kim, Cheol-Hee; Hwang, Jae-Sung et al. (2010): Impact of NAD(P)H:quinone oxidoreductase-1 on pigmentation. In: *The Journal of investigative dermatology* n. 3, 130, pp. 784–792. DOI: 10.1038/jid.2009.280.

Chou, Peter Y.; Fasman, Gerald D. (1974): Prediction of protein conformation. In: *Biochemistry* n. 2, 13, pp. 222–245. DOI: 10.1021/bi00699a002.

Chu, Bei-Bei; Liao, Ya-Cheng; Qi, Wei; Xie, Chang; Du, Ximing; Wang, Jiang et al. (2015): Cholesterol transport through lysosome-peroxisome membrane contacts. In: *Cell* n. 2, 161, pp. 291–306. DOI: 10.1016/j.cell.2015.02.019.

Cichorek, Miroslawa; Wachulska, Malgorzata; Stasiewicz, Aneta; Tyminska, Agata (2013): Skin melanocytes: biology and development. In: *Postepy dermatologii i alergologii* n. 1, 30, pp. 30–41. DOI: 10.5114/pdia.2013.33376.

Clark, Karl J.; Voytas, Daniel F.; Ekker, Stephen C. (2011): A TALE of two nucleases: gene targeting for the masses? In: *Zebrafish* n. 3, 8, pp. 147–149. DOI: 10.1089/zeb.2011.9993.

Clelland, Eric; Peng, Chun (2009): Endocrine/paracrine control of zebrafish ovarian development. In: *Molecular and cellular endocrinology* n. 1-2, 312, pp. 42–52. DOI: 10.1016/j.mce.2009.04.009.

Collins, John E.; White, Simon; Searle, Stephen M. J.; Stemple, Derek L. (2012): Incorporating RNA-seq data into the zebrafish Ensembl genebuild. In: *Genome research* n. 10, 22, pp. 2067–2078. DOI: 10.1101/gr.137901.112.

Cooper, D. N.; Schmidtke, J. (1984): DNA restriction fragment length polymorphisms and heterozygosity in the human genome. In: *Human genetics* n. 1, 66, pp. 1–16.

Cooper, T. G.; Beevers, H. (1969): Beta oxidation in glyoxysomes from castor bean endosperm. In: *The Journal of biological chemistry* n. 13, 244, pp. 3514–3520.

Costin, Gertrude-E; Valencia, Julio C.; Vieira, Wilfred D.; Lamoreux, M. Lynn; Hearing, Vincent J. (2003): Tyrosinase processing and intracellular trafficking is disrupted in mouse primary melanocytes carrying the underwhite (uw) mutation. A model for oculocutaneous albinism (OCA) type 4. In: *Journal of cell science* n. Pt 15, 116, pp. 3203–3212. DOI: 10.1242/jcs.00598.

Curran, Kevin; Raible, David W.; Lister, James A. (2009): Foxd3 controls melanophore specification in the zebrafish neural crest by regulation of Mitf. In: *Developmental biology* n. 2, 332, pp. 408–417. DOI: 10.1016/j.ydbio.2009.06.010.

Dacremont, G.; Vincent, G. (1995): Assay of plasmalogens and polyunsaturated fatty acids (PUFA) in erythrocytes and fibroblasts. In: *Journal of inherited metabolic disease,* 18 Suppl 1, pp. 84–89.

D'Agostino, Giuseppe; Diano, Sabrina (2010): Alpha-melanocyte stimulating hormone: production and degradation. In: *Journal of molecular medicine (Berlin, Germany)* n. 12, 88, pp. 1195–1201. DOI: 10.1007/s00109-010-0651-0.

Dammai, Vincent; Subramani, Suresh (2001): The Human Peroxisomal Targeting Signal Receptor, Pex5p, Is Translocated into the Peroxisomal Matrix and Recycled to the Cytosol. In: *Cell* n. 2, 105, pp. 187–196. DOI: 10.1016/S0092-8674(01)00310-5.

Daniele, Tiziana; Hurbain, Ilse; Vago, Riccardo; Casari, Giorgio; Raposo, Graca; Tacchetti, Carlo; Schiaffino, Maria Vittoria (2014): Mitochondria and melanosomes establish physical contacts modulated by Mfn2 and involved in organelle biogenesis. In: *Current biology : CB* n. 4, 24, pp. 393–403. DOI: 10.1016/j.cub.2014.01.007.

Daniele, Tiziana; Schiaffino, Maria Vittoria (2016): Lipid transfer and metabolism across the endolysosomal-mitochondrial boundary. In: *Biochimica et biophysica acta* n. 8 Pt B, 1861, pp. 880–894. DOI: 10.1016/j.bbalip.2016.02.001.

Darrow, Kiersten O.; Harris, William A. (2004): Characterization and development of courtship in zebrafish, Danio rerio. In: *Zebrafish* n. 1, 1, pp. 40–45. DOI: 10.1089/154585404774101662.

Davis, A. P.; Justice, M. J. (1998): An Oak Ridge legacy: the specific locus test and its role in mouse mutagenesis. In: *Genetics* n. 1, 148, pp. 7–12.

Dawson, Ted M.; Dawson, Valina L. (2003): Molecular pathways of neurodegeneration in Parkinson's disease. In: *Science (New York, N.Y.)* n. 5646, 302, pp. 819–822. DOI: 10.1126/science.1087753.

D'Costa, Allison; Shepherd, Iain T. (2009): Zebrafish development and genetics: introducing undergraduates to developmental biology and genetics in a large introductory laboratory class. In: *Zebrafish* n. 2, 6, pp. 169–177. DOI: 10.1089/zeb.2008.0562.

del Rio, L. A. (2002): Reactive oxygen species, antioxidant systems and nitric oxide in peroxisomes. In: *Journal of experimental botany* n. 372, 53, pp. 1255–1272. DOI: 10.1093/jexbot/53.372.1255.

Den Broeder, Marjo J.; Kopylova, Victoria A.; Kamminga, Leonie M.; Legler, Juliette (2015): Zebrafish as a Model to Study the Role of Peroxisome Proliferating-Activated Receptors in Adipogenesis and Obesity. In: *PPAR research,* 2015, p. 358029. DOI: 10.1155/2015/358029.

Dimitrov, Lazar; Lam, Sheung Kwan; Schekman, Randy (2013): The role of the endoplasmic reticulum in peroxisome biogenesis. In: *Cold Spring Harbor perspectives in biology* n. 5, 5, a013243. DOI: 10.1101/cshperspect.a013243.

Dirkx, Ruud; Vanhorebeek, Ilse; Martens, Katrin; Schad, Arno; Grabenbauer, Markus; Fahimi, Dariush et al. (2005): Absence of peroxisomes in mouse hepatocytes causes mitochondrial and ER abnormalities. In: *Hepatology (Baltimore, Md.)* n. 4, 41, pp. 868–878. DOI: 10.1002/hep.20628.

d'Ischia, Marco; Wakamatsu, Kazumasa; Cicoira, Fabio; Di Mauro, Eduardo; Garcia-Borron, Jose Carlos; Commo, Stephane et al. (2015): Melanins and melanogenesis: from pigment cells to human health and technological applications. In: *Pigment cell & melanoma research* n. 5, 28, pp. 520–544. DOI: 10.1111/pcmr.12393.

Distel, Martin; Wullimann, Mario F.; Koster, Reinhard W. (2009): Optimized Gal4 genetics for permanent gene expression mapping in zebrafish. In: *Proceedings of the National Academy of Sciences of the United States of America* n. 32, 106, pp. 13365–13370. DOI: 10.1073/pnas.0903060106.

Dixit, Evelyn; Boulant, Steeve; Zhang, Yijing; Lee, Amy S. Y.; Odendall, Charlotte; Shum, Bennett et al. (2010): Peroxisomes are signaling platforms for antiviral innate immunity. In: *Cell* n. 4, 141, pp. 668–681. DOI: 10.1016/j.cell.2010.04.018.

D'Mello, Stacey A. N.; Finlay, Graeme J.; Baguley, Bruce C.; Askarian-Amiri, Marjan E. (2016): Signaling Pathways in Melanogenesis. In: *International journal of molecular sciences* n. 7, 17. DOI: 10.3390/ijms17071144.

Dodt, G.; Warren, D.; Becker, E.; Rehling, P.; Gould, S. J. (2001): Domain mapping of human PEX5 reveals functional and structural similarities to Saccharomyces cerevisiae Pex18p and Pex21p. In: *The Journal of biological chemistry* n. 45, 276, pp. 41769–41781. DOI: 10.1074/jbc.M106932200.

Dong, Caihong; Yao, Yijian (2012): Isolation, characterization of melanin derived from Ophiocordyceps sinensis, an entomogenous fungus endemic to the Tibetan Plateau. In: *Journal of bioscience and bioengineering* n. 4, 113, pp. 474–479. DOI: 10.1016/j.jbiosc.2011.12.001.

Dooley, Christopher M.; Mongera, Alessandro; Walderich, Brigitte; Nusslein-Volhard, Christiane (2013a): On the embryonic origin of adult melanophores: the role of ErbB and Kit signalling in establishing melanophore stem cells in zebrafish. In: *Development (Cambridge, England)* n. 5, 140, pp. 1003–1013. DOI: 10.1242/dev.087007.

Dooley, Christopher M.; Schwarz, Heinz; Mueller, Kaspar P.; Mongera, Alessandro; Konantz, Martina; Neuhauss, Stephan C. F. et al. (2013): Slc45a2 and V-ATPase are regulators of melanosomal pH homeostasis in zebrafish, providing a mechanism for human pigment evolution and disease. In: *Pigment cell & melanoma research* n. 2, 26, pp. 205–217. DOI: 10.1111/pcmr.12053.

Dorsky, R. I.; Raible, D. W.; Moon, R. T. (2000): Direct regulation of nacre, a zebrafish MITF homolog required for pigment cell formation, by the Wnt pathway. In: *Genes & development* n. 2, 14, pp. 158–162.

Doyon, Yannick; McCammon, Jasmine M.; Miller, Jeffrey C.; Faraji, Farhoud; Ngo, Catherine; Katibah, George E. et al. (2008): Heritable targeted gene disruption in zebrafish using designed zinc-finger nucleases. In: *Nature biotechnology* n. 6, 26, pp. 702–708. DOI: 10.1038/nbt1409.

Driever, W.; Solnica-Krezel, L.; Schier, A. F.; Neuhauss, S. C.; Malicki, J.; Stemple, D. L. et al. (1996): A genetic screen for mutations affecting embryogenesis in zebrafish. In: *Development (Cambridge, England),* 123, pp. 37–46.

Dupin, Elisabeth; Creuzet, Sophie; Le Douarin, Nicole M. (2006): The contribution of the neural crest to the vertebrate body. In: *Advances in experimental medicine and biology,* 589, pp. 96–119. DOI: 10.1007/978-0-387-46954-6_6.

Dupin, Elisabeth; Sommer, Lukas (2012): Neural crest progenitors and stem cells: from early development to adulthood. In: *Developmental biology* n. 1, 366, pp. 83–95. DOI: 10.1016/j.ydbio.2012.02.035.

Dutton, K. A.; Pauliny, A.; Lopes, S. S.; Elworthy, S.; Carney, T. J.; Rauch, J. et al. (2001): Zebrafish colourless encodes sox10 and specifies non-ectomesenchymal neural crest fates. In: *Development (Cambridge, England)* n. 21, 128, pp. 4113–4125.

Duve, C. de; Baudhuin, P. (1966): Peroxisomes (microbodies and related particles). In: *Physiological reviews* n. 2, 46, pp. 323–357.

Ebberink, Merel S.; Koster, Janet; Visser, Gepke; van Spronsen, Francjan; Stolte-Dijkstra, Irene; Smit, G. Peter A. et al. (2012): A novel defect of peroxisome division due to a homozygous non-sense mutation in the PEX11beta gene. In: *Journal of medical genetics* n. 5, 49, pp. 307–313. DOI: 10.1136/jmedgenet-2012-100778.

Edgar, Robert C. (2004): MUSCLE: a multiple sequence alignment method with reduced time and space complexity. In: *BMC bioinformatics,* 5, p. 113. DOI: 10.1186/1471-2105-5-113.

Edge, R.; d'Ischia, M.; Land, E. J.; Napolitano, A.; Navaratnam, S.; Panzella, L. et al. (2006): Dopaquinone redox exchange with dihydroxyindole and dihydroxyindole carboxylic acid. In: *Pigment cell research / sponsored by the European Society for Pigment Cell Research and the International Pigment Cell Society* n. 5, 19, pp. 443–450. DOI: 10.1111/j.1600-0749.2006.00327.x.

Eisen, Judith S.; Smith, James C. (2008): Controlling morpholino experiments: don't stop making antisense. In: *Development (Cambridge, England)* n. 10, 135, pp. 1735–1743. DOI: 10.1242/dev.001115.

Ekker, Stephen C. (2000): Morphants. A new systematic vertebrate functional genomics approach. In: *Yeast* n. 17, pp. 302–306.

Engelen, Marc; Barbier, Mathieu; Dijkstra, Inge M. E.; Schur, Remmelt; Bie, Rob M. A. de; Verhamme, Camiel et al. (2014): X-linked adrenoleukodystrophy in women: a cross-sectional cohort study. In: *Brain : a journal of neurology* n. Pt 3, 137, pp. 693–706. DOI: 10.1093/brain/awt361.

Esch, Celine de; Slieker, Roderick; Wolterbeek, Andre; Woutersen, Ruud; Groot, Didima de (2012): Zebrafish as potential model for developmental neurotoxicity testing: a mini review. In: *Neurotoxicology and teratology* n. 6, 34, pp. 545–553. DOI: 10.1016/j.ntt.2012.08.006.

Eskelinen, Eeva-Liisa (2006): Roles of LAMP-1 and LAMP-2 in lysosome biogenesis and autophagy. In: *Molecular aspects of medicine* n. 5-6, 27, pp. 495–502. DOI: 10.1016/j.mam.2006.08.005.

Falletta, Paola; Bagnato, Paola; Bono, Maria; Monticone, Massimiliano; Schiaffino, Maria Vittoria; Bennett, Dorothy C. et al. (2014): Melanosome-autonomous regulation of size and number: the OA1 receptor sustains PMEL expression. In: *Pigment cell & melanoma research* n. 4, 27, pp. 565–579. DOI: 10.1111/pcmr.12239.

Fan, C.-Y.; Pan, J.; Chu, R.; Lee, D.; Kluckman, K. D.; Usuda, N. et al. (1996): Hepatocellular and Hepatic Peroxisomal Alterations in Mice with a Disrupted Peroxisomal Fatty Acyl-coenzyme A Oxidase Gene. In: *Journal of Biological Chemistry* n. 40, 271, pp. 24698–24710. DOI: 10.1074/jbc.271.40.24698.

Fang, Yi; Morrell, James C.; Jones, Jacob M.; Gould, Stephen J. (2004): PEX3 functions as a PEX19 docking factor in the import of class I peroxisomal membrane proteins. In: *The Journal of cell biology* n. 6, 164, pp. 863–875. DOI: 10.1083/jcb.200311131.

Faust, Joseph E.; Manisundaram, Arvind; Ivanova, Pavlina T.; Milne, Stephen B.; Summerville, James B.; Brown, H. Alex et al. (2014): Peroxisomes are required for lipid metabolism and muscle function in Drosophila melanogaster. In: *PloS one* n. 6, 9, e100213. DOI: 10.1371/journal.pone.0100213.

Faust, Phyllis L. (2003): Abnormal cerebellar histogenesis in PEX2 Zellweger mice reflects multiple neuronal defects induced by peroxisome deficiency. In: *The Journal of comparative neurology* n. 3, 461, pp. 394–413. DOI: 10.1002/cne.10699.

Ferdinandusse, Sacha; Houten, Sander M. (2006): Peroxisomes and bile acid biosynthesis. In: *Biochimica et biophysica acta* n. 12, 1763, pp. 1427–1440. DOI: 10.1016/j.bbamcr.2006.09.001.

Fink, Maria; Flekna, Gabriele; Ludwig, Alfred; Heimbucher, Thomas; Czerny, Thomas (2006): Improved translation efficiency of injected mRNA during early embryonic development. In: *Developmental Dynamics* n. 12, 235, pp. 3370–3378. DOI: 10.1002/dvdy.20995.

Fu, Yanfang; Sander, Jeffry D.; Reyon, Deepak; Cascio, Vincent M.; Joung, J. Keith (2014): Improving CRISPR-Cas nuclease specificity using truncated guide RNAs. In: *Nature biotechnology* n. 3, 32, pp. 279–284. DOI: 10.1038/nbt.2808.

Fujiki, Yukio (2000): Peroxisome biogenesis and peroxisome biogenesis disorders. In: *FEBS letters* n. 1-2, 476, pp. 42–46. DOI: 10.1016/S0014-5793(00)01667-7.

Fujiki, Yukio; Matsuzono, Yuji; Matsuzaki, Takashi; Fransen, Marc (2006): Import of peroxisomal membrane proteins: the interplay of Pex3p- and Pex19p-mediated interactions. In: *Biochimica et biophysica acta* n. 12, 1763, pp. 1639–1646. DOI: 10.1016/j.bbamcr.2006.09.030.

Fujiki, Yukio; Okumoto, Kanji; Mukai, Satoru; Honsho, Masanori; Tamura, Shigehiko (2014): Peroxisome biogenesis in mammalian cells. In: *Frontiers in physiology,* 5, p. 307. DOI: 10.3389/fphys.2014.00307.

Gagnon, James A.; Valen, Eivind; Thyme, Summer B.; Huang, Peng; Akhmetova, Laila; Pauli, Andrea et al. (2014): Efficient mutagenesis by Cas9 protein-mediated oligonucleotide insertion and large-scale assessment of single-guide RNAs. In: *PloS one* n. 5, 9, e98186. DOI: 10.1371/journal.pone.0098186.

Galindo-Villegas, Jorge (2016): Recent findings on vertebrate developmental immunity using the zebrafish model. In: *Molecular immunology,* 69, pp. 106–112. DOI: 10.1016/j.molimm.2015.10.011.

Garcia-Borron, Jose C.; Abdel-Malek, Zalfa; Jimenez-Cervantes, Celia (2014): MC1R, the cAMP pathway, and the response to solar UV: extending the horizon beyond pigmentation. In: *Pigment cell & melanoma research* n. 5, 27, pp. 699–720. DOI: 10.1111/pcmr.12257.

Gavva, Narender R.; Wen, Shau-Ching; Daftari, Pratibha; Moniwa, Mariko; Yang, Wen-Ming; Yang-Feng, Lan-Ping Teresa et al. (2002): NAPP2, a peroxisomal membrane protein, is also a transcriptional corepressor. In: *Genomics* n. 3, 79, pp. 423–431. DOI: 10.1006/geno.2002.6714.

Gene: PEX3 (ENSG00000034693) - Summary - Homo sapiens - Ensembl genome browser 84. Available online in http://www.ensembl.org/Homo_sapiens/Gene/Summary?db=core;g=ENSG00000034693;r=6:143450807-143490010, retrieved on 6th July 2016.

Ge, Xijin; Yamamoto, Shogo; Tsutsumi, Shuichi; Midorikawa, Yutaka; Ihara, Sigeo; Wang, San Ming; Aburatani, Hiroyuki (2005): Interpreting expression profiles of cancers by genome-wide survey of breadth of expression in normal tissues. In: *Genomics* n. 2, 86, pp. 127–141. DOI: 10.1016/j.ygeno.2005.04.008.

Gerhard, Glenn S.; Kauffman, Elizabeth J.; Wang, Xujun; Stewart, Richard; Moore, Jessica L.; Kasales, Claudia J. et al. (2002): Life spans and senescent phenotypes in two strains of Zebrafish (Danio rerio). In: *Experimental gerontology* n. 8-9, 37, pp. 1055–1068.

Ghaedi, K.; Honsho, M.; Shimozawa, N.; Suzuki, Y.; Kondo, N.; Fujiki, Y. (2000): PEX3 is the causal gene responsible for peroxisome membrane assembly-defective Zellweger syndrome of complementation group G. In: *American journal of human genetics* n. 4, 67, pp. 976–981. DOI: 10.1086/303086.

Ghoneim, Wafaa; El-Bassyouni, Hala T.; Abdel Maksoud, Soheir A. (2011): Peroxisomal biogenesis disorder biomarkers. In: *Clinical laboratory* n. 7-8, 57, pp. 469–480.

Gilmour, Darren T.; Maischein, Hans-Martin; Nüsslein-Volhard, Christiane (2002): Migration and Function of a Glial Subtype in the Vertebrate Peripheral Nervous System. In: *Neuron* n. 4, 34, pp. 577–588. DOI: 10.1016/S0896-6273(02)00683-9.

Giraldez, Antonio J.; Mishima, Yuichiro; Rihel, Jason; Grocock, Russell J.; van Dongen, Stijn; Inoue, Kunio et al. (2006): Zebrafish MiR-430 promotes deadenylation and clearance of maternal mRNAs. In: *Science (New York, N.Y.)* n. 5770, 312, pp. 75–79. DOI: 10.1126/science.1122689.

Giros, M.; Roels, F.; Prats, J.; Ruiz, M.; Ribes, A.; Espeel, M. et al. (1996): Long survival in a case of peroxisomal biogenesis disorder with peroxisome mosaicism in the liver. In: *Annals of the New York Academy of Sciences,* 804, pp. 747–749.

Glaus, Peter; Honkela, Antti; Rattray, Magnus (2012): Identifying differentially expressed transcripts from RNA-seq data with biological variation. In: *Bioinformatics (Oxford, England)* n. 13, 28, pp. 1721–1728. DOI: 10.1093/bioinformatics/bts260.

Goding, C. R. (2000): Mitf from neural crest to melanoma: signal transduction and transcription in the melanocyte lineage. In: *Genes & development* n. 14, 14, pp. 1712–1728.

Goth, Laszlo; Nagy, Terez (2013): Inherited catalase deficiency: is it benign or a factor in various age related disorders? In: *Mutation research* n. 2, 753, pp. 147–154. DOI: 10.1016/j.mrrev.2013.08.002.

Grabacka, Maja; Placha, Wojciech; Urbanska, Krystyna; Laidler, Piotr; Plonka, Przemyslaw M.; Reiss, Krzysztof (2008): PPAR gamma regulates MITF and beta-catenin expression and promotes a differentiated phenotype in mouse melanoma S91. In: *Pigment cell & melanoma research* n. 3, 21, pp. 388–396. DOI: 10.1111/j.1755-148X.2008.00460.x.

Group, Schuler: EST Profile - Dr.79937. Available online in http://www.ncbi.nlm.nih.gov/UniGene/ESTProfileViewer.cgi?uglist=Dr.79937, retrieved on 6th July 2016.

Group, Schuler: HomoloGene - NCBI. Available online in http://www.ncbi.nlm.nih.gov/homologene/2691, retrieved on 6th July 2016.

Gupta, Ankit; Hall, Victoria L.; Kok, Fatma O.; Shin, Masahiro; McNulty, Joseph C.; Lawson, Nathan D.; Wolfe, Scot A. (2013): Targeted chromosomal deletions and inversions in zebrafish. In: *Genome research* n. 6, 23, pp. 1008–1017. DOI: 10.1101/gr.154070.112.

Gupta, Tripti; Mullins, Mary C. (2010): Dissection of organs from the adult zebrafish. In: *Journal of visualized experiments : JoVE* n. 37. DOI: 10.3791/1717.

Guryev, Victor; Koudijs, Marco J.; Berezikov, Eugene; Johnson, Stephen L.; Plasterk, Ronald H. A.; van Eeden, Fredericus J. M.; Cuppen, Edwin (2006): Genetic variation in the zebrafish. In: *Genome research* n. 4, 16, pp. 491–497. DOI: 10.1101/gr.4791006.

Haeussler, Maximilian; Schonig, Kai; Eckert, Helene; Eschstruth, Alexis; Mianne, Joffrey; Renaud, Jean-Baptiste et al. (2016): Evaluation of off-target and on-target scoring algorithms and integration into the guide RNA selection tool CRISPOR. In: *Genome biology* n. 1, 17, p. 148. DOI: 10.1186/s13059-016-1012-2.

Hall, Chris; Crosier, Phil; Crosier, Kathryn (2016): Inflammatory cytokines provide both infection-responsive and developmental signals for blood development: Lessons from the zebrafish. In: *Molecular immunology,* 69, pp. 113–122. DOI: 10.1016/j.molimm.2015.10.020.

Hasan, Sohel; Platta, Harald W.; Erdmann, Ralf (2013): Import of proteins into the peroxisomal matrix. In: *Frontiers in physiology,* 4, p. 261. DOI: 10.3389/fphys.2013.00261.

Hattula, Katarina; Hirschberg, Daniel; Kalkkinen, Nisse; Butcher, Sarah J.; Ora, Ari (2014): Association between the intrinsically disordered protein PEX19 and PEX3. In: *PloS one* n. 7, 9, e103101. DOI: 10.1371/journal.pone.0103101.

Hawkes, J. W. (1974): The structure of fish skin. II. The chromatophore unit. In: *Cell and tissue research* n. 2, 149, pp. 159–172.

He, Yingzi; Tang, Dongmei; Li, Wenyan; Chai, Renjie; Li, Huawei (2016): Histone deacetylase 1 is required for the development of the zebrafish inner ear. In: *Scientific reports,* 6, p. 16535. DOI: 10.1038/srep16535.

Hearing, V. J. (2000): The melanosome: the perfect model for cellular responses to the environment. In: *Pigment cell research / sponsored by the European Society for Pigment Cell Research and the International Pigment Cell Society,* 13 Suppl 8, pp. 23–34.

Hearing, Vincent J. (2005): Biogenesis of pigment granules: a sensitive way to regulate melanocyte function. In: *Journal of dermatological science* n. 1, 37, pp. 3–14. DOI: 10.1016/j.jdermsci.2004.08.014.

Henke, Katrin; Bowen, Margot E.; Harris, Matthew P. (2013): Identification of mutations in zebrafish using next-generation sequencing. In: *Current protocols in molecular biology / edited by Frederick M. Ausubel … [et al.],* 104, Unit 7.13. DOI: 10.1002/0471142727.mb0713s104.

Hettema, E. H.; Girzalsky, W.; van den Berg, M.; Erdmann, R.; Distel, B. (2000): Saccharomyces cerevisiae pex3p and pex19p are required for proper localization and stability of peroxisomal membrane proteins. In: *The EMBO journal* n. 2, 19, pp. 223–233. DOI: 10.1093/emboj/19.2.223.

Heymans, H. S.; Oorthuys, J. W.; Nelck, G.; Wanders, R. J.; Schutgens, R. B. (1985): Rhizomelic chondrodysplasia punctata: another peroxisomal disorder. In: *The New England journal of medicine* n. 3, 313, pp. 187–188.

Hiebler, Shandi; Masuda, Tomohiro; Hacia, Joseph G.; Moser, Ann B.; Faust, Phyllis L.; Liu, Anita et al. (2014): The Pex1-G844D mouse: a model for mild human Zellweger spectrum disorder. In: *Molecular genetics and metabolism* n. 4, 111, pp. 522–532. DOI: 10.1016/j.ymgme.2014.01.008.

Hirata, Masashi; Nakamura, Kei-ichiro; Kanemaru, Takaaki; Shibata, Yosaburo; Kondo, Shigeru (2003): Pigment cell organization in the hypodermis of zebrafish. In: *Developmental dynamics : an official publication of the American Association of Anatomists* n. 4, 227, pp. 497–503. DOI: 10.1002/dvdy.10334.

Hirobe, Tomohisa (2011): How are proliferation and differentiation of melanocytes regulated? In: *Pigment cell & melanoma research* n. 3, 24, pp. 462–478. DOI: 10.1111/j.1755-148X.2011.00845.x.

Hirobe, Tomohisa; Terunuma, Emi (2012): Reduced proliferative and differentiative activity of mouse pink-eyed dilution melanoblasts is related to apoptosis. In: *Zoological science* n. 11, 29, pp. 725–732. DOI: 10.2108/zsj.29.725.

Hodgkinson, C. A.; Moore, K. J.; Nakayama, A.; Steingrimsson, E.; Copeland, N. G.; Jenkins, N. A.; Arnheiter, H. (1993): Mutations at the mouse microphthalmia locus are associated with defects in a gene encoding a novel basic-helix-loop-helix-zipper protein. In: *Cell* n. 2, 74, pp. 395–404.

Hodgkinson, C. A.; Nakayama, A.; Li, H.; Swenson, L. B.; Opdecamp, K.; Asher, J. H., JR et al. (1998): Mutation at the anophthalmic white locus in Syrian hamsters: haploinsufficiency in the Mitf gene mimics human Waardenburg syndrome type 2. In: *Human molecular genetics* n. 4, 7, pp. 703–708.

Holland, P. W.; Garcia-Fernandez, J.; Williams, N. A.; Sidow, A. (1994): Gene duplications and the origins of vertebrate development. In: *Development (Cambridge, England). Supplement*, pp. 125–133.

Home, Philip (2011): Safety of PPAR agonists. In: *Diabetes care,* 34 Suppl 2, S215-9. DOI: 10.2337/dc11-s233.

Honsho, Masanori; Hiroshige, Takanobu; Fujiki, Yukio (2002): The membrane biogenesis peroxin Pex16p. Topogenesis and functional roles in peroxisomal membrane assembly. In: *The Journal of biological chemistry* n. 46, 277, pp. 44513–44524. DOI: 10.1074/jbc.M206139200.

Howe, Kerstin; Clark, Matthew D.; Torroja, Carlos F.; Torrance, James; Berthelot, Camille; Muffato, Matthieu et al. (2013a): The zebrafish reference genome sequence and its relationship to the human genome. In: *Nature* n. 7446, 496, pp. 498–503. DOI: 10.1038/nature12111.

Hsu, Patrick D.; Scott, David A.; Weinstein, Joshua A.; Ran, F. Ann; Konermann, Silvana; Agarwala, Vineeta et al. (2013): DNA targeting specificity of RNA-guided Cas9 nucleases. In: *Nature biotechnology* n. 9, 31, pp. 827–832. DOI: 10.1038/nbt.2647.

Huang, Peng; Xiao, An; Zhou, Mingguo; Zhu, Zuoyan; Lin, Shuo; Zhang, Bo (2011): Heritable gene targeting in zebrafish using customized TALENs. In: *Nature biotechnology* n. 8, 29, pp. 699–700. DOI: 10.1038/nbt.1939.

Huber, Nina; Guimaraes, Sofia; Schrader, Michael; Suter, Ueli; Niemann, Axel (2013): Charcot-Marie-Tooth disease-associated mutants of GDAP1 dissociate its roles in peroxisomal and mitochondrial fission. In: *EMBO reports* n. 6, 14, pp. 545–552. DOI: 10.1038/embor.2013.56.

Hughes, Virginia (2013): Mapping brain networks: Fish-bowl neuroscience. In: *Nature* n. 7433, 493, pp. 466–468. DOI: 10.1038/493466a.

Hunziker, W.; Geuze, H. J. (1996): Intracellular trafficking of lysosomal membrane proteins. In: *BioEssays : news and reviews in molecular, cellular and developmental biology* n. 5, 18, pp. 379–389. DOI: 10.1002/bies.950180508.

Hwang, Woong Y.; Fu, Yanfang; Reyon, Deepak; Maeder, Morgan L.; Tsai, Shengdar Q.; Sander, Jeffry D. et al. (2013): Efficient genome editing in zebrafish using a CRISPR-Cas system. In: *Nature biotechnology* n. 3, 31, pp. 227–229. DOI: 10.1038/nbt.2501.

Ignatius, Myron S.; Moose, Holly E.; El-Hodiri, Heithem M.; Henion, Paul D. (2008): colgate/hdac1 Repression of foxd3 expression is required to permit mitfa-dependent melanogenesis. In: *Developmental biology* n. 2, 313, pp. 568–583. DOI: 10.1016/j.ydbio.2007.10.045.

Ignatius, Myron S.; Unal Eroglu, Arife; Malireddy, Smitha; Gallagher, Glen; Nambiar, Roopa M.; Henion, Paul D. (2013): Distinct functional and temporal requirements for zebrafish Hdac1 during neural crest-derived craniofacial and peripheral neuron development. In: *PloS one* n. 5, 8, e63218. DOI: 10.1371/journal.pone.0063218.

Imazaki, Ai; Tanaka, Aiko; Harimoto, Yoshiaki; Yamamoto, Mikihiro; Akimitsu, Kazuya; Park, Pyoyun; Tsuge, Takashi (2010): Contribution of peroxisomes to secondary metabolism and pathogenicity in the fungal plant pathogen Alternaria alternata. In: *Eukaryotic cell* n. 5, 9, pp. 682–694. DOI: 10.1128/EC.00369-09.

Islinger, Markus; Grille, Sandra; Fahimi, H. Dariush; Schrader, Michael (2012): The peroxisome: an update on mysteries. In: *Histochemistry and cell biology* n. 5, 137, pp. 547–574. DOI: 10.1007/s00418-012-0941-4.

Islinger, Markus; Li, Ka Wan; Seitz, Jurgen; Volkl, Alfred; Luers, Georg H. (2009): Hitchhiking of Cu/Zn superoxide dismutase to peroxisomes--evidence for a natural piggyback import mechanism in mammals. In: *Traffic (Copenhagen, Denmark)* n. 11, 10, pp. 1711–1721. DOI: 10.1111/j.1600-0854.2009.00966.x.

Ito, S.; Prota, G. (1977): A facile one-step synthesis of cysteinyldopas using mushroom tyrosinase. In: *Experientia* n. 8, 33, pp. 1118–1119.

Ivashchenko, Oksana; van Veldhoven, Paul P.; Brees, Chantal; Ho, Ye-Shih; Terlecky, Stanley R.; Fransen, Marc (2011): Intraperoxisomal redox balance in mammalian cells: oxidative stress and interorganellar cross-talk. In: *Molecular biology of the cell* n. 9, 22, pp. 1440–1451. DOI: 10.1091/mbc.E10-11-0919.

Jansen, Gerbert A.; Wanders, Ronald J. A. (2006): Alpha-oxidation. In: *Biochimica et biophysica acta* n. 12, 1763, pp. 1403–1412. DOI: 10.1016/j.bbamcr.2006.07.012.

Jao, Li-En; Wente, Susan R.; Chen, Wenbiao (2013): Efficient multiplex biallelic zebrafish genome editing using a CRISPR nuclease system. In: *Proceedings of the National Academy of Sciences of the United States of America* n. 34, 110, pp. 13904–13909. DOI: 10.1073/pnas.1308335110.

Jin, Yui; Strunk, Bethany S.; Weisman, Lois S. (2015): Close encounters of the lysosome-peroxisome kind. In: *Cell* n. 2, 161, pp. 197–198. DOI: 10.1016/j.cell.2015.03.046.

Jinek, Martin; Chylinski, Krzysztof; Fonfara, Ines; Hauer, Michael; Doudna, Jennifer A.; Charpentier, Emmanuelle (2012): A programmable dual-RNA-guided DNA endonuclease in adaptive bacterial immunity. In: *Science (New York, N.Y.)* n. 6096, 337, pp. 816–821. DOI: 10.1126/science.1225829.

Kasahara, Masahiro; Naruse, Kiyoshi; Sasaki, Shin; Nakatani, Yoichiro; Qu, Wei; Ahsan, Budrul et al. (2007): The medaka draft genome and insights into vertebrate genome evolution. In: *Nature* n. 7145, 447, pp. 714–719. DOI: 10.1038/nature05846.

Kassmann, Celia M.; Lappe-Siefke, Corinna; Baes, Myriam; Brugger, Britta; Mildner, Alexander; Werner, Hauke B. et al. (2007): Axonal loss and neuroinflammation caused by peroxisome-deficient oligodendrocytes. In: *Nature genetics* n. 8, 39, pp. 969–976. DOI: 10.1038/ng2070.

Kemp, Stephan; Berger, Johannes; Aubourg, Patrick (2012): X-linked adrenoleukodystrophy: clinical, metabolic, genetic and pathophysiological aspects. In: *Biochimica et biophysica acta* n. 9, 1822, pp. 1465–1474. DOI: 10.1016/j.bbadis.2012.03.012.

Kessler, Mirjam; Rottbauer, Wolfgang; Just, Steffen (2015): Recent progress in the use of zebrafish for novel cardiac drug discovery. In: *Expert opinion on drug discovery* n. 11, 10, pp. 1231–1241. DOI: 10.1517/17460441.2015.1078788.

Kettleborough, Ross N. W.; Busch-Nentwich, Elisabeth M.; Harvey, Steven A.; Dooley, Christopher M.; Bruijn, Ewart de; van Eeden, Freek et al. (2013): A systematic genome-wide analysis of zebrafish protein-coding gene function. In: *Nature* n. 7446, 496, pp. 494–497. DOI: 10.1038/nature11992.

Kiel, J. A.; Keizer-Gunnink, I. K.; Krause, T.; Komori, M.; Veenhuis, M. (1995): Heterologous complementation of peroxisome function in yeast: the Saccharomyces cerevisiae PAS3 gene restores

peroxisome biogenesis in a Hansenula polymorpha per9 disruption mutant. In: *FEBS letters* n. 3, 377, pp. 434–438.

Kienow, Lucie; Schneider, Katja; Bartsch, Michael; Stuible, Hans-Peter; Weng, Hua; Miersch, Otto et al. (2008): Jasmonates meet fatty acids: functional analysis of a new acyl-coenzyme A synthetase family from Arabidopsis thaliana. In: *Journal of experimental botany* n. 2, 59, pp. 403–419. DOI: 10.1093/jxb/erm325.

Kim, Dongkyun; Song, Jinsoo; Kang, Yeonho; Park, Sujung; Kim, Yong-Il; Kwak, Seongae et al. (2016): Fis1 depletion in osteoarthritis impairs chondrocyte survival and peroxisomal and lysosomal function. In: *Journal of molecular medicine (Berlin, Germany). DOI:* 10.1007/s00109-016-1445-9.

Kim, Peter K.; Mullen, Robert T.; Schumann, Uwe; Lippincott-Schwartz, Jennifer (2006): The origin and maintenance of mammalian peroxisomes involves a de novo PEX16-dependent pathway from the ER. In: *The Journal of cell biology* n. 4, 173, pp. 521–532. DOI: 10.1083/jcb.200601036.

Kimmel, C. B.; Ballard, W. W.; Kimmel, S. R.; Ullmann, B.; Schilling, T. F. (1995): Stages of embryonic development of the zebrafish. In: *Developmental dynamics : an official publication of the American Association of Anatomists* n. 3, 203, pp. 253–310. DOI: 10.1002/aja.1002030302.

Kinkel, Mary D.; Prince, Victoria E. (2009): On the diabetic menu: zebrafish as a model for pancreas development and function. In: *BioEssays : news and reviews in molecular, cellular and developmental biology* n. 2, 31, pp. 139–152. DOI: 10.1002/bies.200800123.

Kirkman, Henry N.; Gaetani, Gian F. (2007): Mammalian catalase: a venerable enzyme with new mysteries. In: *Trends in biochemical sciences* n. 1, 32, pp. 44–50. DOI: 10.1016/j.tibs.2006.11.003.

Kleinstiver, Benjamin P.; Prew, Michelle S.; Tsai, Shengdar Q.; Topkar, Ved V.; Nguyen, Nhu T.; Zheng, Zongli et al. (2015): Engineered CRISPR-Cas9 nucleases with altered PAM specificities. In: *Nature* n. 7561, 523, pp. 481–485. DOI: 10.1038/nature14592.

Klouwer, Femke C. C.; Berendse, Kevin; Ferdinandusse, Sacha; Wanders, Ronald J. A.; Engelen, Marc; Poll-The, Bwee Tien (2015): Zellweger spectrum disorders: clinical overview and management approach. In: *Orphanet journal of rare diseases,* 10, p. 151. DOI: 10.1186/s13023-015-0368-9.

Knight, Robert D.; Nair, Sreelaja; Nelson, Sarah S.; Afshar, Ali; Javidan, Yashar; Geisler, Robert et al. (2003): lockjaw encodes a zebrafish tfap2a required for early neural crest development. In: *Development (Cambridge, England)* n. 23, 130, pp. 5755–5768. DOI: 10.1242/dev.00575.

Knoblach, Barbara; Sun, Xuejun; Coquelle, Nicolas; Fagarasanu, Andrei; Poirier, Richard L.; Rachubinski, Richard A. (2013): An ER-peroxisome tether exerts peroxisome population control in yeast. In: *The EMBO journal* n. 18, 32, pp. 2439–2453. DOI: 10.1038/emboj.2013.170.

Koch, Johannes; Pranjic, Kornelija; Huber, Anja; Ellinger, Adolf; Hartig, Andreas; Kragler, Friedrich; Brocard, Cecile (2010): PEX11 family members are membrane elongation factors that coordinate peroxisome proliferation and maintenance. In: *Journal of cell science* n. Pt 19, 123, pp. 3389–3400. DOI: 10.1242/jcs.064907.

Koo, Taeyoung; Lee, Jungjoon; Kim, Jin-Soo (2015): Measuring and Reducing Off-Target Activities of Programmable Nucleases Including CRISPR-Cas9. In: *Molecules and cells* n. 6, 38, pp. 475–481. DOI: 10.14348/molcells.2015.0103.

Koscielny, Gautier; Yaikhom, Gagarine; Iyer, Vivek; Meehan, Terrence F.; Morgan, Hugh; Atienza-Herrero, Julian et al. (2014): The International Mouse Phenotyping Consortium Web Portal, a unified point of access for knockout mice and related phenotyping data. In: *Nucleic acids research* n. Database issue, 42, D802-9. DOI: 10.1093/nar/gkt977.

Kragt, Astrid; Voorn-Brouwer, Tineke; van den Berg, Marlene; Distel, Ben (2005): Endoplasmic reticulum-directed Pex3p routes to peroxisomes and restores peroxisome formation in a Saccharomyces cerevisiae pex3Delta strain. In: *The Journal of biological chemistry* n. 40, 280, pp. 34350–34357. DOI: 10.1074/jbc.M505432200.

Krysko, Olga; Hulshagen, Leen; Janssen, Anneleen; Schutz, Gunter; Klein, Rudiger; Bruycker, Melina de et al. (2007): Neocortical and cerebellar developmental abnormalities in conditions of selective elimination of peroxisomes from brain or from liver. In: *Journal of neuroscience research* n. 1, 85, pp. 58–72. DOI: 10.1002/jnr.21097.

Krysko, Olga; Stevens, Mieke; Langenberg, Tobias; Fransen, Marc; Espeel, Marc; Baes, Myriam (2010): Peroxisomes in zebrafish: distribution pattern and knockdown studies. In: *Histochemistry and cell biology* n. 1, 134, pp. 39–51. DOI: 10.1007/s00418-010-0712-z.

Kurtzman, Mark S.; Craig, Michael P.; Grizzle, Brenda K.; Hove, Jay R. (2010): Sexually segregated housing results in improved early larval survival in zebrafish. In: *Lab animal* n. 6, 39, pp. 183–189. DOI: 10.1038/laban0610-183.

Kushimoto, T.; Basrur, V.; Valencia, J.; Matsunaga, J.; Vieira, W. D.; Ferrans, V. J. et al. (2001): A model for melanosome biogenesis based on the purification and analysis of early melanosomes. In: *Proceedings of the National Academy of Sciences of the United States of America* n. 19, 98, pp. 10698–10703. DOI: 10.1073/pnas.191184798.

Lamason, Rebecca L.; Mohideen, Manzoor-Ali P. K.; Mest, Jason R.; Wong, Andrew C.; Norton, Heather L.; Aros, Michele C. et al. (2005): SLC24A5, a putative cation exchanger, affects pigmentation in zebrafish and humans. In: *Science (New York, N.Y.)* n. 5755, 310, pp. 1782–1786. DOI: 10.1126/science.1116238.

Land, E. J.; Ito, S.; Wakamatsu, K.; Riley, P. A. (2003): Rate constants for the first two chemical steps of eumelanogenesis. In: *Pigment cell research / sponsored by the European Society for Pigment Cell Research and the International Pigment Cell Society* n. 5, 16, pp. 487–493.

Land, Edward J.; Ramsden, Christopher A.; Riley, Patrick A. (2003): Tyrosinase autoactivation and the chemistry of ortho-quinone amines. In: *Accounts of chemical research* n. 5, 36, pp. 300–308. DOI: 10.1021/ar020062p.

Land, Edward J.; Ramsden, Christopher A.; Riley, Patrick A.; Yoganathan, Gnanamoly (2003): Mechanistic studies of catechol generation from secondary quinone amines relevant to indole formation and tyrosinase activation. In: *Pigment cell research / sponsored by the European Society for Pigment Cell Research and the International Pigment Cell Society* n. 4, 16, pp. 397–406.

Lawrence, Christian (2011): Advances in zebrafish husbandry and management. In: *Methods in cell biology,* 104, pp. 429–451. DOI: 10.1016/B978-0-12-374814-0.00023-9.

Lawrence, Christian; Ebersole, John P.; Kesseli, Richard V. (2007): Rapid growth and out-crossing promote female development in zebrafish (Danio rerio). In: *Environ Biol Fish* n. 2, 81, pp. 239–246. DOI: 10.1007/s10641-007-9195-8.

Lazarow, P. B.; Duve, C. de (1976): A fatty acyl-CoA oxidizing system in rat liver peroxisomes; enhancement by clofibrate, a hypolipidemic drug. In: *Proceedings of the National Academy of Sciences of the United States of America* n. 6, 73, pp. 2043–2046.

Lazarow, P. B.; Fujiki, Y. (1985): Biogenesis of peroxisomes. In: *Annual review of cell biology,* 1, pp. 489–530. DOI: 10.1146/annurev.cb.01.110185.002421.

Lazarow, Paul B. (2006): The import receptor Pex7p and the PTS2 targeting sequence. In: *Biochimica et biophysica acta* n. 12, 1763, pp. 1599–1604. DOI: 10.1016/j.bbamcr.2006.08.011.

Le, Hong-Gam T.; Dowling, John E.; Cameron, D. Joshua (2012): Early retinoic acid deprivation in developing zebrafish results in microphthalmia. In: *Visual neuroscience* n. 4-5, 29, pp. 219–228. DOI: 10.1017/S0952523812000296.

Le Douarin, Nicole M.; Couly, Gerard; Creuzet, Sophie E. (2012): The neural crest is a powerful regulator of pre-otic brain development. In: *Developmental biology* n. 1, 366, pp. 74–82. DOI: 10.1016/j.ydbio.2012.01.007.

Ledent, Valerie (2002): Postembryonic development of the posterior lateral line in zebrafish. In: *Development (Cambridge, England)* n. 3, 129, pp. 597–604.

Lee, Joong Sun; Choi, You Mi; Kang, Hee Young (2007): PPAR-gamma agonist, ciglitazone, increases pigmentation and migration of human melanocytes. In: *Experimental dermatology* n. 2, 16, pp. 118–123. DOI: 10.1111/j.1600-0625.2006.00521.x.

Lepiller, Sandrine; Laurens, Veronique; Bouchot, Andre; Herbomel, Philippe; Solary, Eric; Chluba, Johanna (2007): Imaging of nitric oxide in a living vertebrate using a diamino-fluorescein probe. In: *Free radical biology & medicine* n. 4, 43, pp. 619–627. DOI: 10.1016/j.freeradbiomed.2007.05.025.

Lerner, A. B. (1993): The discovery of the melanotropins. A history of pituitary endocrinology. In: *Annals of the New York Academy of Sciences,* 680, pp. 1–12.

Lessman, Charles A. (2011): The developing zebrafish (Danio rerio): a vertebrate model for high-throughput screening of chemical libraries. In: *Birth defects research. Part C, Embryo today : reviews* n. 3, 93, pp. 268–280. DOI: 10.1002/bdrc.20212.

Levine, Beth; Kroemer, Guido (2008): Autophagy in the pathogenesis of disease. In: *Cell* n. 1, 132, pp. 27–42. DOI: 10.1016/j.cell.2007.12.018.

Levy, Carmit; Khaled, Mehdi; Fisher, David E. (2006): MITF: master regulator of melanocyte development and melanoma oncogene. In: *Trends in molecular medicine* n. 9, 12, pp. 406–414. DOI: 10.1016/j.molmed.2006.07.008.

Li, X.; Baumgart, E.; Dong, G.-X.; Morrell, J. C.; Jimenez-Sanchez, G.; Valle, D. et al. (2002): PEX11 Is Required for Peroxisome Proliferation in Response to 4-Phenylbutyrate but Is Dispensable for Peroxisome Proliferator-Activated Receptor Alpha-Mediated Peroxisome Proliferation. In: *Molecular and cellular biology* n. 23, 22, pp. 8226–8240. DOI: 10.1128/MCB.22.23.8226-8240.2002.

Li, Xiaoling; Baumgart, Eveline; Morrell, James C.; Jimenez-Sanchez, Gerardo; Valle, David; Gould, Stephen J. (2002): PEX11 beta deficiency is lethal and impairs neuronal migration but does not abrogate peroxisome function. In: *Molecular and cellular biology* n. 12, 22, pp. 4358–4365.

Lister, J. A.; Close, J.; Raible, D. W. (2001): Duplicate mitf genes in zebrafish: complementary expression and conservation of melanogenic potential. In: *Developmental biology* n. 2, 237, pp. 333–344. DOI: 10.1006/dbio.2001.0379.

Lister, James A.; Cooper, Cynthia; Nguyen, Kim; Modrell, Melinda; Grant, Kelly; Raible, David W. (2006): Zebrafish Foxd3 is required for development of a subset of neural crest derivatives. In: *Developmental biology* n. 1, 290, pp. 92–104. DOI: 10.1016/j.ydbio.2005.11.014.

Liu, Yang; Kretz, Colin A.; Maeder, Morgan L.; Richter, Catherine E.; Tsao, Philip; Vo, Andy H. et al. (2014): Targeted mutagenesis of zebrafish antithrombin III triggers disseminated intravascular coagulation and thrombosis, revealing insight into function. In: *Blood* n. 1, 124, pp. 142–150. DOI: 10.1182/blood-2014-03-561027.

Logan, Darren W.; Burn, Sally F.; Jackson, Ian J. (2006): Regulation of pigmentation in zebrafish melanophores. In: *Pigment cell research / sponsored by the European Society for Pigment Cell Research and the International Pigment Cell Society* n. 3, 19, pp. 206–213. DOI: 10.1111/j.1600-0749.2006.00307.x.

Loughran, Patricia A.; Stolz, Donna B.; Barrick, Stacey R.; Wheeler, David S.; Friedman, Peter A.; Rachubinski, Richard A. et al. (2013): PEX7 and EBP50 target iNOS to the peroxisome in hepatocytes. In: *Nitric oxide : biology and chemistry / official journal of the Nitric Oxide Society,* 31, pp. 9–19. DOI: 10.1016/j.niox.2013.02.084.

Luciani, Flavie; Champeval, Delphine; Herbette, Aurelie; Denat, Laurence; Aylaj, Bouchra; Martinozzi, Silvia et al. (2011): Biological and mathematical modeling of melanocyte development. In: *Development (Cambridge, England)* n. 18, 138, pp. 3943–3954. DOI: 10.1242/dev.067447.

Ma, Alvin C.; Lee, Han B.; Clark, Karl J.; Ekker, Stephen C. (2013): High efficiency In Vivo genome engineering with a simplified 15-RVD GoldyTALEN design. In: *PloS one* n. 5, 8, e65259. DOI: 10.1371/journal.pone.0065259.

Mahalwar, Prateek; Walderich, Brigitte; Singh, Ajeet Pratap; Nusslein-Volhard, Christiane (2014): Local reorganization of xanthophores fine-tunes and colors the striped pattern of zebrafish. In: *Science (New York, N.Y.)* n. 6202, 345, pp. 1362–1364. DOI: 10.1126/science.1254837.

Makky, Khadijah; Duvnjak, Petar; Pramanik, Kallal; Ramchandran, Ramani; Mayer, Alan N. (2008): A whole-animal microplate assay for metabolic rate using zebrafish. In: *Journal of biomolecular screening* n. 10, 13, pp. 960–967. DOI: 10.1177/1087057108326080.

Malek, Renae L.; Sajadi, Hedieh; Abraham, Joseph; Grundy, Martin A.; Gerhard, Glenn S. (2004): The effects of temperature reduction on gene expression and oxidative stress in skeletal muscle from adult zebrafish. In: *Comparative biochemistry and physiology. Toxicology & pharmacology : CBP* n. 3, 138, pp. 363–373. DOI: 10.1016/j.cca.2004.08.014.

Mandrekar, Noopur; Thakur, Narsinh L. (2009): Significance of the zebrafish model in the discovery of bioactive molecules from nature. In: *Biotechnology letters* n. 2, 31, pp. 171–179. DOI: 10.1007/s10529-008-9868-1.

Manga, P.; Boissy, R. E.; Pifko-Hirst, S.; Zhou, B. K.; Orlow, S. J. (2001): Mislocalization of melanosomal proteins in melanocytes from mice with oculocutaneous albinism type 2. In: *Experimental eye research* n. 6, 72, pp. 695–710. DOI: 10.1006/exer.2001.1006.

Mangelsdorf, D. J.; Thummel, C.; Beato, M.; Herrlich, P.; Schutz, G.; Umesono, K. et al. (1995): The nuclear receptor superfamily: the second decade. In: *Cell* n. 6, 83, pp. 835–839.

Marks, M. S.; Seabra, M. C. (2001): The melanosome: membrane dynamics in black and white. In: *Nature reviews. Molecular cell biology* n. 10, 2, pp. 738–748. DOI: 10.1038/35096009.

Marles, Lee K.; Peters, Eva M.; Tobin, Desmond J.; Hibberts, Nigel A.; Schallreuter, Karin U. (2003): Tyrosine hydroxylase isoenzyme I is present in human melanosomes: a possible novel function in pigmentation. In: *Experimental dermatology* n. 1, 12, pp. 61–70.

Marshall, Owen J. (2004): PerlPrimer: cross-platform, graphical primer design for standard, bisulphite and real-time PCR. In: *Bioinformatics (Oxford, England)* n. 15, 20, pp. 2471–2472. DOI: 10.1093/bioinformatics/bth254.

Mathelier, Anthony; Fornes, Oriol; Arenillas, David J.; Chen, Chih-Yu; Denay, Gregoire; Lee, Jessica et al. (2016): JASPAR 2016: a major expansion and update of the open-access database of transcription factor binding profiles. In: *Nucleic acids research* n. D1, 44, D110-5. DOI: 10.1093/nar/gkv1176.

Matsui, Shuji; Funahashi, Masuko; Honda, Ayako; Shimozawa, Nobuyuki (2013): Newly identified milder phenotype of peroxisome biogenesis disorder caused by mutated PEX3 gene. In: *Brain & development* n. 9, 35, pp. 842–848. DOI: 10.1016/j.braindev.2012.10.017.

Mattiazzi Usaj, M.; Brloznik, M.; Kaferle, P.; Zitnik, M.; Wolinski, H.; Leitner, F. et al. (2015): Genome-Wide Localization Study of Yeast Pex11 Identifies Peroxisome-Mitochondria Interactions through the ERMES Complex. In: *Journal of molecular biology* n. 11, 427, pp. 2072–2087. DOI: 10.1016/j.jmb.2015.03.004.

Maxit, C.; Denzler, I.; Marchione, D.; Agosta, G.; Koster, J.; Wanders, R. J. A. et al. (2016): Novel PEX3 Gene Mutations Resulting in a Moderate Zellweger Spectrum Disorder. In: *JIMD reports. DOI:* 10.1007/8904_2016_10.

Mayor, Roberto; Carmona-Fontaine, Carlos (2010): Keeping in touch with contact inhibition of locomotion. In: *Trends in cell biology* n. 6, 20, pp. 319–328. DOI: 10.1016/j.tcb.2010.03.005.

McClure (1999): Development and evolution of melanophore patterns in fishes of the genus Danio (Teleostei: Cyprinidae). In: *Journal of morphology* n. 1, 241, pp. 83–105. DOI: 10.1002/(SICI)1097-4687(199907)241:1<83::AID-JMOR5>3.0.CO;2-H.

McKeown, Sonja J.; Wallace, Adam S.; Anderson, Richard B. (2013): Expression and function of cell adhesion molecules during neural crest migration. In: *Developmental biology* n. 2, 373, pp. 244–257. DOI: 10.1016/j.ydbio.2012.10.028.

McKinney, Mary C.; Fukatsu, Kazumi; Morrison, Jason; McLennan, Rebecca; Bronner, Marianne E.; Kulesa, Paul M. (2013): Evidence for dynamic rearrangements but lack of fate or position restrictions in premigratory avian trunk neural crest. In: *Development (Cambridge, England)* n. 4, 140, pp. 820–830. DOI: 10.1242/dev.083725.

McNew, J. A. (1994): An oligomeric protein is imported into peroxisomes in vivo. In: *The Journal of cell biology* n. 5, 127, pp. 1245–1257. DOI: 10.1083/jcb.127.5.1245.

Meijer, Wiebe H.; Gidijala, Loknath; Fekken, Susan; Kiel, Jan A. K. W.; van den Berg, Marco A.; Lascaris, Romeo et al. (2010): Peroxisomes are required for efficient penicillin biosynthesis in Penicillium chrysogenum. In: *Applied and environmental microbiology* n. 17, 76, pp. 5702–5709. DOI: 10.1128/AEM.02327-09.

Milet, Cecile; Monsoro-Burq, Anne H. (2012): Neural crest induction at the neural plate border in vertebrates. In: *Developmental biology* n. 1, 366, pp. 22–33. DOI: 10.1016/j.ydbio.2012.01.013.

Miller, Jeffrey C.; Tan, Siyuan; Qiao, Guijuan; Barlow, Kyle A.; Wang, Jianbin; Xia, Danny F. et al. (2011): A TALE nuclease architecture for efficient genome editing. In: *Nature biotechnology* n. 2, 29, pp. 143–148. DOI: 10.1038/nbt.1755.

Miller BF (2003): Miller-Keane Encyclopedia and Dictionary of Medicine, Nursing, and Allied Health. Saunders. Philadelphia.

Milos, N.; Dingle, A. D.; Milos, J. P. (1983): Dynamics of pigment pattern formation in the zebrafish, Brachydanio rerio. III. Effect of anteroposterior location of three-day lateral line melanophores on colonization by the second wave of melanophores. In: *The Journal of experimental zoology* n. 1, 227, pp. 81–92. DOI: 10.1002/jez.1402270112.

Mongera, Alessandro; Singh, Ajeet P.; Levesque, Mitchell P.; Chen, Yi-Yen; Konstantinidis, Peter; Nusslein-Volhard, Christiane (2013): Genetic lineage labeling in zebrafish uncovers novel neural crest contributions to the head, including gill pillar cells. In: *Development (Cambridge, England)* n. 4, 140, pp. 916–925. DOI: 10.1242/dev.091066.

Moore, John C.; Langenau, David M. (2016): Allograft Cancer Cell Transplantation in Zebrafish. In: *Advances in experimental medicine and biology,* 916, pp. 265–287. DOI: 10.1007/978-3-319-30654-4_12.

Moreno-Mateos, Miguel A.; Vejnar, Charles E.; Beaudoin, Jean-Denis; Fernandez, Juan P.; Mis, Emily K.; Khokha, Mustafa K.; Giraldez, Antonio J. (2015): CRISPRscan: designing highly efficient sgRNAs for CRISPR-Cas9 targeting in vivo. In: *Nature methods* n. 10, 12, pp. 982–988. DOI: 10.1038/nmeth.3543.

Mort, Richard L.; Jackson, Ian J.; Patton, E. Elizabeth (2015): The melanocyte lineage in development and disease. In: *Development (Cambridge, England)* n. 7, 142, p. 1387. DOI: 10.1242/dev.123729.

Moser, A. B.; Rasmussen, M.; Naidu, S.; Watkins, P. A.; McGuinness, M.; Hajra, A. K. et al. (1995): Phenotype of patients with peroxisomal disorders subdivided into sixteen complementation groups. In: *The Journal of pediatrics* n. 1, 127, pp. 13–22.

Mosimann, Christian; Puller, Ann-Christin; Lawson, Katy L.; Tschopp, Patrick; Amsterdam, Adam; Zon, Leonard I. (2013): Site-directed zebrafish transgenesis into single landing sites with the phiC31 integrase system. In: *Developmental dynamics : an official publication of the American Association of Anatomists* n. 8, 242, pp. 949–963. DOI: 10.1002/dvdy.23989.

Motley, Alison M.; Nuttall, James M.; Hettema, Ewald H. (2012): Pex3-anchored Atg36 tags peroxisomes for degradation in Saccharomyces cerevisiae. In: *The EMBO journal* n. 13, 31, pp. 2852–2868. DOI: 10.1038/emboj.2012.151.

Munck, Joanne M.; Motley, Alison M.; Nuttall, James M.; Hettema, Ewald H. (2009): A dual function for Pex3p in peroxisome formation and inheritance. In: *The Journal of cell biology* n. 4, 187, pp. 463–471. DOI: 10.1083/jcb.200906161.

Muntau, A. C.; Mayerhofer, P. U.; Paton, B. C.; Kammerer, S.; Roscher, A. A. (2000): Defective peroxisome membrane synthesis due to mutations in human PEX3 causes Zellweger syndrome, complementation group G. In: *American journal of human genetics* n. 4, 67, pp. 967–975. DOI: 10.1086/303071.

Nakayama, Minoru; Sato, Hiroyasu; Okuda, Takayuki; Fujisawa, Nao; Kono, Nozomu; Arai, Hiroyuki et al. (2011): Drosophila carrying pex3 or pex16 mutations are models of Zellweger syndrome that reflect its symptoms associated with the absence of peroxisomes. In: *PloS one* n. 8, 6, e22984. DOI: 10.1371/journal.pone.0022984.

Nasevicius, A.; Ekker, S. C. (2000): Effective targeted gene 'knockdown' in zebrafish. In: *Nature genetics* n. 2, 26, pp. 216–220. DOI: 10.1038/79951.

Nathan, Carl; Ding, Aihao (2010): SnapShot: Reactive Oxygen Intermediates (ROI). In: *Cell* n. 6, 140, 951-951.e2. DOI: 10.1016/j.cell.2010.03.008.

Ni, Terri T.; Lu, Jianjun; Zhu, Meiying; Maddison, Lisette A.; Boyd, Kelli L.; Huskey, Lindsey et al. (2012): Conditional control of gene function by an invertible gene trap in zebrafish. In: *Proceedings of the National Academy of Sciences of the United States of America* n. 38, 109, pp. 15389–15394. DOI: 10.1073/pnas.1206131109.

Niimi, A. J.; LaHam, Q. N. (1974): Influence of breeding time interval on egg number, mortality, and hatching of the zebra fish Brachydanio verio. In: *Canadian journal of zoology* n. 4, 52, pp. 515–517.

Nishikawa, M.; Hagishita, T.; Yurimoto, H.; Kato, N.; Sakai, Y.; Hatanaka, T. (2000): Primary structure and expression of peroxisomal acetylspermidine oxidase in the methylotrophic yeast Candida boidinii. In: *FEBS letters* n. 3, 476, pp. 150–154.

Okamoto, Koji (2014): Organellophagy: eliminating cellular building blocks via selective autophagy. In: *The Journal of cell biology* n. 4, 205, pp. 435–445. DOI: 10.1083/jcb.201402054.

Osumi, T.; Imamura, A.; Tsukamoto, T.; Fujiwara, C.; Hashiguchi, N.; Shimozawa, N. et al. (2000): Temperature sensitivity in peroxisome assembly processes characterizes milder forms of peroxisome biogenesis disorders. In: *Cell biochemistry and biophysics,* 32 Spring, pp. 165–170.

Overwijk, W. W.; Restifo, N. P. (2001): B16 as a mouse model for human melanoma. In: *Current protocols in immunology / edited by John E. Coligan … [et al.],* Chapter 20, Unit 20.1. DOI: 10.1002/0471142735.im2001s39.

Pacher, Pal; Beckman, Joseph S.; Liaudet, Lucas (2007): Nitric oxide and peroxynitrite in health and disease. In: *Physiological reviews* n. 1, 87, pp. 315–424. DOI: 10.1152/physrev.00029.2006.

Pagon, Roberta A.; Adam, Margaret P.; Ardinger, Holly H.; Wallace, Stephanie E.; Amemiya, Anne; Bean, Lora J. H. et al. (1993): GeneReviews(R). University of Washington, Seattle. Seattle (WA).

Panieri, E.; Santoro, M. M. (2016): ROS homeostasis and metabolism: a dangerous liason in cancer cells. In: *Cell death & disease* n. 6, 7, e2253. DOI: 10.1038/cddis.2016.105.

Parichy, D. M.; Ransom, D. G.; Paw, B.; Zon, L. I.; Johnson, S. L. (2000): An orthologue of the kit-related gene fms is required for development of neural crest-derived xanthophores and a subpopulation of adult melanocytes in the zebrafish, Danio rerio. In: *Development (Cambridge, England)* n. 14, 127, pp. 3031–3044.

Parichy, D. M.; Rawls, J. F.; Pratt, S. J.; Whitfield, T. T.; Johnson, S. L. (1999): Zebrafish sparse corresponds to an orthologue of c-kit and is required for the morphogenesis of a subpopulation of melanocytes, but is not essential for hematopoiesis or primordial germ cell development. In: *Development (Cambridge, England)* n. 15, 126, pp. 3425–3436.

Parichy, David M.; Elizondo, Michael R.; Mills, Margaret G.; Gordon, Tiffany N.; Engeszer, Raymond E. (2009): Normal table of postembryonic zebrafish development: staging by externally visible anatomy of the living fish. In: *Developmental dynamics : an official publication of the American Association of Anatomists* n. 12, 238, pp. 2975–3015. DOI: 10.1002/dvdy.22113.

Park, H. Y.; Kosmadaki, M.; Yaar, M.; Gilchrest, B. A. (2009): Cellular mechanisms regulating human melanogenesis. In: *Cellular and molecular life sciences : CMLS* n. 9, 66, pp. 1493–1506. DOI: 10.1007/s00018-009-8703-8.

Pattanayak, Vikram; Guilinger, John P.; Liu, David R. (2014): Determining the specificities of TALENs, Cas9, and other genome-editing enzymes. In: *Methods in enzymology,* 546, pp. 47–78. DOI: 10.1016/B978-0-12-801185-0.00003-9.

Pawelek, J. M. (1985): Studies on the Cloudman melanoma cell line as a model for the action of MSH. In: *The Yale journal of biology and medicine* n. 6, 58, pp. 571–578.

Pawelek, J. M.; Chakraborty, A. K.; Osber, M. P.; Orlow, S. J.; Min, K. K.; Rosenzweig, K. E.; Bolognia, J. L. (1992): Molecular cascades in UV-induced melanogenesis: a central role for melanotropins? In: *Pigment cell research / sponsored by the European Society for Pigment Cell Research and the International Pigment Cell Society* n. 5 Pt 2, 5, pp. 348–356.

Pennisi, Elizabeth (2013): The CRISPR craze. In: *Science (New York, N.Y.)* n. 6148, 341, pp. 833–836. DOI: 10.1126/science.341.6148.833.

Petriv, Oleh I.; Pilgrim, David B.; Rachubinski, Richard A.; Titorenko, Vladimir I. (2002): RNA interference of peroxisome-related genes in C. elegans: a new model for human peroxisomal disorders. In: *Physiological genomics* n. 2, 10, pp. 79–91. DOI: 10.1152/physiolgenomics.00044.2002.

Pillai, Renjitha; Coverdale, Louise E.; Dubey, Gaytri; Martin, C. Cristofre (2004): Histone deacetylase 1 (HDAC-1) required for the normal formation of craniofacial cartilage and pectoral fins of the zebrafish.

In: *Developmental dynamics : an official publication of the American Association of Anatomists* n. 3, 231, pp. 647–654. DOI: 10.1002/dvdy.20168.

Pillaiyar, Thanigaimalai; Manickam, Manoj; Jung, Sang-Hun (2015): Inhibitors of melanogenesis: a patent review (2009 - 2014). In: *Expert opinion on therapeutic patents* n. 7, 25, pp. 775–788. DOI: 10.1517/13543776.2015.1039985.

Pinto, Manuel P.; Grou, Claudia P.; Fransen, Marc; Sa-Miranda, Clara; Azevedo, Jorge E. (2009): The cytosolic domain of PEX3, a protein involved in the biogenesis of peroxisomes, binds membrane lipids. In: *Biochimica et biophysica acta* n. 11, 1793, pp. 1669–1675. DOI: 10.1016/j.bbamcr.2009.08.007.

Plonka, P. M.; Passeron, T.; Brenner, M.; Tobin, D. J.; Shibahara, S.; Thomas, A. et al. (2009): What are melanocytes really doing all day long…? In: *Experimental dermatology* n. 9, 18, pp. 799–819. DOI: 10.1111/j.1600-0625.2009.00912.x.

Poirier, Yves; Antonenkov, Vasily D.; Glumoff, Tuomo; Hiltunen, J. Kalervo (2006): Peroxisomal beta-oxidation--a metabolic pathway with multiple functions. In: *Biochimica et biophysica acta* n. 12, 1763, pp. 1413–1426. DOI: 10.1016/j.bbamcr.2006.08.034.

Porteus, Matthew H.; Carroll, Dana (2005): Gene targeting using zinc finger nucleases. In: *Nature biotechnology* n. 8, 23, pp. 967–973. DOI: 10.1038/nbt1125.

Postlethwait, John H. (2007): The zebrafish genome in context: ohnologs gone missing. In: *Journal of experimental zoology. Part B, Molecular and developmental evolution* n. 5, 308, pp. 563–577. DOI: 10.1002/jez.b.21137.

Potterf, S. B.; Virador, V.; Wakamatsu, K.; Furumura, M.; Santis, C.; Ito, S.; Hearing, V. J. (1999): Cysteine transport in melanosomes from murine melanocytes. In: *Pigment cell research / sponsored by the European Society for Pigment Cell Research and the International Pigment Cell Society* n. 1, 12, pp. 4–12.

Prota, G. (1995): The chemistry of melanins and melanogenesis. In: *Fortschritte der Chemie organischer Naturstoffe = Progress in the chemistry of organic natural products. Progres dans la chimie des substances organiques naturelles,* 64, pp. 93–148.

Que, Syril Keena T.; Weston, Gillian; Suchecki, Jeanine; Ricketts, Janelle (2015): Pigmentary disorders of the eyes and skin. In: *Clinics in dermatology* n. 2, 33, pp. 147–158. DOI: 10.1016/j.clindermatol.2014.10.007.

Ran, F. Ann; Hsu, Patrick D.; Lin, Chie-Yu; Gootenberg, Jonathan S.; Konermann, Silvana; Trevino, Alexandro E. et al. (2013): Double nicking by RNA-guided CRISPR Cas9 for enhanced genome editing specificity. In: *Cell* n. 6, 154, pp. 1380–1389. DOI: 10.1016/j.cell.2013.08.021.

Raposo, G.; Tenza, D.; Murphy, D. M.; Berson, J. F.; Marks, M. S. (2001): Distinct protein sorting and localization to premelanosomes, melanosomes, and lysosomes in pigmented melanocytic cells. In: *The Journal of cell biology* n. 4, 152, pp. 809–824.

Raposo, Graca; Marks, Michael S. (2007): Melanosomes--dark organelles enlighten endosomal membrane transport. In: *Nature reviews. Molecular cell biology* n. 10, 8, pp. 786–797. DOI: 10.1038/nrm2258.

Reyon, Deepak; Khayter, Cyd; Regan, Maureen R.; Joung, J. Keith; Sander, Jeffry D. (2012): Engineering designer transcription activator-like effector nucleases (TALENs) by REAL or REAL-Fast assembly. In: *Current protocols in molecular biology / edited by Frederick M. Ausubel … [et al.],* Chapter 12, Unit 12.15. DOI: 10.1002/0471142727.mb1215s100.

Rhodin, J. (1954): Correlation of Ultrastructural Organization: And Function in Normal and Experimentally Changed Proximal Convoluted Tubule Cells of the Mouse Kidney: an Electron Microscopic Study: Department of Anatomy, Karolinska Institutet. Available online in https://books.google.de/books?id=suneOwAACAAJ.

Rokka, Aare; Antonenkov, Vasily D.; Soininen, Raija; Immonen, Hanna L.; Pirila, Paivi L.; Bergmann, Ulrich et al. (2009): Pxmp2 is a channel-forming protein in Mammalian peroxisomal membrane. In: *PloS one* n. 4, 4, e5090. DOI: 10.1371/journal.pone.0005090.

Romero-Graillet, C.; Aberdam, E.; Biagoli, N.; Massabni, W.; Ortonne, J. P.; Ballotti, R. (1996): Ultraviolet B radiation acts through the nitric oxide and cGMP signal transduction pathway to stimulate

melanogenesis in human melanocytes. In: *The Journal of biological chemistry* n. 45, 271, pp. 28052–28056.

Rottensteiner, Hanspeter; Kramer, Achim; Lorenzen, Stephan; Stein, Katharina; Landgraf, Christiane; Volkmer-Engert, Rudolf; Erdmann, Ralf (2004): Peroxisomal membrane proteins contain common Pex19p-binding sites that are an integral part of their targeting signals. In: *Molecular biology of the cell* n. 7, 15, pp. 3406–3417. DOI: 10.1091/mbc.E04-03-0188.

Russell, David W. (2003): The enzymes, regulation, and genetics of bile acid synthesis. In: *Annual review of biochemistry,* 72, pp. 137–174. DOI: 10.1146/annurev.biochem.72.121801.161712.

Sander, Jeffry D.; Maeder, Morgan L.; Reyon, Deepak; Voytas, Daniel F.; Joung, J. Keith; Dobbs, Drena (2010): ZiFiT (Zinc Finger Targeter): an updated zinc finger engineering tool. In: *Nucleic acids research* n. Web Server issue, 38, W462-8. DOI: 10.1093/nar/gkq319.

Santoro, Massimo M. (2014): Zebrafish as a model to explore cell metabolism. In: *Trends in endocrinology and metabolism: TEM* n. 10, 25, pp. 546–554. DOI: 10.1016/j.tem.2014.06.003.

Sasselli, Valentina; Pachnis, Vassilis; Burns, Alan J. (2012): The enteric nervous system. In: *Developmental biology* n. 1, 366, pp. 64–73. DOI: 10.1016/j.ydbio.2012.01.012.

Sato, Yasuhiko; Shibata, Hiroyuki; Nakano, Hiroaki; Matsuzono, Yuji; Kashiwayama, Yoshinori; Kobayashi, Yuji et al. (2008): Characterization of the interaction between recombinant human peroxin Pex3p and Pex19p: identification of TRP-104 IN Pex3p as a critical residue for the interaction. In: *The Journal of biological chemistry* n. 10, 283, pp. 6136–6144. DOI: 10.1074/jbc.M706139200.

Sato, Yasuhiko; Shibata, Hiroyuki; Nakatsu, Toru; Nakano, Hiroaki; Kashiwayama, Yoshinori; Imanaka, Tsuneo; Kato, Hiroaki (2010): Structural basis for docking of peroxisomal membrane protein carrier Pex19p onto its receptor Pex3p. In: *The EMBO journal* n. 24, 29, pp. 4083–4093. DOI: 10.1038/emboj.2010.293.

Schallreuter, K. U.; Lemke, K. R.; Hill, H. Z.; Wood, J. M. (1994): Thioredoxin reductase induction coincides with melanin biosynthesis in brown and black guinea pigs and in murine melanoma cells. In: *The Journal of investigative dermatology* n. 6, 103, pp. 820–824.

Schallreuter, K. U.; Wood, J. M. (1989): Free radical reduction in the human epidermis. In: *Free radical biology & medicine* n. 5, 6, pp. 519–532.

Schiaffino, Maria Vittoria (2010): Signaling pathways in melanosome biogenesis and pathology. In: *The international journal of biochemistry & cell biology* n. 7, 42, pp. 1094–1104. DOI: 10.1016/j.biocel.2010.03.023.

Schluter, Agatha; Fourcade, Stephane; Ripp, Raymond; Mandel, Jean Louis; Poch, Olivier; Pujol, Aurora (2006a): The evolutionary origin of peroxisomes: an ER-peroxisome connection. In: *Molecular biology and evolution* n. 4, 23, pp. 838–845. DOI: 10.1093/molbev/msj103.

Schmelzer, Constance; Okun, Jurgen G.; Haas, Dorothea; Higuchi, Keiichi; Sawashita, Jinko; Mori, Masayuki; Doring, Frank (2010): The reduced form of coenzyme Q10 mediates distinct effects on cholesterol metabolism at the transcriptional and metabolite level in SAMP1 mice. In: *IUBMB life* n. 11, 62, pp. 812–818. DOI: 10.1002/iub.388.

Schmidt, Friederike; Dietrich, Denise; Eylenstein, Roy; Groemping, Yvonne; Stehle, Thilo; Dodt, Gabriele (2012a): The role of conserved PEX3 regions in PEX19-binding and peroxisome biogenesis. In: *Traffic (Copenhagen, Denmark)* n. 9, 13, pp. 1244–1260. DOI: 10.1111/j.1600-0854.2012.01380.x.

Schmidt, Friederike; Treiber, Nora; Zocher, Georg; Bjelic, Sasa; Steinmetz, Michel O.; Kalbacher, Hubert et al. (2010): Insights into peroxisome function from the structure of PEX3 in complex with a soluble fragment of PEX19. In: *The Journal of biological chemistry* n. 33, 285, pp. 25410–25417. DOI: 10.1074/jbc.M110.138503.

Schrader, M.; Bonekamp, N. A.; Islinger, M. (2012): Fission and proliferation of peroxisomes. In: *Biochimica et biophysica acta* n. 9, 1822, pp. 1343–1357. DOI: 10.1016/j.bbadis.2011.12.014.

Schrader, Michael; Costello, Joseph; Godinho, Luis F.; Islinger, Markus (2015): Peroxisome-mitochondria interplay and disease. In: *Journal of inherited metabolic disease* n. 4, 38, pp. 681–702. DOI: 10.1007/s10545-015-9819-7.

Schrader, Michael; Costello, Joseph L.; Godinho, Luis F.; Azadi, Afsoon S.; Islinger, Markus (2016): Proliferation and fission of peroxisomes - An update. In: *Biochimica et biophysica acta* n. 5, 1863, pp. 971–983. DOI: 10.1016/j.bbamcr.2015.09.024.

Schrader, Michael; Fahimi, H. Dariush (2006a): Growth and Division of Peroxisomes. In: A survey of cell biology, t. 255. Amsterdam: Elsevier (International Review of Cytology, v. 255), pp. 237–290.

Schrader, Michael; Fahimi, H. Dariush (2006b): Peroxisomes and oxidative stress. In: *Biochimica et biophysica acta* n. 12, 1763, pp. 1755–1766. DOI: 10.1016/j.bbamcr.2006.09.006.

Schrader, Michael; Fahimi, H. Dariush (2008): The peroxisome: still a mysterious organelle. In: *Histochemistry and cell biology* n. 4, 129, pp. 421–440. DOI: 10.1007/s00418-008-0396-9.

Schrader, Michael; Grille, Sandra; Fahimi, H. Dariush; Islinger, Markus (2013): Peroxisome interactions and cross-talk with other subcellular compartments in animal cells. In: *Sub-cellular biochemistry,* 69, pp. 1–22. DOI: 10.1007/978-94-007-6889-5_1.

Schrul, Bianca; Kopito, Ron R. (2016): Peroxin-dependent targeting of a lipid-droplet-destined membrane protein to ER subdomains. In: *Nature cell biology* n. 7, 18, pp. 740–751. DOI: 10.1038/ncb3373.

Scislowski, P. W.; Slominski, A. (1983): The role of NADP-dependent dehydrogenases in hydroxylation of tyrosine in hamster melanoma. In: *Neoplasma* n. 2, 30, pp. 239–243.

Scislowski, P. W.; Slominski, A.; Bomirski, A. (1984): Biochemical characterization of three hamster melanoma variants--II. Glycolysis and oxygen consumption. In: *The International journal of biochemistry* n. 3, 16, pp. 327–331.

Seabra, Miguel C.; Coudrier, Evelyne (2004): Rab GTPases and myosin motors in organelle motility. In: *Traffic (Copenhagen, Denmark)* n. 6, 5, pp. 393–399. DOI: 10.1111/j.1398-9219.2004.00190.x.

Sehring, Ivonne M.; Jahn, Christopher; Weidinger, Gilbert (2016): Zebrafish fin and heart: what's special about regeneration? In: *Current opinion in genetics & development,* 40, pp. 48–56. DOI: 10.1016/j.gde.2016.05.011.

Semple, Robert K.; Chatterjee, V. Krishna K.; O'Rahilly, Stephen (2006): PPAR gamma and human metabolic disease. In: *The Journal of clinical investigation* n. 3, 116, pp. 581–589. DOI: 10.1172/JCI28003.

Seth, Asha; Stemple, Derek L.; Barroso, Ines (2013): The emerging use of zebrafish to model metabolic disease. In: *Disease models & mechanisms* n. 5, 6, pp. 1080–1088. DOI: 10.1242/dmm.011346.

Shaklee, J. B.; Christiansen, J. A.; Sidell, B. D.; Prosser, C. L.; Whitt, G. S. (1977): Molecular aspects of temperature acclimation in fish: contributions of changes in enzyme activities and isozyme patterns to metabolic reorganization in the green sunfish. In: *The Journal of experimental zoology* n. 1, 201, pp. 1–20. DOI: 10.1002/jez.1402010102.

Shamseldin, Hanan E.; Alshammari, Muneera; Al-Sheddi, Tarfa; Salih, Mustafa A.; Alkhalidi, Hisham; Kentab, Amal et al. (2012): Genomic analysis of mitochondrial diseases in a consanguineous population reveals novel candidate disease genes. In: *Journal of medical genetics* n. 4, 49, pp. 234–241. DOI: 10.1136/jmedgenet-2012-100836.

Shibata, Eri; Sasaki, Makoto; Tohyama, Koujiro; Otsuka, Kotaro; Endoh, Jin; Terayama, Yasuo; Sakai, Akio (2008): Use of neuromelanin-sensitive MRI to distinguish schizophrenic and depressive patients and healthy individuals based on signal alterations in the substantia nigra and locus ceruleus. In: *Biological psychiatry* n. 5, 64, pp. 401–406. DOI: 10.1016/j.biopsych.2008.03.021.

Shimozawa, N.; Imamura, A.; Zhang, Z.; Suzuki, Y.; Orii, T.; Tsukamoto, T. et al. (1999): Defective PEX gene products correlate with the protein import, biochemical abnormalities, and phenotypic heterogeneity in peroxisome biogenesis disorders. In: *Journal of medical genetics* n. 10, 36, pp. 779–781.

Shimozawa, N.; Suzuki, Y.; Zhang, Z.; Imamura, A.; Ghaedi, K.; Fujiki, Y.; Kondo, N. (2000): Identification of PEX3 as the gene mutated in a Zellweger syndrome patient lacking peroxisomal remnant structures. In: *Human molecular genetics* n. 13, 9, pp. 1995–1999.

Singh, Ajeet Pratap; Nusslein-Volhard, Christiane (2015): Zebrafish stripes as a model for vertebrate colour pattern formation. In: *Current biology : CB* n. 2, 25, R81-92. DOI: 10.1016/j.cub.2014.11.013.

Singh, Ajeet Pratap; Schach, Ursula; Nusslein-Volhard, Christiane (2014): Proliferation, dispersal and patterned aggregation of iridophores in the skin prefigure striped colouration of zebrafish. In: *Nature cell biology* n. 6, 16, pp. 607–614. DOI: 10.1038/ncb2955.

Sitaram, Anand; Marks, Michael S. (2012): Mechanisms of protein delivery to melanosomes in pigment cells. In: *Physiology (Bethesda, Md.)* n. 2, 27, pp. 85–99. DOI: 10.1152/physiol.00043.2011.

Slominski, A.; Paus, R.; Schadendorf, D. (1993): Melanocytes as "sensory" and regulatory cells in the epidermis. In: *Journal of theoretical biology* n. 1, 164, pp. 103–120. DOI: 10.1006/jtbi.1993.1142.

Slominski, Andrzej; Tobin, Desmond J.; Shibahara, Shigeki; Wortsman, Jacobo (2004): Melanin pigmentation in mammalian skin and its hormonal regulation. In: *Physiological reviews* n. 4, 84, pp. 1155–1228. DOI: 10.1152/physrev.00044.2003.

Smith, Jennifer J.; Aitchison, John D. (2013): Peroxisomes take shape. In: *Nature reviews. Molecular cell biology* n. 12, 14, pp. 803–817. DOI: 10.1038/nrm3700.

Sone, Michio; Orlow, Seth J. (2007): The ocular albinism type 1 gene product, OA1, spans intracellular membranes 7 times. In: *Experimental eye research* n. 6, 85, pp. 806–816. DOI: 10.1016/j.exer.2007.08.016.

Song, Zhu; Zhang, Xiaoli; Jia, Shuo; Yelick, Pamela C.; Zhao, Chengtian (2016): Zebrafish as a Model for Human Ciliopathies. In: *Journal of genetics and genomics = Yi chuan xue bao* n. 3, 43, pp. 107–120. DOI: 10.1016/j.jgg.2016.02.001.

South, S. T.; Baumgart, E.; Gould, S. J. (2001): Inactivation of the endoplasmic reticulum protein translocation factor, Sec61p, or its homolog, Ssh1p, does not affect peroxisome biogenesis. In: *Proceedings of the National Academy of Sciences of the United States of America* n. 21, 98, pp. 12027–12031. DOI: 10.1073/pnas.221289498.

Spence, R.; Fatema, M. K.; Ellis, S.; Ahmed, Z. F.; Smith, C. (2007): Diet, growth and recruitment of wild zebrafish in Bangladesh. In: *J Fish Biology* n. 1, 71, pp. 304–309. DOI: 10.1111/j.1095-8649.2007.01492.x.

Spence, Rowena; Gerlach, Gabriele; Lawrence, Christian; Smith, Carl (2008): The behaviour and ecology of the zebrafish, Danio rerio. In: *Biological reviews of the Cambridge Philosophical Society* n. 1, 83, pp. 13–34. DOI: 10.1111/j.1469-185X.2007.00030.x.

Sprong, H.; Degroote, S.; Claessens, T.; van Drunen, J.; Oorschot, V.; Westerink, B. H. et al. (2001): Glycosphingolipids are required for sorting melanosomal proteins in the Golgi complex. In: *The Journal of cell biology* n. 3, 155, pp. 369–380. DOI: 10.1083/jcb.200106104.

Sprote, Petra; Brakhage, Axel A.; Hynes, Michael J. (2009): Contribution of peroxisomes to penicillin biosynthesis in Aspergillus nidulans. In: *Eukaryotic cell* n. 3, 8, pp. 421–423. DOI: 10.1128/EC.00374-08.

Steinberg, Steven J.; Dodt, Gabriele; Raymond, Gerald V.; Braverman, Nancy E.; Moser, Ann B.; Moser, Hugo W. (2006): Peroxisome biogenesis disorders. In: *Biochimica et biophysica acta* n. 12, 1763, pp. 1733–1748. DOI: 10.1016/j.bbamcr.2006.09.010.

Stollery, Nigel (2015): Pigmentation disorders. In: *The Practitioner* n. 1786, 259, pp. 30–31.

Stolz, Donna Beer; Zamora, Ruben; Vodovotz, Yoram; Loughran, Patricia A.; Billiar, Timothy R.; Kim, Young-Myeong et al. (2002): Peroxisomal localization of inducible nitric oxide synthase in hepatocytes. In: *Hepatology (Baltimore, Md.)* n. 1, 36, pp. 81–93. DOI: 10.1053/jhep.2002.33716.

Strausberg, Robert L.; Feingold, Elise A.; Grouse, Lynette H.; Derge, Jeffery G.; Klausner, Richard D.; Collins, Francis S. et al. (2002): Generation and initial analysis of more than 15,000 full-length human and mouse cDNA sequences. In: *Proceedings of the National Academy of Sciences of the United States of America* n. 26, 99, pp. 16899–16903. DOI: 10.1073/pnas.242603899.

Subramani, Suresh (1992): Targeting of proteins into the peroxisomal matrix. In: *J. Membarin Biol.* n. 2, 125. DOI: 10.1007/BF00233350.

Sugden, Mary C.; Caton, Paul W.; Holness, Mark J. (2010): PPAR control: it's SIRTainly as easy as PGC. In: *The Journal of endocrinology* n. 2, 204, pp. 93–104. DOI: 10.1677/JOE-09-0359.

Suhre, Karsten; Gieger, Christian (2012): Genetic variation in metabolic phenotypes: study designs and applications. In: *Nature reviews. Genetics* n. 11, 13, pp. 759–769. DOI: 10.1038/nrg3314.

Svetic, Valentina; Hollway, Georgina E.; Elworthy, Stone; Chipperfield, Thomas R.; Davison, Claire; Adams, Richard J. et al. (2007): Sdf1a patterns zebrafish melanophores and links the somite and melanophore pattern defects in choker mutants. In: *Development (Cambridge, England)* n. 5, 134, pp. 1011–1022. DOI: 10.1242/dev.02789.

Symington, Lorraine S.; Gautier, Jean (2011): Double-strand break end resection and repair pathway choice. In: *Annual review of genetics,* 45, pp. 247–271. DOI: 10.1146/annurev-genet-110410-132435.

Tachibana, M.; Takeda, K.; Nobukuni, Y.; Urabe, K.; Long, J. E.; Meyers, K. A. et al. (1996): Ectopic expression of MITF, a gene for Waardenburg syndrome type 2, converts fibroblasts to cells with melanocyte characteristics. In: *Nature genetics* n. 1, 14, pp. 50–54. DOI: 10.1038/ng0996-50.

Takahara, Shigeo (1952): PROGRESSIVE ORAL GANGRENE PROBABLY DUE TO LACK OF CATALASE IN THE BLOOD (ACATALASÆMIA). In: *The Lancet* n. 6745, 260, pp. 1101–1104. DOI: 10.1016/S0140-6736(52)90939-2.

Tam, Yuen Yi C.; Fagarasanu, Andrei; Fagarasanu, Monica; Rachubinski, Richard A. (2005): Pex3p initiates the formation of a preperoxisomal compartment from a subdomain of the endoplasmic reticulum in Saccharomyces cerevisiae. In: *The Journal of biological chemistry* n. 41, 280, pp. 34933–34939. DOI: 10.1074/jbc.M506208200.

Taylor, J. S.; van de Peer, Y.; Meyer, A. (2001): Revisiting recent challenges to the ancient fish-specific genome duplication hypothesis. In: *Current biology : CB* n. 24, 11, R1005-8.

Theos, Alexander C.; Berson, Joanne F.; Theos, Sarah C.; Herman, Kathryn E.; Harper, Dawn C.; Tenza, Daniele et al. (2006): Dual loss of ER export and endocytic signals with altered melanosome morphology in the silver mutation of Pmel17. In: *Molecular biology of the cell* n. 8, 17, pp. 3598–3612. DOI: 10.1091/mbc.E06-01-0081.

Theveneau, Eric; Mayor, Roberto (2011): Collective cell migration of the cephalic neural crest: the art of integrating information. In: *Genesis (New York, N.Y. : 2000)* n. 4, 49, pp. 164–176. DOI: 10.1002/dvg.20700.

Thieringer, H. (2003): Modeling human peroxisome biogenesis disorders in the nematode Caenorhabditis elegans. In: *Journal of cell science* n. 9, 116, pp. 1797–1804. DOI: 10.1242/jcs.00380.

Thisse, Christine; Thisse, Bernard (2008): High-resolution in situ hybridization to whole-mount zebrafish embryos. In: *Nature protocols* n. 1, 3, pp. 59–69. DOI: 10.1038/nprot.2007.514.

Thompson, J. D.; Higgins, D. G.; Gibson, T. J. (1994): Improved sensitivity of profile searches through the use of sequence weights and gap excision. In: *Computer applications in the biosciences : CABIOS* n. 1, 10, pp. 19–29.

Thoms, Sven; Harms, Imke; Kalies, Kai-Uwe; Gartner, Jutta (2012): Peroxisome formation requires the endoplasmic reticulum channel protein Sec61. In: *Traffic (Copenhagen, Denmark)* n. 4, 13, pp. 599–609. DOI: 10.1111/j.1600-0854.2011.01324.x.

Thorrez, Lieven; van Deun, Katrijn; Tranchevent, Leon-Charles; van Lommel, Leentje; Engelen, Kristof; Marchal, Kathleen et al. (2008): Using ribosomal protein genes as reference: a tale of caution. In: *PloS one* n. 3, 3, e1854. DOI: 10.1371/journal.pone.0001854.

Tiso, Natascia; Moro, Enrico; Argenton, Francesco (2009): Zebrafish pancreas development. In: *Molecular and cellular endocrinology* n. 1-2, 312, pp. 24–30. DOI: 10.1016/j.mce.2009.04.018.

Toyama, Reiko; Chen, Xiongfong; Jhawar, Nupur; Aamar, Emil; Epstein, Jonathan; Reany, Nir et al. (2009): Transcriptome analysis of the zebrafish pineal gland. In: *Developmental dynamics : an official publication of the American Association of Anatomists* n. 7, 238, pp. 1813–1826. DOI: 10.1002/dvdy.21988.

Toyofuku, Kazutomo; Valencia, Julio C.; Kushimoto, Tsuneto; Costin, Gertrude-E; Virador, Victoria M.; Vieira, Wilfred D. et al. (2002): The etiology of oculocutaneous albinism (OCA) type II: the pink protein modulates the processing and transport of tyrosinase. In: *Pigment cell research / sponsored by the European Society for Pigment Cell Research and the International Pigment Cell Society* n. 3, 15, pp. 217–224.

Trapnell, Cole; Hendrickson, David G.; Sauvageau, Martin; Goff, Loyal; Rinn, John L.; Pachter, Lior (2013): Differential analysis of gene regulation at transcript resolution with RNA-seq. In: *Nature biotechnology* n. 1, 31, pp. 46–53. DOI: 10.1038/nbt.2450.

Tsai, Shengdar Q.; Wyvekens, Nicolas; Khayter, Cyd; Foden, Jennifer A.; Thapar, Vishal; Reyon, Deepak et al. (2014): Dimeric CRISPR RNA-guided FokI nucleases for highly specific genome editing. In: *Nature biotechnology* n. 6, 32, pp. 569–576. DOI: 10.1038/nbt.2908.

Tseng, Yung-Che; Chen, Ruo-Dong; Lucassen, Magnus; Schmidt, Maike M.; Dringen, Ralf; Abele, Doris; Hwang, Pung-Pung (2011): Exploring uncoupling proteins and antioxidant mechanisms under acute cold exposure in brains of fish. In: *PloS one* n. 3, 6, e18180. DOI: 10.1371/journal.pone.0018180.

Tusnady, G. E.; Simon, I. (2001): The HMMTOP transmembrane topology prediction server. In: *Bioinformatics (Oxford, England)* n. 9, 17, pp. 849–850.

van den Bosch, H.; Schutgens, R. B.; Wanders, R. J.; Tager, J. M. (1992): Biochemistry of peroxisomes. In: *Annual review of biochemistry,* 61, pp. 157–197. DOI: 10.1146/annurev.bi.61.070192.001105.

van der Velden, Yme U.; Wang, Liqin; Zevenhoven, John; van Rooijen, Ellen; van Lohuizen, Maarten; Giles, Rachel H. et al. (2011): The serine-threonine kinase LKB1 is essential for survival under energetic stress in zebrafish. In: *Proceedings of the National Academy of Sciences of the United States of America* n. 11, 108, pp. 4358–4363. DOI: 10.1073/pnas.1010210108.

van der Zand, Adabella; Gent, Jurgen; Braakman, Ineke; Tabak, Henk F. (2012): Biochemically distinct vesicles from the endoplasmic reticulum fuse to form peroxisomes. In: *Cell* n. 2, 149, pp. 397–409. DOI: 10.1016/j.cell.2012.01.054.

van Maldergem, L.; Moser, A. B.; Vincent, M-F; Roland, D.; Reding, R.; Otte, J-B et al. (2005): Orthotopic liver transplantation from a living-related donor in an infant with a peroxisome biogenesis defect of the infantile Refsum disease type. In: *Journal of inherited metabolic disease* n. 4, 28, pp. 593–600. DOI: 10.1007/s10545-005-0593-9.

van Roermund, C. W.; van den Berg, M.; Wanders, R. J. (1995): Localization of peroxisomal 3-oxoacyl-CoA thiolase in particles of varied density in rat liver: implications for peroxisome biogenesis. In: *Biochimica et biophysica acta* n. 3, 1245, pp. 348–358.

Vander Heiden, Matthew G.; Cantley, Lewis C.; Thompson, Craig B. (2009): Understanding the Warburg effect: the metabolic requirements of cell proliferation. In: *Science (New York, N.Y.)* n. 5930, 324, pp. 1029–1033. DOI: 10.1126/science.1160809.

Varshney, Gaurav K.; Pei, Wuhong; LaFave, Matthew C.; Idol, Jennifer; Xu, Lisha; Gallardo, Viviana et al. (2015): High-throughput gene targeting and phenotyping in zebrafish using CRISPR/Cas9. In: *Genome research* n. 7, 25, pp. 1030–1042. DOI: 10.1101/gr.186379.114.

Varshney, Gaurav K.; Sood, Raman; Burgess, Shawn M. (2015): Understanding and Editing the Zebrafish Genome. In: *Advances in genetics,* 92, pp. 1–52. DOI: 10.1016/bs.adgen.2015.09.002.

Vilella, Albert J.; Severin, Jessica; Ureta-Vidal, Abel; Heng, Li; Durbin, Richard; Birney, Ewan (2009): EnsemblCompara GeneTrees: Complete, duplication-aware phylogenetic trees in vertebrates. In: *Genome research* n. 2, 19, pp. 327–335. DOI: 10.1101/gr.073585.107.

Vossen, Rolf H. A. M.; Aten, Emmelien; Roos, Anja; den Dunnen, Johan T. (2009): High-resolution melting analysis (HRMA): more than just sequence variant screening. In: *Human mutation* n. 6, 30, pp. 860–866. DOI: 10.1002/humu.21019.

Vouillot, Lena; Thelie, Aurore; Pollet, Nicolas (2015): Comparison of T7E1 and surveyor mismatch cleavage assays to detect mutations triggered by engineered nucleases. In: *G3 (Bethesda, Md.)* n. 3, 5, pp. 407–415. DOI: 10.1534/g3.114.015834.

Walker, M. B.; Kimmel, C. B. (2007): A two-color acid-free cartilage and bone stain for zebrafish larvae. In: *Biotechnic & histochemistry : official publication of the Biological Stain Commission* n. 1, 82, pp. 23–28. DOI: 10.1080/10520290701333558.

Wallner, Stefan; Schmitz, Gerd (2011): Plasmalogens the neglected regulatory and scavenging lipid species. In: *Chemistry and physics of lipids* n. 6, 164, pp. 573–589. DOI: 10.1016/j.chemphyslip.2011.06.008.

Wanders, R. J.; Denis, S.; Ruiter, J. P.; Schutgens, R. B.; van Roermund, C. W.; Jacobs, B. S. (1995): Measurement of peroxisomal fatty acid beta-oxidation in cultured human skin fibroblasts. In: *Journal of inherited metabolic disease,* 18 Suppl 1, pp. 113–124.

Wanders, R. J. A.; Ferdinandusse, S.; Brites, P.; Kemp, S. (2010): Peroxisomes, lipid metabolism and lipotoxicity. In: *Biochimica et biophysica acta* n. 3, 1801, pp. 272–280. DOI: 10.1016/j.bbalip.2010.01.001.

Wanders, Ronald J. A. (2014): Metabolic functions of peroxisomes in health and disease. In: *Biochimie,* 98, pp. 36–44. DOI: 10.1016/j.biochi.2013.08.022.

Wanders, Ronald J. A.; Komen, Jasper; Ferdinandusse, Sacha (2011): Phytanic acid metabolism in health and disease. In: *Biochimica et biophysica acta* n. 9, 1811, pp. 498–507. DOI: 10.1016/j.bbalip.2011.06.006.

Wang, Joshua X.; Fukunaga-Kalabis, Mizuho; Herlyn, Meenhard (2016): Crosstalk in skin: melanocytes, keratinocytes, stem cells, and melanoma. In: *Journal of cell communication and signaling. DOI:* 10.1007/s12079-016-0349-3.

Wasmeier, Christina; Hume, Alistair N.; Bolasco, Giulia; Seabra, Miguel C. (2008): Melanosomes at a glance. In: *Journal of cell science* n. Pt 24, 121, pp. 3995–3999. DOI: 10.1242/jcs.040667.

Wasserman, Wyeth W.; Sandelin, Albin (2004): Applied bioinformatics for the identification of regulatory elements. In: *Nature reviews. Genetics* n. 4, 5, pp. 276–287. DOI: 10.1038/nrg1315.

Waterham, Hans R.; Ebberink, Merel S. (2012): Genetics and molecular basis of human peroxisome biogenesis disorders. In: *Biochimica et biophysica acta* n. 9, 1822, pp. 1430–1441. DOI: 10.1016/j.bbadis.2012.04.006.

Waterham, Hans R.; Ferdinandusse, Sacha; Wanders, Ronald J. A. (2016): Human disorders of peroxisome metabolism and biogenesis. In: *Biochimica et biophysica acta* n. 5, 1863, pp. 922–933. DOI: 10.1016/j.bbamcr.2015.11.015.

Waterham, Hans R.; Koster, Janet; van Roermund, Carlo W. T.; Mooyer, Petra A. W.; Wanders, Ronald J. A.; Leonard, James V. (2007): A lethal defect of mitochondrial and peroxisomal fission. In: *The New England journal of medicine* n. 17, 356, pp. 1736–1741. DOI: 10.1056/NEJMoa064436.

Waterhouse, Andrew M.; Procter, James B.; Martin, David M. A.; Clamp, Michele; Barton, Geoffrey J. (2009): Jalview Version 2--a multiple sequence alignment editor and analysis workbench. In: *Bioinformatics (Oxford, England)* n. 9, 25, pp. 1189–1191. DOI: 10.1093/bioinformatics/btp033.

Wehrle-Haller, B.; Meller, M.; Weston, J. A. (2001): Analysis of melanocyte precursors in Nf1 mutants reveals that MGF/KIT signaling promotes directed cell migration independent of its function in cell survival. In: *Developmental biology* n. 2, 232, pp. 471–483. DOI: 10.1006/dbio.2001.0167.

Westerfield, Monte (2000): The zebrafish book. A guide for the laboratory use of zebrafish (Danio rerio). 4th ed. Eugene: Univ. of Oregon Press.

Wiese, Sebastian; Gronemeyer, Thomas; Ofman, Rob; Kunze, Markus; Grou, Claudia P.; Almeida, Jose A. et al. (2007): Proteomics characterization of mouse kidney peroxisomes by tandem mass spectrometry and protein correlation profiling. In: *Molecular & cellular proteomics : MCP* n. 12, 6, pp. 2045–2057. DOI: 10.1074/mcp.M700169-MCP200.

Williams, Chris; Opalinski, Lukasz; Landgraf, Christiane; Costello, Joseph; Schrader, Michael; Krikken, Arjen M. et al. (2015): The membrane remodeling protein Pex11p activates the GTPase Dnm1p during peroxisomal fission. In: *Proceedings of the National Academy of Sciences of the United States of America* n. 20, 112, pp. 6377–6382. DOI: 10.1073/pnas.1418736112.

Wolfe, K. (2000): Robustness--it's not where you think it is. In: *Nature genetics* n. 1, 25, pp. 3–4. DOI: 10.1038/75560.

Wood, Andrew J.; Lo, Te-Wen; Zeitler, Bryan; Pickle, Catherine S.; Ralston, Edward J.; Lee, Andrew H. et al. (2011): Targeted genome editing across species using ZFNs and TALENs. In: *Science (New York, N.Y.)* n. 6040, 333, p. 307. DOI: 10.1126/science.1207773.

Wu, Xufeng; Hammer, John A. (2014): Melanosome transfer: it is best to give and receive. In: *Current opinion in cell biology,* 29, pp. 1–7. DOI: 10.1016/j.ceb.2014.02.003.

Yale Journal of Biology and Medicine (1980): The Coat Colors of Mice. A Model for Mammalian Gene Action and Interaction. Con la collaborazione di Vijay Thadani. Available online in http://www.ncbi.nlm.nih.gov/pmc/articles/PMC2595761/, modified on March 1st 1980, retrieved in 19th July 2016.

Yamaguchi, Yuji; Brenner, Michaela; Hearing, Vincent J. (2007): The regulation of skin pigmentation. In: *The Journal of biological chemistry* n. 38, 282, pp. 27557–27561. DOI: 10.1074/jbc.R700026200.

Yamaguchi, Yuji; Hearing, Vincent J.; Maeda, Akira; Morita, Akimichi (2010): NADPH:quinone oxidoreductase-1 as a new regulatory enzyme that increases melanin synthesis. In: *The Journal of investigative dermatology* n. 3, 130, pp. 645–647. DOI: 10.1038/jid.2009.378.

Yamashita, Shun-ichi; Abe, Kakeru; Tatemichi, Yuki; Fujiki, Yukio (2014): The membrane peroxin PEX3 induces peroxisome-ubiquitination-linked pexophagy. In: *Autophagy* n. 9, 10, pp. 1549–1564. DOI: 10.4161/auto.29329.

Yan, Jingmin; Fujii, Kenji; Yao, Junjie; Kishida, Hideyuki; Hosoe, Kazunori; Sawashita, Jinko et al. (2006): Reduced coenzyme Q10 supplementation decelerates senescence in SAMP1 mice. In: *Experimental gerontology* n. 2, 41, pp. 130–140. DOI: 10.1016/j.exger.2005.11.007.

Yan, Yi-Lin; Miller, Craig T.; Nissen, Robert M.; Singer, Amy; Liu, Dong; Kirn, Anette et al. (2002): A zebrafish sox9 gene required for cartilage morphogenesis. In: *Development (Cambridge, England)* n. 21, 129, pp. 5065–5079.

Yao, Qi; DeSmidt, Alexandra A.; Tekin, Mustafa; Liu, Xuezhong; Lu, Zhongmin (2016): Hearing Assessment in Zebrafish During the First Week Postfertilization. In: *Zebrafish* n. 2, 13, pp. 79–86. DOI: 10.1089/zeb.2015.1166.

Yik, Wing Yan; Steinberg, Steven J.; Moser, Ann B.; Moser, Hugo W.; Hacia, Joseph G. (2009): Identification of novel mutations and sequence variation in the Zellweger syndrome spectrum of peroxisome biogenesis disorders. In: *Human mutation* n. 3, 30, E467-80. DOI: 10.1002/humu.20932.

Yin, Linlin; Maddison, Lisette A.; Li, Mingyu; Kara, Nergis; LaFave, Matthew C.; Varshney, Gaurav K. et al. (2015): Multiplex Conditional Mutagenesis Using Transgenic Expression of Cas9 and sgRNAs. In: *Genetics* n. 2, 200, pp. 431–441. DOI: 10.1534/genetics.115.176917.

Zamani, Mostafa; Taher, Jennifer; Adeli, Khosrow (2016): Complex role of autophagy in regulation of hepatic lipid and lipoprotein metabolism. In: *Journal of biomedical research,* 30. DOI: 10.7555/JBR.30.20150137.

Zehmer, John K.; Huang, Youguo; Peng, Gong; Pu, Jing; Anderson, Richard G. W.; Liu, Pingsheng (2009): A role for lipid droplets in inter-membrane lipid traffic. In: *Proteomics* n. 4, 9, pp. 914–921. DOI: 10.1002/pmic.200800584.

Zucca, Fabio A.; Basso, Emy; Cupaioli, Francesca A.; Ferrari, Emanuele; Sulzer, David; Casella, Luigi; Zecca, Luigi (2014): Neuromelanin of the human substantia nigra: an update. In: *Neurotoxicity research* n. 1, 25, pp. 13–23. DOI: 10.1007/s12640-013-9435-y.

Zucca, Fabio A.; Giaveri, Giuseppe; Gallorini, Mario; Albertini, Alberto; Toscani, Marco; Pezzoli, Gianni et al. (2004): The neuromelanin of human substantia nigra: physiological and pathogenic aspects. In: *Pigment cell research / sponsored by the European Society for Pigment Cell Research and the International Pigment Cell Society* n. 6, 17, pp. 610–617. DOI: 10.1111/j.1600-0749.2004.00201.x.

10 Abbreviations

°C	Degrees Celsius
µ	Micro-
A	Adenine
A	Anterior
Adat	Adenosine deaminase, tRNA-specific
Agps	Alkylglycerone phosphate synthase
AMO	Antisense morpholino oligonucleotide
Amsh	α-melanocyte stimulating hormone
AP	Alkaline phosphatase
ATP	Adenosine triphosphate
BAAT	Bile Acid-CoA-Amino acid N-acyltransferase
BCIP	5-bromo-4-chloro-3'-indolyphosphate
BLAST	Basic Local Alignment Search Tool
bp	Base pairs
BSA	Bovine Serum Albumin
C	Cytosine
cAMP	Cyclic adenosine monophosphate
Cas	CRISPR associated protein
Cat	Catalase
Cdkn	Cyclin dependent kinase inhibitor
cDNA	Complementary DNA
Cebp	CCAAT/enhancer binding protein
CIL	Contact-Inhibition of locomotion
CMV	Cytomegalovirus
CNC	Cephalic neural crest
CNS	Central nervous system
CoA	Coenzyme A
CoQ_2	Coenzyme Q2
CoQ_2H_2	Reduced coenzyme Q2
Cpt	Carnitine palmitoyltransferase
CRISPR	Clustered regularly interspaced short palindromic repeats
crRNA	CRISPR RNA
D	Dorsal
Da	Dalton
DAF-FM	4-Amino-5-Methylamino-2’,7’-Difluorofluorescein diacetate
DAPI	4',6-diamidino-2-phenylindole
dATP	Deoxyadenosine triphosphate
Dct	Dopachrome tautomerase

del	Deletion
DHA	Docosahexanoic acid
Dhapat	Dihydroxyacetone-phosphate acyltransferase
DHCA	Dihydroxycholic acid
DHI	5,6-Dihydroxyindole
DHICA	5,6-Dihydroxyindole-2-carboxilic acid
DM	Drosophila melanogaster
DMEM	Dulbecco/Vogt modified Eagle's minimal essential medium
DMF	N-N-dimethylformamide
DMSO	Dimethyl sulfoxide
DNA	Deoxyribonucleic acid
DNAse	Deoxyribonuclease
DOPA	Dihydroxyphenylalanine
dpf	Days post fertilization
DR	Danio rerio
DSB	Double strand break
ECL	enhanced chemiluminescence
EDTA	Ethylenediaminetetraacetic acid
eGFP	Enhanced green fluorescent protein
Elf	Elongation factor
EMT	Epithelium-to-mesenchyme transition
ENU	N-ethyl-N-nitrosourea
ER	Endoplasmic reticulum
EST	Expressed sequence tag
EZRC	European Zebrafish Resource Centre
f	Femto-
FCS	Fetal Calf Serum
FL	Full length
FLASH	Fast ligation based automable solid phase high throughput
Fox	Forkhead box
g	local acceleration due to gravity
g	Gram
G	Guanine
GEO	Gene expression omnibus
GFP	Green fluorescent protein
Gnpat	Glyceronephosphate O-acyltransferase
Hdac	Histone deacetylase
HDR	Homology-directed repair
HEPES	4-(2-hydroxyethyl)-1-piperazineethanesulfonic acid
Hmox	Heme oxygenase 2
hpf	Hours post fertilization
HRMA	High resolution melting analysis

HS	Homo sapiens
IgG	Immunoglobulin G
iNOS	Inducible nitric oxide synthase
IRD	Infantile Refsum Disease
k	Kilo-
K	Lysine
kb	Kilobase
Kit	V-kit Hardy-Zuckerman 4 feline sarcoma viral oncogene homolog
l	Litre
L	Left
L	Leucine
LAMP	Lysosome-associated membrane glycoproteins
LB	Lysogeny broth (or Luria-Bertani medium)
M	Molar concentration
m	Meter
m	Milli-
MART	Melanoma antigen recognized by T-cells
Mc1r	Melanocortin 1 receptor
min	Minute
Mitf	Microphthalmia-associated transcription factor
MM	Mus musculus
mol	Mole
mRNA	Messenger RNA
Mt-nd	Mitochondrial NADH-ubiquinone oxidoreductase chain
MTS	Melanosome targeting signal
n	Nano-
N	Any nucleotide
NAD	Nicotinamide adenine dinucleotide
NADP	Nicotinamide adenine dinucleotide phosphate
NALD	Neonatal adrenoleukodystrophy
NBT	nitro-blue tetrazolium
NC	Neural crest
NHEJ	Non-homologous end joining
OMIM	Online Mendelian Inheritance in Man
ORF	Open reading frame
p	Pico-
P	Posterior
PAGE	Polyacrylamide gel electrophoresis
PAM	Protospacer adjacent motif
PBD	Peroxisomal biogenesis disorder
PBS	Phosphate buffered saline
PCR	Polymerase chain reaction

PED	Peroxisomal enzyme deficiency
Pex	Peroxin
Pmel	Premelanosomal protein
PMP	Peroxisomal membrane protein
Polg	DNA polymerase gamma, catalytic subunit
POMC	Pro-opiomelanocortin
Ppar	Peroxisome proliferator-activated receptor
Ppargc	Peroxisome proliferator-activated receptor γ coactivator
PTS	Peroxisomal targeting signal
PTU	Phenylthiourea
qRT-PCR	Quantitative real-time polymerase chain reaction
R	Right
RCDP	Rhizomelic chondrodysplasia punctate
RFLP	Restriction fragment length polymorphism
RFP	Red fluorescent protein
RNA	Ribonucleic acid
RNAi	RNA interference
RNAse	Ribonuclease
RNS	Reactive Nitrogen Species
ROS	Reactive Oxygen Species
Rpl	Ribosomal protein
rpm	Rotation per minute
RVD	Repeat variable di-residue
S	Serine
SDS	Sodium dodecyl sulphate
sec	Second
sgRNA	Single guide RNA
Slc	Solute carrier
SNP	Single nucleotide polymorphism
SOD	Superoxide dismutase
Sox	(Sex determining region Y)-box
SSC	Saline sodium citrate
T	Thymine
TALEN	Transcription activator-like effector nuclease
TB	Translational blocker
TBS	Tris-buffered saline
THCA	Trihydroxycholic acid
TNC	Trunk neural crest
tracrRNA	Transactivating RNA
tRNA	Transfer RNA
Tyr	Tyrosinase
Tyrp	Tyrosine related protein

U	Unit
UAS	Upstream activating sequence
UTP	Uridine-5'-triphosphate
UTR	Untranslated region
UV	Ultraviolet
V	Ventral
v/v	Volume per volume
VLCFA	Very long chain fatty acid
w/v	Weight per volume
wt	Wildtype
X-ALD	X-linked adrenoleukodystrophy
Y	Tyrosine
ZFN	Zinc finger nuclease
ZMP	Zebrafish mutation project
ZS	Zellweger syndrome
Δ	Deletion
Φ	Bulky hydrophobic amino acid